AN INTELLIGENT ELECTRIC VEHICLE CHARGING INFRASTRUCTURE

A

Thesis submitted

in Partial Fulfilment of the Requirements

for the Degree of

Doctor of Philosophy

by

Bikash Sah

Department of Electronics and Electrical Engineering
Indian Institute of Technology Guwahati
Guwahati - 781039, Assam, India

October 2021

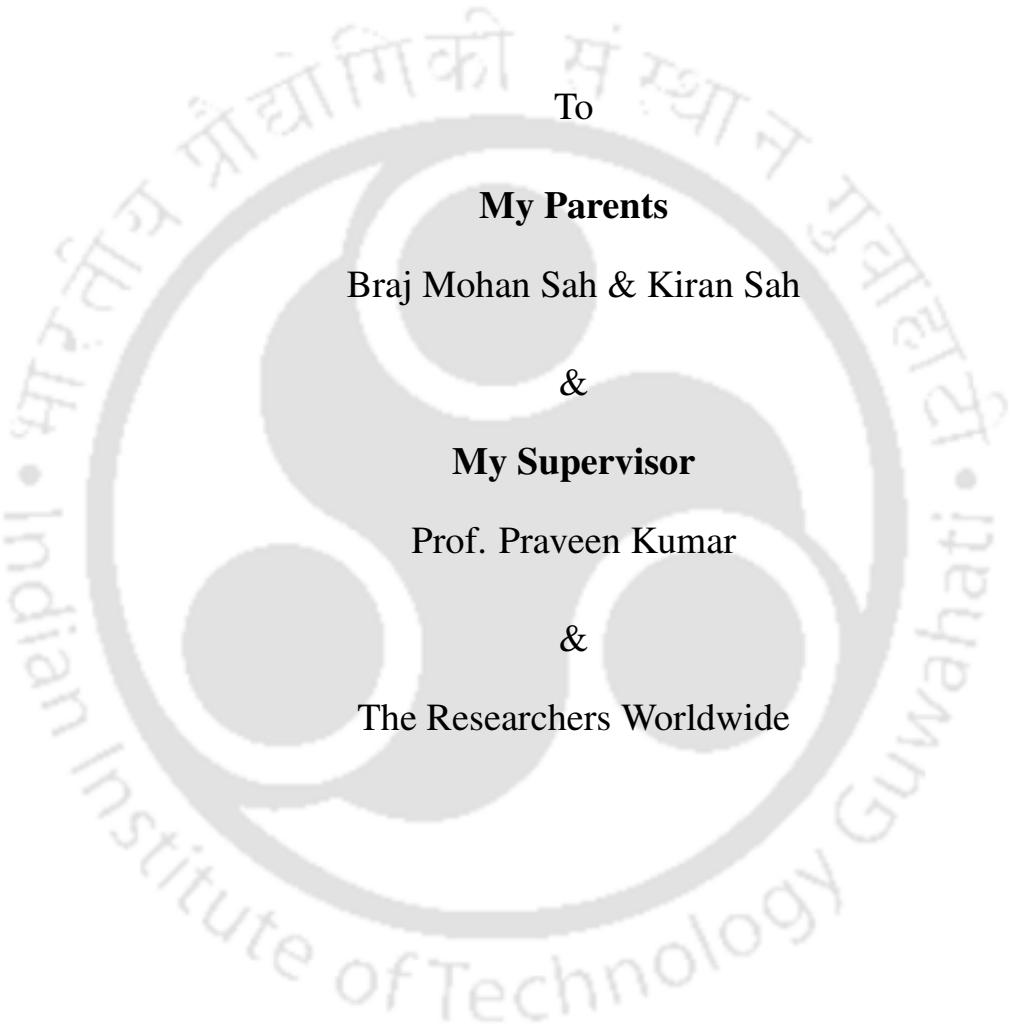

To

My Parents

Braj Mohan Sah & Kiran Sah

&

My Supervisor

Prof. Praveen Kumar

&

The Researchers Worldwide

Certificate

This is to certify that the thesis entitled "**An Intelligent Electric Vehicle Charging Infrastructure**", submitted by **Bikash Sah** (156102015), a research scholar in the *Department of Electronics and Electrical Engineering, Indian Institute of Technology Guwahati*, for the award of the degree of **Doctor of Philosophy**, is a record of an original research work carried out by him under our supervision and guidance. The thesis has fulfilled all requirements as per the regulations of the institute and, in our opinion, has reached the standard needed for submission. The results embodied in this thesis have not been submitted to any other University or Institute for the award of any degree or diploma.

Date:

Place: Guwahati

Prof. Praveen Kumar

Dept. of Electronics and Electrical Engg.,

Indian Institute of Technology Guwahati,

Guwahati - 781 039, Assam, India.

Acknowledgements

The works carried out to fulfil the requirement of this doctoral degree does not conclude merely with the addition of a higher academic degree that, of course, will help me boost my carrier. It also adds diverse learning that will help me live a flourishing life. These learning or life lessons are attributed to many people who readily supported me throughout the journey. To start with, it is my genuine pleasure and a great privilege to express my deepest and most sincere gratitude to my supervisor Prof. Praveen Kumar for their excellent guidance throughout my study. I feel fortunate to get an opportunity to work with him as his PhD student. His kindness, dedication, hard work and attention to detail have been a great inspiration to me. My heartfelt thanks to him for the unlimited support and patience shown to me. I sincerely thank him for patiently scrutinizing every work I presented to him and offering critical comments for improvements.

With utmost gratitude, I would further like to thank Prof. Sanjay Kumar Bose for his humble support by giving suggestions to improve my works, guiding, and correcting my manuscripts. I am also very thankful to my doctoral committee members Prof. Sisir Kumar Nayak, Dr Praveen Tripathy and Prof. Karuna Kalita, for sparing their precious time out of their busy schedule to evaluate my progress and enrich it with their invaluable suggestions and feedbacks.

I would also like to thank the Head of the Department and other faculty members for their kind help in carrying out this work. I am also grateful to all the members of the research and technical staff of the department, especially Mr Ridib Bharali, Mr Jatin Rabha and Mr Sibananda Sonowal. They have helped enormously by helping in sharing measurement equipment. My special thanks to Mr Dimpul Gogoi, who helped me in PCB printing and maintained the Electric Machine lab cum Electric Mobility Lab, where I worked for my PhD dissertation.

My special thanks to my closest friends - Chandan Kumar and Darpan Mishra, who were always there to hear my reasons for disappointments, resentment, happiness and success stories. Their spirit to positively boost me irrespective of the causes of failure or successes will always be appreciated and remembered. Further, I would like to thank Moon Moon Bordeori for being always there for me. It has been an immense pleasure to spend time with my colleagues in

the lab, Mr Rajendra Kumar and Binita Nanda, with whom I discussed our shared challenges, motivations and positivities.

Profusely, I also thank my seniors and mentors, Abhishek Kumar, Kashyap Kumar Prabhakar, Gautam Rituraj, C Upendra Reddy, Ankit Dalal, Mridul Kanti Malakar, Krishana Pavan Inala, and Brijesh Kushwaha, my colleagues Ankit Vishway and Tarique Sayeed, my friends and batchmates- Mohit Mishra, Manoranjan Minz, Nupur, Eedara Prabhakararao, Vineeta Das, Satyajit Borah, Rahul Sharma, Rishav Roshan, Sunil Mohan, and many others for being the part of this journey.

My deepest gratitude goes to my family member, especially my father and mother, for nurturing me beautifully. Withal, the support of my elder sister (Mrs Manisha Sah) and brother in law (Mr Neeraj Kumar), brother and sister in law (Mr Vishal Sah and Mrs Laxmi Pandiyar) is no less. I am heartily grateful to my family members for freeing me from all the responsibilities throughout my studies. My accomplishments made to date were always backed by their support and sacrifices.

I am also thankful to the Ministry of Education (previously Ministry of Human Resource Development) for financially supporting me from July 2015 to July 2020 by providing scholarship.

Finally, I thank all whose names are not mentioned for their delightful support in various forms.

(Bikash Sah)

Abstract

Electric vehicle charging infrastructure is the foundation for ensuring wider acceptance of electric vehicles (EVs). Governments and organisations worldwide are working on policies for deeper penetration of EVs in the transportation sector. The infrastructure comprises various stakeholder who communicates with each other. The communication ensures an optimal operation of each entity in the infrastructure, meeting the requirements of all the stakeholders. Although the present electricity infrastructure is able to support the charging of EVs, there are challenges of integrating bidirectional power flow between EVs and electric grid, developing appropriate communication infrastructure and support systems, motivating users to perform coordinated charging, and options to utilise EVs for ancillary services. Apart from the challenges in the electric grid, the requirement of fast charge with constrained battery degradation is another major challenge to persuade user acceptance. Henceforth, the work presented in the thesis proposes controllers, algorithms, estimation procedures, and techniques to develop an intelligent infrastructure that can perform coordinated charging with the least disturbances in the electric grid and meet the requirement of fast charge with constrained degradation at the user end.

The objective of developing an intelligent charging infrastructure is attempted by four major contributions described in the thesis. The potential of EVs to reduce the share of overall carbon emission by the transportation sector and provide ancillary services are best utilised in a vehicle to grid system. The vehicle to grid (V2G) system is comprised of an electric grid, controllers, aggregators, charging stations and electric vehicles as a major entity. The first two works of the thesis are focused on

developing an intelligent controller to reduce the impact of any issue with the data communicated between entities in the V2G systems. A practical scenario of data being transmitted to the controller utilising different data rates and communication channels is considered. In the first work, the importance of fast and equal data rate for the data reaching the controller are determined for optimal operation. A fuzzy logic controller (FLC) is used in this work. A process to synchronise the data rate is proposed, and modifications in the FLC are discussed to ensure the best operation even at a lower sampling rate.

In the second work, an artificial neural network (ANN) and FLC based controller is designed and verified to reduce the impact of issues such as delay, error and loss of data when transmitted by a communication channel. The intelligent controller performs data integrity checks using a trained ANN and corrects based on an algorithm if required. Since the intelligent controller ensured optimal power flow between EVs and the electric grid, the next challenge of intelligent charging infrastructure is to perform fast charge, constrain battery degradation and reduce the impact of charging in the electric grid. The battery degradation can be constrained by accurately estimating battery parameters and states during charging appropriately.

Hence, in the third work, a technique to estimate the battery parameters and states is proposed incorporating based on real-time impedance estimation. The impedance is a major parameter to interpret the ageing in EVs. Since the battery is an electrochemical device, a study incorporating electrochemistry in the development of charging techniques is necessary. Thus, the fourth work develops a new charging technique by analysing the electrochemical models and building insights on the variation of electrochemical, mechanical, and electrical parameters. The thesis concludes with the proposal of an intelligent controller for the V2G system and the development of an intelligent charger with battery-friendly charging techniques to fast charge and reduce battery degradation.

Contents

List of Figures

List of Tables

List of Acronyms

AC	Alternating Current.
APDCL	Assam power distribution corporation limited.
AHR	Ampere Hour .
ANN	Artificial Neural Network.
BER	Bit Error Rate.
CSs	Charging stations.
CC	Constant Current.
CCCV	Constant Current Constant Voltage.
CP	Constant Power.
CTCV	Constant Temperature Constant Voltage.
DICC	Data integrity check and correction.
DC	Direct Current.
EVs	Electric Vehicles.
ECM	Electrical Circuit Model.
EIS	Electrochemical Impedance Spectroscopy.
EKF	Extended Kalman Filter.
FLC	Fuzzy Logic Controller.
GHG	Green House Gas.
G2V	Grid to Vehicle.
IEC	International Electrotechnical Commission.
IoT	Internet of Things.
LCO	Lithium Cobalt Oxide.

LMO	Lithium Manganese Oxide.
LFP	Lithium Iron Phosphate.
LTO	Lithium Titanate Oxide.
MFs	Membership Functions.
MCS	Multi Charging Stations.
MAPE	Mean average percentage error.
MFs	Membership functions.
OCV	Open Circuit Voltage.
PFC	Power Factor Correction.
PI	Proportional Integrator.
LTE	Long Term Evolution.
PLC	Power Line Communication.
RMSE	Root mean square error.
RLS	Recursive Least Square.
RLSEF	Recursive Least Square Estimation using Exponential Forgetting.
SEI	Solid Electrolyte Interface.
SoC	State of charge.
SNR	Signal to Noise Ration.
ToU	Time of Usage.
TCP	Transmission Control Protocol.
UDP	User Datagram Protocol.
UMTS	Universal Mobile Telecommunication System.
V2G	Vehicle to Grid.
VPLC	Variants of Power Line Communication.

List of Symbols

SoC_{lt}	Minimum state of charge.
C^{lt}_{rate}	Maximum charge or discharge rate.
$SoC_{initial}$	Initial SoC.
C_{rate}	Charging rate.
P_{bni}	Power available or required at the n^{th} CS by the i^{th} EV.
V_{ni}	Voltage of the i^{th} EV at the n^{th} CS.
Ahr_{ni}	Current ampere hour rating of the i^{th} EV at n^{th} CS.
Ahr_{rated}	Rated ampere hour capacity of battery.
SoC_r	Remaining SoC of the battery.
SoC_c	Current SoC of the battery.
E_{evb}	Energy in the batteries of each EV connected to the i^{th} CS.
$P_{CS_{G2V}}$	Power required by the CSs to charge EVs.
$P_{CS_{V2G}}$	Power available at the CSs to support grid.
E_{evcs}	Total energy computed in the real time at each CS.
η_c	Charging efficiency.
η_d	Discharging efficiency.
P_T	Total power decided by the controller.
P_{evb}	Power available or required by the EVs.
$V(PU)_{fc}$	Forecasted values of node voltage.
$V(PU)_{grid}$	Value of node voltage of the grid.
$V_{controller}$	Final value of the given controller.
tol^*	Tolerance.

T_{out}	Maximum delay.
T_1	Fixed value of time which is equal to the sum of propagation and processing delays.
T_2	Random value of time which is exponentially distributed over a mean of 1.
P_L	Probability of data loss.
P_D	Probability of delay in data reaching the controller.
E_0	Constant voltage of battery.
Exp (s)	Exponential zone dynamics (V).
Sel (s)	Battery operating mode- 0 for discharge and 1 for charge.
L	Polrisation current ($Ah^{(} - 1$)).
i^*	Low frequency current dynamics (A).
i	Battery current (A).
Q	Maximum battery capacity (Ah).
A	Exponential voltage (V).
B	Exponential capacity (Ah).
P_{bni}	Power of battery in an EV at a CS.
V_{ni}	Voltage of battery in an EV at a CS.
Ahr_{ni}	Ampere hour of a battery in a EV at CS.
$X_{s\&H,i}$	Value of parameter with sampler in V2G.
$X_{RT,i}$	Value of parameter for base case (Plot without FLC in Fig. 2.7).
n	Number of samples.
$LiCoO_2$	Lithium Cobalt Oxide.
$I_o(t)$	Output current of DC-DC converter.
I_{dc}	DC offset current.
I_{ac}	Peak value of sinusoid added of I_{dc}.
f_p	Frequency of sinusoid added of I_{dc}.
d(t)	Duty cycle of output of DC-DC converter.
D_{dc}	Duty cycle for constant offset current of DC-DC converter.

D_{ac}	Duty cycle of the sinusoidal component in DC-DC converter.
ϕ_v	Phase angle of voltage in a battery.
ϕ_i	Phase angle of current in a battery.
Z	Impedance of the battery.
V_1 and V_0	Polarization voltage and drop across series resistance, respectively.
$V_T(s)$	Terminal voltage of the battery.
$V_{OC}(SoC)$	SoC dependant open circuit voltage of the battery.
Φ_T	Parameter vector.
$\theta(k)$	Regression vector.
$\Delta\varepsilon$	Effect of input noise.
t_{on}	On-time in pulse charging.
t_{off}	Off-time in pulse charging.

List of Publications

Patent application

1. **Bikash Sah**, Praveen Kumar, "A Rule-Based Charging Technique Incorporating Electrochemistry of Battery to Fast Charge and Constrain Battery Degradation," Indian Patent 202131028110, filled on June 23, 2019 (supported by Office of Dean, Industrial Interaction & Special Initiatives, IIT Guwahati).

Journal Publications Published

1. **Bikash Sah**, P. Kumar and S. K. Bose, "A Fuzzy Logic and Artificial Neural Network-Based Intelligent Controller for a Vehicle-to-Grid System," in IEEE Systems Journal, vol. 15, no. 3, pp. 3301-3311, Sept. 2021, doi: 10.1109/JSYST.2020.3006338.
2. **Bikash Sah**, P. Kumar, R. Rayudu, S. K. Bose and K. P. Inala, "Impact of Sampling in the Operation of Vehicle to Grid and Its Mitigation," in IEEE Transactions on Industrial Informatics, vol. 15, no. 7, pp. 3923-3933, July 2019, doi: 10.1109/TII.2018.2886633.

Journal under review

1. **Bikash Sah**, Praveen Kumar. An Insight into the Battery Degradation for a Proposal of a Battery Friendly Charging Technique, 09 August 2021, PREPRINT (Version 2) available at Research Square [https://doi.org/10.21203/rs.3.rs-710085/v2]

Book Chapters

1. **Bikash Sah**, P. Kumar, D.P Kothari, ”Application of Fuzzy Logic in the Operation of a V2G system in Smart Grid” accepted to be published in book titled ”Smart Charging Solutions on Hybrid and Electric Vehicle”, in Springer Nature.
2. **Bikash Sah**, P. Kumar, ”Smart charging: an outlook towards its role and impacts, enablers, markets, and the global energy system” accepted to be published in book titled ”Smart Charging Solutions on Hybrid and Electric Vehicle”, in Wiley–Scrivener Publishing.

1

Introduction to the EV Charging Infrastructure

Contents

"Take up one idea. Make that one idea your life — think of it, dream of it, live on that idea. Let the brain, muscles, nerves, every part of your body, be full of that idea, and just leave every other idea alone. This is the way to success."

– Swami Vivekananda

1.1 Introduction

Over the years, increasing greenhouse gas (GHG) emissions and deteriorating air quality have been of global concern. According to the recent report on climate change by the inter-governmental panel on climate change (IPCC), each decade is warmer than the previous one in the last four decades. As per the increase determined from the observed temperature data, the global surface temperature has increased by approximately 1.3°. Human influence on the environment is primarily the main driver for climate change [3]. GHG is one of the major reasons for the increase in global surface temperature.

The transportation sector is a major contributor to the release of GHG in the environment. The transport sector dominates one-quarter of the GHG emitted from energy-related services [4]. Hence, countries worldwide are working on various projects and policies to improve air quality for their citizens. Regrettably, only Europe and North America are reported to have improvements [5]. A potential solution to reduce vehicular emissions would facilitate the wider adoption of electric vehicles (EVs). Researches and reports suggest utilising electric vehicles (EVs) for transportation and renewable energy sources for power generation to reduce GHG emissions and improve air quality [6–8].

The replacement of conventional vehicles with EVs will help reduce the dependency on conventional fuels, apparently increasing energy security [9–11]. Further, it is to be noted that complete dependence on the EVs would instead increase GHG emissions from the energy sector if renewable sources are not used for generation. A case study in California shows a need to utilise the potential renewable energy sources and EVs as energy storage to reduce greenhouse gas (GHG) emissions. The utilisation of EVs in a coordinated way can help cut the GHG emissions to 42.9 % by 2050 compared to 2010 levels [12]. Hence, added utilisation of the potential renewable energy with coordinated recharging and discharging of EVs will help in

improving the environmental degradation and energy security collaterally [6, 13].

The benefits of EVs are not limited to energy security and air quality. Researchers have also proposed the utilisation of EVs as ancillary services. Voltage and frequency regulation, renewable energy support are the few most common application of EVs mentioned in literature [14, 15].

However, large scale deployment of EVs will demand an intelligent infrastructure that can ensure that the connected utility services to the electric grid remain least affected. There are two major challenges in this perspective. First, the recharging (G2V) and discharging (V2G) of EVs act as an additional load and distributed energy technology respectively to the utility grid [16, 17]. This will demand an overhaul of the overall management of the existing power system (generation, transmission and distribution). Secondly, a proper operation of EVs' recharging and discharging will require an intelligent controller to decide the amount of power to be exchanged between the utility grid and the EVs [18, 19]. The controller's working will depend on the node voltage of the grid and the energy available in the EVs connected. The node voltage in the grid gives an idea of the load connected to the utility grid, and the amount of energy in the EVs proclaim the capacity to recharge or discharge. This will require a robust information exchange system to communicate data between various entities of a V2G system [20].

Apart from the works to reduce the impact of charging in the electric grid and connected utility services, the requirements of fast charge with constrained battery degradation is another challenge in the EV charging infrastructure [21]. The battery degradation or the phenomenon of reduction in capacity due to ageing demands replacements or maintenance of EV battery packs. The replacements and maintenance increase the overall investment in EV for the EV users, which demotivates ardour or EV adoption [22, 23].

The two directions of the research described in the literature - the impact of charging on the electric grid and battery degradation are mostly divergent. The work described in the thesis bridges the gap between two directions. It proposes appropriate algorithms for controllers that coordinate the exchange of power between the electric grid and EVs and charging techniques that consider the electric grid's conditions and the phenomenon of battery degradation

before deciding the rate of charge. In this chapter, a brief discussion on the works done in EV infrastructure, challenges in the development of intelligent EV infrastructure and a need for intelligent chargers in EV infrastructure. Further, the objectives, contributions and organisations of the thesis will also be presented.

1.2 EV charging infrastructure

Infrastructure is a set of entities connected together using technologies, hardware and software systems, and standards to meet a common goal. The EV charging infrastructure is developed to meet EVs' charging requirements with the least impact on the electric grid infrastructure and connected stakeholders. Fig. 1.1 shows an example of EV charging infrastructure. The infrastructure is broadly divided into two: (i) electric grid side and (ii) user side. The infrastructure's electric grid side comprises power plants generating power and transmitting to a connected network called the electric grid. The connected network transfers the power to various feeder lines or local substations. The connected network transfers the power to various feeder lines or local substations. The distribution of power for utility services and charging stations (CSs) is done by the controllers in substations. The user end is characterised by the various devices connected at the CSs to control the charging of EVs.

Recent years have witnessed an increase in the penetration of renewables in the present electric grid infrastructure. Hence, the design of EV charging infrastructure should also consider the additional challenges emerging with the penetration of renewables. Altogether, the EV charging infrastructure should incorporate the following objectives [18, 20, 24–26]:

(i) The infrastructure should be able to facilitate providing power to utility services and charging stations or charging of EVs based on the available resources and variations of load.

(ii) The addition of new technologies and services to the existing electric grid infrastructure should be done without doing a complete overhaul.

(iii) The power flow from different types of generating stations to the loads and between EVs and the electric grid should be done using an intelligent controller. The infrastructure

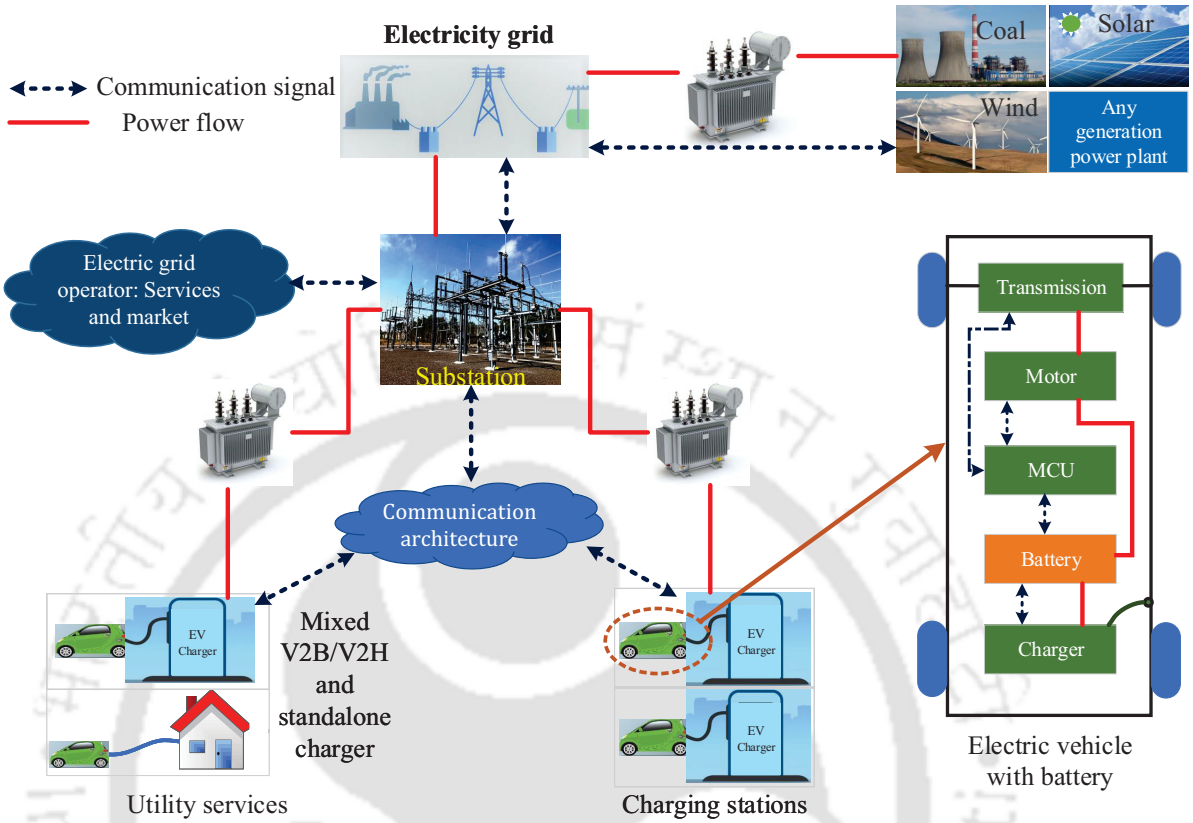

Fig. 1.1: EV charging infrastructure with various entities communicating and exchanging power between them.

should assist the participation of distributed generations and microgrids and support the participation of EV users and utility loads in improving existing grid infrastructure.

(iv) All the stakeholders should be connected via a common platform, and the dynamic control and pricing should concur with each other.

The bidirectional flow of power mentioned in the objectives is challenging but required to explore the potential of EVs such as ancillary services (voltage and frequency regulation) and act as distributed generations. Vehicle to grid (V2G) is a technique that helps to explore the potential of EVs.

1.3 Literature review and research directions

The potential of EVs has not limited to the curb the menace of environmental degradation. The potential is extended to provide support to the existing electric grid infrastructure [16]. The EVs remained parked for more than 60% of the time in a day [18, 22]. Hence, the batteries

in EVs, which are generally of more than 50kWh, can be used to provide services such as load levelling and ancillary services to the electric grid or act as a distributed generation by supporting local supplies. The V2G systems support these services from the EVs.

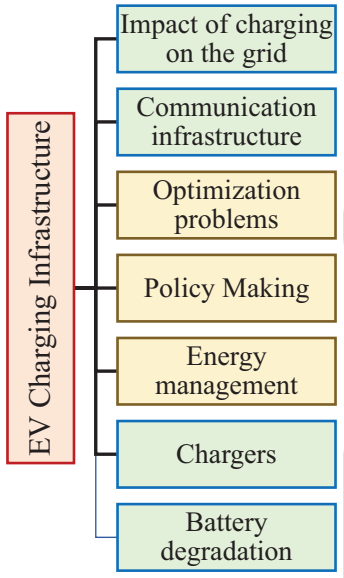

Fig. 1.2: Classification of research in the EV charging infrastructures

Fig. 1.2 shows a broad classification of the research in the EV charging infrastructure. The classification is based on the studies reported in the literature, which are independent in nature. A work describing the impact of EV charging does not consider the role of communication architecture. The optimization problems, policymaking, source side and load side energy management are mostly reported as separate studies [27–34]. Further, works in chargers and batteries are also separate and independent of challenges in EV charging infrastructure [35–41]. It is to be noted that each research topic is related, and an independent study will lead to multiple assumptions. For example, a study on the design of the V2G system with a focus on the impact of the electric grid assumes data are communicated ideally from one entity to another via an appropriate communication channel. Hence, the impact of erroneous data received at the entity will not be known. Similarly, battery degradation due to charging is always studied as a separate topic, although charging significantly impacts the electric grid. Further, a wider acceptance of EVs depends on the economic benefit a user is able to get. If the user has to spend on purchasing a new battery repeatedly, the users will restrain to purchase an EV.

The work described in this thesis is an attempt to analyse the EV charging infrastructure by not considering the research topics as an independent study. The scope of the thesis will be very wide if each topic is taken into consideration. Hence, the work is limited to challenges in the impact of charging on the electric grid, communication infrastructure, chargers and battery degradation. The optimisation, policymaking, and energy management are not directly taken into account. These involve surveys, inputs from experts, and various technical, economic and social analyses [22], which are out of the scope of this thesis. The previous sections discussed briefly the electric grid side and user side of an EV charging infrastructure. Although each side is dependant on the other, in literature, these two sides are discussed incoherently.

The increase in the number of EVs in the transportation sector will increase the demand for power to charge batteries. Increased demand for power will act as an additional load to the electric grid. Hence, the generation capacity, equipment for electric power transfer such as transmission lines, transformers and substations should be upgraded appropriately. Various research has proposed coordinated charging as a solution to reduce the impact of charging on the electric grid [42, 43]. As per coordinated charging, the EVs will charge during off-peak hours only. During peak load hours, since the service provider does not deny the charging, the cost of charging is increased. The increased cost discourages the users from charging during peak load hours [43–45].

Additional functionalities of load levelling and ancillary services are attributed to the bidirectional flow of power [14, 15]. The bidirectional flow of power is linked to the V2G systems. The conventional flow of power from the electric grid to EVs is called grid to vehicle (G2V). Similarly, the flow of power from EVs to the electric grid is called a vehicle to grid (V2G). The process of V2G is confined to an administered environment in which a controller decides the instance in which V2G and G2V is required [18, 20, 46]. In general, the decision of V2G and G2V is based on the connected loads and required power in the electric grid. The implementation of V2G is found to be beneficial in increasing the stability, efficiency, power dispatch and overall reliability [47]. The benefits of V2G is not limited to the technical domain; instead extends to economic and social sectors as well. An EV owner is expected to earn up to $ 4000

per year [22, 26, 47]. Further, V2G services will help in the upliftment of society in terms of air quality, constraining the rise of global temperature, and related health benefits [48].

The functionalities integrated into the V2G system require a robust communication system that can transfer data from one entity to another [46, 49]. The decisions made by the controller are based on these data. Hence, the communication architecture is reliable with an assurance of integrity in data. Literature mention various communication technologies such as narrow-band power line communication, vehicular power line communications, WiMAX, WiFi, long term evolution protocol, Ethernet, universal mobile telecommunication system, and other IoT based systems. The proposal of the utilisation of communication technologies and appropriate architecture is supported by performing analysis of parameters such as maximum round-trip delay, end-to-end delay, processing time with the variation in the number of EVs, control cycle duration, demand settling time, authentication delay, bit error rate (BER), signal to noise ratio (SNR) and a few others [50–59].

The user side of the infrastructure is visualised by the chargers and the batteries. The works on chargers remain focussed on different power electronics converter topologies and control techniques that can appropriately charge the EV batteries. The requirements of fast charge further demand high power converters. The high power is usually met by using converters in parallel. Further, these converters should be highly efficient and of high power density. Hence, high switching frequencies are used, which help in reducing the size of passive components. The other requirements like total harmonic distortion, impact on the power factor of source, bidirectional power flow and isolation are also looked into while proposing topologies [35–38]. The commercially available chargers have two stages: AC to DC with power factor correction (PFC) and DC to DC converters to charge batteries. The AC to DC stage with PFC have configurations such as totem pole PFC, multi-level PFC, Vienna PFC and variants of neutral point clamped converters. Conventional phase-shifted full bridge, LLC resonant converters, and dual active bridge based converters are popular topologies for the DC-DC stage [60].

Battery degradation is another major aspect of the user side. The battery is one of the costliest parts of an EV. The battery is an electrochemical device. Hence, it undergoes a variety

of required and superfluous reactions. The required reactions lead to charging and discharging. In contrast, the superfluous reactions lead to the formation of various byproducts that reduce the reactants for required reactions. Since the reactants for charging and discharging are reduced, the overall capacity to store energy by charging reduces [39, 40]. Further, the formation of products due to superfluous reactions adds resistance to the flow of ions in the battery. These superfluous reactions are also called side reactions [61]. These side reactions are triggered by a variety of factors like change in charge rate and discharge rate, change in internal and ambient temperatures, external or internal pressure or incorrect parameters estimated while charging or discharging [41].

The works in the thesis will ensure the challenges of EV charging infrastructure discussed in this section are studied in a correlated manner. The organisations, researchers and policymakers working in the development of EV charging infrastructure will be supported by the works with simulated and experimental models, results and analysis done on systems close to the real-time systems.

1.4 Motivation

The EV charging infrastructure is a complex system, with the design of each subsystem being a challenge. On the grid side, the controllers in the EV charging infrastructure requires data from connected entities to implement functionalities such as direction and amount of power flow between EVs and electric grid and any other as per requirements. The data is communicated by an appropriate network of communication technologies defined by the communication architecture [19, 62]. Communication of incorrect data from one entity to another, especially to the controller, have a turbulent impact on the whole system. For example, in a V2G system, during peak load hours, when V2G operation is supposed to be decided, the controller decides G2V operation. The decision of G2V will add EVs as an extra load to the electric grid during peak load hours, further supplementing the instability to the V2G system. Moreover, since the data is communicated via communication channels, there is a possibility of data becoming erroneous. Thus, there is a requirement for an intelligent controller which is robust and supports

the data integrity check and correction.

Meeting the requirements of EV users along with satisfying the electric grid standards is a challenging task. A paramount requirement of EV users is the ability to fast charge. Unfortunately, increasing the charge rate (C_{rate}) amplifies the rate of battery degradation, which is not required [1]. Further, increasing the C_{rate} increases the internal temperature of batteries leading to safety challenges such as thermal runaway, cell venting, and fires [63, 64]. The type of charging is another factor impacting battery degradation. Chargers to date are studied as power electronics devices with appropriate control.

In contrast, batteries are studied to determine the causes of degradation and the process to constrain degradation. However, the flow of power to the battery during charging is from the electric grid to the battery, which aligns with the studies in directions to determine the impact of charging on the electric grid. Thus, intelligent controllers decide the appropriate amount of power to be exchanged between the electric grid and EVs along with intelligent chargers which can fast charge and constrain battery degradation and consider the condition of the electric grid while deciding C_{rate} to charge is the need of the hour.

1.5 Objectives of thesis

The literature reviewed and the motivation have discussed the challenges in developing an intelligent EV charging infrastructure. Considering the discussions presented in previous sections, the following are the objectives of the thesis:

(i) To develop a controller for a V2G system that can decide the correct amount of power to be exchanged between EVs and electric grid irrespective of the asynchronous data reaching the controller.

(ii) To develop an intelligent controller which can perform data integrity check and control before providing data as an input to the controller.

(iii) To develop intelligent chargers which can perform accurate parameter and state estimations of the EV batteries to perform appropriate charging without incrementing the rate of battery degradation.

(iv) To study the causes of battery degradation and determine the relation between electro-chemical and mechanical parameters leading to proposals for charging at a varied range of temperature and specific to application (power intensive or energy intensive).

(v) To develop an intelligent charging technology that can fast charge and constrain battery degradation considering the results obtained from the previous study and reduce the impact of charging on the electric grid.

1.6 Contributions

Based on the work reported in the literature and their limitations, the contributions of this thesis are as follows:

(i) **Improvements in the controller of a vehicle to grid system to mitigate the impact of sampling**

The work explores two issues: (i) What impact does the communication system have on the grid? (ii) How can the controller(s) used in V2G be designed taking into account the communication network? In this work, communication between the various entities of a V2G system is investigated by transmitting data at different sampling rates. The contribution of this work is to examine various case scenarios developed based on the modelled system and analyse the impact of sampling on the V2G controller. Based on the analysis, the modifications in the controller are proposed to overcome the issues that arise from sampling.

(ii) **Development of an intelligent controller for a vehicle-to-grid systems**

The communication channels in the V2G system help to exchange information between entities to control the amount of power flow between the electric grid and EVs. These communication channels, while transmitting data, experiences delay, data corruption and data loss. Hence, in this work, a two-layer framework intelligent controller using fuzzy logic and artificial neural network (ANN) is proposed, which will perform V2G or G2V operation based on the inputs from both the electric grid side and the EV charging infrastructure. The controller will also perform suitable control actions, even if the required

data (grid node voltage) are lost. The data loss in the communication channel can be due to network congestion or if the receiver does not accept the data as it did not pass the error check or if it is excessively delayed. In addition, an algorithm is developed to integrate the intelligent controller with the V2G system. The algorithm considers the real-time per unit voltage (V(PU)) data sent from the grid, the data forecasted using the ANN, and the historical trend of V(PU) for checking the integrity. The algorithm further takes corrective steps taken in case errors are detected. The data in this work are the magnitude of the quantities measured at the electric grid side and the EV charging infrastructure. Further, the performance of the proposed algorithm is compared with an existing fuzzy logic controller (FLC) and found to be better.

(iii) **Charger integrated coestimation of parameters and states of battery**

This work directly towards the development of an intelligent charger with parameter and state estimation. Accurate estimation of these parameters and states will help perform charging with constrained battery degradation and reduce the impact of charging in the electric grid. In this work, an algorithm to estimate impedance online and use the impedance values in SoC and capacity estimation is proposed. An online impedance measurement technique for the battery is proposed in this work by modifying the reference signal of the DC-DC converter, which perform charging using any type of technique (constant current (CC), constant voltage (CV), CC-CV, and variants of pulse-based charging). The equivalent circuit model (ECM) parameters of the battery are also determined online. These parameters and impedance are used to estimate other states. The OCV of the battery is determined using the impedance. At the same time, the SoC estimation is realised utilising an extended Kalman filter based on the ECM parameters determined online. The real-time estimation of parameters in the EKF makes the estimation process suitable for all types of Li-ion batteries irrespective of their age and chemistries. The battery's capacity is estimated using a rule-based estimator, which takes OCV and SoC as inputs. Since the OCV and SoC are calculated in real-time, the impact of ageing in capacity is also incorporated with increased accuracy and reduction in complexity. The

proposed algorithms are verified for suitability in three types of charging techniques viz: CC, pulse charging without discharge and pulse charging with discharge.

(iv) **An Insight into the Battery Degradation for a Proposal of a Battery Friendly Charging Technique** Battery being an electrochemical system requires a deeper insight into the variation of electrochemical parameters. Further, these electrochemical phenomenon impacts the mechanical properties of the electrode as well. However, there is a lack of studies that provide a deeper insight by describing the variation of both types of parameters of battery with change in charging technique. The parameters widely studied in the literature are inactive material, SEI layer thickness, overpotential, lithiation, porosity, tortuosity, and particle crack length. The variation of the parameters results in the change in charging time, capacity, energy and power. Moreover, the parameters are dependant on the ambient temperature of the battery. The studies related to the impact on the battery parameters with change in the ambient temperature with change in charging types are also missing in the literature. Hence, via this work, the authors describe the impact of C_{rate} on the rate of chemical and mechanical degradation, the suitability of charging techniques at different ambient temperatures, and the suitability of the type of charging for high power and low power application. Further, for the first time, a commercially feasible and practically implementable novel charging technique suitable for all applications and ambient temperatures, considering the user's requirements and conditions of the electric grid, is proposed to fast charge with constrained degradation.

1.7 Organisation of thesis

A structural organization of the thesis is shown in Fig. 1.3. The organization of this thesis is as follows: The renaming thesis chapters are organized as follows:

- **Chapter 1:** A paradigm shift in the transportation sector is visible with the introduction of electric vehicles (EVs). Sustainable growth in usage requires a robust charging infrastructure. This chapter will discuss the works done to date for developing infrastructure. There are various challenges since the development of infrastructure is evolving with the

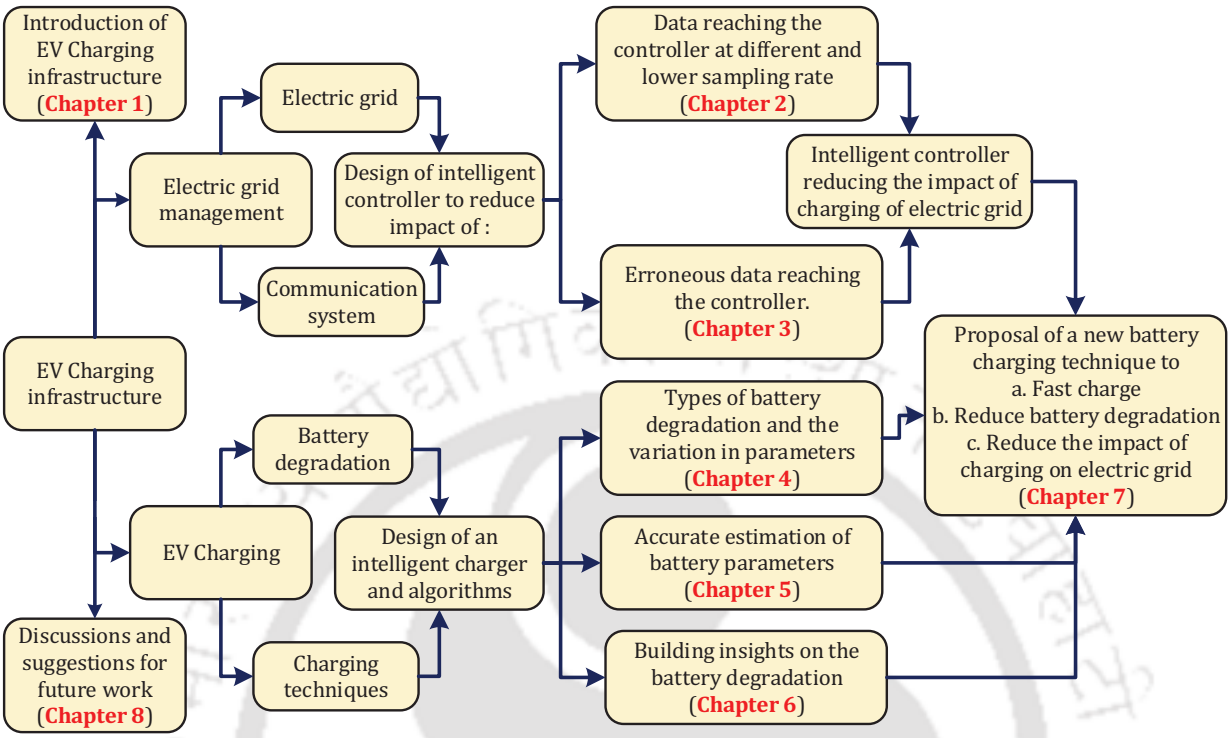

Fig. 1.3: Thesis organization

requirements of power system operators, users and other stakeholders of the EV ecosystem. These challenges will be comprehensively discussed to describe the need for an intelligent charger in the EV infrastructure. The objectives of the thesis and the contributions will also be discussed. The chapter will conclude with the organisation of the thesis and conclusions.

✍ **Chapter 2:** The vehicle to grid (V2G) systems is an integral part of the EV charging infrastructure. The V2G systems comprise of electric grid, controllers, aggregations, charging stations and EVs. These are connected to each other to exchange power. The amount of power exchange is decided by a controller, which requires appropriate data to be communicated between entities. Hence, the rate at which data reaches the controller and the controller types have a major role to play in the V2G system. A fuzzy logic controller is used to determine the amount of power to be exchanged between EVs and the electric grid. This chapter describes the process of optimizing the performance of the controller by synchronizing the data reaching the controller and updating the membership functions of the fuzzy logic controller.

- ✍ **Chapter 3:** The previous chapter remains focused on updating the controller of the V2G system, but the data reaching the controller via a communication channel also impacts the operation of the controller. The data reaching the controller can either be delayed, lost or become erroneous. Hence, in this work, modifications in the modified fully logic controller and algorithms are proposed to perform data integrity check and correction (DICC). The algorithm uses a trained artificial neural network to perform DICC. This chapter describes the modifications in the controller with the integration of the DICC block and the results obtained with the new controller.
- ✍ **Chapter 4:** Battery degradation is another challenge in the EV charging infrastructure. Hence, after optimising the controller of V2G, the other chapters focus on developing an intelligent charger to constrain the battery degradation. This chapter introduces the types of batteries, the electrochemical phenomenon in the battery that leads to charging and degradation, parameters studied in the literature to study the causes of degradation, and charging techniques proposed to reduce the battery degradation. Further, the requirement of an optimal charging algorithm incorporating challenges of electric grid loading and battery degradation is also discussed in this chapter.
- ✍ **Chapter 5:** The battery degradation is best determined by estimating the parameters of the battery. Impedance is an important parameter that can describe the rate of degradation and the health of the battery. Although various impedance estimation techniques are proposed in the literature, those are not easily integrable in the chargers. This chapter describes the proposal of an impedance estimation technique that can be incorporated into the charger. Further, the estimation of other states based on the impedance estimated is also described in this chapter. The algorithms proposed are validated using an experimental setup developed in the laboratory. The results obtained are further presented and compared to validate algorithms in real-time and verify the accuracy when compared to conventional techniques.
- ✍ **Chapter 6:** The proposals presented in the previous chapter were based on an electrical equivalent circuit model. The battery is an electrochemical system that requires multiple

other electrochemical parameters to constrain the battery degradation. These studies of electrochemical parameters are performed using models and experiments. The experimental approach is time-consuming. Hence, accurate electrochemical models are used in this work. This chapter describes the models used to perform charge and discharge, degradation- solid electrolyte interface formation, particle cracking and thermal changes. Further, parameters of different charging techniques used in this work, viz. constant current, constant current constant voltage, pulse charging without discharge and pulse charging with discharge, are also described. The selected electrochemical model of the battery is simulated for various charging types, C_{rate}, and ambient temperatures. The results obtained are described in this chapter. The parameters analysed are classified into three types, namely, electrochemical, mechanical and electrical. The chapter further describes the proposal of new types of charging techniques that help fast charging with constrained battery degradation and reduce the impact of charging in the electric grid.

✍ **Chapter 7:** The work described in this thesis will be summarised in this chapter. An outlook of the work will be discussed to show the usefulness to the various stakeholder involved in the EV charging infrastructure. The possibilities of the extension of this work will also be presented.

2

V2G Controller: Design and Mitigation on the Impact of Slower Sampling Rates

Contents

"There's always some room for improvisation."

– Satyajit Ray

2.1 Introduction

The growing concerns of government worldwide over energy security and environmental degradation have led to policies to reduce harmful gaseous emissions from the generation and transportation sector. The generation of power using renewable sources and electrifying the transportation sector is a possible solution to the problem. However, increased electrification of the transport sector requires a reliable and robust infrastructure. This infrastructure should be intelligent to meet the appropriate demands of both the user and generation sides. Further, the infrastructure should balance the generation and demand by coordinating between different entities involved.

The coordination requirement between entities of the infrastructure is to ensure the least changes in the existing electric grid systems. The existing electric grid has a limited generation, transmission and distribution capacity [19, 65]. An increase in the number of EVs on the road will demand power to charge batteries, increasing the load on the electric grid. An increase in load will lead to voltage instability, further stimulating voltage collapse [19, 66, 67]. This leads to outages locally and a wider blackout of the power system. Apart from the impact on the voltage, the injection of harmonics and the power factor are the other issues reported in the literature due to EV chargers and batteries [47].

The goal of the EV infrastructure is henceforth related to performing charging smartly such that the electric grid is least burdened. Smart charging is generally described in the literature as a grid to vehicle or G2V. Moreover, EVs have a large battery bank enough to power two houses for a day when fully charged. Hence, EVs are also suitable to be used as a power source or distributed generations. The idea further establishes the requirements of coordination between entities. The electric grid is at peak load hours during the evening when maximum electric utilities are being used and at off-peak conditions during late night and early morning hours, mostly rest periods for humans. The large battery capacity in the EVs makes it suitable to

supply power to the electric grid during peak load hours. During off-peak hours, the EVs can be charged.

The flow of power from EVs to the electric grid is conceptualised as a vehicle to grid or V2G [25, 68, 69]. The V2G systems incorporate the functionality of both G2V and V2G. They help provide peak shaving during peak load hours and valley filling by controlling the discharging and recharging of EVs to the electric grid. V2G also supports the electric grid by providing ancillary services such as frequency and voltage regulations, reserve power supply, and reactive power support [70, 71]. The functionalities reported in the literature require extensive information and data exchange between the entities. Hence, communication infrastructure is also a requirement in the EVs' smart charging infrastructure. The communication infrastructure has a vital role in ensuring the smart, efficient and reliable operation of the EV smart charging infrastructure.

Kempton and Letendre in 1987 proposed the use of EVs to support electric grid and local utility loads. Since then, a significant amount of work has been done and widely reported in the literature on V2G systems [47, 72–76]. However, a primary drawback of the works done in the V2G systems is that when the electrical aspects are studied, the communication aspects are neglected, or vice-versa [65, 77]. The works on the electrical aspects overlook the possibility of issues if the communication system fails [78–82]. Similarly, the works on communication proposed various technologies and analysed related parameters but do not look into the impact on the operation of the electric grid or the V2G system [50–59, 83–85]. Extensive reviews on the EV charging infrastructure leads to a common conclusion on the drawback [47, 86, 87].

Voltage and frequency regulation, load following, scheduling and dispatch, loss compensation, and energy balance are a few ancillary services reported in the literature directly or in another form. The impact of charging of EVs on the electric grid distribution network is the initial step to propose techniques. Various studies are reported in the literature to determine the impact of charging on the distribution network of the electric grid. Shao et al. discussed the impact of charging of EVs on the distribution network in the residential area, considering different types of EVs, charging profiles, and EV penetration [80]. Similar studies reported in

the literature considered a variation of voltage, frequency, and power quality [18, 88, 89].

The proposals to reduce the impact of EV charging in the electric grid is no less explored. A possible idea of frequency regulation is done by optimal scheduling of charge, and discharge between EVs and electric grid using aggregator [78]. Planned demand response in a distribution network with EVs is another strategy to reduce the impact of charging. The strategy requires modelling of V2G fleet using parameters of both charging stations and electric grid (such as energy, power, node voltage) in the context of a smart distribution network [81]. Similar models are proposed and investigated for optimal charging and control of V2G functionalities in [82]. EVs are mobile systems; hence, it is impractical to model a system by considering a fixed charging or discharging point in any node of the electric grid. Mobility of EVs is explored to manage the demand in [84]. Although varieties of techniques are proposed in the literature, operational cost to the power system operator and the reliability of the overall system is another major aspect that needs to be analysed. Fard et al. proposed the reconfiguration of distribution feeder in the context of an optimisation problem to cut down the operational cost of the network, reliability of the system, and the optimal dispatch in the V2G network [85]. The works described in the literature are focused on the V2G system as an electrical nodus. However, the proposed strategies are not practically implementable without the use of communication systems.

Proposals of communication systems or architectures and standards are another set of advancement required in the V2G systems. These technologies help to communicate or exchange data between entities to implement appropriate control. Technologies such as WiFi, long term evolution (LTE) protocol, universal mobile telecommunication system (UMTS), transmission control protocol (TCP), user datagram protocol (UDP), variants of power line communication (PLC), WiMAX and various others are reported in the literature with their suitability for V2G system. Each of the technologies is claimed to be suitable for communication between specific entities based on the distance between them, requirements of data rate and accuracy and topography of the region [50, 51]. WiFi is found to be a suitable communication for home area networks to communicate. At the same time, Ethernet is suitable to communicate between EV charging equipment and aggregator, and a communication system realised based on IEC-61850

standard is proposed appropriate between EVs and aggregator [50]. Renewable power generation is also an essential aspect of EV charging infrastructure. Hence suitable communication is required between the renewable generating station and other entities. A TCP based connection is considered in [53] between EVs and renewable energy generating systems. Further parameters which define the suitability of the TCP is also analysed. A similar study is done in [55], where UDP is used to communicate between EVs and aggregators.

The aspects of security in communicating data between entities are also investigated in a few studies reported in the literature [54, 90]. The VPLC and the narrowband PLC is used to communicate between plug-in EVs and electric grid, and EVs and aggregators, respectively. Similarly, WiMAX protocol is modelled to communicate between EVs and aggregator, and EVs and CSs [58, 59]. [59] proposed an authentication framework considering anonymity to connect between EVs and CSs. In a similar way, various other proposals of communication technologies for connecting between entities of V2G systems are reported in the literature. These proposals are validated by analyses of communication parameters related to the technologies. Authentication delay, bite error rate (BER), signal to noise ratio (SNR), loads and delay in bits/sec, database entry response time, traffic in sending and receiving, and path loss are a few parameters analysed in all the works described to determine the reliability and suitability for the proposed technique [50–59, 83]. Restating, the works described for developing communication systems for EV charging infrastructure fall short to explore the impact on the electrical parameters related to the electric grid, controllers, EVs and aggregators.

The literature reviewed in the previous paragraphs shows that both communication and electrical aspects are not studied together, nor the dependence between each other is reported. Further, the electrical perspective is neglected when communication systems for V2G are analysed or proposed, and the communication outlook is deserted when V2G is modelled to study electrical aspects. The discussions motivated me to explore the following concerns:

(i) How does the communication system impact the operation of the electric grid?

(ii) What should be the design of the controller(s) for use in the V2G systems considering the issues caused by the communication network?

The above concerns require an extensive study on the V2G model with appropriate electrical and communication systems. Hence, there is a requirement to develop a model of electric grid and communication systems together. However, both models are computationally intensive when simulated individually. Further, if simulating both models together will add the computational requirements. The fundamental step to determine the influence of communication on the electric grid will be to look into the impact of different sampling rates of the data.

The chapter approaches the fundamental step by modelling a V2G system where data communicated are in defined sampling rates. Different case scenarios are developed, which is studied using the modelled system. The results obtained are inclined to develop and perform necessary modifications in the controllers such that the issues due to changes in the sampling rates are reduced.

The rest of the chapter is organized as follows: Section II discusses the different components of the V2G system and its modelling, Section III help in the formation of problem statement by analysing the behaviour of the controller with inputs coming at different sampling rates, Section IV explores various options to tune the controller and Section V outlines the major conclusions of this chapter.

2.2 System modelling

A generic V2G system can be proposed to comprise of five major entities viz, the electric grid, controller, aggregator, CSs and EVs. Fig. 2.1 shows the general architecture with the mentioned entities. The previous sections described the requirements of the bidirectional flow of power. Hence, the idea of a bidirectional flow of power is shown using arrows. The real time systems exchanges data in the form of packets, which contains the data samples. In this work, the transmission is assumed to be discrete and in the form of samples. Moreover, the entities of the V2G system are located in different geographical locations. A coherent operation of the system will require appropriate communication architectures to interconnect the entities. The dashed line in the Fig. 2.1 shows the flow of information via any suitable communication systems between the entities.

In this section, the description of the V2G system modelled for meeting the objectives of this work is described. The electric grid part of the V2G system is based on the actual electric distribution grid of the Guwahati city located in the Assam state of India. A set of CSs called the Multi Charging Stations (MCS) are modelled to support the electric grid via a selected node in the distribution network. The only simplification in work is done by neglecting the interaction between power electronics converters and the electric grid. Similar assumptions are made in various other works reported in the literature [18, 25, 91–98]. Further, the work is technical analysis; hence, economic aspects are not discussed and considered.

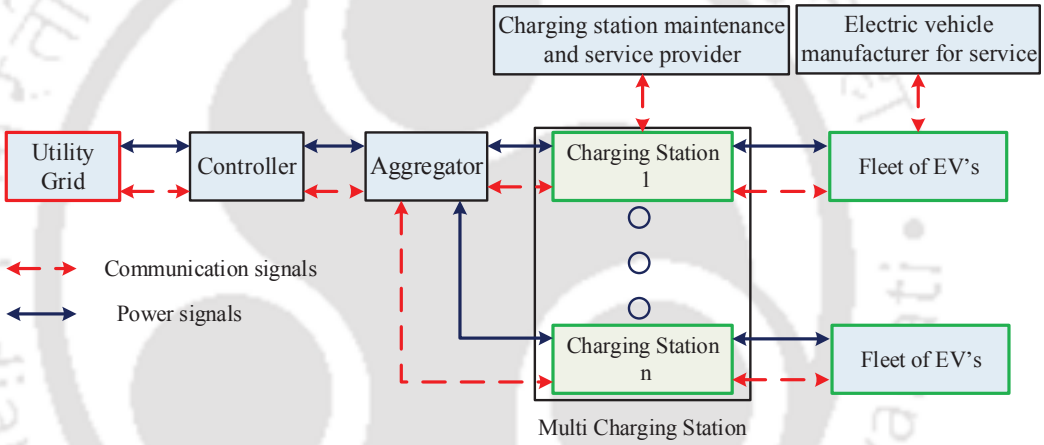

Fig. 2.1: A schematic of V2G system representing communication channels for information exchange and power flow between entities

2.2.1 Distribution System

The distribution system modelled in this work is a section of the overall Guwahati city electric grid network. The Guwahati city electric grid network consists of feeders, substations and nodes of different voltage levels. The data about the city is collected from the office of Assam Power Distribution Corporation Limited (APDCL). The transmission lines comprised of four 320 kV, five 220 kV and nineteen 132 kV feeders, which sum up to 28 high voltage feeders. The distribution side is characterised by a voltage equal to or below 33 kV. There are twenty-seven 33 kV substations from which one hundred thirty-five sub feeders of 11 kV branch out. The distribution system of the electric grid feeds both 11 kV and 440 V loads. If required, the 440 V, which is in three-phase, is stepped down further to feed single phase home loads.

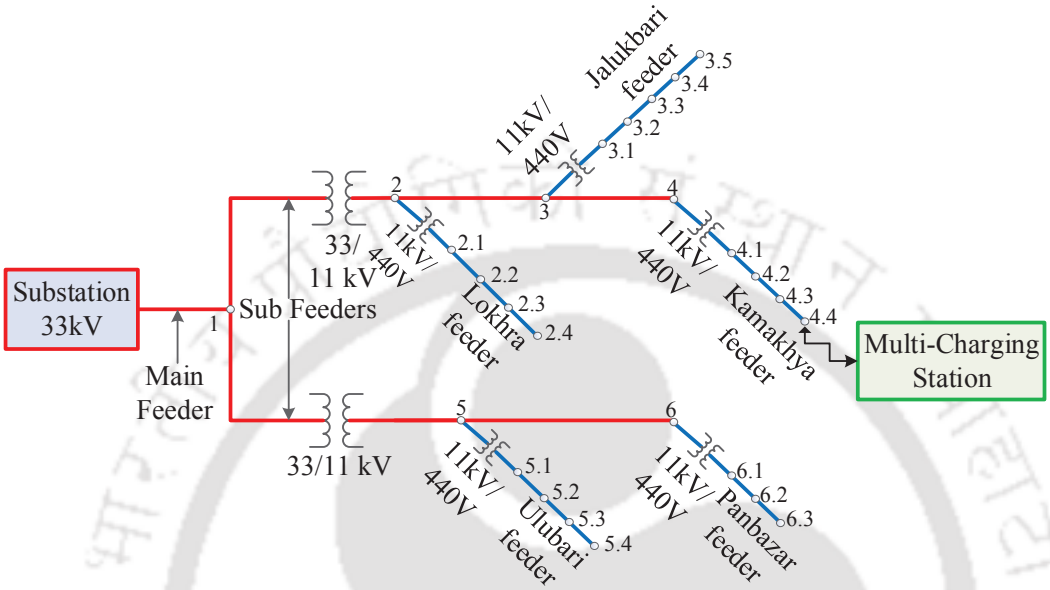

Fig. 2.2: Radial test distribution of 33kV node of Guwahati city

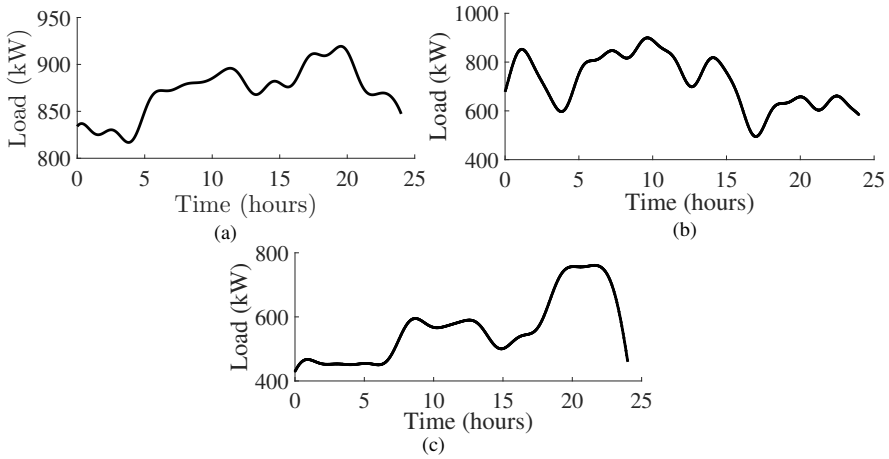

Fig. 2.3: Load profiles simulated at nodes (a) 4.4, (b) 5.4, and (c) 6.3

Appropriate transformers are used to step down voltages at the different parts of the electric grid.

Fig.2.2 shows a section of the electric grid that is modelled in this work. The section is a 33 kV feeder catering the loads in Lokhra, Jalukbari, Kamakhya, Panbazar and Ulubari. The 33 kV feeder branches out to 11 kV feeders. The nodes 2 to 6 are 440 V feeders, which are branched from 11 kV feeders using step down transformers. These nodes represent the Lokhra, Jalukbari, Kamakhya, Panbazar, and Ulubari areas, respectively, of Guwahati city. The selection of this 33kV feeder is based on the diversity in types of loads connected. Ulubari and Panbajar regions are commercial areas, Lokhra is residential, and Kamakhya and Jalukbari are a mix of both commercial and residential loads. The total numbers of nodes modelled in the section are 20.

The 24 hours load profile used in work is based on the data provided by the 33 kV substation of APDCL. The 24 hour load profiles for node 4.4 (residential area), 5.4 (office area) and 6.3 (commercial area) is shown in Fig. 2.3 (a), Fig. 2.3 (b) and, Fig. 2.3 (c) respectively. The work further analyses the complete system and the related parameters of the entities considering two patterns: mobile and immobile EVs. The deviation of node voltage when EVs are immobile is studied at node 4.4. while the node voltages of nodes 4.4, 5.4 and 6.3 are analyses when EVs are mobile. The selection of the node for study and analysis is based on the fact that the last node of a node series in an electrical network is most vulnerable to voltage deviations [99].

The work is further focussed on determining the efficacy of the controller in a V2G system and the performance of the V2G system. Hence, nodes 4 and 6 of the Fig.2.2 are found to be suitable for connecting MCS. However, the load profile of node 6 is smoother as compared to node 4. Node 4, being a mix of commercial and residential load, have more sharp slopes and more number of peaks. Hence in this work, node 4.4 is selected as a basic node in which MCS will be connected. The node voltages in other nodes (4.4, 5.4 and 6.3) will be analysed only when EV is considered mobile. A controller performs the decision to determine the amount of power to be exchanged between connected MCS in the electric grid nodes. The controller is described in the next subsection.

2.2.2 Multicharging Station

The MCS comprises of the main aggregator and the CSs. The subsystem shown in Fig. 2.6 represents the MCS. The main aggregator communicates with various other aggregators at CS and is the controller of the V2G system. Each entity of the MCS is explained in this subsection.

2.2.2.1 Charging Stations (CSs):

A CS is the point of connection between EVs and electric grid. The power from the electric grid is available via a node in CS. By using appropriate power electronics converters, control and communication systems, the EVs exchange the power. The modelled CS in this work comprises of communication between the main aggregator and several aggregators at CSs and 40 EVs. These EVs are modelled as batteries in this work. Five types of EVs are considered in this work, and the battery of each type are given in Table 3.1.

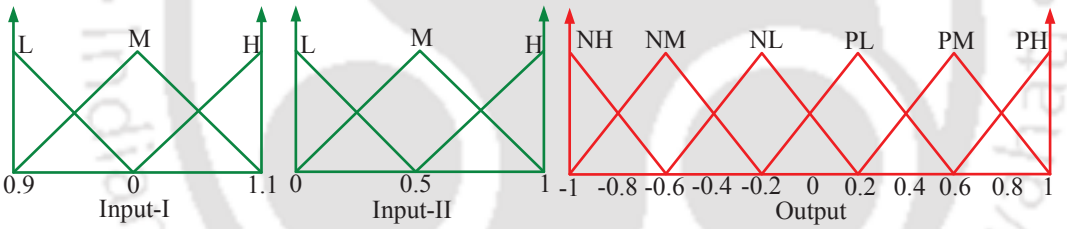

Fig. 2.4: Fuzzy membership functions; Input-I (V[PU]), Input-II (E_i) and Output (Power)

The table lists the energy and ampere-hour (AHR) ratings, values of types of state of charge (SoC) viz. $SOC_{initial}$ and SOC_{limit} and maximum charging rate limit C_{rate}^{limit}. Of the mentioned, $SOC_{initial}$ and SOC_{limit} need special mention and consideration while developing the algorithm to charge and discharge as per the decision of the V2G controller. $SOC_{initial}$ is the value of SoC which is sensed by CS or communicated by EVs on connecting an EV to the charging port. $SOC_{initial}$ value help to determine if the batteries in EVs are suitable to charge or discharge. SOC_{limit} is the value of the SoC at which the EV owner constrain EVs from participating in the V2G mode of operation. Basically, SOC_{limit} is the minimum value of SoC set by the EV owner to maintain in his EV.

The batteries in the EV used in the V2G model are the ones available in the Electric Drives/Extra Sources library of MATLAB Simulink. The model is a generic battery model

Table 2.1: Specifications of the batteries in the EVs

Types of battery	Energy (kWh)	$SOC_{initial}$ (%)	SOC_{limit} (%)	AhR	C_{rate}^{limit}	No. of EVs
A	8	70	25	32	3	40
B	10	40	45	40	2.5	40
C	16	50	30	64	3	40
D	20	85	40	80	4	40
E	24	30	20	96	4	40

with options to select electrochemistry. Further, the model is validated with experimental data from various datasheets of different chemistry. In this work, Li-ion battery chemistry is used whose charging and discharging are defined by Eqn. 2.1 and 2.2 [100, 101].

$$f_1(it, i^*Exp) = E_o - k.\frac{Q}{Q-it}.i^* - k\frac{Q}{Q-it} + L^{-1}\left(\frac{Exp(s)}{Sel(s)}.0\right) \tag{2.1}$$

$$f_1(it, i^*Exp) = E_o - k.\frac{Q}{it-0.1Q}.i^* - k\frac{Q}{Q-it}it + L^{-1}\left(\frac{Exp(s)}{Sel(s)}.\frac{1}{s}\right) \tag{2.2}$$

where E_0 is the constant voltage (V), Exp(s) is the exponential zone dynamics (V), Sel(s) represents the battery mode (Sel(s) = 0 during battery discharge, Sel(s) = 1 during battery charging), K is the polarization constant (Ah^{-1}) or polarization resistance (Ohms), i^* is the low frequency current dynamics (A), it is the extracted capacity (Ah), i is the battery current (A), Q is the maximum battery capacity (Ah), A is the exponential voltage (V) and B is the exponential capacity (Ah^{-1}) of battery.

The user defined values SOC_{limit} and other mentioned in the previous paragraphs are used to determine value of C_{rate}, energy in the batteries E_{evb} and related parameters. Comprehensively, the algorithm is defined in Algorithm 2.2.2.1.

The C_{rate} as an input to the algorithm is determined using (2.3).

$$C_{rate} = P_{bni}/(V_{ni}Ahr_{ni}) \tag{2.3}$$

where P_{bni} and V_{ni} and Ahr_{ni} are the data of battery from an EV at the CS. The value of Ahr_{ni} in (2.3) is computed based on the current SoC and the rated Ah capacity of battery which are

Algorithm 1 Algorithm at CS end

Calculate C_{rate}
if $C_{rate} < C^{lt}_{rate}$ **then**
    C_{rate}=C_{rate}
else if $C_{rate} > C^{lt}_{rate}$ **then**
    C_{rate}=C^{lt}_{rate}
end if
Calculate Ahr_{bj}
Calculate SoC_c
if $SoC_c < SoC_{lt}$ **then**
    No V2G participation, only G2V
    Calculate A_j
else if $SoC_c > SoC_{lt}$ **then**
    Calculate A_j
end if
Calculate E_b

related using (2.4).

$$Ahr_{ni} = (Ahr_{rated} SoC_r)/100 \tag{2.4}$$

The computation of SoC_r vary for cases when EV is charging and discharging. During charging, the SoC_r is equal to (100- SoC_c) while in case of discharging, it is equal to (SoC_c-SoC_{lt}). SoC_c is defined as the current or real time SoC of the battery. The amount of current (A_{ni}) for recharging or discharging of EV at the CS is given by (2.5).

$$A_{ni} = Ahr_{ni} C_{rate} \tag{2.5}$$

The energy in the batteries E_{evb} is computed based on the value of SoC_r determined from the EVs connected at the CSs using (2.6).

$$E_{evb} = (SoC_r V_{ni} Ahr_{rated})/100 \tag{2.6}$$

2.2.2.2 Aggregator:

The aggregator is an intermediary entity in the V2G system whose functionality is to regulate the distribution of power and energy among the electric grid and the CSs [102]. This work defines two types of aggregators: the main aggregator connecting the controller and several aggregators at the CS level. The main aggregator communicates between CSs and the controller to aggregate the data reaching it via communication channels. The controller decides the direction

and amount of power flow between EVs and the electric grid. At the same time, the aggregators distribute the power among the CSs connected to it. The distribution of power in the case of charging is based on (2.7) and (2.8) in the case of discharging.

$$P_{i_{G2V}} = (\frac{E_i}{E}P)\eta \tag{2.7}$$

$$P_{i_{V2G}} = (\frac{E_i}{E}P)\frac{1}{\eta} \tag{2.8}$$

where, P is the power drawn/supplied from/to the node, P_i is the net power exchanged at the i^{th} CS, E_i is the available/required batteries energy of the i^{th} CS and E is the total energy available/required by the MCS. Here, η is the charging/discharging efficiency of the system [25].

Similarly the aggregator at the CS level coordinates between EVs and the main aggregator. If (P_i) is the power to be distributed to each i^{th} EVs at CSs, (2.9) computes the power available/required (Pb_{ij}) by the j^{th} battery of i^{th} CS [25].

$$Pb_{ij} = \frac{Eb_{ij}}{\sum_{j=1}^{m} Eb_{ij}} P_i \tag{2.9}$$

Apart from the regulation and distribution of power, the aggregator also determines if the CS is capable of delivering power to the electric grid or the needs of power from the electric grid to charge connected EVs. For example, if the electric grid is at peak load condition, and the SoC of an EV is more than SoC_{limit}, the aggregator confirms to deliver power to the grid, but if the SoC of the EV has reached SoC_{limit}, the aggregator aborts the delivery of power to grid. The functionalities of the aggregator are redefined based on the developer of the V2G system. Overall, communication systems are the common requirement to ensure reliable operation of V2G as shown in Fig. 2.6. In this work, the data is assumed to be exchanged between entities in the form of samples at varied sampling rates. The next section will discuss in detail the variety of sampling rates for data communicated by the channels as shown in Fig. 2.6. The work does not model the actual communication channels between each entity of the V2G system.

2.2.3 Controller

The controller is the entity deciding the appropriate amount of power to be exchanged between the electric grid and the EVs. The operation of the controller is decided by the connected entities and the information shared by them using communication channels as shown in Fig. 2.6. The controller in this work is connected to the Kamakhya feeder at node 4.4. Fig. 2.6 shows the detailed schematic of the controller. In this work, a fuzzy logic based controller (FLC) is designed for this purpose. The selection of the FLC is contrary to existing conventional controllers like a proportional integral derivative. The conventional controllers require detailed mathematical modelling of the system to calculate appropriate gains. The calculation further is restricted by the limitations of boundary conditions defined while mathematically formulating the system [18, 103]. The system model for the V2G system is given load profiles at various nodes. These load profiles widely vary over time.

Further, the number of EVs at the CSs are also not always the same. Hence, such variations of parameters and operating points of a model will be a challenge to incorporate in the mathematical model. On the other end, the FLC provides ample flexibility in the design of the controller because it is not dependent on the mathematical modelling of the system. The design of FLC is based on a set of rules which are frames by experts who have significant knowledge of the system operation. These properties promote the use of FLC to model uncertainty and complex decision processes [104, 105].

The FLC operates based on two inputs viz. (a) the node voltage in per unit (PU) of the electric grid at which the MCS is connected (V(PU)) and (b) the total energy available in the batteries of EVs (Energy). These inputs are initially fuzzified into linguistic variables with a range of values. The linguistic variables are passed to an inference system supported by the rule base. The output of the inference system is passed to a defuzzification system which gives a crisp value. A Mamdani type FLC is used in this work, and the crisp value is calculated using the centroid defuzzification method. The feature of interpretability and intuitively designing the rule base led to the selection of Mamdani type FLC. Further, triangular membership functions (MFs) are used over other shapes because of the ease in implementation and its ability to

yield optimal values of outputs [19, 106]. The triangular MF used is represented in Fig. 2.5. Mathematically it can be defined by Eqn. 2.10 [107, 108].

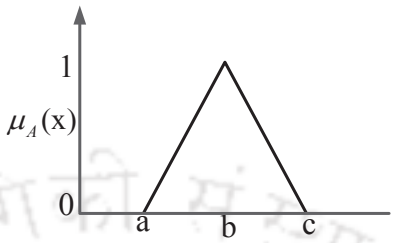

Fig. 2.5: A triangular membership function of FLC

$$\mu_A(x) = \begin{cases} 0 \text{ if } x \in]-\infty, a] \cup [c, \infty] \\ \dfrac{x-a}{b-a} \text{ if } x \in [a, b] \\ \dfrac{x-c}{b-c} \text{ if } x \in [b, c] \\ 0 \text{ if } c \leq x \end{cases} \tag{2.10}$$

where $\mu_A(x)$ is a function of x; a, b and c are the scalar values such that $a < b < c$ as shown in Fig. 2.5.

The two inputs are represented by three membership functions viz. low (L), medium (M) and high(H). Six membership functions represent the output: negative low (NL), negative medium (NM), negative high (NH), positive low (PL), positive medium (PM) and positive high (PH). The membership functions are shown in Fig. 2.4. A positive value of output power from the controller corresponds to the charging of EVs, and negative values correspond to discharging of EVs. The rule base used is given in Table 2.2. The MCS is described in the following subsection.

Table 2.2: Rules for V2G controller

Inputs		Output	Inputs		Output
V (PU)	Energy	Power	V (PU)	Energy	Power
L	L	PL	H	L	PH
L	M	NM	H	M	PM
L	H	NL	H	H	PL
M	L	PL	M	H	NL
M	M	NM	.	.	.

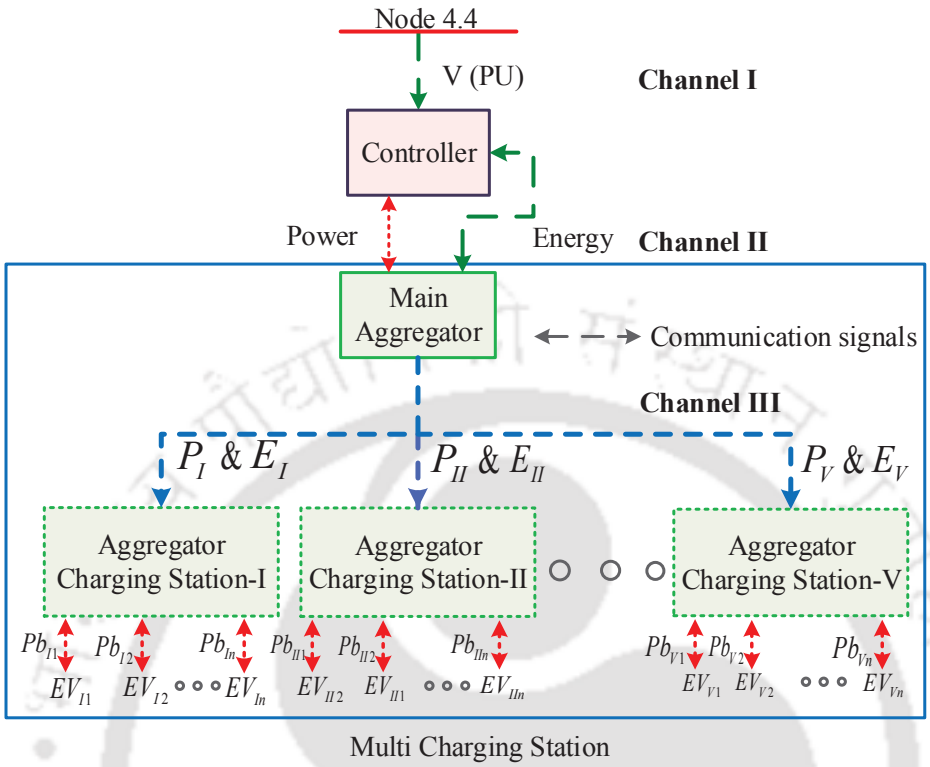

Fig. 2.6: Detailed view of the node at which CSs are connected with entities of V2G interacting with each other

2.3 Behavior Of Controller With Sampling Rate

In this section, the impact on the output of the controller due to changes in the sampling rate of the inputs is reported. The input data required for the controller are discussed in the previous sections. A data (V(PU)) is coming from the electric grid end while the other (Energy) is transmitted from the CS end. The V2G system operates when the electric grid is at peak load condition while G2V is functional during the vice-versa. The efficacy of the controller is hypothesised to vary with the sampling rate because a faster sampling will increase precision resulting inaccurate computation of output. Further, the study is performed for two conditions, viz. when the EVs are stationary and when the EVs are mobile. Stationary EVs means the EVs are connected to a particular CS for the whole day or 24 hours. Considering simplicity, the results for determining efficacy and proposal for improvisations are based on the case when EVs are stationary. The proposed improvisations are validated for the case when EVs are mobile.

The functioning of the FLC is verified by checking the variation of voltage profile with and without the use of the controller. Fig. 2.7 shows the smoothing of the voltage profile with the

use of a controller. The use of a controller signifies that the MCS is supporting the operation of the electric grid. A similar scenario is shown in many previous works [78–82] including the work of Mukesh et.al. in [25]. These works considered the continuous transmission of data between entities rather than at discrete time intervals. However, the plots shown in Fig. 2.7 is for the cases when data are transmitted as samples at discrete time intervals.

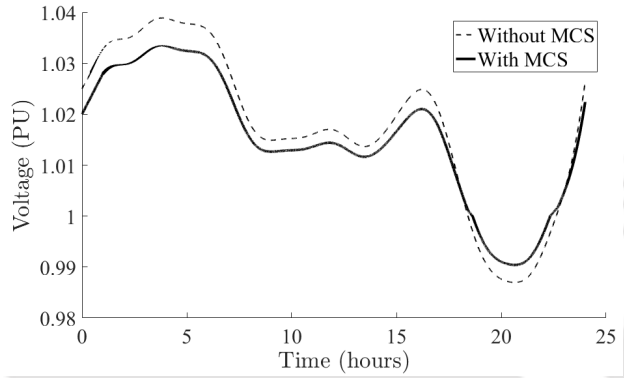

Fig. 2.7: Improvement in the node voltage profile due to support from MCS

A base case for comparing the results with the variation of sampling rate is required. Fig. 2.7, which shows the voltage profile when the controller is connected, is taken as a base case. The work in this chapter tries to capture all the aspects of the impact on the sampling. Initially, the impact of faster and slower sampling rates are studied, followed by analysing the requirement of synchronisation of inputs of the controller at the same data rates. Further, the impact of synchronisation of samples at faster and slower sampling rates are also studied. These studies provide insights into the design of FLC with increased efficacy. Initially, all the channels are assumed to be transmitting data sampled at the same data rate. As EVs' incoming and outgoing pattern is unpredictable, a sampling rate of 1000 samples per second (i.e. sampling interval=1 ms) is assumed at the CS end. Fig. 2.8(a) shows the variation of node voltage results obtained when the sampling rate of 1 ms for all the channels.

Similarly, the case where all the signals are sampled at the rate of 1 sample/s (sampling interval = 1 s) is also examined. Corresponding results are shown in Fig. 2.8(b). From Fig. 7(a) and 7(b), it can be seen that, when the sampling interval is 1 ms, the results are close to the base case scenario, the results for which were shown in Fig. 2.7. However, when the sampling

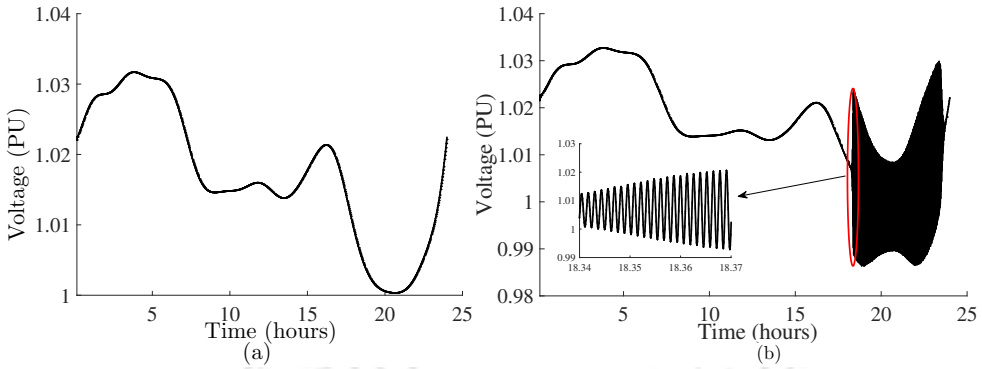

Fig. 2.8: A comparison of voltage profile when all channels are at same sampling rate. (a): Sampling rate of 1 sample/ms (b) Sampling rate of 1 sample/s

is done at 1s intervals, the voltage profile oscillates between 16 and 24 hours, i.e. during peak load hours.

Between 1600 to 2200 hours, the voltage per unit (V (PU))) lies in the range of 0.99 to 1.01. For the V (PU) value in this range, as per the rules defined, two MFs (NL and PL) are activated in the output. These MFs, as seen in Fig. 2.4 lie in the region around [-0.4, 0.4]. The output of the controller in this region determines the operation, either V2G or G2V. A negative value decided by the controller means that the controller is performing V2G operation, and a positive value is decided for G2V operation. The transitioning of V2G to G2V or vice versa is a critical decision to be taken by the controller. The decision to be taken by the controller will depend on its input. Fig. 2.9 shows the activated MFs when the FLC is operating in this region. A small change in input changes the value of output to either positive or negative when the controller operates in this region. The peak load hours start at 18 hours, and the controller should change the operation of G2V to V2G. For incorrect values of the input, the controller decides erroneous output values that do not meet the demand of the grid. This leads to oscillations in power decided by the controller, which introduces oscillations in the voltage profile of the node in which MCS is connected. The oscillations in the output of the controller imply that the charging and discharging of EVs connected at CS are wobbling. The wobbling can have an adverse impact on the EVs and introduce imbalance in the electric grid. The abrupt change from charge and discharge at EVs end will accelerate ageing in the battery. Similarly, transient oscillations will be introduced in the electric grid, adding to the events leading to

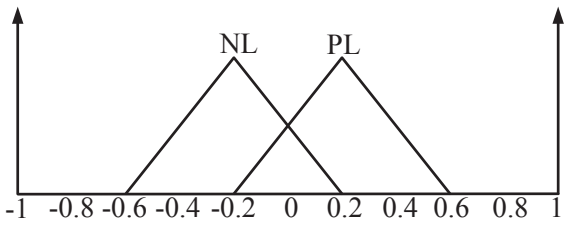

Fig. 2.9: Activated MF in the region when the V2G to G2V or vice versa operation takes place

instability and even collapse.

From the above discussion, it is clear that fast sampling would ensure the smooth operation of the controller. However, using a sampling interval of 1ms at the grid end is not a feasible option as the practically advanced systems like supervisory control and data acquisition (SCADA) and data acquisition using phasor measurement unit (PMU) work in lower sampling rates. SCADA has a resolution of 1 sample every 2-4 seconds (steady-state observability), and PMU has a resolution of 10-60 samples per second (dynamic observability) [109]. Therefore, it may be necessary to have different sampling rates in different parts of the system, eventually leading to different data rates for different channels. To determine the sampling and the data rates, three channels are considered between the entities of the V2G system of Fig. 2.6.

(i) ***Channel I:*** This channel is between the grid and the controller. The per-unit voltage signal $V(PU)$ data is sent from the substation of the grid to the controller on this channel. This is the slowest channel as the grid has high inertia, and its dynamics are slow [18,110]. The developed model is simulated for different sampling intervals (D) varied from 1 s to 15 s in steps of 1 s.

(ii) ***Channel II:*** This channel is between the controller and the main aggregator and is used to send data on the energy ((E_I)) and power (P_I) signals. The sampling interval has to be shorter than that of Channel I, i.e. faster sampling. The sampling interval for this is represented by xD where x is a variable that varies from 0.1 to 0.5 in steps of 0.1. (A lower value of x implies faster sampling at the controller.) In general, a fast channel is needed to ensure good support to the grid from the MCS as the energy from the MCS will vary dynamically based on the arrivals and departures of the EVs.

(iii) ***Channel III:*** This channel transmits data on the energy (E_n) and power (P_n) signals be-

tween the main aggregator and the several aggregators at CSs. Since the arrivals and departures of EVs are unpredictable, Channel III should be capable of sending data at a rate as fast as possible so that the system can support sampling rates as high as possible. The sampling interval of this channel is assumed to be $0.5xD$.

The communication channels described above for the purpose to transmit the data between entities of a V2G system will depend on the topography of the region. Literature gives valued suggestions and analysis for selecting a suitable communication channel to transmit the data [50–55]. Channel I can be an optical fibre or Ethernet-based channel, while Channel II can be an Ethernet or WiMAX based channel, and Channel III can be a WiMAX or WiFi-based channel.

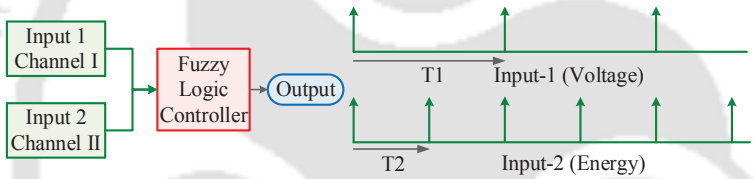

Fig. 2.10: Asynchronous inputs to the FLC. The input-I is sampled at $T1$ time period and $T2$ is the time period of input-II

The data communicated by the three channels are at different sampling rates. Hence, the inputs to the controller are asynchronous, as shown in Fig. 2.10. However, the controller requires synchronized data as inputs because, at a particular instant, both inputs are required to infer from the rule base. Suppose at a discrete-time interval; only one input reaches the controller. In that case, the other input will be any garbage value which will lead to incorrect output. Hence, for the proper operation of the controller, data have to be synchronized. There are two options for synchronization:

Case a) Synchronize both the inputs with respect to V(PU) or

Case b) Synchronize both the inputs with respect to E_I.

To analyse the effect of synchronization, the results for both **cases (a) and (b)** are compared with that of the base case. For comparison, the Root Mean Square Error (RMSE) is used and it

is defined as:

$$RMSE = \sqrt{\frac{\sum_{i=1}^{n} (X_{S\&H,i} - X_{RT,i})^2}{n}} \tag{2.11}$$

where $X_{S\&H,i}$= Value of parameter with sampler in V2G

$X_{RT,i}$= Value of parameter for base case (Plot without FLC in Fig. 2.7)

n=number of samples

Case (a): Synchronization w.r.t. V(PU)

V(PU) signal has a time period of $T1$, whereas the E_I has a time period of $T2$. A sample and hold is added before input-2 (energy), as shown in Fig. 2.11. The sample and hold in Fig. 2.11 is triggered at every $T1^{th}$ time interval. This ensures that both the signals are synchronized at the controller end. The simulations are run for the developed model at different sampling intervals, as described earlier in the section, and the RMSE for V(PU) w.r.t the base case (Fig. 2.7) is calculated. The RMSE for different sampling intervals is shown in Fig. 2.12.

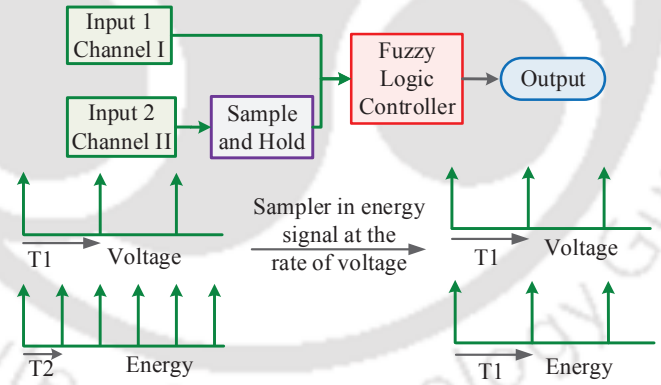

Fig. 2.11: Synchronizing the FLC at a slower sampling option V(PU)

Case (b): Synchronization w.r.t. Energy

The inputs, in this case, are synchronised at a faster sampling rate. Since [V(PU)] is at a slower sampling rate, a sample and hold are placed before the input 1 signal as shown in 2.13. The sample and hold are triggered at every $T2^{th}$ time interval, which ensures that both the inputs are synchronised at the controller end. As done in the previous case, the RMSE of [V(PU)] is determined, and the plot is shown in Fig. 2.14.

Further from Fig.2.12 and Fig. 2.14, the following can be observed:

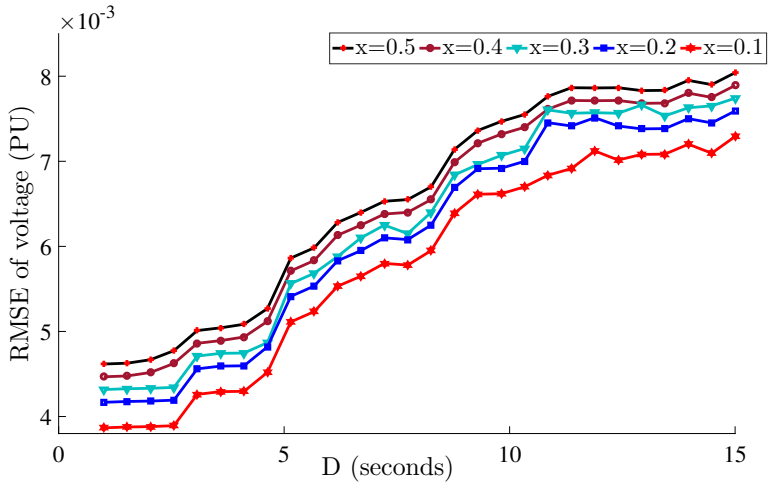

Fig. 2.12: Plot of RMSE obtained when slower sampling option is explored

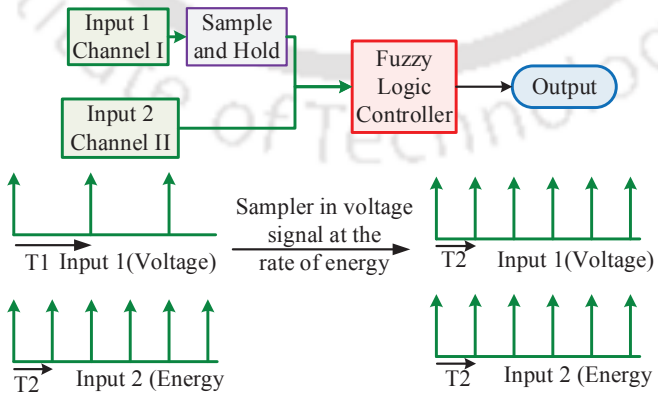

Fig. 2.13: Synchronising the FLC using the faster sampling option (E_I)

(i) The value of RMSE of the voltage increases with an increase in the D for a given value of x.

(ii) The RMSE of the voltage increases with and increase in x, for a given value of D (i.e. slower sampling at the controller end).

(iii) Comparing the results in Fig.2.14 and 2.12, it can be observed that for given values of D and x, the RMSE of voltage is lower when the sampling rate is higher.

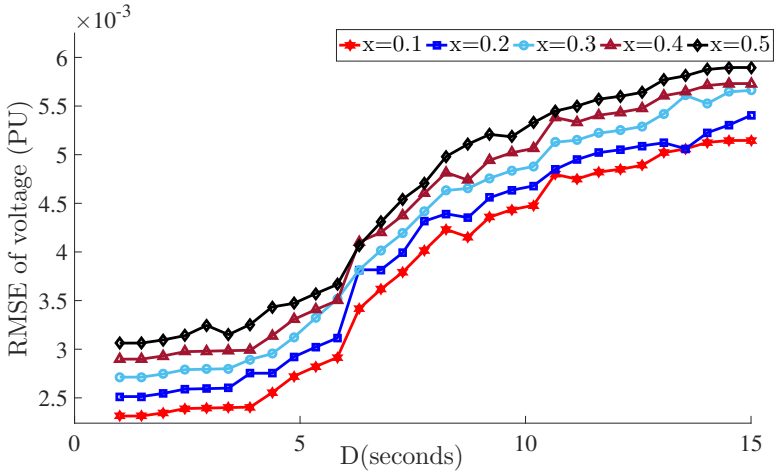

Fig. 2.14: Plot of RMSE when faster sampling option is explored

Fig. 2.15 and Fig. 2.16 shows that for both slower and faster sampling cases, as the sampling intervals in channel II and III decrease, the error in power and energy (over a 24-hour cycle) decreases. It is also observed that the error for power and energy is less for the faster channel.

The beginning of Section III concluded that, when data is transmitted by performing sampling at a lower sampling rate (instead of continuous sampling), oscillations are observed in the node voltage at which MCS is connected. The voltage profile for different data rates for cases (a) and (b) are shown in Fig. 2.17 and Fig. 2.18. These figures help to conclude the following:

(i) A higher oscillations are observed during the transition from V2G to G2V or vice-versa when the synchronization is done w.r.t V(PU), i.e. at a slower synchronization rate.

(ii) The oscillations does not die out fast rather sustains for a period of time even after the point at which transition from V2G to G2V or vice-versa.

(iii) The oscillations tend to increase with a decrease in the sampling, i.e. D increases.

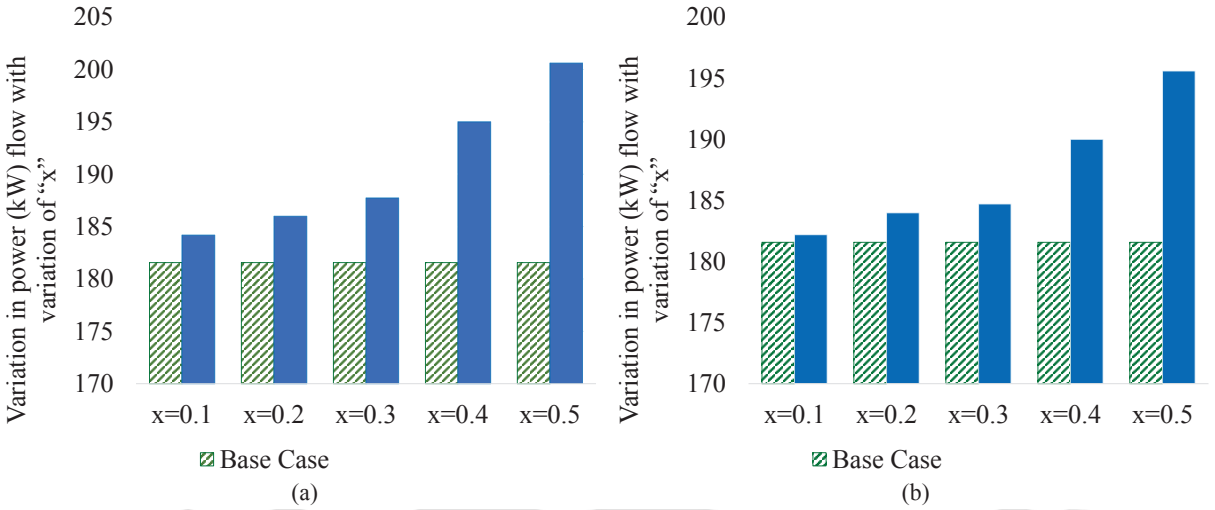

Fig. 2.15: Comparison of power with variation of x (D=1 sec) when synchronisation is done w.r.t. (a) V(PU) ; (b) E_I

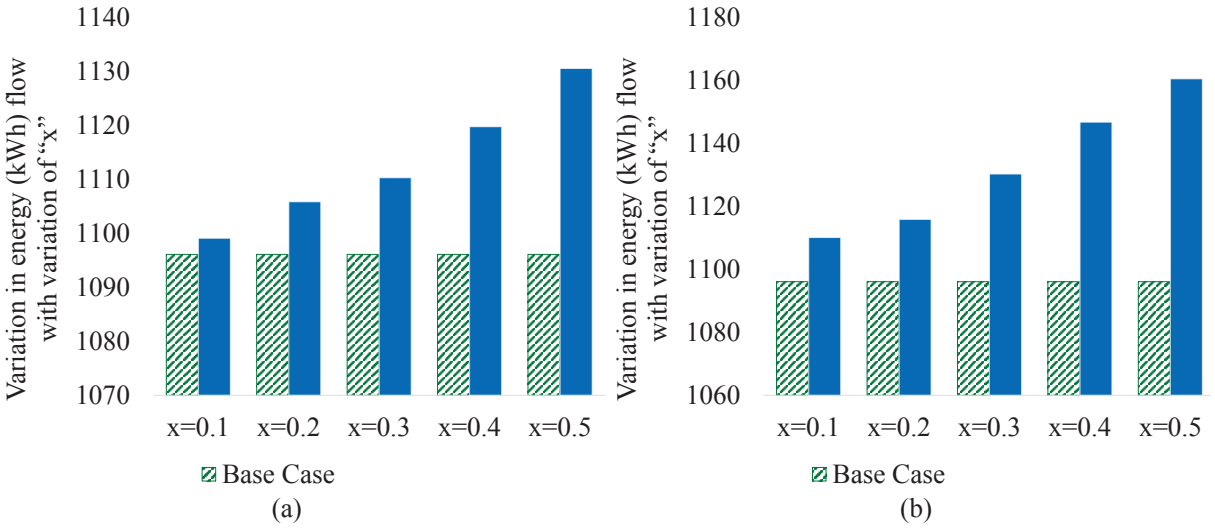

Fig. 2.16: Comparison of energy with variation of x (D=1 sec) when synchronisation is done w.r.t. (a) V(PU) ; (b) E_I

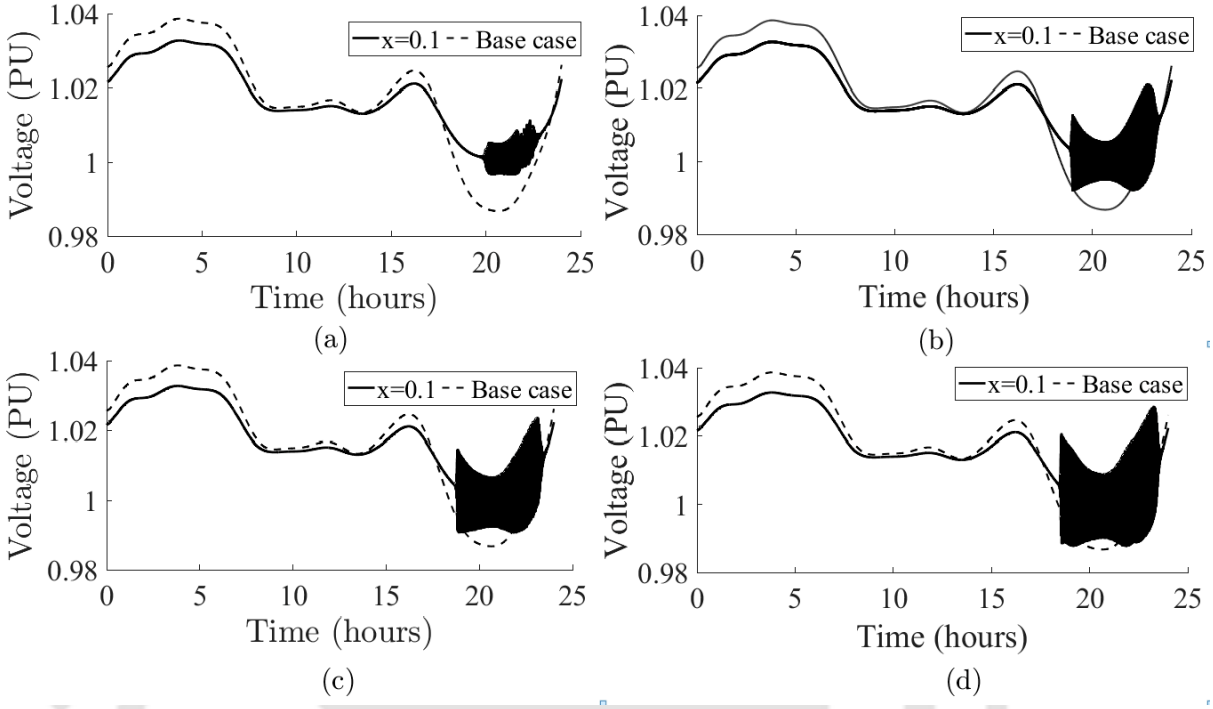

Fig. 2.17: The oscillations seen in V(PU) when synchronisation is done w.r.t. V(PU) by increasing the value of D and keeping x constant. (a)Plot of V(PU) for D=1 s ; (b)Plot of V(PU) for D=2 s ; (c) Plot of V(PU) for D=3 s ; (d)Plot of V(PU) for D=4 s

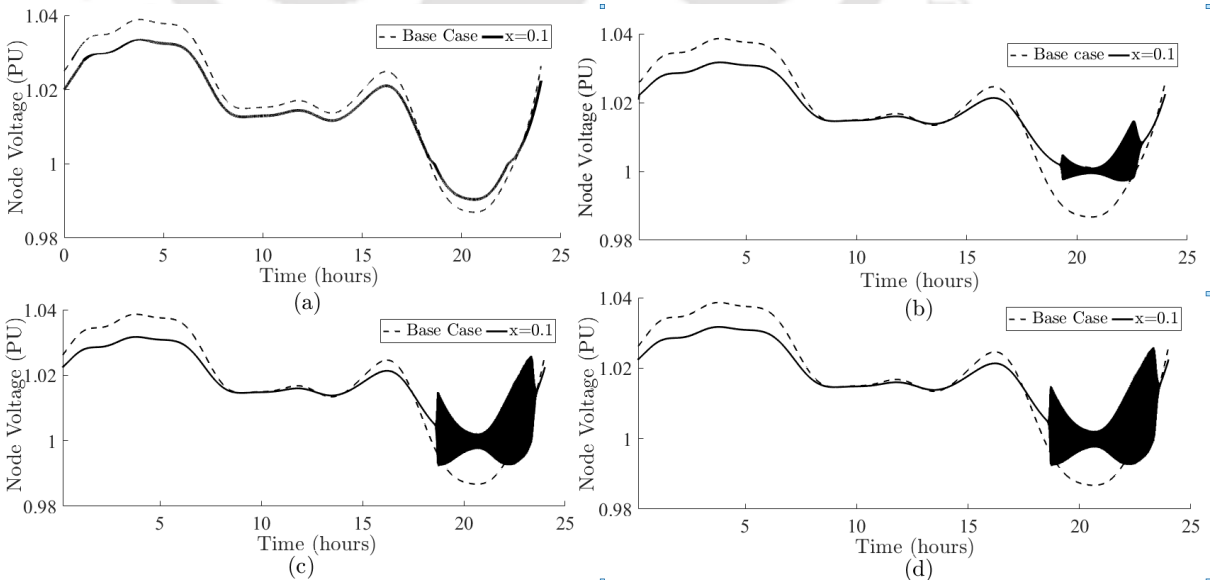

Fig. 2.18: No oscillations is observed in (a). Oscillations increases with increase in the value of D keeping x =0.1 when synchronisation is done w.r.t. E_I. (a)Plot of V(PU) for D=1 s ; (b)Plot of V(PU) for D=2 s ; (c) Plot of V(PU) for D=3 s ; (d)Plot of V(PU) for D=4 s

Case (b) shows no oscillations at the fastest sampling time ($D = 1sec$ and $x = 0.1$). With the increase in either value of D or x, the oscillations also increase. However, the oscillations for the faster synchronization option, case (b), are smaller than those for the slower synchronization option of the case (a) for all values of D and x. Therefore, case (b) is further considered in this work and used to fine-tune the controller.

2.4 Decreasing Impact Of Sampling Interval In Controller

The previous section discussed the issue of an increase in oscillations in the node voltage when sampling rates are increases. If the sampling rates are lower, a higher cost on the sampler (analog to digital converter) is to be spent. Hence, the challenge of ensuring the efficient operation of the controller at higher sampling rates is investigated in this section. Appropriate options to tune the controller is proposed for an FLC based on the findings when the membership functions are modified. There are two possibilities of modifications in an FLC to reduce the oscillations:

(A) Modifying the shape of MF.

(B) Increasing the rule base.

2.4.1 Changing the Shape of MF

The work reported in this chapter used triangular MFs. The reasons for the selection is also discussed in the previous section. However, there are many other shapes of MFs reported in the literature. The following MFs are investigated in this work to check for any improvement in the operation of FLC:

(i) Trapezoidal shape (Fig. 2.19 (a))

(ii) Gaussian shape (Fig. 2.19 (b))

(iii) Bell shape (Fig. 2.19 (c))

These shapes of MFs are the most frequently used in the literature [111–116]. Hence, possibilities of efficiency improvisation are explored for the above three MFs only. Fig. 2.20 shows the node voltages obtained by changing the shape of MFs. The oscillations at the point where V2G to G2V or vice-versa happens still remain and continue to sustain for a period of time,

inferring that the change in MFs in the FLC does not eliminate the oscillations.

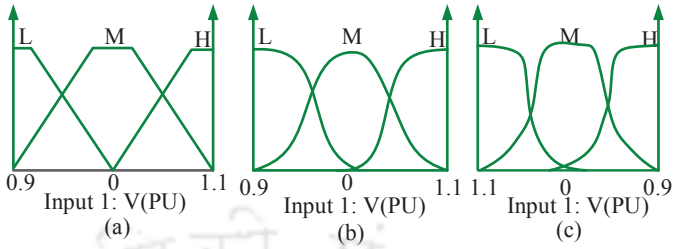

Fig. 2.19: Shape of MF explored to reduce oscillations. (a)Trapezoidal MF; (b) Gaussian MF; (c) Bell MF

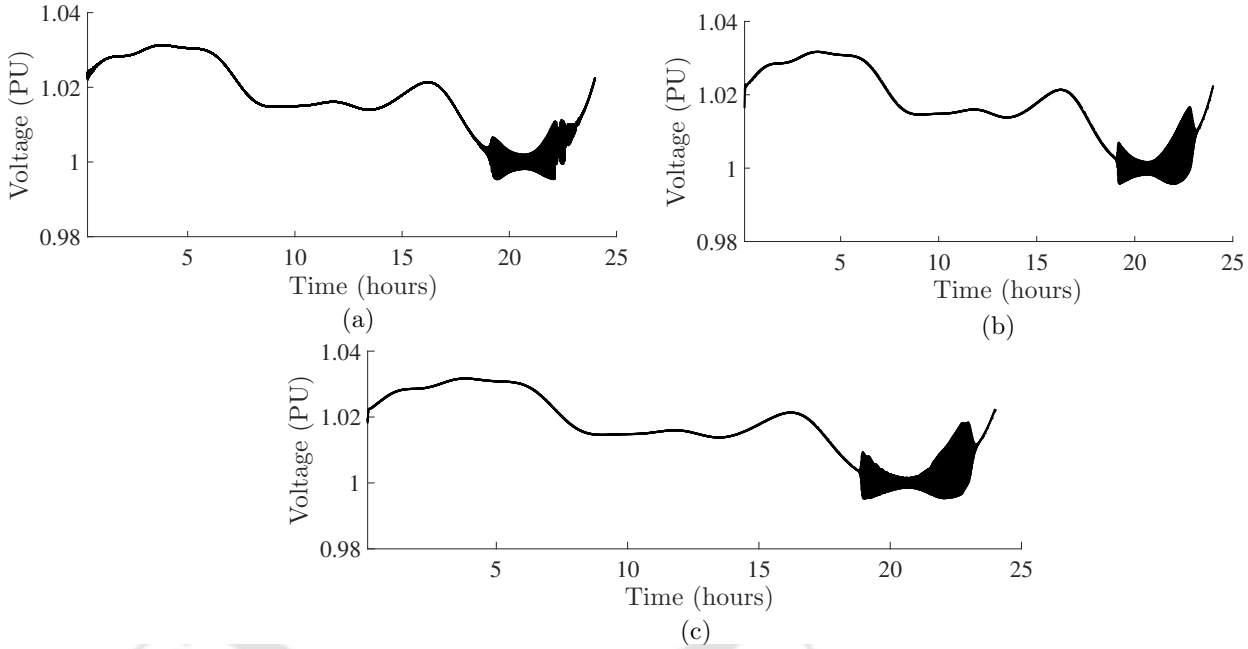

Fig. 2.20: Oscillations exists in voltage waveforms on checking by changing shapes of MF for D=2 sec and x=0.2. (a) Trapezoidal MF (b) Gaussian MF (c) Bell MF.

2.4.2 Increasing Rule Base

Since the change in the shape of MFs does not impact the oscillations in the node voltage, the second option of increasing the rule base is explored. So far, each input V(PU) and E_I were represented using three MFs only. The impact of the increase in the rule base on the oscillation of node voltage is investigated by adding two more MFs.

Case I: The number of MF in input-I (V(PU)) are increased (Fig. 2.21 (a)) and the new set of rules are given in Table III.

Case II: The number of MF in input-II (E_I) is increased(Fig. 2.21(b)) and the rule base is given in Table IV.

Case III: The number of MF in both inputs are increased. This is a combination of cases I and II and the rule base is given in Table V.

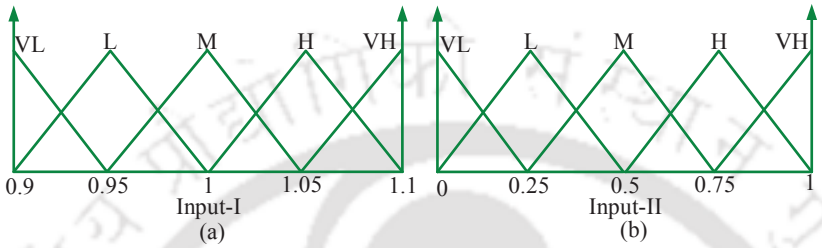

Fig. 2.21: (a) Addition of two MF-VL and VH in input-I ; (b) Addition of two MF-VL and VH in input II

Table 2.3: Rules for V2G controller with increased number of MF in input-I

Inputs		Output	Inputs		Output	Inputs		Output
V(PU)	E_I	Power	V(PU)	E_I	Power	V(PU)	E_I	Power
VL	L	PL	M	M	NM	VH	L	PM
VL	M	NM	M	H	NL	VH	M	PM
VL	H	NH	H	H	PL	M	L	PL
L	L	PL	H	M	PM	VH	H	PL
L	M	NM	H	L	PH	L	H	NL

Table 2.4: Rules for V2G controller with increased number of MF in input-II

Inputs		Output	Inputs		Output	Inputs		Output
V(PU)	E_I	Power	V(PU)	E_I	Power	V(PU)	E_I	Power
V	VL	PL	M	M	NM	L	VH	PL
M	VL	PM	M	H	NL	M	VH	NM
H	VL	PH	H	H	PL	M	L	PL
L	L	PL	H	M	PM	H	VH	NH
L	M	NM	H	L	PH	L	H	NL

Table 2.5: Rules for V2G controller with increased MF number of in both inputs

Inputs		Output	Inputs		Output	Inputs		Output
V(PU)	E_I	Power	V(PU)	E_I	Power	V(PU)	E_I	Power
VL	L	PL	M	M	NM	VH	VL	PH
VL	M	NM	M	H	NL	H	VH	PH
VL	H	NH	H	H	PL	H	VL	PL
L	L	PL	H	M	PM	M	VH	NM
L	M	NM	H	L	PH	VH	VH	PL
L	H	NL	VH	H	PL	M	VL	PM
M	L	PL	VH	M	PM	L	VH	NH
VH	L	PM	VL	VL	PL	L	VL	PL
VL	VH	NH	.	.	.	.	.	.

Fig. 2.22 shows the plots of node voltage obtained when the number of rule bases in the FLC is increased. The elimination or constraining of oscillations are clearly visible for all three scenarios. Since all the three cases show similar results, RMSE of node voltage is calculated using (2.11) to look for the best option. Fig. 2.24 shows the plots of the RMSE when compared to the base case.

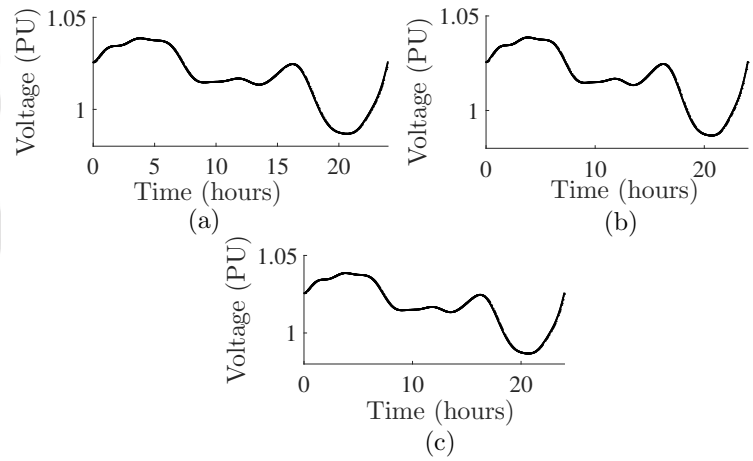

Fig. 2.22: The oscillations in voltage are removed by increasing the number of MF for D=2 sec and x=0.2 when synchronization is done at faster sampling rate. (a) Increase in granularity in input I (V(PU)) ; (b) Increase in granularity in input II (E_I); (c) Increasing granularity in both inputs.

The above idea of increasing the rule base to reduce the oscillations is further explored when synchronization of the inputs is done at a slower sampling rate. Fig. 2.23 shows the plots of node voltage obtained, and Fig. 2.24 shows the value of RMSE for the three cases, viz., base case, synchronization at a faster sampling rate and synchronization at the slower sampling rate.

Based on the above investigations, it can be observed that:

(i) Change in the shape of membership functions does not remove oscillations in the node voltage as shown in Fig. 2.22.

(ii) Considering the shape of MF, triangular-shaped MF is found to be more accurate and give a better performance as compared to trapezoidal, Gaussian and Bell-shaped MF.

(iii) Increasing the number of rule bases removes the oscillations. Hence, the response of the considered fuzzy system is sensitive to the change in the number of MF.

(iv) The RMSE values for the case when synchronization is done at a faster sampling rate is

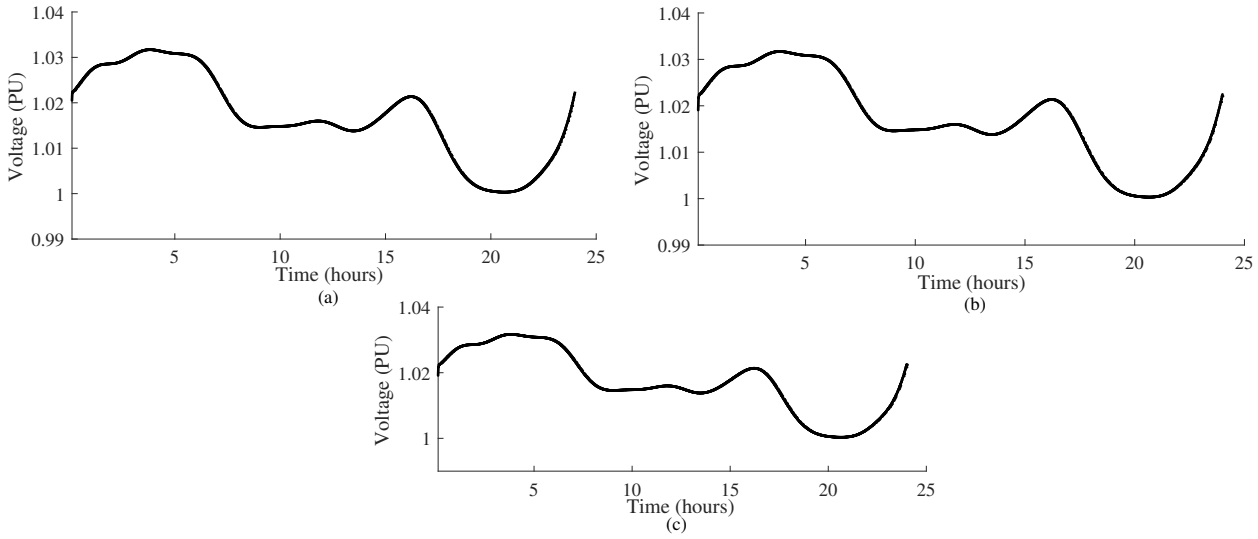

Fig. 2.23: The oscillations in voltage are removed by increasing the number of MF for D=2 sec and x=0.1 when synchronization is done at slower sampling rate. (a) Increase in granularity in input I (V(PU)) ; (b) Increase in granularity in input II (E_1); (c) Increasing granularity in both inputs.

lower as compared to slower sampling rate as seen in Fig. 2.24.

(v) The RMSE values (Fig. 2.24) for cases I and III are the least, and either of the two can be used. However, case I is better compared to case III because it has a smaller rule base and hence needs less computation time.

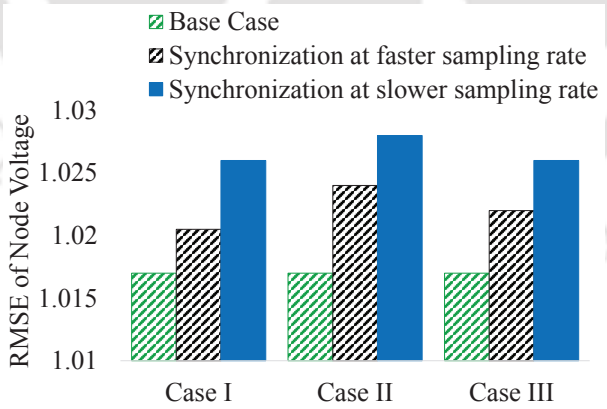

Fig. 2.24: Plot of comparison of RMS for the three cases of increasing MFs with respect to base case for synchronization at faster and slower sampling rates.

2.4.3 Verification of the Results By Implementing With Mobility Of EVs

The proposal of the improvements in the controller when EVs were stationary, parked and connected at one of the CSs are further extended for the case when EVs are mobile. A similar required scenario of mobility of EVs presented in [25] is used for validation in this work. The

33kV section of the Guwahati grid is assumed to be distributed in three types of destination viz. residential, office, and commercial area. These areas are marked at node 4.4, 5.4 and 6.3 of the radial test distribution of Guwahati city, respectively, as shown in Fig. 2.2 in Section II. Out of the five CSs, it is assumed that there are three CSs in the residential area and the remaining one each are in the official and commercial area. The EVs in each CSs move between these regions based on the time of the day. The following realistic scenario is assumed while validating the proposals:

- The number of EVs are more in the office area from 0900 hrs and 1700 hrs as compared to commercial and residential area.
- The number of EVs are more in the commercial area from 1700 hrs and 2000 hrs as compared to office and residential area.
- The number of EVs are more in the residential area from 2000 hrs and 0900 hrs as compared to commercial and office area.
- The EVs which are not in any of the areas are in transit and 10 % of the SOC is consumed when moving from one area to another [25].

The above scenario is represented in Fig. 2.25 with the number of EVs at a particular time at each area.

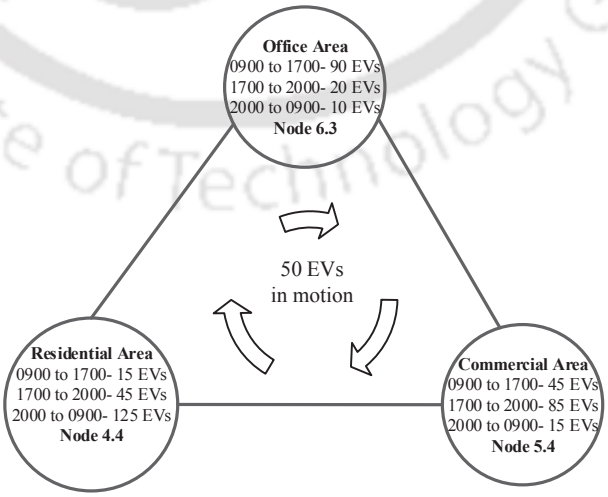

Fig. 2.25: Number of EVs in three areas at different time intervals

50 EVs are assumed to be at transit at different time instances. The remaining EVs which are

parked and connected in the CSs (as given Fig. 2.25) are either supporting the grid or charging based on the decision of V2G or G2V operation by the controller. Based on the assumptions defined, the V2G system described in Section II is analysed for different numbers for EVs. The proposal of an increased number of rule bases (as given in Table 3.2) of the controller is used in the analysis. The selection of this particular rule base in Table 3.2 is based on the least value of RMSE in node voltage obtained among previous results as shown in Fig. 2.24.

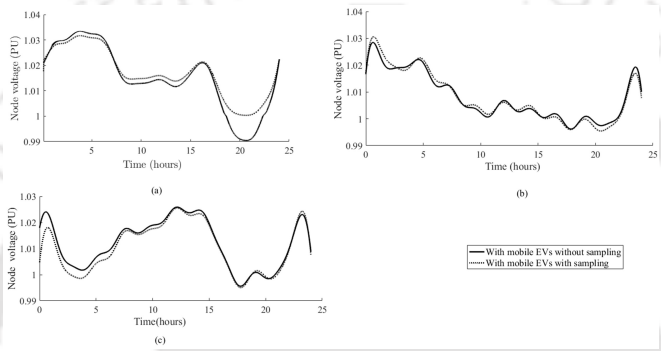

Fig. 2.26: Variation of node voltages with mobility of EVs- with and without sampling for three areas- (a) Residential, (b) Office and (c) Commercial

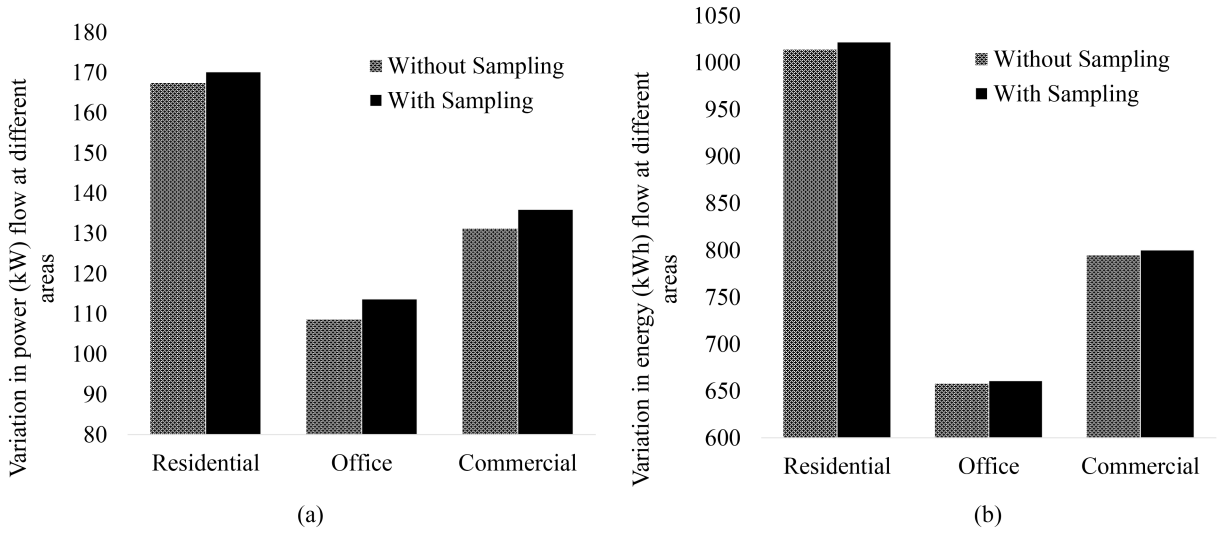

Fig. 2.27: Variation of power and energy with mobility of EVs- with and without sampling for three areas- (a) Residential, (b) Office and (c) Commercial

The variation of the node voltage with the changes in the number of EVs at the three regions are shown in Fig. 2.26. The node voltages for the two cases (without and with sampling) in the present scenario is shown in Fig. 2.26. Furthermore, the power decided by the controller

and the energy available at the MCS is shown in Fig. 2.27. It is observed that even with the reduction in the number of EVs at a particular node due to mobility, the power decided by the controller to be exchanged between EVs and the electric grid is sufficient to support the electric grid. The difference in the power decided by the controller and energy at MCS in the two cases are less. The oscillations in the node voltage are also not found.

Further, the number of EVs also impacts the amount of power exchanged in an area. Since the residential area has a higher number of EVs, the power and energy exchange is also higher when compared to commercial and office areas. The observations from the results obtained for the case when EVs are mobile or varying at a node in the electric grid validates the operation and performance of the controller.

2.5 Conclusion

In this paper, a V2G system consisting of a network, collector, controller, MCS and EVs is designed. The effect of changing the sampling rate of the signal transmitted between entities was investigated. This study shows how the sample rate of the input data affects the FLC output. Synchronizing input data at a faster sampling rate reduces errors compared to operating at a slower sampling rate, but oscillations remain. The output oscillations were found to be larger as the data sampling rate decreased. For further analysis, operation of the controller unit in a sensitive area where V2G to G2V or vice-versa takes place was identified as the cause. Possible solutions to reduce vibration are explored by changing the shape of the MFs and increasing the rule base by increasing the number of MFs. The MFs shape does not dampen oscillations, but with an increase in the number of rules or the input MFs, the oscillations in the node voltage are reduced. We also conclude that increasing MFs can improve controller performance when synchronization is performed even at lower sample rates. Realistic scenarios for mobile EVs confirm this finding. MCS can support the network even in this scenario. This work provides guidance for investigating the impact of network and communications and networking-related challenges such as delays, data loss, and other related issues such as system security in V2G scenarios.

3

V2G Controller: Intelligent Operation to eliminate Challenges of Communication

Contents

"A computer would deserve to be called intelligent if it could deceive a human into believing that it was human."

– Alan Turing

3.1 Introduction

The growing consensus among nations worldwide to drive the adoption of EVs has led to an increase in the demand for electric power to recharge their batteries [117]. The increased demand for power needs attention to plan appropriate measures to reduce the capital investment cost on a complete overhaul of the power system. If planned appropriately, the cost of overhaul can be diverted to the up-gradation of a few types of equipment and the addition of new entities. The negative impacts of the unplanned increase in the power demand due to recharging of EVs are visible in the form of voltage deviations, phase imbalance, harmonic distortions, and decreased life of transformers [118, 119].

Nevertheless, EVs have the potential to support the operation of the electric grid as well. This potential extends to providing support to the electric grid, spinning reserve, and ancillary services such as voltage and frequency regulation. The services provided by the EVs are not limited to the mentioned. They have capabilities to fulfill various other goals of the prospective transportation system of future [14, 15]. Apart from the mentioned, EVs have high energy batteries which can power multiple homes. Hence, they are also suitable for use as distributed energy storage systems (DESS). Furthermore, the renewable energy sources, which are mostly intermittent in nature, can also be integrated into the electric grid by using EVs as DESS [120, 121].

The previous chapters have already described that the comprehensive benefit of EVs can be reaped only with a reliable and intelligent infrastructure. The infrastructure acts as a common platform where different entities and stakeholders will interact and coordinate with each other. The coordination ensures that either side of the infrastructure- power system operator or the EVs/users are not burdened with supporting each other. MCS, aggregators and controllers are the three major entities of the EV charging infrastructure. Each entity communicates required information by the controller appropriately to support the decision-making process. The substa-

tion communicates the condition of the electric grid (voltage level), and the MCS communicates the energy available in the EVs connected at CSs. These data help the controller to decide V2G or G2V operation and the amount of power to be exchanged. The efficiency and correctness of the operation of the controller depend on the credibility of the data received at the inputs. Hence, it will be inappropriate to allow the controller to take decisions without verifying the correctness of the data. This necessity is the foundation of the work described in this chapter. The controller should be supported by algorithms or systems that verify the integrity of the data and perform corrective steps if required.

3.2 Literature review

The requirements of EV charging infrastructure for wider acceptance and deployment of EVs is widely discussed in the literature. The works reported in the literature examine V2G either as an electrical system or as a communication system which is discussed in the previous chapter. The analysis as an electrical system look into the impact of EV recharging on the electric grid in a coordinated or uncoordinated manner, use of EVs to provide ancillary services, active power support, and reactive power compensation. Further, the support of EVs in the iteration of renewable into the electric grid is also discussed [14, 15, 78, 80, 82]. The other type of analysis incorporating communication aspects models communication channels for exchanging data between entities and proposes the use of standard communication technology for a V2G system such as Ethernet, Long Term Evolution (LTE), Vehicular Power Line Communication (VPLC), narrowband Power Line Communication (PLC), Universal Mobile Telecommunication System (UMTS), WiFi, WiMAX, and others. The proposals of communication channels and technology are validated by analysing related parameters for improving performance, reliability and security [50–59].

Although the literature presents details of modelling a V2G system to perform an electrical and communication-based analysis; the real-time implementation requires a solution to the challenge of designing an intelligent controller. The intelligent controller for V2G is expected to be robust, reliable, less computationally intensive, designed with the least assumptions and

boundary conditions, easily implementable, and features to verify the inputs to ensure distinct and precise output.

Literature reports a few controllers with a few functionalities. A proportional-integral (PI) controller for load frequency regulation is presented in [122]. The PI controller requires the computation of accurate gains to ensure efficient operation. Further, these gains require a mathematical model of the system to compute gain values. However, in this work, particle swarm optimisation with fixed structure mixed H_2/H_∞ technique is utilised to compute the gains which inclined towards a few functionalities expected in an intelligent controller. [123] proposed using EVs for supporting a workplace microgrid system using an intelligent energy management controller. The potential of the EVs is determined by forecasting the travel pattern of the EV users using random forest methodology, and appropriate scheduling of charging and discharging is done for the management of energy. The possibility of using EVs to regulate frequency using fractional order control is proposed and elaborated in [124]. Goal representation adaptive dynamic programming is used to develop a supplementary intelligent controller in [125]. The controller is used to enhance the stability of the frequency in an island electric grid comprising of EVs, photovoltaic, and wind energy systems. In another work, intelligent fuzzy logic-based load and voltage controllers are proposed to tap prospective benefits of EVs in a smart grid system [126]. The controller is designed to perform load levelling and monitor peak power, voltage regulation, and balancing control.

The controllers discussed in the previous paragraph has in one way or the other coordinated the process of recharging of EV batteries. Hence, such recharging is called coordinated charging. Coordinated charging is also a widely discussed topic in literature to reduce the adverse impact on the electric grid due to the recharging of EVs. The idea of coordinated charging derives and realises relations between losses, node voltage, load factor, load variance, and optimises parameters like time of use (ToU) tariffs and user inputs [127–129].

However, non of the works considered the issue of erroneous data reaching the controller. As discussed earlier, the controller decides the mode of operations viz. V2G or G2V is based on the data sent by the MCS and substations via communication channels. These entities are located at

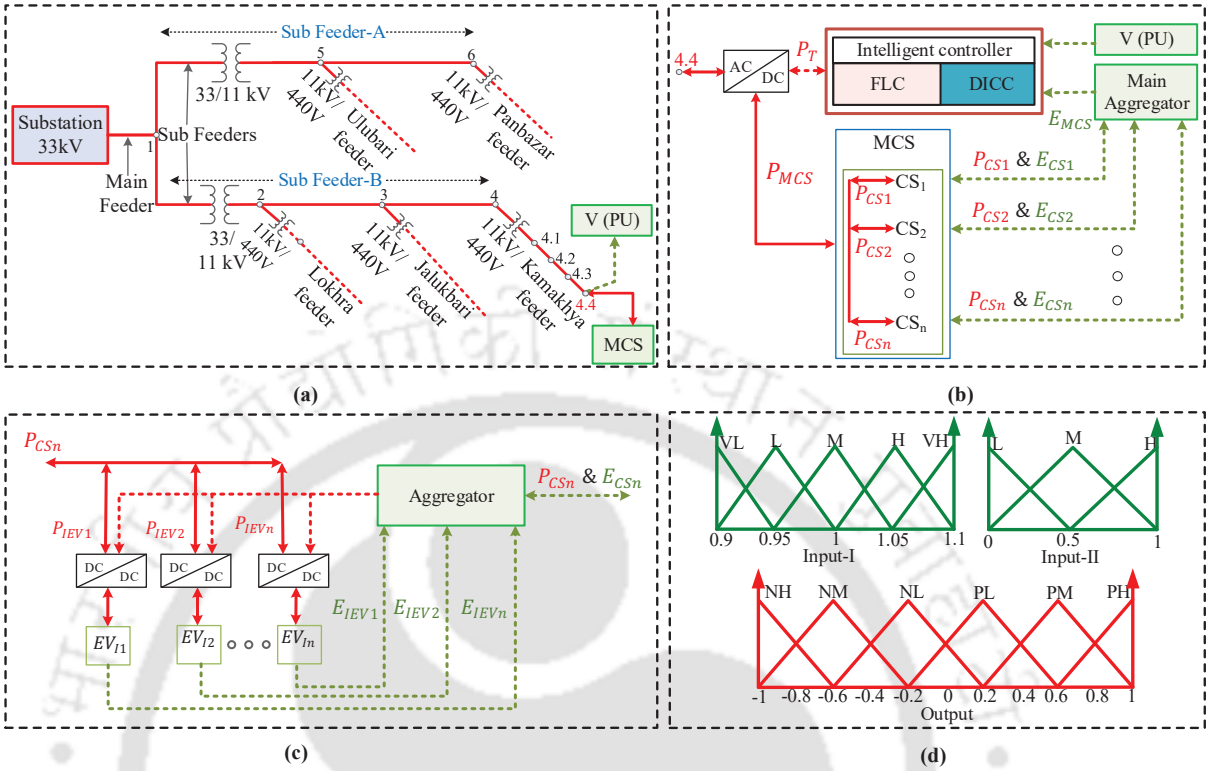

Fig. 3.1: Modeled V2G system for verification of the proposal of intelligent controller. (a), Single line diagram of 33 kV feeder of Guwahati city with MCS considered for study (b), Details of MCS with intelligent controller. The dotted line shows the communication system and the other is power lines. (c), Details of a entities in a CS with appropriate lines showing communication and power lines. (d), The inputs and output membership functions of FLC with range of each.

different topographical locations. The noise added by the channels while transmitting data can add errors. If the inputs to the controller are erroneous, the output follows the same. A similar scenario was discussed in the previous chapter while describing the need for synchronisation. Suppose one data reaches at a discrete time, while the other is not found. In that case, the controller works with a garbage value and give false decisions. These false decisions could add to instability in the electric grid (increases losses, voltage and frequency deviations, etc.) or accelerate the degradation mechanism of the battery [119]. Hence, if the controller has inbuilt algorithms, with the help of which it can determine the correctness of data reaching as inputs and perform repair, an intelligent controller with all the required functionalities can be realised.

3.3 Contributions

Based on the literature reviewed, discussions presented, and the challenges outlined in the previous sections, the following are the contributions of this chapter:

(i) Modifications in the V2G system modelled in the previous chapter is upgraded with appropriate algorithms to simulate the errors due to communication systems. Further, the model enables the development and integration of the intelligent controller for the EV charging infrastructure.

(ii) The novel intelligent controller comprising of two-layer framework: an artificial neural network and support algorithm in the first layer, and a fuzzy logic controller in the second layer is designed. Apart from the function of deciding V2G or G2V operation and the amount of power to be exchanged between the EVs and the electric grid described in the previous chapter, the controller also performs correction for cases when data reaching the controller is erroneous to ensure the best operation.

(iii) The intelligent controller developed is capable of performing a data integrity check using the forecasted data from the ANN and the trend of data reaching the controller. Further, in case of detection of any error, the controller performs corrections as well, which ensures the output of the controller is not affected, thereby eliminating the impact of communication channels.

The work in this chapter details the analysis of the modelled infrastructure for the challenges due to the communication channel. The first challenge is the data loss in which the data transmitted from the sending end does not reach the receiving end; the second challenge is the delay in which the data is received after an excessive delay or effectively lost. The third challenge is analysed by combining the first and second challenges. These analyses in this chapter help reveal the intelligent operation of the developed controller.

Section I and II discussed the works presented in the literature and discussions on the drawbacks. Section III discussed the contributions of this work. Section IV will presents the comprehensive modelling of the system. The design of EV infrastructure is further discussed in

Table 3.1: Specifications of the EVs battery

Battery types	Energy (kWh)	$SoC_{initial}$ (%)	SOC_{lt} (%)	AhR	C^{lt}_{rate}	No. of EVs
A	8	45	25	32	3	40
B	10	40	45	40	2.5	40
C	16	50	30	64	3	40
D	20	65	40	80	4	40
E	24	30	20	96	4	40

Section V. The modelling of the the primary challenge of data loss and delay in the communication systems are discussed in the Section VI. The results obtained with and without the use of intelligent controller will be presented in Section VII. Section VIII presents the conclusions of the work.

3.4 Modeling Of The System

The V2G system modelled in the previous chapter will be used in this chapter also. Hence, the entities in which modifications are performed will be comprehensively discussed in this chapter. The other subsection will describe the modifications and addition of algorithms in the V2G system.

3.5 EV Charging Infrastructure

Node 4.4 is the point at which the MCS is connected. The intelligent controller help to decide the power flow between node 4.4 and the MCS. The intelligent controller is majorly supported by the electric substation, aggregators, MCS, CSs and the fleet of EVs. The schematic of the EV charging infrastructure modelled in this work is shown in Fig 3.1(b) and Fig 3.1(c). The intelligent controller designed in this work is the core of the EV charging infrastructure. The intelligent controller comprises a two-layer framework. The first layer is the DICC block supported by a trained ANN, while the second layer is an FLC layer. The details of the FLS is already discussed in the previous chapter. The variants of EVs and the details of the battery also remains the same as described in the previous chapter yet rewritten for ease in reading as given in Table 3.1.

Table 3.2: Rules for V2G controller with increased number of MF in input-I

Inputs		Output	Inputs		Output	Inputs		Output
V(PU)	E_I	Power	V(PU)	E_I	Power	V(PU)	E_I	Power
VL	L	PL	M	M	NM	VH	L	PM
VL	M	NM	M	H	NL	VH	M	PM
VL	H	NH	H	H	PL	M	L	PL
L	L	PL	H	M	PM	VH	H	PL
L	M	NM	H	L	PH	L	H	NL

3.5.1 Design of FLC

The FLC is the chief component of the intelligent controller. The FLC deicides the flow of power between node 4.4 of the electric grid and the MCS. The FLC described in the previous chapter, which resulted in the best results, is used in work as well. The two inputs, viz. per unit voltage from grid node 4.4 and the total energy available at the MCS, are used to compute the required power to be exchanged between EVs and the electric grid. These two inputs are fuzzified into five MFs represented by linguistic variables, and 6 MFs are used to represent outputs. Mamdani type FLC with triangular MFs is modelled. The rule base used to compute the output of the FLC is listed in Table 3.2.

The inputs to the controllers are data transmitted via communication channels that have a likelihood of delay or data loss. These data are henceforth checked and corrected by the proposed DICC block in the intelligent controller. The DICC block will be described in the following subsections.

3.5.2 Data Integrity Check and Correction Block

The DICC block comprises of two modules. The first module is the filter block, while the other is the decision block. The filter of the DICC block allows passing values of node voltages which are in the ANSI standard tolerance limit of the electric grid. As per standard, the value lies between (0.95 to 1.05) PU [130]. The node voltage values which are not in the range are not allowed to pass. However, the controller will require a value in a particular discrete time. Hence, the requirement of the value is fulfilled by the forecasted value of node voltage ($V(PU)_{fc}$) from the next module called the decision block.

The functioning of the decision block is based on a supported algorithm facilitated by a ma-

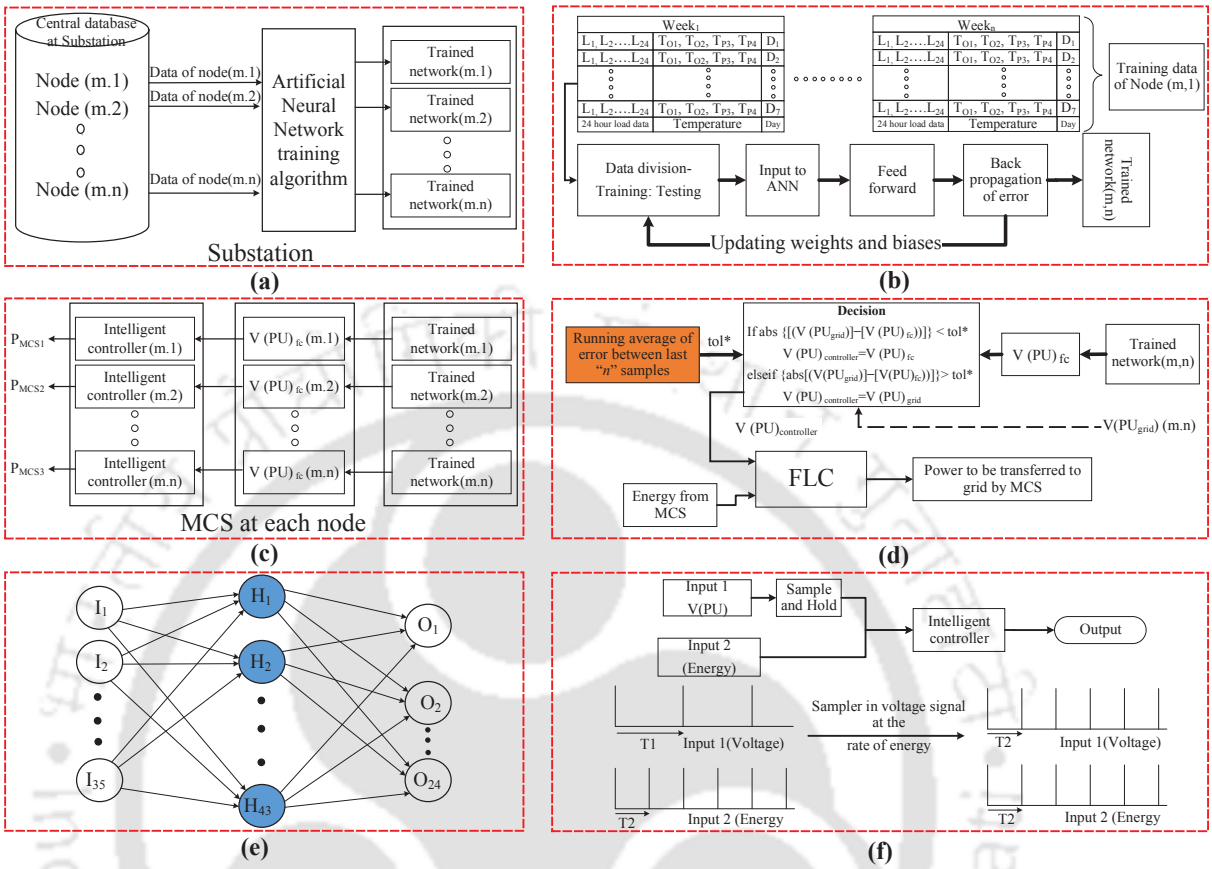

Fig. 3.2: Proposed intelligent controller for a V2G system with error check and correction mechanism. a-f,(a),A block diagram of the operation of ANN at substation by communicating between central database. (b), Process of training of the ANN (c), $V(PU)_{fc}$, which is the output of trained ANN is given as an input to the intelligent controller. (d), Illustrates the process of DICC (e), Structure of the ANN. (f), Synchronisation of the samples before giving as an input to the DICC block of the intelligent controller.

chine learning (ML) technique called -artificial neural network (ANN). The occurrence of delay, data loss and combination of both is a non-deterministic process. To deal with such issues, the controller should have its in-built intelligence to decide the integrity of data. The ML technique, which uses historical data to determine the current values, is found to be suitable for the purpose. Although the deployment of such algorithms demands high computational environment support, yet the benefits of the electric grid and the EV users or the overall infrastructure motivate its use. The ANN is one of the oldest and simplest techniques. Since the focus of the work is to show the requirement of an intelligent controller, ANN is used.

Further, it is assumed that the MCS will be equipped with a high computational facility that can monitor, control and perform computations to implement the proposed algorithms. Moreover, the historical data can be regularly updated or added to the database, which would

Algorithm 2 Algorithm running in decision block

if abs($V(PU)_{grid}$-$V(PU)_{fc}$) >= tol^* **then**
  $V(PU)_{controller}$= $V(PU)_{fc}$
else if abs($V(PU)_{grid}$-$V(PU)_{fc}$) < tol^* **then**
  $V(PU)_{controller}$= $V(PU)_{grid}$
end if

further benefit the controller by improving efficiency. Overall, the addition of the DICC would add benefits such as generalization, scalability, speed and accuracy, which is required for a V2G system operating in real-time [131].

Fig. 3.2 details the DICC. Each component is shown to visualise the operation of the system. The ANN requires historical data to train; hence, a data centre to store appropriate data required for training is kept at the substation. Fig. 3.2(a) shows the data centre which stores the 24 hours load data of the loads connected to the node at which MCS is connected, temperature and the day of the week in which it is recorded. The ANN at the MCS is regularly retrained by the updated data added every week. The trained ANN is transferred by physical or cyber means to the place where the controller is housed to use for performing data check and correction processes.

3.5.3 Artificial Neural Network

The ANN used in the system is trained based on the data saved by the data centre in the substation. Fig. 3.2(b) presents the training process of the ANN. The ANN comprises neurons for input and output, layers and neurons. The ANN used in this work (shown in Fig. 3.2(e)) is made of a double layer, 59 inputs, 24 outputs, and 43 hidden neurons. The number of layers and other relevant values were determined based on an iterative process that resulted in the least testing error.

59 inputs to the ANN correspond to the hourly data of node voltage and power for a data, the number of days in a week, minimum and maximum temperature of the previous day and the one forecasted for the current day. The 24 output neutrons in the ANN gives the value of forecasted node voltage or the target values. Log sigmoid and linear functions are used as activation functions for the hidden and output layer, respectively. These activation functions are selected considering their property of ease in computation and interpretability. The data set for

the use of ANN is divided into 2 subsets, viz. training and testing in the proportion of (80:20)%. Further, the training is run for 20000 epochs to get appropriate results.

The training and testing of the ANN are validated by computing the mean average percentage error (MAPE). On validation of the trained ANN, the MAPE for the training set and testing set is found to be 3% and 4%, respectively, as shown in Fig. 3.3. The accuracy of the ANN increases with an increase in the number of epochs. Suppose the testing error for the ANN is found to be less. In that case, the corresponding trained network is used to forecast the node voltage at which MCS is connected in the current day, as shown in Fig. 3.2(c). It is to be noted that the ANN trained for a particular node is not suitable for use in any other node unless the testing error is less and acceptable. At every discrete time instant, the node voltage $(V(PU)_{fc})$ data is forecasted based on inputs to the trained ANN. The node voltage $(V(PU)_{fc})$ data is given as an input to the decision block, which is shown in Fig. 3.2(d).

The decision block performs data integrity check and correction using three inputs viz; $(V(PU)_{grid})$ of the node at which MCS is connected, $V(PU)_{fc}$, communicated real-time voltage, and a value of tolerance (tol^*). Of the three, tol^* is determined as a running average of the difference between n^{th} and $(n-1)^{th}$ voltage data sample in real-time. It is given by (3.1), where n is the number of samples and, $V(PU)_{n-1}$ and $V(PU)_n$ are the values of the voltage sample received from the node at which MCS is connected. The process of computation of tolerance and its use in the decision block has a significant role in performing necessary checks of the incoming data before inputting it into the controller. The algorithm is given in Algorithm 2.

$$tol^* = \sum_{n=1}^{n-1} \frac{V(PU)_{n-1} - V(PU)_n}{n} \tag{3.1}$$

The results from the previous chapter showed that synchronisation of the inputs to the controller is required for better outputs. Further, synchronisation at a faster sampling rate resulted in better results when compared to the case when synchronisation at a slower sampling rate is done. In this work, the data reaching the controller from the MCS is a faster sampling rate than the data coming from node 4.4. of the electric grid. Further, the synchronisation of the data is

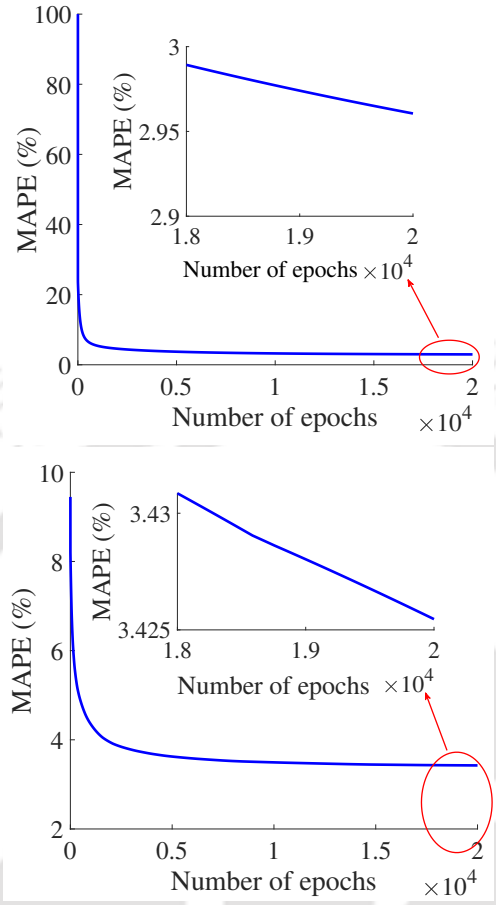

Fig. 3.3: Variation of MAPE with increase in the number of epochs.(a), Variation of MAPE (%) for training set. (b), Variation of MAPE (%) for testing set

done at a faster sampling rate before giving as an input to DICC, as shown in Fig. 3.2(f).

3.6 Modeling Scenarios Of Data Loss And Delay

The modelling of the scenarios of data loss and delay due to transmission of data using communication channels should be based on the present scenario. The present scenario uses GPS-synchronised data of voltage and frequency. One of the works reported in the literature by Huang et al. found that the data loss due to data transmission between phasor measurement unit and local phasor data concentrator is 10%. The work was based on the data collected over four weeks using GPS-synchronized wide-area FNET/GridEye network [132]. In another study on real-time data transmission in a smart grid system, it is reported that the latency should be less than 10 ms in a wide area monitoring system for data delivery in a smart grid [133]. These findings are used as a base in formulating the three scenarios- data loss, data delay and a

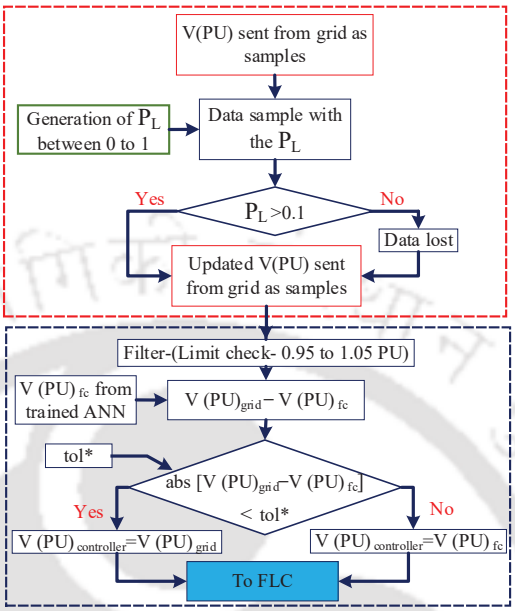

Fig. 3.4: Flow chart of the algorithm describing the scenario of data loss. R_n is a random number between 0 and 1. Red and black dotted box distinguish between the working of error simulator and the intelligent controller, respectively.

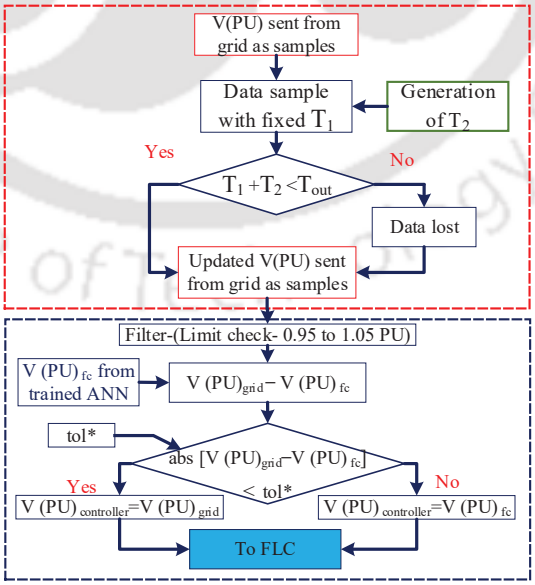

Fig. 3.5: Flow chart of the algorithm describing the scenario of delay. T_1 and T_2 are the fixed and random delay for samples reaching the receiving end. Red and black dotted box distinguish between the working of error simulator and the intelligent controller, respectively

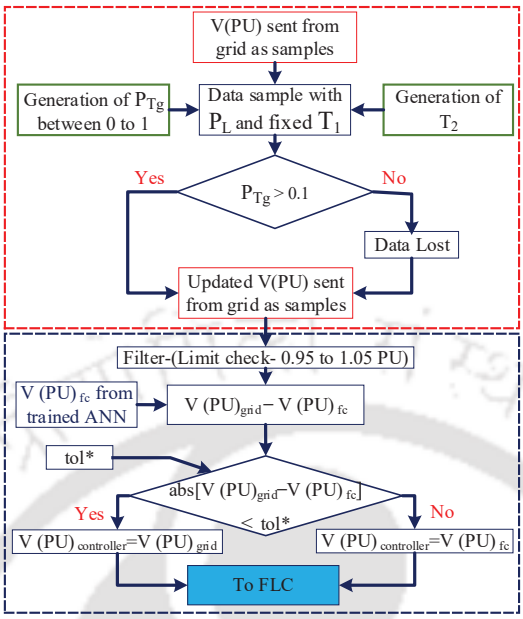

Fig. 3.6: Flow chart of the algorithm describing the realistic scenario. Red and black dotted box distinguish between the working of error simulator and the intelligent controller, respectively combination of both.

Since the limits at which loss and delay are to be considered are determined, the next step is to introduce the two phenomena in the system. Appropriate algorithms are developed to perform data loss and delay. To simulate the phenomenon of loss, at every discrete time interval, the simulation generates and couple a random number between 0 and 1 with the data being transmitted by the substation. These random numbers denote the event probability. A value of probability less than 0.1 corresponds to data loss, while a value greater than 0.1 means that the data is received without loss in less than 10 ms. The event of a loss can be due to the failure of the data to pass the inbuilt error check algorithms like cyclic redundancy check (CRC) or due to congestions in the network. Let us assume that the substation which is the sender in this work generates a sample at time t and sends it to the intelligent controller. Let T_{out} be the maximum allowable delay in reaching the sample at the receiver end, and T_1 be a fixed value which is equal to the sum of the propagation and processing delays.

The three scenario of data loss, delay and the combination of both due which is the realistic one is shown in Fig. 3.4, Fig. 3.5 and Fig. 3.6. The data from the electric grid (substation) is sent every second as samples with the randomly generated event probabilities (P_L) coupled to it. The event of data loss is considered when the attached (P_L) to the data is less than 0.1. The

remaining data passing through the DICC block as explained in the previous sections.

Fig. 3.5 shows the process of simulating the phenomenon of data delay. Fixed delay and a variable delay is considered in this work. The fixed delay is a constant delay. The variable delay depends on the network congestion and the distance between two ends of the channel (sending and receiving). Let us assume that T_1 is the constant delay in sending the samples via a communication channel [134]. Let T_2 be another random number defining the variable delay. The T_2 is also generated in the simulator, which is exponentially distributed over a mean of 1. The probability of a larger delay is very less as compared to a smaller delay. Hence, exponential distribution is selected to generate T_2. These two delays are added together to get a resultant random delay of T_1+T_2. The resultant random delay is compared with T_{out}. If it is less than T_{out}, the data is considered for further process in DICC; else, the data is considered to be impacted by the phenomenon of delay and considered to be lost.

The combination of the two cases results in the realistic case where both- the event of data loss or delay can happen randomly. The scenario is shown in Fig. 3.6. The samples sent are attached with both- random delay (T_{out}) and an event probability (P_L). The probability that both the event will happen is defined by $(1-P_L)(1-P_D)$ where P_L and P_D are the probabilities of each event defined above. A random number generated for each sample is compared with the probability of both the events -$(1-P_L)(1-P_D)$. If the generated random number is smaller, the data is considered to be lost.

3.7 Results And Discussion

Based on the model developed and algorithms to add the phenomenon of data loss and delay, simulations are performed to determine the impact on the use of DICC. This section will present the plots of node voltages for different scenarios and cases (when DICC is used and when DICC is not used).

3.7.1 Impact of Erroneous Input to the Controller

The impact on the electric grid due to the errors described in the previous sections is presented in this section. Initially, the values of P_L and P_D are varied to perform a sensitivity

analysis. The resultant plots of node voltage at node 4.4 at different values of P_L and P_D are summarised in the Fig. 3.10. The data being communicated between entities are moved in the direction of realistic scenarios by the works in this thesis. Initially, the data was simulated in continuous time states, followed by the case when data was transmitted in the form of samples (results described in the previous chapter). In this chapter, the data were exchanged between entities in the form of samples with different types of errors (data loss, delay or both). These three different types of data communication between the entities and their impact on the electric grid are shown in the plots of Fig. 3.10. Further, the scenarios of data loss, delay and the combination of both are also shown for comparison.

The impact of data loss is clearly visible in the plots shown in Fig. 3.7.1 – Fig. 3.7.1. The node voltage has oscillations at only those points where the event of data loss is triggered. Since the FLC computes at every discrete time, at a particular time, if one of the inputs is not received, the FLC computes the output with a garbage value resulting in erroneous output. Further, the MFs (Fig. 3.1d) are assigned a range of values, and the rules are framed as per the range. In case the input is a garbage value that is not in the range, the controller will give an unexpected random erroneous output.

A similar analysis for the case of delay is shown in Fig. 3.7.1 – Fig. 3.7.1. The oscillations in the node voltage are noted to be generated during peak load hours. The oscillations during peak load hours infer the requirement of better accuracy in the controller's output during peak load hours as compared to off-peak load. The time to switch from V2G to G2V is critical. The error in the input of FLC can easily change the signs of the output values. If the output is negative, the V2G operation will be decided and vice-versa for positive values. For example, the peak load hours start after 18:00 hours as per the load data collected from the APDCL. During peak load hours, the power system operator expects help from the connected EVs in the MCS. The support is to be decided by the controller. Since the data reaching the controller is erroneous, the power decided to support the electric grid by the controller can be either less than the expected or the controller continue to work on G2V mode. The resultant of the incorrect decision by the controller burden the electric grid leads to voltage oscillations and citing unstable operation.

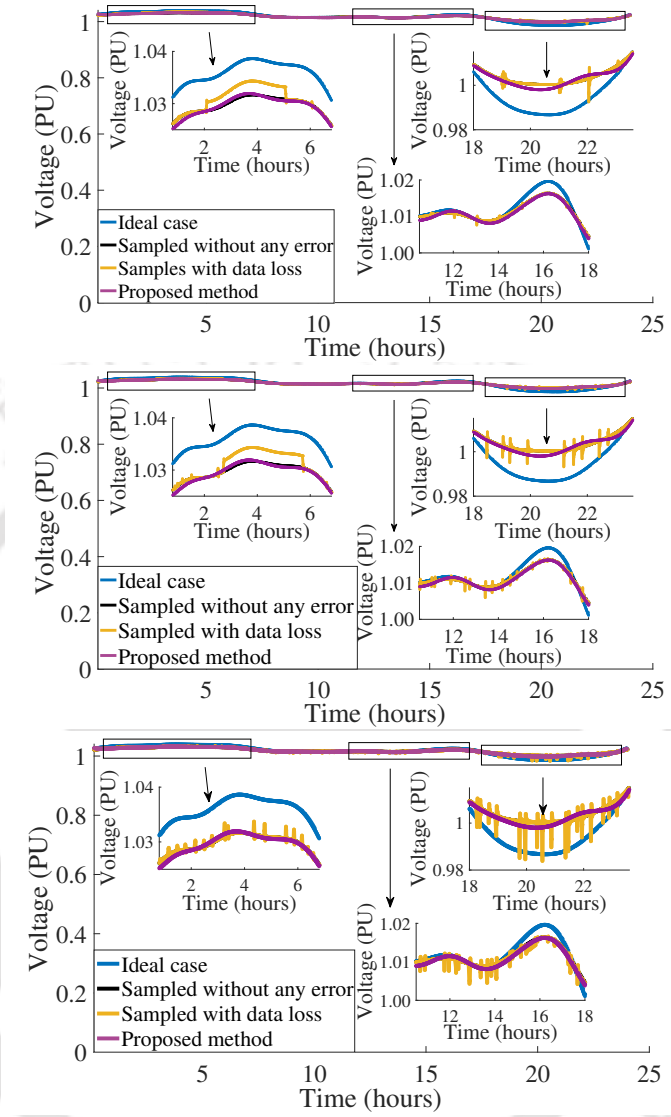

Fig. 3.7: Variation of node voltage in which MCS is connected for four cases- ideal, sampled without any error (I), sampled with error (II) and, with the proposed algorithm of intelligent controller (III),.(a-c), Variation of V(PU) in the event of data loss - P_L=0.01, 0.05 and 0.1, respectively.

A similar case will be observed if the controller decides incorrect values during off-peak hours. The power decided during V2G, or G2V operations are further dependant on the individual charging stations and the connected EVs in there. The power decided by the FLC is to be exchanged based on 1 and 2. Further, the power decided by the controller is distributed among CSs using (3). Since the power decided by the controller to charge or discharge is misleading, the users will be demotivated to participate in the process of V2G considering safety concerns. Further, suppose the oscillations are at the critical point where V2G and G2V switching takes place. In that case, the EV batteries health will also be impacted due to swinging between

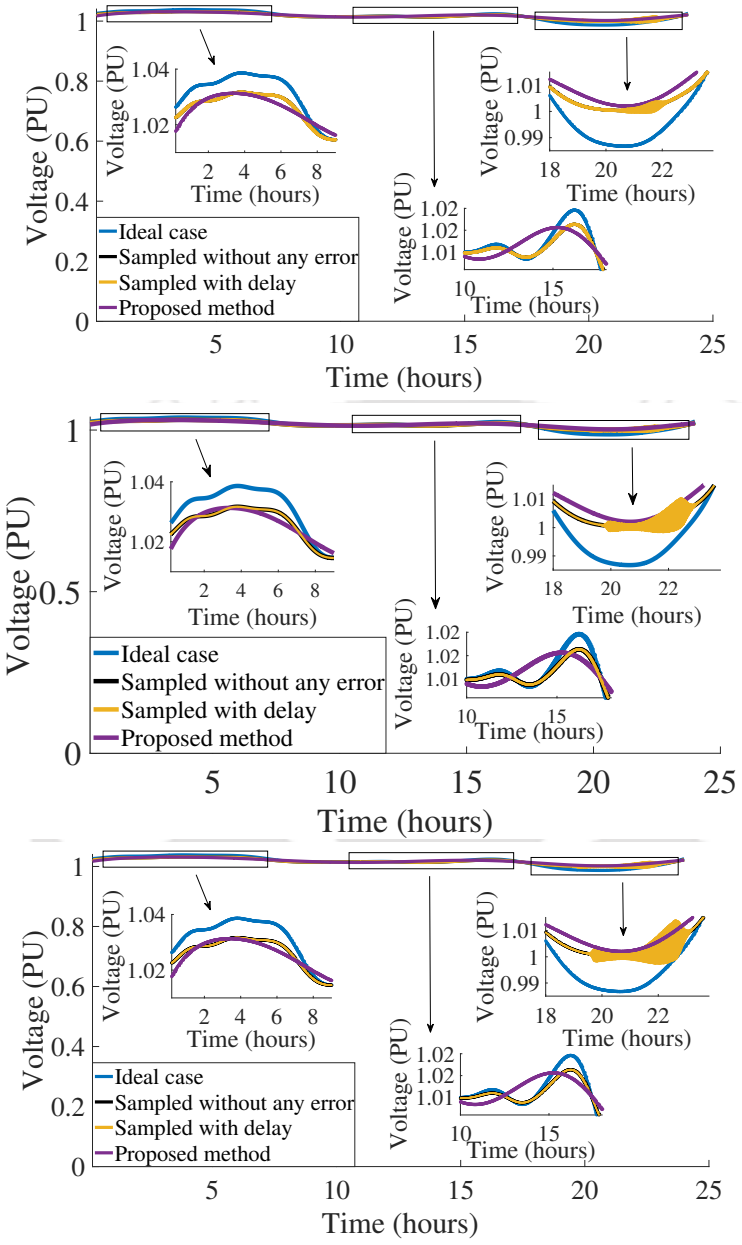

Fig. 3.8: Variation of node voltage in which MCS is connected for four cases- ideal, sampled without any error (I), sampled with error (II) and, with the proposed algorithm of intelligent controller (III),.(a-c), Variation of $V(PU)$ in the event of excessive delay-P_D = 1ms, 5ms and 10ms, respectively.

charging and discharging abruptly. The other resultant impacts in the electric grid, such as voltage deviations, imbalance in phase, harmonic distortions, and negative impact on the life of the transformers, are well described in the literature [135–137].

The results shown and discussed in this subsection confirms the requirement of an intelligent controller with error check and correction mechanism. The plots of node voltages with the realistic scenario (both errors introduced randomly) is shown in Fig. 3.7.1 – Fig. 3.7.1.

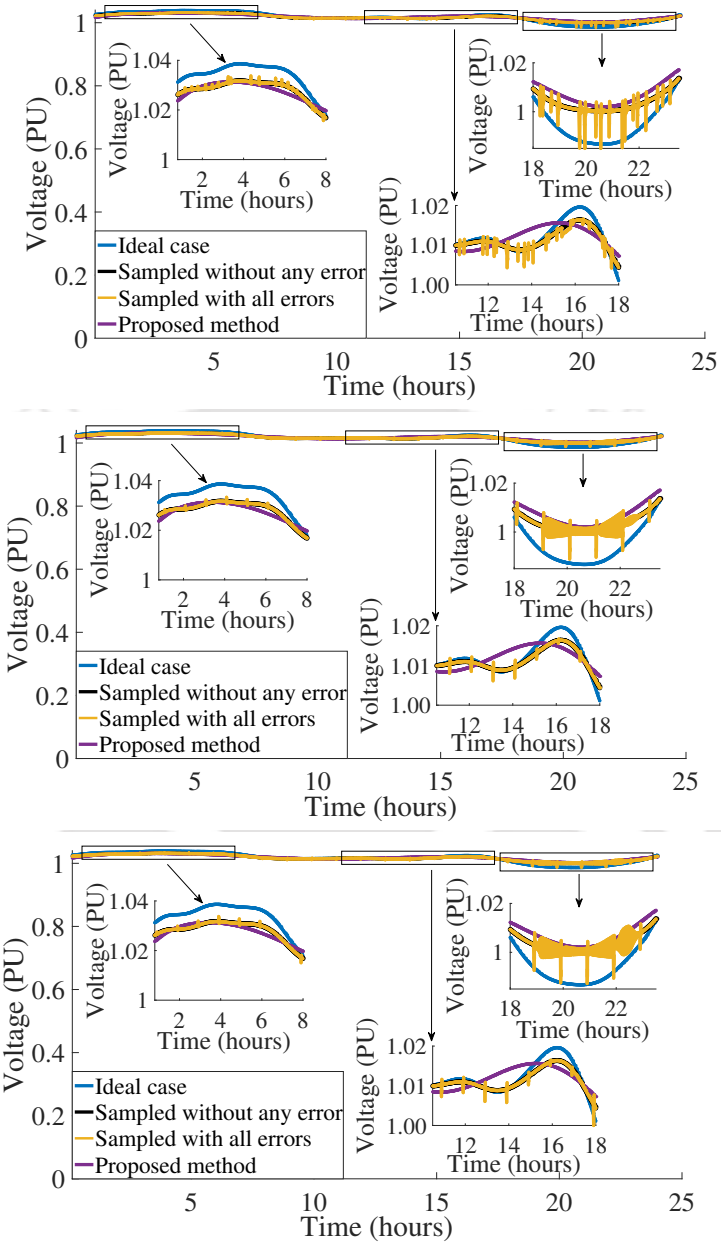

Fig. 3.9: Variation of node voltage in which MCS is connected for four cases- ideal, sampled without any error (I), sampled with error (II) and, with the proposed algorithm of intelligent controller (III),. (a-c), Variation of $V(PU)$ in the realistic scenario- P_L and P_D= 0.1 and 1ms, 0.01 and 10 ms, and 1 and 10 ms, respectively.

3.7.2 Influence of the Proposed Controller in the V2G System

The intelligent controller described in the modelling section is introduced in the V2G system by replacing the FLC. The intelligent controller comprises of filters, ANN-based forecasting system and data integrity check and correction algorithm. The intelligent controller is proposed to handle the errors mentioned in the previous section, viz. data loss and delay. The intelligent

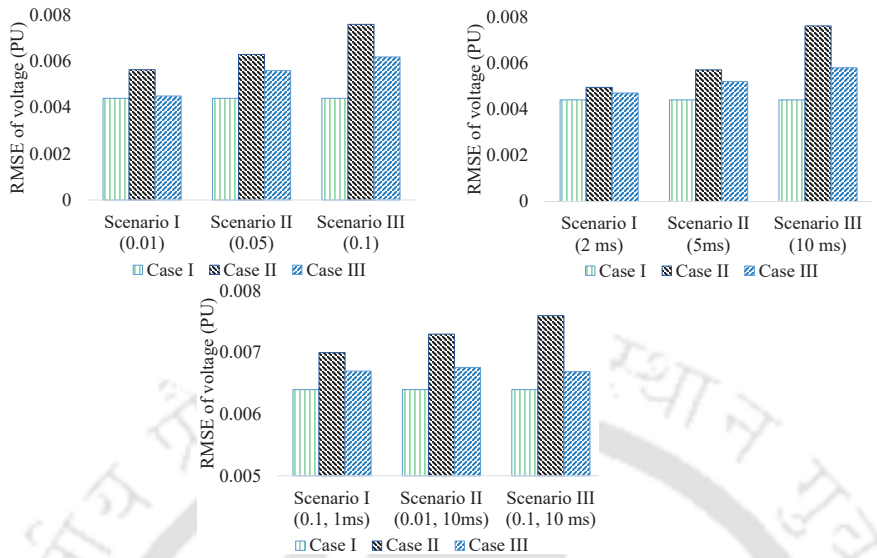

Fig. 3.10: Variation of node voltage in which MCS is connected for four cases- ideal, sampled without any error (I), sampled with error (II) and, with the proposed algorithm of intelligent controller (III),.(a-c), A comparison of the three cases with ideal one using RMSE.

controller is able to perform data integrity checks and corrections irrespective of the type of errors due to the communication channel or sending end. The process of data integrity check and correction process is explained relating to the simulated V2G system.

The process of correction is described in flow charts in Fig. 3.4–Fig. 3.6. In all the scenarios, the samples received from the node ($V(PU)_{grid}$) at which MCS is connected are initially passed through the filter and then compared with the samples generated using a trained ANN ($V(PU)_{fc}$). If the difference between $V(PU)_{grid}$ and $V(PU)_{fc}$ is greater than the tolerance(tol^*) value (determined using (3.1) given in Section II), ($V(PU)_{fc}$) is taken as the final value for input to FLC, else $V(PU)_{grid}$ is taken. The importance of using tol^* value is to check the consistency in the data, and this value is calculated based on the last 125 samples of ($V(PU)_{grid}$) sent from the substation in this work. Since the substation sends the $V(PU)$ every second, a total of 125 samples mean that the data of the last 125 seconds is used for tol^*. This value is determined based on the simulation of the modelled system in which the number of samples for calculation of tol^* is varied from 50 to 200 in steps of 25. Two plots of node voltage depicting the influence of the number of samples in the calculation of tol^* and hence, working of the algorithm are shown in Fig. 3.11. For the number of samples less than 125, oscillations existed in node voltage. In contrast, for a number of samples equal to or more than 125, no oscillations were

found in node voltage. Hence, to reduce computational intensiveness, 125 samples are used for the calculation of tol^* in this work. The value of tol^* act as a threshold beyond which the impact of errors will be visible in the FLC.

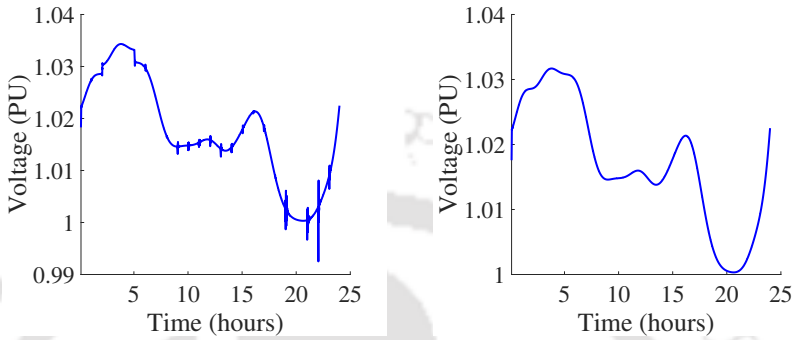

Fig. 3.11: Plot of node voltage for tolerance calculated using last.(a), 50 samples. (b), 125 samples.

In case of data loss ($P_L < 0.1$), two-time instances are defined. First (t_x), the time at which the $(V(PU)_{grid})$ arrives at DICC and; second (T_1), the time at which $(V(PU)_{fc})$ is computed. Explaining with an example, let the data is lost based on the flowchart shown in Fig. 3.4 at time t_x. The magnitude of the difference of $(V(PU)_{grid})$ and $(V(PU)_{fc})$ is compared with the tolerance (tol_*) value at time t_x+ T_1. If the data is lost, the magnitude of the difference is equal to $(V(PU)_{fc})$. As the difference is larger than the tol^*, $(V(PU)_{fc})$ is taken as $(V(PU)_{controller})$ which is the input to the FLC.

The scenario of delay (Fig. 3.5 and Fig. 3.6 in samples reaching the input of controller is tackled based on three time instances. The two time instances (t_x and T_1) are the same as defined in the case of data loss, while the third time instance is (T_2), which is a randomly generated delay exponentially distributed over a mean of 1 as described in Section III. If the sample of data does not reach the FLC by (t_x+T_1+T_2), the data is considered to be lost. Based on Algorithm 2, further computation takes place similar to the case of data loss which decides the value of $(V(PU)_{controller})$. Like the scenario of data loss and delay, the process is done in the third (realistic) scenario, which creates a combination of both (data loss and delay) to compute the final value for input to FLC. The process is explained in Fig. 3.6.

The improvement in the node voltage is shown in Fig. 3.7.1 – 3.7.1. In each case, the node voltage is smoother and without oscillations. The intelligent controller is able to ensure that

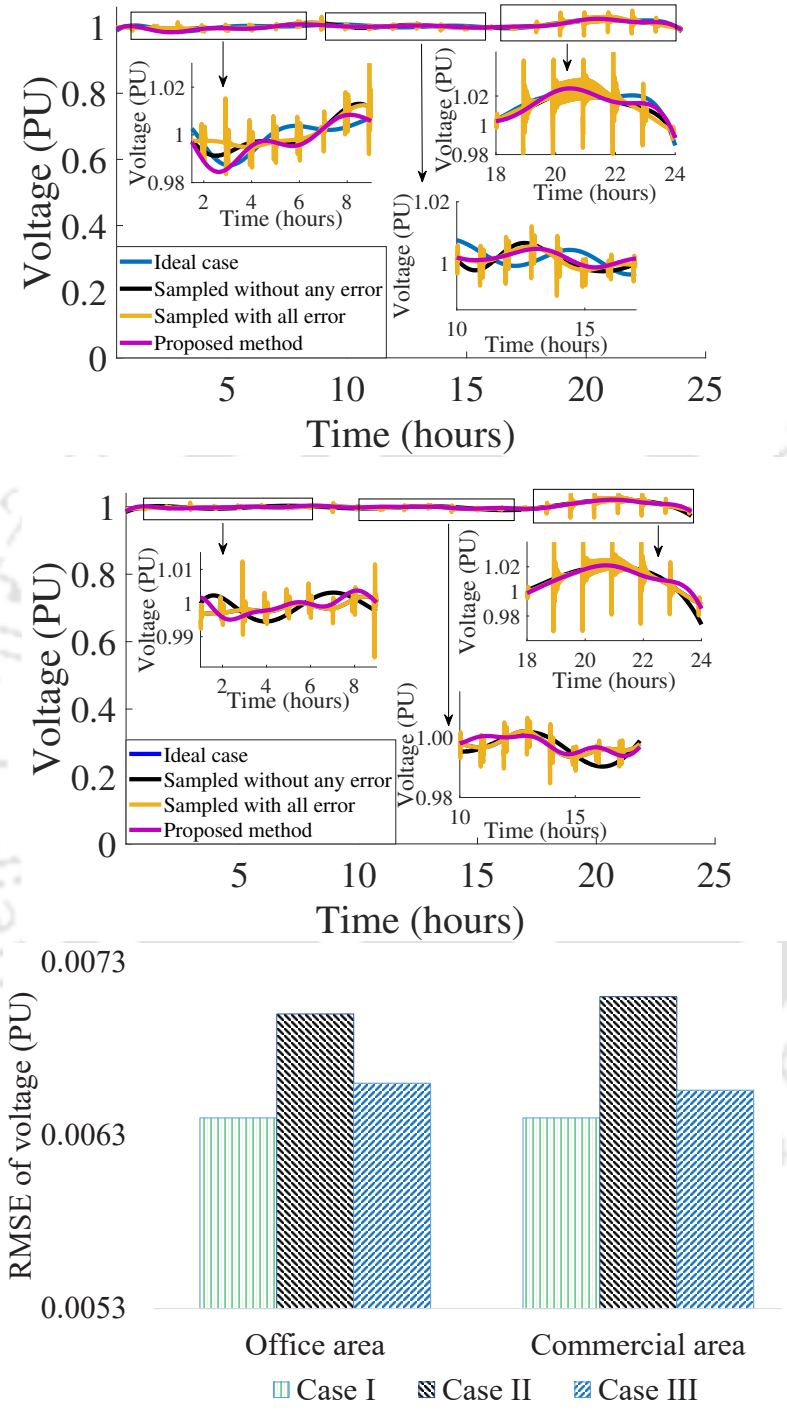

Fig. 3.12: Variation of node voltage in which MCS is connected for four cases- ideal, sampled without any error (I), sampled with error (II) and, with the proposed algorithm of intelligent controller (III).(a), Office area. (b), Commercial area.(c), Plot of RMSE for the three cases also defined in Fig. 3.10.

the controller (FLC) gets acceptable values at the inputs. The sudden change in the magnitude of the values is also stabilised because of the integration of tolerance values in the data check and correction algorithm. A sudden change in the inputs can abruptly change the output of the

controller. The abrupt change in the output will impact the operation of various entities of the V2G system. Since the power decided by the controller is consistent (does not abruptly change), the amount of power to be exchanged between the electric grid and EVs via MCS is consistent, accurate, and as per the requirements of the electric grid and EV users. The correct decision by the FLC due to the addition of supporting algorithms ensures that the impact of errors in the data communicated between entities is eliminated.

Fig. 3.7.1, 3.7.1, and 3.7.1 show the root mean square error (RMSE) in the node voltage corresponding to the ideal case. The case in which data is being transmitted continuously (not as samples) is considered the ideal case [138]. The plots infer that RMSE is less for the case when the data is communicated as samples without errors as compared to the case when samples are communicated with errors. Further, minimal RMSE is seen when the proposed intelligent controller is used, and samples are exchanged with errors. The finding validates that the proposed controller is able to reduce the impact of data loss and excessive delay in data communication. The proposed controller is further verified using two different load profiles: office and commercial. The plots of node voltages are shown in Fig. 3.7.2 and 3.7.2. The performance of the proposed controller is better even with the change in load profiles.

3.8 Conclusion

In this work, fuzzy logic and ANN-based intelligent controller comprising of DICC, ANN, and FLC are proposed to counter the issue of data loss and delay between entities of a V2G system. The proposed intelligent controller performs data integrity checks and correction at the input of FLC based on the real-time data of the node voltage transmitted, the data forecasted using ANN, and the historical trend of node voltage. The checks and corrections ensure the data reaching the inputs of FLC are consistent and also corroborates that the output decided by the controller is as per requirements of the electric grid and MCS. Hence, oscillations in the node voltage at which the MCS is connected is eliminated. The conventional FLC is compared with the proposed intelligent controller to check the performances during the issue of data loss and delay. The intelligent controller is further validated for three different load profiles collected

from APDCL, Guwahati, using the developed V2G system model. These load profiles are of three different areas, namely, residential, office, and commercial. The proposed controller can be implemented similarly for all the distribution networks where there is a central database of load data.

Moreover, the self-learning and adaptive nature of the controller due to the use of fuzzy logic and ANN make it suitable to be utilized for the V2G system operating in the smart grid scenario. This work opens direction for the formulation of a similar data check and correction algorithm for the data from the MCS side. The formulation will be challenging due to the unpredictable nature of the incoming and outgoing of EVs at CSs.

4

An Introduction to the Impact of Charging on Li-ion Battery Degradation

Contents

"The greatest challenge to any thinker is stating the problem in a way that will allow a solution."

– Bertrand Russell

4.1 Introduction

Batteries are an integral component of EVs. The previous chapters have discussed the requirements of the electrification of the transportation sector and power generation using renewable for the possibility to curb the increase in pollution [4]. Although governments worldwide have set up goals to electrify the vehicles on the road, the penetration rate is still low due to a lack of consumer acceptance. One of the major reasons for low penetration is range anxiety which can be addressed by developing fast chargers with technology to mitigate the problem of battery degradation [139].

Batteries are electrochemical devices that can store and transfer electrical energy to electrical equipment. They are categorised as primary and secondary batteries [140]. Primary batteries being non-rechargeable, are limited to alkaline, mercury, zinc, nickel and magnesium chemistries. Conversely, secondary batteries are rechargeable; hence, a wide range of chemistries are explored and researched [141]. Aluminium, zinc, sulphur, lead, vanadium, iron, potassium, tin, calcium, nickel, manganese, beryllium, sodium, polymer, glass and organic material chemistries have been described in the literature. The chemistry of secondary batteries has different characteristics, which vary for different load profiles. Hence, the selection of battery for usage in electric vehicle (EV) application is a challenge [142–144].

There are a few specific requirements and challenges of batteries for use in EVs. Reduction in the overall weight of vehicles in transportation is a universal need. EVs have a strong relationship between the weight of vehicles, range and energy consumption. An increase in the weight of the vehicle leads to an increase in the size of energy storage to meet the specified range. The cost of batteries, which are the costliest part of EVs because of the engineering complexity in design and material used, is another challenge. A higher cost leads to demand for a larger life cycle of batteries by EV users. Safety while charging and EV operation is also a challenge and requirement in selecting batteries. Moreover, the requirement of fast charge

capability batteries has remained a common goal of organisations worldwide to motivate using EVs for transportation.

Variation in ambient temperature is another issue affecting the optimal performance of EV battery, limiting the acceptance of EVs. Li-ion batteries at present have liquid electrolytes. Hence, the conductivity of electrolytes decreases at a lower temperature affecting the performance of the battery. Furthermore, at higher temperatures, operating voltage and State of Charge (SoC), the electrolyte undergoes secondary exothermic reactions [145]. These reactions increase internal cell temperature, supporting the formation of gaseous products and increases pressure within the battery. Thermal runaway, cell venting and explosions are the outcomes of the process leading to the safety concerns related to the use of Li-ion batteries in EVs [146,147]. A rise in the internal battery temperature due to high charge or discharge rate and applied voltage also have a similar impact on the battery performance [146, 147]. Further, the secondary exothermic reactions lead to the capacity fade in Li-ion batteries. Hence, an optimal ambient temperature considering the chemical composition of electrolyte and electrode material is required for the best performance of the battery [41, 145].

Capacity fade due to ageing is another major issue related to Li-ion batteries. Calendar and cycle ageing are the two types of ageing characterised in batteries. Calendar ageing is linked to the storage conditions of batteries, SoC and the ambient temperature of the storage area impact the calendar ageing phenomenon. An increased storage temperature leads to secondary reactions such as corrosion and electrolyte degradation. Such reactions lead to loss of active lithium, formation of passivation layers, and an increase in the self-discharge rate. A higher SoC further instigates the secondary reactions [148]. On the other end, cyclic ageing is characterised by the degradation in the battery due to the charge-discharge cycle. Structural change in electrodes, solid electrolyte layer formation, chemical decomposition, or dissolution is a few resultants of cyclic ageing [39].

4.1.1 Components of battery

Fig. 4.1 shows the structure of a Lithium-ion battery, which comprises two electrodes, an electrolyte and a porous separator. The two electrodes are called anode and cathode. The anode

gives electrons to the connected circuit, hence called reducing electrode. It gets oxidized by electrochemical reactions. On the other side, the cathode accepts electrons sent by the anode via an externally connected circuit, hence called an oxidizing electrode. The cathode is reduced during electrochemical reactions. The electrolyte act as a medium to perform ionic transfer between cathode and anode. Various types of electrolytes are reported in the literature, such as solid, polymer, acids, gel type, alkalis, and liquid with dissociated salts. The electrolyte has a unique property to allow only ionic transfer while remains electrically non-conductive for electrons. The electronic insulation ensures the avoiding of internal short circuits between anode and cathode.

However, since the electrodes are stacked together, the possibility to get shorted is not reduced due to compression during manufacturing or pressure due to external elements while in use. Hence, a solid material called a separator is used in the battery, which is also electronically insulating like an electrolyte. Further, the selection of separator is made to ensure the permeability of electrolyte is maintained without impacting the ionic conductivity. Apart from the mentioned, various other entities support the operation of batteries, like current collectors and binders. The electrodes are made using active material particles held together using binders, and their structure help in storing lithium. Current collectors are connected to the electrodes for electrical connection.

4.1.2 Electrochemical reactions and principles

The electrochemical reactions in the battery to charge and discharge depends on the type of the battery-primary or secondary, and the chemistry of electrodes and electrolytes. With extensive research to develop high energy/power density batteries, varieties of chemistries are available in the market. However, the basic principle of oxidation and reduction in the electrodes remains the same. The cathode or the positive electrode is characterised by metal oxide such as lithium cobalt oxide ($LiCoO_2$), while the anode or the negative electrode is graphite (carbon). Both cathode and anode are the layered structure that helps ions to insert or extract in between during charging and discharging. Based on the types of reactions- oxidation and reduction, the cathode is attached to aluminium as a current collector while the anode is attached to copper as

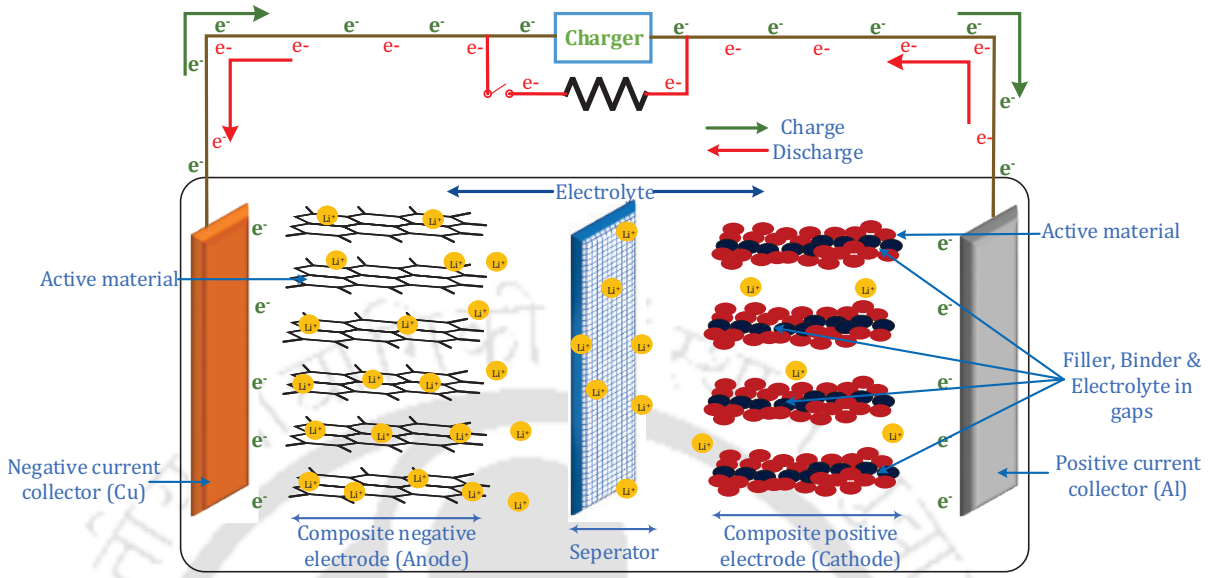

Fig. 4.1: The model of the battery with all components depicting the process of charging and discharging using the direction of flow of electrons. The arrows and ions in red depicts the process of discharge while the green depicts charging process. The electrons flow via the connecting wires and the positive ions diffuse to either electrodes (positive or negative) depending on the process of charging and discharging via electrolyte.
a current collector.

The Li-ions shuttle between anode and cathode during the charging and discharging process. Hence, these batteries are also called rocking chair batteries. The direction of the flow of lithium determines the state of charge and discharge in the battery. The intercalated lithium in the negative electrode diffuses to the surface during discharge, initiating an electrochemical reaction. The electrochemical reaction leads to the release of Li^+ ion and an electron. The electrolyte prevents the flow of electrons but allows Li^+ ion to diffuse towards the positive electrode. Hence, the electron via the electrode and current collector travels to the positive electrode. At the surface of the positive electrode, the Li^+ ion combines with the electron to form a lithium atom and intercalate in the positive electrode particle. The process of reversible insertion of ions into the layered structure of electrodes is called an intercalation reaction. The process reverses in the case of charging. The equations describing the process are:

$$LiCoO_2 \underset{discharging}{\overset{charging}{\longleftrightarrow}} Li_{1-x}CoO_2 + xLi^+ + xe^- \tag{4.1}$$

$$C + yLi^+ + ye^- \underset{discharging}{\overset{charging}{\longleftrightarrow}} Li_yC \tag{4.2}$$

$$LiCoO_2 + \frac{x}{y}C \underset{discharging}{\overset{charging}{\longleftrightarrow}} \frac{x}{y}Li_yC + Li_{1-x}CoO_2 \tag{4.3}$$

4.2 Phenomenon of degradations in Li-ion battery

Apart from the required intercalation reactions to charge and discharge, Lithium-ion batteries undergo various other reactions which are not desirable called the secondary reactions. These secondary reactions lead to products that are irreversible and hence, are a major reason for battery degradation. The amplitude, frequency, and time to charge or discharge impact the rate of secondary reactions. Two types of degradation mechanisms are reported in the literature, viz. chemical and mechanical. Further, the temperature and states of the battery also impact the rate of either degradation mechanism. Chemical degradation dominates at a lower applied current at normal ambient temperature, while a higher applied current and higher ambient temperature lead to fast mechanical degradation [1, 149]. Hence, changing the pattern of current while charging is often explored to reduce the degradation of batteries.

The reduction in the rate of battery degradation is a major challenge to ensure accelerated acceptance of EVs by people worldwide. The degradation impacts by reducing the discharge opacity and power density increases internal resistance and the ability to fast charge [40, 150]. The causes of battery degradation, which are widely discussed in the literature, are shown in Fig. 4.2. These causes are classified into a capacity fade and power fade. Capacity fade is related to the decrease in the discharge capacity of the battery, while power fade is the reduction in the ability to supply required current to the load without the rise in internal temperature above safety limits. These causes are further related to the electrodes-anode and cathode. The solid electrolyte interface (SEI) layer formation, decrease in porosity, lithium plating and lithium dendrite formation is noted in the anode side, while in the cathode side, binder decomposition, metal dissolution and phase transitions are dominant [151].

The regions in which interface of the phase change (solid-liquid or liquid-solid) are more vulnerable to side reactions [40]. Overall, the degradation in the battery is the sum of degradation in its different components. However, the degradation modes are widely reviewed, describing two fundamental processes- loss of lithium and loss of active material. The loss of

lithium-ion is on the anode side, while the loss of active material is mostly reported on the cathode side. The temperature too has a major role in demising the rate of degradation.

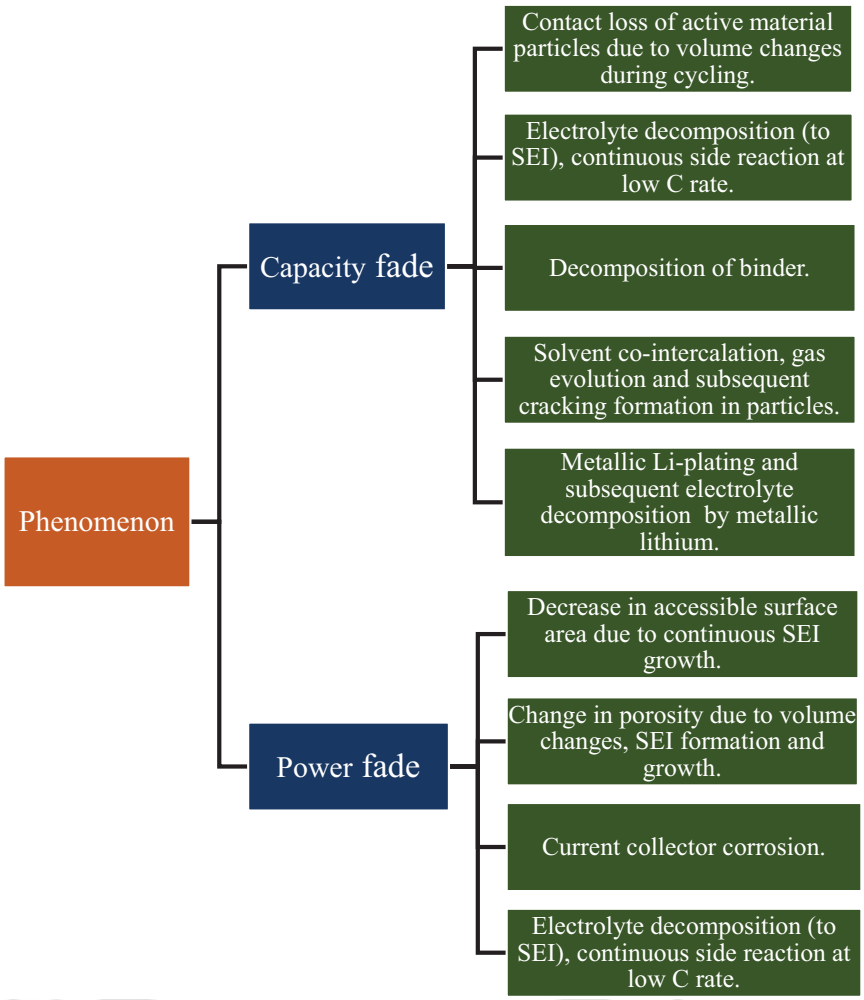

Fig. 4.2: A few causes of battery widely studied in literature

The SEI layer formation is one of the most common causes of degradations. The layer is required to ensure the solid and liquid phase does not react viciously. The lithium potential makes the electrolyte unstable and vulnerable to the reaction, which leads to the loss of lithium and a reduction in the overall capacity of batteries. Hence, while manufacturing, a formation cycle is run, which ensure a layer of SEI is formed in the electrode. With an increase in the side reactions in the battery, these layers start thickening. The thickening of the layer changes the area of contact in the active material. The reduction reduces the porosity of the electrodes in which the process of intercalation and deintercalation is to be performed. Since the amount of required reaction is reduced, the discharge capacity is impacted.

The discussion further leads to the fact that the byproducts of the reactions are irreversible. Hence, losses are noted in both phases-solid electrode and liquid electrolyte. These products diffuse in either direction of electrodes, further adding to the degradation of the battery. Apart from the solid byproducts of the side reactions, the gaseous products are no less formed. These gaseous products further add to the internal pressure of the battery and instigate the rise in temperature. The side reactions in the battery follow the Arrhenius temperature dependence. The reaction rate is increased, adding to further degradation. The complete degradation phenomenon is a sequence of interdependent events.

The overall degradation phenomenon is related to the rise in the resistance of the battery as well. The formation of irreversible products consumes the required active materials, deteriorates the electrolyte properties, and changes the volume/structure due to changes in pressure. These changes modify the rate of diffusivity of ions towards each electrode. At a higher C_{rare}, the ions are expected to diffuse fast. The ions already are diffusing fast, but the ions did not diffuse at the required rate due to the reduction in diffusivity. Since the movement/velocity of ions is fast, the temperature of the battery increases. The resistance to diffuse further increases the temperature and adds to both mechanical and chemical instability. The rise in resistance is a major cause of the increase in I^2R losses in the battery.

Further, the increase supplements the phenomenon of self-discharge of batteries also. A similar phenomenon of blocking ions and an increase in temperature is seen when the battery is operated at a high discharge rate. Numerous processes and phenomena are reported in the literature to describe battery degradation. Correspondingly, various approaches to constrain the rate of degradation is no less discussed. The study of the variation of the parameters of the battery is the basic step towards the challenge.

4.3 Parameters studied in literature to describe the phenomenon of degradation

The parameters of Li-ion batteries studied in the literature are either electrical or electrochemical or mechanical in nature. The electrical parameters studied are impedance, SoC, SoH,

capacity (fade, retention, relative, incremental, utilisation), energy efficiency, variations in OCV voltage, and specific energy are. Electrochemical parameters include side reactions rate, over-potential, active material volume concentration in electrodes, SEI (thickness, density, film resistance, potential), lithium loss, side reaction exchange current density, electrode potentials, and polarisation voltage. Porosity, electrode particle cracking, structural disordering, stress and expansion of cell (width and length) are the mechanical parameters studied in the literature. The temperature rise, change in charging time, and rate of capacity fade results from variation in these parameters.

The CC-CV is the oldest and standard technique described in the literature. Hence, all the new proposed charging algorithms have compared the variation of parameters listed above with CC-CV. Moreover, impedance is the most commonly studied parameter in earlier studies because of the possibility to relate with the variation of SoC and battery degradation [152–156]. Table 4.1 list the types of parameter studied for different types of charging techniques. The electrical model requires least number of parameters to be modelled but help in deriving required health status. The electrochemical model is computationally expensive and demands numerous parameters which are either available only with the manufacturer or determined using sophisticated test and equipments. The mechanical model is also similar to the electrochemical model but the governing equations used are different. Both electrochemical and mechanical model help in determining the health of the battery. Maximum parameters are studied in CC-CV charging technique being the oldest and a standard charging technique. In contrast, the least number of parameters are studied in the temperature-based charging technique [157].

The study of variation in the type of parameters for each charging technique is important to determine the causes of degradation. For example, for a CC charging at constant ambient temperature, if the C_{rate} is increased, the chemical kinetics (velocity of movement of Li-ions) in the Li-ion battery increases [153]. The increased kinetics lead to an increase in the internal battery temperature of the battery. The increase in temperature affects the electrical, chemical and mechanical behaviour of the battery. An increase in overpotential leads to an increase in the terminal voltage of the battery bringing change in the electrical behaviour [158]. Further,

increase in lithiation, side reactions, formation of inactive material, loss of lithium and electrolyte, and change in thickness, density or resistance of solid electrolyte interface (SEI) are examples of change in the chemical phenomenon [2, 159]. The mechanical changes include a change in electrode porosity, an increase in stress on the electrode particles leading to particle cracking or fracture of the electrode, and cell expansion due to increased internal pressure and any other structural disordering [158, 160].

Table 4.1: Different types of parameters studied or used in models reported to date.

Charging technique	Electrical	Electrochemical	Mechanical
CCCV	Capacity, impedance, efficiency (charge and energy), OCV, SoC, and SoH	Electrode potential, side reaction rate, active material concentration, Lithium loss, SEI (thickness, density, resistance), and exchange current density.	Porosity, stress, expansion (cell width and length), structural disordering
Pulse charging	Capacity, impedance, SoC, efficiency (charge and energy)	Li-loss, surface concentration, transfer reaction	Structuring disordering and porosity
Model based	Impedance, differential voltage, SoC, SoH, ohmic loss, capacity, energy	Polarization voltage, SEI (thickness and potential), electrode potential, Li concentration, active material concentration	
Boost charging	Capacity, charge efficiency	Concentration (electrolyte, surface) transfer reaction	Porosity
Temperature based	SoC, impedance, capacity, SoH and end-of-life		

The study of variation in the type of parameters for each charging technique is associated with the rate of battery degradation. Although the literature has described multiple studies on each charging technique to prove the suitability of fast charge and reduced battery degradation, there is a lack of studies that associate all the three types of parameters -electrical, chemical, and mechanical. Further, only a few works describe the effect on the parameters due to an increase or decrease in the ambient temperature. Hence, the commercially used charging techniques-

CC, CCCV, pulse charging (with negative pulse and without negative pulse) and variable frequency/duty charge pulse will be analysed in detail to understand and associate the change in the three types of parameter with the degradation phenomenon.

Various parameters are studied in the literature to describe the phenomenon of capacity fade in batteries. Each of the parameters studied is justified with the variation of values of related variables. The literature on this theme is mostly focused on the changes in a few battery parameters under specific operating conditions. For example, Sikha et al. studied the changes in porosity on the capacity fade [158], Zhang et al. studied CC, CP and multistage CC charging techniques and analysed impedance to describe the cause of capacity fade [161]. Furthermore, Shaoqing described the capacity fade in a Li-ion battery when subjected to pulse charging using strain on the electrode particles [162]. Many similar studies are presented in the literature. However, none of the works relates the variation of chemical, mechanical, electrical parameters to describe the process of capacity fade in Li-ion batteries. Hence, in this work, we related the three types of parameters to explain the causes of battery degradation when subjected to different charging techniques described in Table 4.3.

Table 4.3: The table shows different types of charging techniques simulated in the work. The t_{on}, t_{off} and t_{dis} are the time during a period of pulse to turn on to charge, turn off to rest and discharge, respectively. Each charging technique is simulated on a DFN model with incorporated degradation models at different charging rates. The empty spaces resembles that the specific parameter is not relevant for the charging type.

Sl.No	Charging techniques	Sub category	$t_{on}(s)$	$t_{off}(s)$	$t_{dis}(s)$
1	CC				
2	CCCV				
3	Pulse charge without discharge	Type 1	5	0.2	
4	Pulse charge without discharge	Type 2	3	0.2	
5	Pulse charge without discharge	Type 3	1	0.2	
6	Pulse charge without discharge	Type 4	5	0.1	
7	Pulse charge without discharge	Type 5	3	0.1	
8	Pulse charge without discharge	Type 6	1	0.1	
9	Pulse charge with discharge	Type 1	5	0.2	0.2
10	Pulse charge with discharge	Type 2	3	0.2	0.2
11	Pulse charge with discharge	Type 3	1	0.2	0.2
12	Pulse charge with discharge	Type 4	5	0.2	0.2
13	Pulse charge with discharge	Type 5	5	0.2	0.2
14	Pulse charge with discharge	Type 6	3	0.2	0.2
15	Pulse charge with discharge	Type 7	3	0.2	0.2

In this work, overpotential, the extent of lithiation in electrodes, inactive material volume fraction, SEI layer thickness in electrodes are studied as chemical parameters. The porosity, tortuosity, and the phenomenon of particle cracking in the electrodes are included in mechanical parameters, while the resultant parameters such as energy, power and capacity fade are analysed as electrical properties. Li-ion batteries undergo two reactions during charging and discharging-primary intercalation reactions and secondary electrochemical reactions (also called side reactions). The intercalation reactions are responsible for the charge and discharge of batteries. In contrast, the side reactions lead to the loss of lithium and materials, which intervenes in intercalation reactions called active materials. It also leads to electrolyte oxidation and reduction, passivation, structural disordering, particle cracking and thickening of the SEI layer. The resultants of side reactions lead to the capacity fade in the battery, which will be described in the subsequent subsections. SEI layer thickness, particle cracking, change in internal cell temperature are the major parameters impacting the discharge capacity of batteries. Hence, they are included in the main study, while others are described in the supplementary section.

Various parameters are studied in the literature to describe the phenomenon of capacity fade in batteries. Each of the parameters studied is justified with the variation of values of related variables. The literature on this theme is mostly focused on the changes in a few battery parameters under specific operating conditions. For example, Sikha et al. studied the changes in porosity on the capacity fade [158], Zhang et al. studied CC, CP and multistage CC charging techniques and analyzed impedance to describe the cause of capacity fade [161]. Furthermore, Shaoqing described the capacity fade in a Li-ion battery when subjected to pulse charging using strain on the electrode particles [162]. Many similar studies are presented in the literature.

However, none of the works relates the variation of chemical, mechanical, electrical parameters to describe the process of capacity fade in Li-ion batteries. Hence, in this work, we related the three types of parameters to explain the causes of battery degradation when subjected to different charging techniques described in Table 4.3. [1] hypothesized and showed the dominating influence of the chemical degradation process in the reduction of battery capacity during low charging rates.

4.4 Charging techniques proposed in literature

Fig. 4.3 shows the different types of charging proposed in the literature to fast charge and control the degradation of the battery. The charging techniques can be classified into conventional, active control, sinusoidal ripple, boost, constant temperature-constant voltage (CT-CV) and model-based charging. Each type of charging technique is proposed to increase the charging efficiency, reduce charging time, and reduce battery degradation in comparison to conventional techniques (mostly CC-CV).

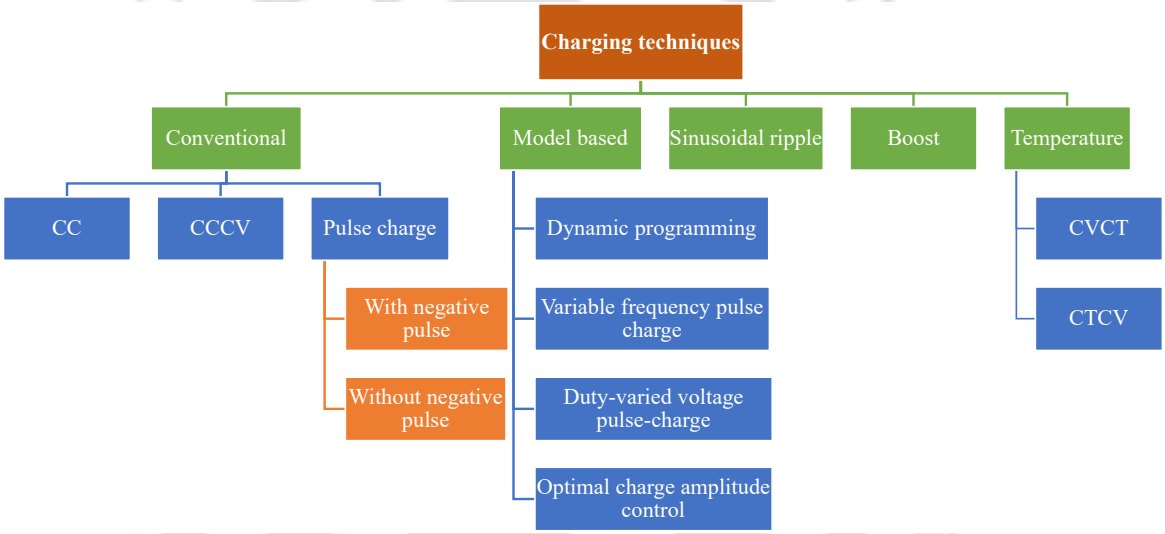

Fig. 4.3: Types of charging techniques reported in literature and a few typical current and voltage waveforms; All the types of charing reported in the literature are extensively reviewed and classified appropriately.

4.4.1 Charging techniques discussed in literature

Constant current (CC) was the first technique to charge the battery. The battery is considered to be fully charged when charging with a constant current leads to an increase in terminal voltage to a fixed cut-off voltage. Since the battery is an electrochemical system, it experiences a reduction in open-circuit voltage after a specified time of turn off. Hence, and a new technique of constant current-constant voltage (CC-CV) was proposed in which the battery is charged with a fixed value of current up to the specified cut-off voltage during CC [156, 161]. On reaching cut-off voltage, the CV gets activated in which the voltage is kept constant and current starts reducing. At a specified value of current (50 mA), the battery is considered to be fully

charged [153]. The reduction of current in the case of CV significantly increases the charging time. However, it allows the settling of mass and ions in the battery, helping to reduce the concentration gradients within the electrode and leading to more energy storage for a specified maximum voltage. The simplicity in implementing CC-CV and its ability to transfer more energy to the battery has made it a standard charging protocol for charging [151].

The idea of settling ions or mass in the battery is further exploited in pulse charging by the researchers. In pulse charge, the continuous current is interrupted periodically to give rest phases, or discharge pulses [162, 163]. These rest phases and discharge pulses help to settle the kinetics of ions and compounds in the battery. Three types of pulse charging are reported in the literature: pulse charging without discharge, pulse charging with different current amplitude stages, and pulse charging with short discharge pulses [164, 165]. The rest and discharge phases aim to reduce the following: (a)the mechanical stress in electrode particles due to uneven insertion and extraction of lithium in the solid particles, (b) the possibility of electrochemical potential at anode becoming negative and concentration polarisation. Researches have shown other benefits, such as inhibition of dendrite formation in battery, better charge and discharge efficiency, and active material utilisation [166].

Works in literature have shown that application of high current when the battery is at a state of high open-circuit voltage (OCV) and high SoC accelerates the battery degradation due to increased intercalation of Li^+ ions in electrodes and side reactions in the surrounding region of electrodes in battery [158]. However, at the state of low OCV and SoC, the battery can be charged at high currents. Hence, Notten et al. proposed a charging technique called boost charging [167]. Boost charging is characterised by a high charge current (1C) for a short period leading to a fast charge up to one-third of the battery capacity. After that, conventional controlled low current CCCV is used to charge the remaining capacity. Although boost charging resulted in fast charge with controlled degradation, the implementation is a challenge because of the unknown high current that flows into the battery due to high voltage at the charger terminals. Moreover, the temperature rise and the degradation studies are not yet well discussed in the literature for boost charging. Compared to other charging techniques like CCCV, boost charging

is able to input more charge in the battery when recorded in the initial fast charge period. However, the rise in battery temperature during boost charge was another challenge [162, 167, 168].

Numerous studies have shown a rise in temperature with an increase in the number of charge-discharge cycles. The temperature rise in the battery is due to an increase in the impedance or the chemical kinetics on the application of high current to charge or both [153]. Hence, considering the impact of temperature in ageing, Xiaosong analysed a new type of charging protocol, constant voltage constant temperature using the electro-thermal-ageing model. The analysis showed a tradeoff between charge time and the ageing of the battery. Constant temperature constant voltage (CTCV) charging protocol is another technique proposed considering the importance of temperature in the ageing of battery [157]. CTCV has simplicity in implementation and results in 20% faster charging when compared with CCCV.

Chen introduced sinusoidal ripple charging (SRC), claiming reduced charging time, charging efficiency and lifetime of battery with a controlled temperature rise of battery [169]. A challenge in using SRC for practical chargers is precise control of the magnitude and frequency of the charging current. The frequency should be optimal to have a low impedance of the battery. Further, the magnitude of the ripple, which affects polarisation in battery and selection of components in the charger, need to be monitored [170–173]. Hence, a new power electronics converter topology for the charger and precise control of outputs (current and voltage) with the ability to reduce power quality for vehicle-to-grid issues is proposed in [172]. Further, suppression of dendrite growth in the battery is another benefit demonstrated in [174]. On the contrary, Bessman showed using experiments on prismatic cells and a physics-based model that the claimed benefits of SRC are not true as mentioned in literature [175].

In recent years, a new research direction has opened towards the model-based charging system. Information gathered from electrical and electrochemical modelling of batteries can be utilised to optimise the charging for a battery. The model-based charging technique uses electrical, electrochemical and thermal models and computes parameters for the battery [160, 176–182]. The parameters computed using the electrical model include impedance and SoC. The electrochemical model computes SEI potential or thickness, active material concentration,

and anode potential. Capacity, temperature and SoH are common to the model-based charging techniques. The works in this research direction also demonstrated a decrease in charge time and control of the rise in battery temperature. However, a few considered the effect of battery degradation during charging. Further, the advantage of model-based charging is demonstrated in simulation due to the requirements of multiple battery parameters and extensive computational cost.

4.5 Outlook and discussions

The literature has studied battery degradation and the EV charging infrastructure as two different problem statements. However, a wider acceptance of EVs demands a relation between infrastructure requirements and battery degradation. Although the EV infrastructure can be robust and reliable if the rate of battery degradation is not constrained, the repetitive capital investment to replace the battery will for sure question the adoption of EVs. Hence, the infrastructure should consider the causes of battery degradation and look for the processes and algorithms to constrain it. Further, the processes and algorithms should ensure the reliability of the infrastructure is not impacted and help in improving electric grid stability.

The discussions in the battery degradation is incomplete with the mention of the impact of ambient temperature. The changes in the ambient temperature bring changes in the internal battery temperature, which influences the reaction rate of the required (intercalation and deintercalation) and the side reactions. A similar phenomenon of changes due to variation in internal temperature as described in the previous section is reported for this case as well. Hence, the processes and algorithms to utilise EVs optimally to reduce vehicular emission and to ensure electric grid stability should consider the impact of ambient temperature as well. The next chapters will attempt to solve the challenge.

5

Li-ion Battery Degradation: Charger Side Online Parameter Estimation

Contents

"There is always room at the top."

– Daniel Webster

5.1 Introduction

A literature review of all the proposed techniques can be presented. This chapter is based on the paper to be submitted in Transactions on Industrial applications. The title of the paper will be "Online parameters and states estimation of battery based on impedance".

The increase in the demand for transportation electrification worldwide has stimulated the application of energy storage systems. Li-ion batteries have emerged as the best solution because of high specific power and energy densities, longer life and lower weight. A major challenge to optimally utilise the Li-ion batteries require accurate determination of parameters and states. The parameters of the battery vary over a long period while states change rapidly. The value of the parameters and states guide the user to decide the charging and discharging capabilities. The operation of Li-ion batteries with an inaccurate prediction of its parameter and states leads to fast degradation and safety concerns. Battery parameters like impedance and states such as state of charge (SoC) and capacity majorly impact the battery's performance.

The impedance of the battery provides valuable information about the degradation, ageing, possible rise in internal temperature, deviation in open circuit voltage (OCV), and possible safety concerns [183]. An increase in the impedance directs towards the electrochemical phenomenon that leads to an increase in the solid electrolyte interface layer thickness, changes in the diffusivity of ions and viscosity of electrolyte, decrease in the porosity and increase in tortuosity [39]. The increasing impedance adds to I^2R losses, reducing the charge and discharge efficiency and increasing self-discharge and the internal rise of battery temperature. Cell venting, fire or explosions are a few outcomes when heating exceeds safety limits [64]. Further, impedance is an important parameter for estimating other battery states, such as state of charge (SoC) and capacity. Hence, an accurate estimation of the battery impedance will lead to it's optimal utilisation within safety limits.

Electrochemical impedance spectroscopy (EIS) is the most widely used and accurate impedance

estimation technique. EIS give complex values of impedance for a wider range of frequencies. The values help to build deeper insight into the electrochemical characteristics, which varies for different frequencies. The values of impedance at low frequency are in the range of a few mΩ. Hence, the need for accuracy and precision in measurement makes the equipment costly, especially when the frequency range is from μHz to MHz. Another major drawback of this measurement technique is integrating a separate hardware system that does not support online estimation. Hence, EIS is mostly limited to laboratory applications. Approaches are discussed in the literature to perform the online estimation. Broadband impedance spectroscopy, which uses multi-sine wave excitation and a connected electronic load, is another approach to the online estimation of impedance [184]. Apart from using a new device for impedance estimation, integrating the online impedance estimation in the charger or connected power-electronics converter is another widely discussed approach.

A calibration device coupled with a power converter to perform precise measurement of the battery's response to a particular excitation is an initial step to such an approach. Discrete Fourier transform is used to determine the impedance of a VLRA AGM battery [185]. In an another work, the duty cycle of the control signal of a DC-DC converter is perturbed to get sinusoidal current and voltage with offset [186]. Since the battery impedance is unknown, the idea of perturbing the duty cycle in [186] suffered from a drawback of the unknown response of voltage and current. Motor controller excitation is used as a tool to generate multi-sine signals and noise excitation signals in [187]. The response of the battery is calibrated, filtered, and using a statistical correlation approach, the information of impedance is extracted. Reinhold et al. supplemented the charger with a switched-mode amplifier for generating required current waveforms to perform impedance spectroscopy [188]. The d-q transformation is also explored to estimate impedance in a high-power charger in [189]. A statistical approach such as the cross-correlation technique integrated into a DC-DC converter is also presented in the literature to determine impedance [190]. With different algorithms proposed in the literature, sinusoidal excitation and extraction of information from the battery response remain a common approach. The differences are in either device used for excitation or the process of information extraction.

The impedance information determined from the proposed techniques is used for estimating states such as SoC, OCV and capacity.

Accurate SoC estimation is a challenge to date that researchers are trying to solve using various algorithms. The algorithms are either direct measurement-based, model-based, or hybrid. Coulomb counting, SoC-OCV curve, and lookup table are the simplest and most common direct measurement methods. These techniques use filtered charging current to the battery and terminal voltage to estimate SoC. The drawbacks of the direct measurement methods are the measurement error, error integration, and dependency on the accuracy of measured OCV [146]. Model-based estimations are widely used for real-time estimation because of the possibility to update estimates based on a feedback mechanism. These models are electrochemical, electrical or data-driven [191]. The electrochemical model is based on sets of governing equations and values of parameters that describe the characteristics of a specific battery. Electrical models use properties of voltage and current sources, resistors, and capacitors to model the behaviour of batteries. Data-driven models utilise machine learning algorithms such as artificial neural networks, deep neural networks, and support vector machines, to model battery properties [192, 193]. These estimations based on the models are supplemented by feedback algorithms such variants of least square, adaptive observers, Kalman Filters, and their combinations [146, 190, 191, 194].

Capacity estimation is another important state for determining the health of the battery. Ampere hour counting, internal resistances based, OCV-SoC curve deviation, and model-based (electrochemical, electrical and data-driven) are widely proposed techniques in the literature. The major disadvantages of these techniques are the sensitivity to measurement error, environmental errors, mathematical complexity, and computational cost. Hence, there is a requirement of an estimation technique that is not directly dependant on accurately estimated parameters, less complex for easier implementation and computationally limited. Further, impedance which varies based on the electrochemical phenomenon and ageing in battery is an important parameter which impacts the estimation of all the states. Hence, if impedance estimation is accurate and incorporated in states estimation, accuracy in other state estimation process can be improvised

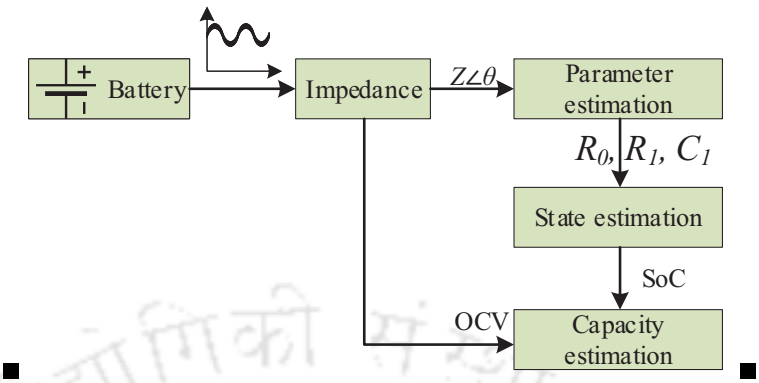

Fig. 5.1: A schematic representation of the proposed algorithm

irrespective if ageing of batteries.

Taking into consideration of all the challenges and requirements discussed in previous paragraphs, in this work, an algorithm to estimate impedance online, and use the impedance values in SoC and capacity estimation is proposed. The contributions of the work are:

(i) An online impedance measurement technique for the battery is proposed in this work by modifying the reference signal of the DC-DC converter, which perform charging using any type of technique (constant current (CC), constant voltage (CV), CC-CV, and variants of pulse-based charging).

(ii) The equivalent circuit model (ECM) parameters of the battery are also determined online. These parameters and impedance are used to estimate other states. The OCV of the battery is determined using the impedance, while the SoC estimation is realised utilising an extended Kalman filter based on the ECM parameters determined online. The real-time estimation of parameters in the EKF makes the estimation process suitable for all types of Li-ion batteries irrespective of their age and chemistries.

(iii) The battery's capacity is estimated using a rule-based estimator, which takes OCV and SoC as inputs. Since the OCV and SoC are calculated in real-time, the impact of ageing in capacity is also incorporated with increased accuracy and reduction in complexity.

(iv) The proposed algorithms are verified for their suitability for using in three types of charging techniques viz: CC, pulse charging without discharge and pulse charging with discharge.

The remaining sections of the chapter is organised in three sections. Section II describes the al-

gorithms proposed for estimating impedance, SoC and capacity. Section III presents the results obtained on implementing the algorithms in an experimental setup comprising of power electronics converters and digital signal processer for control and estimation. Section IV concludes the work with a comprehensive discussion on the outcome of the work.

5.2 Proposal of online parameter estimation

The battery's impedance varies with change in SoC, internal or ambient temperature, C_{rate} and discharge rate, ageing and any change in electrochemistry. The rate of change in impedance is not predictable, which makes the impedance estimation a challenge. The drawbacks of the works in literature are discussed in the previous section. The proposed algorithm in this work eliminates the drawbacks of the existing methods, such as requirements of a separate device, integration of computationally extensive calibration and estimation algorithms into a device connected with the power converter. In this work, the perturbation is performed in the reference signals used in the power converter connecting the battery. Since the battery charge using DC inputs, the reference current and voltage values to charge the battery are constant. A sinusoidal component is added to these constant DC values such that the converter does not go in a discontinuous mode of operation. Since the reference signals are controlled, the output voltage and current at the battery are known and remain under limits.

The controlled DC-DC converter in a charger gives an output of either CC, CV or pulsed current. The value of load current in CC and pulse charging and the voltage across the load in CV is decided based on the reference values. Hence, the reference values are updated to get a sinusoidal current and voltage for estimating impedance at the output of the DC-DC converter, which charges the battery. A detailed schematic of the proposed impedance measurement algorithm is given in Fig. 5.2. Consider a controlled DC-DC converter that is operating to charge using CC charging mode. The reference $I_o(t)$ is defined as:

$$I_o(t) = I_{dc} + I_{ac} Sin(2\pi f_p t + \phi_i) \tag{5.1}$$

where, I_{dc} is the DC offset current over which a sinusoid of peak magnitude I_{ac} and frequency

f_p is superimposed. The value of I_{dc} should be less than or equal to $|I_o - I_{ac}|$. If the converter operates in the CV mode of charging, the variable I can be replaced by V. In response to the reference, the controller of the DC-DC converter will produce duty cycle as:

$$d(t) = D_{dc} + D_{ac} Sin(2\pi f_p t + \phi_i) \tag{5.2}$$

where, D_{dc} is the duty cycle for constant offset current, D_{ac} and f_p are the peak magnitude of duty cycle and frequency of waveform to generate $I_o(t)$, respectively. Since the battery is both resistive and capacitive nature, the output voltage also follows a sinusoidal pattern with a change in phase angle.

$$V_o(t) = V_{dc} + V_{ac} Sin(2\pi f_p t + \phi_v) \tag{5.3}$$

where, V_o is the voltage at the load, V_{dc} is the offset output voltage, V_{ac} is the peak amplitude of sinusoidal voltage output, and ϕ_v is the phase angle of voltage. It is to be noted that all the sinusoids ($I_o(t), d(t)$ and $V_o(t)$) are in the same f_p. For determining the battery's impedance, a cycle of data is stored in the buffer from which the peak to peak values of voltage ($V_{ac_{pp}}$) and current ($I_{ac_{pp}}$) are determined. The impedance (Z) of the connected battery is determined by measuring the peak-to-peak values of V_{ac} and I_{ac} and the change in phase angle ($\phi_v - \phi_i$) for a cycle.

$$Z = \frac{V_{ac_{pp}}}{I_{ac_{pp}}} \angle \phi_v - \phi_i \tag{5.4}$$

The estimated impedance is used to determine the OCV using (5.5).

$$OCV = V_{battery} + I_{battery} \times Z \tag{5.5}$$

The OCV is a function of SoC of battery. Further, the capacity is also related in a similar manner as SoC.

5.2.1 Determination of equivalent circuit parameters

The state estimations in this work are performed using a dynamic electrical model that can capture the characteristics of the battery during charge and discharge. These electrical models comprise mostly the combination of RC components. If the impedance estimated is accurate,

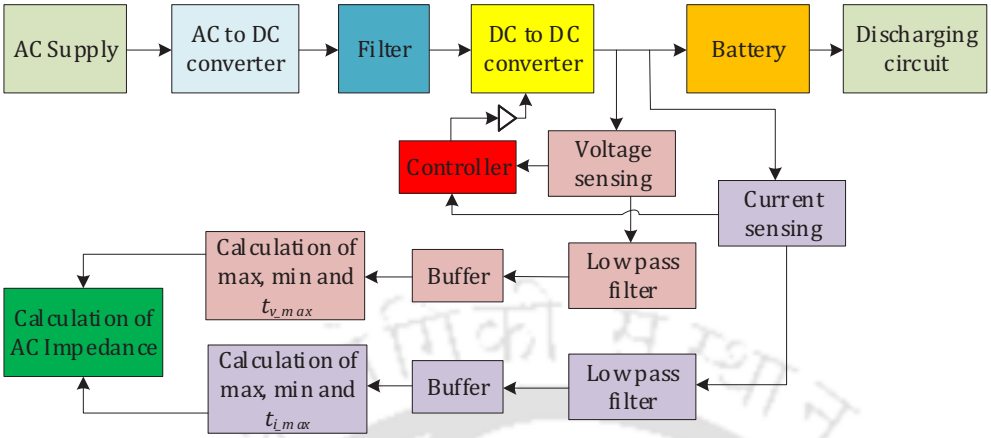

Fig. 5.2: A schematic representation of the impedance estimation

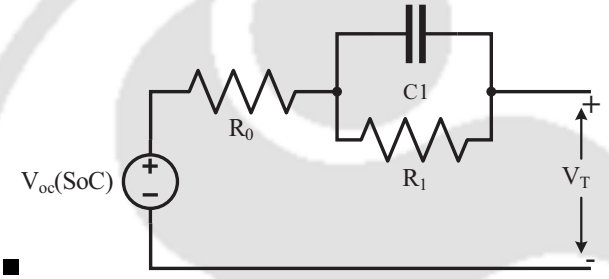

Fig. 5.3: Electrical model of battery

the RC components can be determined appropriately to improve the accuracy and increase the application spectrum. Since the impedance and corresponding R and C values are estimated in real-time, the estimated states easily accounts for the model and measurement uncertainty, thereby complementing the estimation accuracy. The RC model used in this work is relatively simple but captures the dynamics of the battery as described in [189,195]. The equivalent circuit model (ECM) of the battery is shown in Fig. 5.3. The ECM comprises of a resistance in series (R_0) with a single RC network (R_1 and C_1) that captures the response of the battery during transients and a DC source representing the OCV as a function of SoC. The values of these components are required to be computed for implementing any model based state estimation algorithms. The ECM for a charge current i_l in Fig. 5.3 is described in (5.6).

$$\left.\begin{aligned} V_0 &= i_l R_0 \\ \dot{V}_1 &= \tfrac{i_l}{C_1} - \tfrac{V_1}{R_1 C_1} \\ V_T &= V_{oc}(SoC) - V_1 - V_0 \\ SoC_{t+1} &= SoC_t + \int_t^{t+1} \tfrac{\eta \times i_l}{Q} dt \end{aligned}\right\} \tag{5.6}$$

where, V_1 and V_0 are the polarisation voltage and the drop across series resistance, respectively, η is the charge efficiency, and Q is the capacity of the battery. The equation in (5.6) is used to determine the values of (R_0), (R_1) and (C_1) using recursive least square with variable direction forgetting. Recursive least square (RLS) estimation and its variants viz. weighted RLS, RLS with forgetting factor and moving window RLS are widely used for parameter identification [196–199]. The recursive least square estimation using exponential forgetting (RLSEF) is used for parameter identification in this work. RLSEF uses the forgetting factor, which decays the droop in the covariance matrix. Further, RLSEF has a faster estimation ability with less prediction error [200]. Since the implementation is to be done online in a real time systems, the (5.6) is to be converted into the discrete domain. Hence, the required equation is converted to frequency domain and discretised using bilinear transformation. The characteristics of the ECM in frequency domain is expressed in (5.7).

$$V_T(s) - V_{oc}(SoC)(s) = i_l(s)\left[R_0 + \frac{R_1}{1 + R_1 C_1 s}\right] \tag{5.7}$$

The transfer function (G(s)) of the system is

$$G(s) = \frac{V_L(s)}{i_l(s)} = \left[\frac{R_0 + R_1 + R_0 R_1 C_1 s}{1 + R_1 C_1 s}\right] \tag{5.8}$$

where V_L is $V_T(s)$ - V_{oc}. The discretisation 5.8 is performed using bilinear transformation $s = \frac{2-z^{-1}}{T+z^{-1}}$ which results in values of R_0, R_1 and C_1 as given in (5.9).

$$R_0 = \frac{-(a_1 - a_2)}{1 + a_0}, R_1 = \frac{-2(a_0 a_1 + a_2)}{1 - a_0^2}, C_1 = \frac{T(1 + a_0)^2}{4(a_0 a_1 + a_2)}\Bigg) \tag{5.9}$$

where, the variable a_0, a_1, a_2 are given by (5.10) and the discretised transfer function in simplified form in defined by (5.11)

$$\begin{aligned} a_0 &= -\frac{T-2R_1C_1}{T+2R_1C_1}, a_1 = -\frac{R_0T+R_1T+2R_0R_1C_1}{T+2R_1C_1}, \\ a_2 &= -\frac{R_0T+R_1T-2R_0R_1C_1}{T+2R_1C_1} \end{aligned} \tag{5.10}$$

$$G(z^{-1}) = \frac{a_1 + a_2 z^{-1}}{1 - a_0 z^{-1}} \tag{5.11}$$

where, z^{-1} is the unit backward shift operator and T is the sampling time. Using a_0, a_1, a_2 , the (5.7) is dicretised as (5.12).

$$V_T[k] = (1 - a_0)V_{oc}(SoC)[k] + a_0 V_L[k-1] + a_1 i_l[k] + a_2 i_l[k-1] \tag{5.12}$$

The parameter identification starts by rearranging (5.12) into (5.13)

$$y[k] = \phi^T[k]\theta[k] + \Delta\varepsilon \tag{5.13}$$

where, ϕ^T is the parameter vector, $\theta[k]$ is the regression vector and $\Delta\varepsilon$ is the effect of input noise in the system. Each vector is characterised in equation (5.14) and (5.15).

$$\theta[k] = \begin{bmatrix} 1 & V_T[k-1] & i_l[k] & i_l[k-1] \end{bmatrix}^T \tag{5.14}$$

$$\phi[k] = \begin{bmatrix} (1 - a_0)V_{oc}(SoC)[k] & a_0 & a_1 & a_2 \end{bmatrix}^T \tag{5.15}$$

With the determination of values in (5.14) and (5.15), the RLSEF is employed for estimating parameters of ECM. The RLSEF is comprehensively presented in Algorithm 1. K[k] is the adaption gain in the given algorithm.

Algorithm 3 RLSEF estimation for parameter identification

Initialise: $\theta(0)$, $P(0)$, and $\lambda(0)$
Input $\phi[k]$ based on (5.15)
Update covariance matrix using P[k]=$\frac{1}{\lambda}[1 - K[k]\phi^T[k-1]P[k-1]]$
Compute weighing factor using K[k] = P[k]$\phi[k]$
Prediction error $\varepsilon[k]$ = y[k] - ϕ^T[k - 1]$\hat{\theta}[k-1]$
Estimation $\hat{\theta}[k]$ = $\hat{\theta}[k-1]$ + K[k]$\varepsilon[k]$
Identify parameters using (5.9)

5.2.2 Estimation of the state of charge

Coulomb counting is the simplest technique that requires the use of measured current to determine SoC. However, the method does not incorporate methods to reduce the noises in the measurement and accumulation of error during estimation. Kalman filter, which uses a solution methodology called sequential probabilistic inference, is the most popular method to estimate SoC. The Kalman filter relies on using a dynamic electrical model (described in the previous subsection) that can capture the characteristics of the battery during charge and discharge.

Linear, extended, unscented or sigma point and particle filters are different approaches of Kalman filters used to date for estimating SoC. Extended Kalman filters (EKF) and Unscented Kalman filters (UKF) are widely used in literature for estimating SoC. However, EKF is less complex and computationally inexpensive when compared with UKF. Literature has also shown that the precision in estimating states is also not compromised [201,202]. Further, UKF relies on some unpredictable values to solve the equation to estimate states [201]. Hence, EKF with the values of components of ECM estimated using the algorithm in the previous subsection is used in this work to estimate SoC. EKF relies on the minimum value of the mean square estimate to determine the state and hence mitigates the impact of measurement noise and accumulated error.

Based on (5.6), the state equations in discrete form describing the dynamics are given in (5.16) and (5.17).

$$\begin{bmatrix} SOC_{k+1} \\ V_{1_{k+1}} \end{bmatrix} = \begin{bmatrix} 1 & 0 \\ 0 & e^{\left(-\frac{\Delta t}{R_1 C_1}\right)} \end{bmatrix} \begin{bmatrix} SOC_k \\ V_{1_k} \end{bmatrix} + \begin{bmatrix} \eta \frac{\Delta t}{C_n} \\ 1 - e^{\left(-\frac{\Delta t}{R_1 C_1}\right)} \end{bmatrix} i_k + w_k \tag{5.16}$$

$$y_{k+1} = OCV\,(SOC_{k+1}) + R_o i_k + V_{1_{k+1}} + v_{k+1} \tag{5.17}$$

The value of R_0, R_1 and C_1 is taken from the 5.2.1. The battery is a complex electrochemical system which is non-linear in nature. These non linearities are incorporated in mathematical

equations which can be represented using (5.18) and (5.19).

$$x_{k+1} = f(x_k, u_k) + w_k \tag{5.18}$$

$$y_{k+1} = f(x_{k+1}, u_k) + v_{k+1} \tag{5.19}$$

where x_k=$[SOC_k V_{fk}]^T$ are the states at time k, u_k is the input current at time k, $f(x_k, u_k)$ symbolises the dynamic of states at time step k, y_{k+1} is the system measurement at time step $k+1$, and $h(x_{k+1}, u_k)$ represents the measurement model. The EKF estimates the value of sates and determine the process using a feedback control mechanism involving steps of time and measurement update. The current and forward states are determined during time update while the measurement update is responsible for improving the posteriori estimate based on new measurement. An EKF is initialised with a state estimate of $\hat{x}(0)$, error covariance ($P(0)$), process noise covariance (Q) and R as the measurement noise covariance. The estimation of SoC is given in Algorithm 2, where, $\hat{x}_{k|k}$ is the posteriori estimate of the state at time step k given measurements up to time step k with a corresponding posteriori covariance $\hat{P}_{k|k}$, $F = \frac{\partial f}{\partial x}\Big|_{\hat{x}_{k|k}, u_k}$ is the linearized state transition matrix, and B is the input matrix applied to the current input, u_k, as in (5.16). The EKF has been shown to be successful at accurate SOC state estimation especially when it is fed with the correct covariance magnitudes for the state and measurement noise processes, Q and R. Further, the system model uncertainty with change in battery is incorporated by real time estimation of parameters used in EKF.

Algorithm 4 EKF estimation for SoC estimation

Input: $\hat{x}(0)$, $P(0)$, Q, R

Prediction steps

(I) **Priori estimate time update** $\hat{x}_{k+1|k} = F\hat{x}_{k|k} + Bu_k$

(II) **Error covariance time update** $\hat{P}_{k+1|k} = F\hat{P}_{k|k}F^T + Q_k$

Measurement update steps

(I) **Kalman gain matrix** $K_{k+1} = \hat{P}_{k+1|k}H_{k+1}^T (S_{k+1})^{-1}$

(II) **Posteriori estimate** $\hat{x}_{k+1|k+1} = \hat{x}_{k+1|k} + K_{k+1}\left[y_{k+1} - (h(x_{k+1}, u_{k+1}))\right]$

(III) **Error covariance measurement update** $\hat{P}_{k+1|k+1} = (I - K_{k+1}H_{k+1})\hat{P}_{k+1|k}$

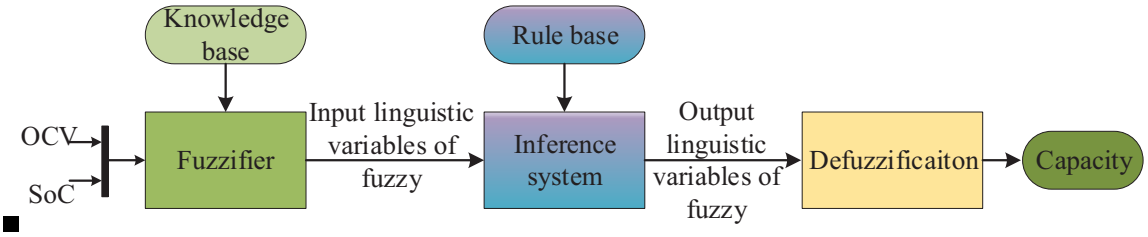

Fig. 5.4: A schematic representation of the capacity estimation

5.2.3 Capacity

Capacity is estimated using a fuzzy logic estimator (FLE). Unlike other state estimators, FLE does not require mathematical equations describing the dynamics of the system. The operation of the FLE is based on a set of rules defined by the developer using the knowledge base. The rules are framed to capture the non-linearity of a system. Further, studies have shown an increase in the accuracy of output of a FLE when an appropriate shape and number of membership functions are selected [19, 20]. In this work, the inputs to FLE are SoC estimated using EKF and the OCV computed based on impedance of the battery.

Mamdani and Sugeno are the two types of fuzzy logic systems widely discussed in the literature. Of the two, in this work, the Mamdani type FLE is used to determine capacity because of the possibility to define the rule base based on the developer's intuitive nature and the property of interpretability. The rules are defined using triangular MFs because of the simplicity in implementation, less computational cost and ability to yield optimal outputs. The two inputs viz. SoC and OCV are translated into 10 and 20 triangular MFs, respectively, while 20 MFs represent the output (capacity). Fig. 5.4 shows the structure of the FLE. Inputs are fuzzified and passed through an inference system. The inference system is supported by the rule base designed by developers, And, Or, implication and aggregation process. The centroid method is used for the defuzzification process. The output of the defuzzification process of FLE is the crisp value (capacity).

5.3 Experimental validation

To validate and check the effectiveness of the proposed battery parameter and state estimation algorithms, a practical setup is developed. Hardware-in-loop testing is a simplistic and fast

Table 5.1: Specifications of Experimental Setup

AC-DC converter	
Model	Description
M5060TB1000	1kV, 60 A
Output filter	1.5mH, 470uF
DC-DC Converter	
Parameters/Items	Description
Input and output voltages (Vin and Vdc)	200 V, 8 to 20 V
Input and output filter capacitors	470 uF, 10 uF
Inductor	8 mH
Switching frequency	30 kHz
Power MOSFET	IRP4768PbF
Power diode	40EPS16
Gate driver IC	HCPL-3120
Closed loop control	
Items	Description
Voltage transducer	LEM LV25-P,
Current transducer	LEM HO 50-S
Isolated power supply	ECL30UT03 GP 1132
Digital Signal Processor	TMS320F28335
Electronic Load	
Parameter	Description
Model	EL 2400,
Power	50-2400 W
Voltage and current control	(0-160) V and (0-100)A

approach to test the proposed algorithm in a practical system. The experimental setup developed to test algorithms is shown in Fig. 5.5. The setup comprises of a Crydom rectifier module-M5060TB1000, diode bridge rectifier with output LC filter, a DC-DC converter (buck topology), a controlled discharge circuit comprising of resistive load and Heliocentris programmable electronic load (EL2400), LEM LV25-P and LEM HO 50-S as voltage and current transducers, respectively. The specifications of the power converter and electronic load are given in Table 5.1. TMS320F28335, a 32-bit microcontroller with 12 bit, 12.5 M samples/second ADCs, is used to realize the close loop digital controller. The monitoring desktop is configured to perform a real-time simulation of the estimation algorithms, including impedance, SoC, and capacity of the battery. The proposed algorithm is verified in a new and an old battery based on the availability in the laboratory. The batteries are of lithium iron phosphate (LFP) electrochemistry. Both batteries are rated at 12.8 V nominal voltage and 12 Ah capacity. The details of the batteries are given in Table. 5.2. Apart from the mentioned details of the experimental setup, YOKOGAWA 700924 differential voltage probe and HAMEG HZ050 current probe are used to record appropriate current and voltage waveforms using YOKOGAWA DLM2054 oscilloscope.

Table 5.2: Specifications of batteries used

Details of battery		
Parameters	Old	New
Capacity	12 Ah	12 Ah
Nominal Voltage	12 V	12 V
Electrochemistry	LiFePO4	LiFePO4
Max charge voltage	14.6 V	14.6 V
Cut-off voltage	8 V	8 V

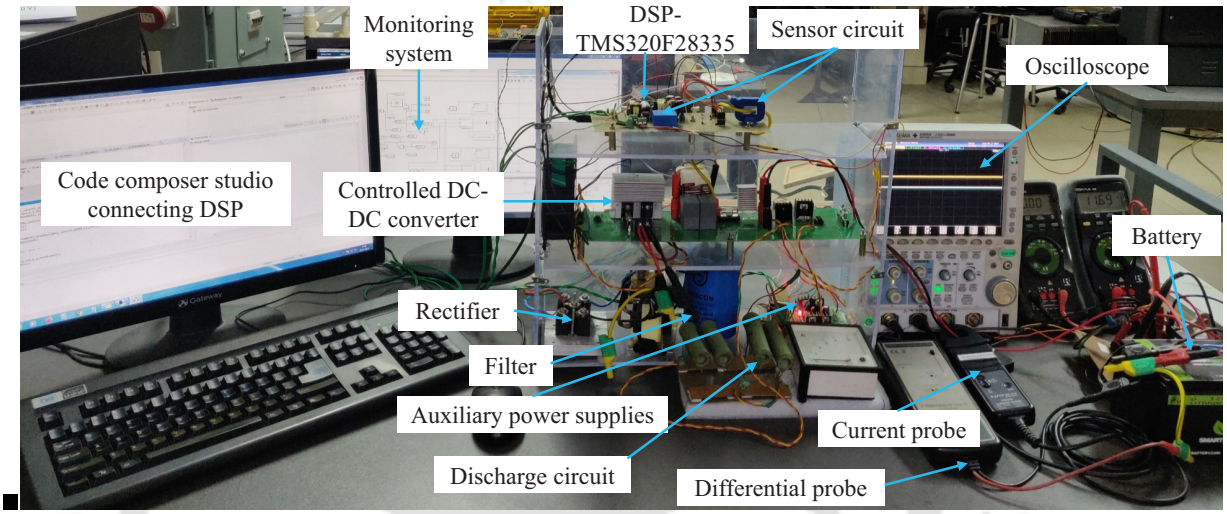

Fig. 5.5: A schematic representation of all the estimation

An overview of the algorithms implemented in the experimental setup is shown in Fig. 5.6. The figure comprehensively present all the algorithms and show the utilisation of the estimated impedance and related parameters of ECM. The state estimation starts only after the parameters are estimated.

5.3.0.1 Impedance estimation

The estimated impedance based on the process described in section 5.2. The impedance is used to determine the OCV and capacity. The parameters of the battery are identified online using RLSEF (5.2.1) is given in 5.3. The estimated values shows a higher ageing has a high value of impedance when compared to the new battery. Further, the resistance (R_0) of old is approximately 4 to 5 times higher in comparison with a new battery.

5.3.1 Parameter identification of the batteries

The process of estimation of the states requires parameters of the battery. This subsection will describe the process of identification of the battery.

Table 5.3: The parameters of the battery determined from test

ECM parameters of battery			
Parameters	R0	R1	C1
Old	0.898	0.17	3500F
New	0.19	0.05	1600F

5.3.1.1 OCV-SoC test

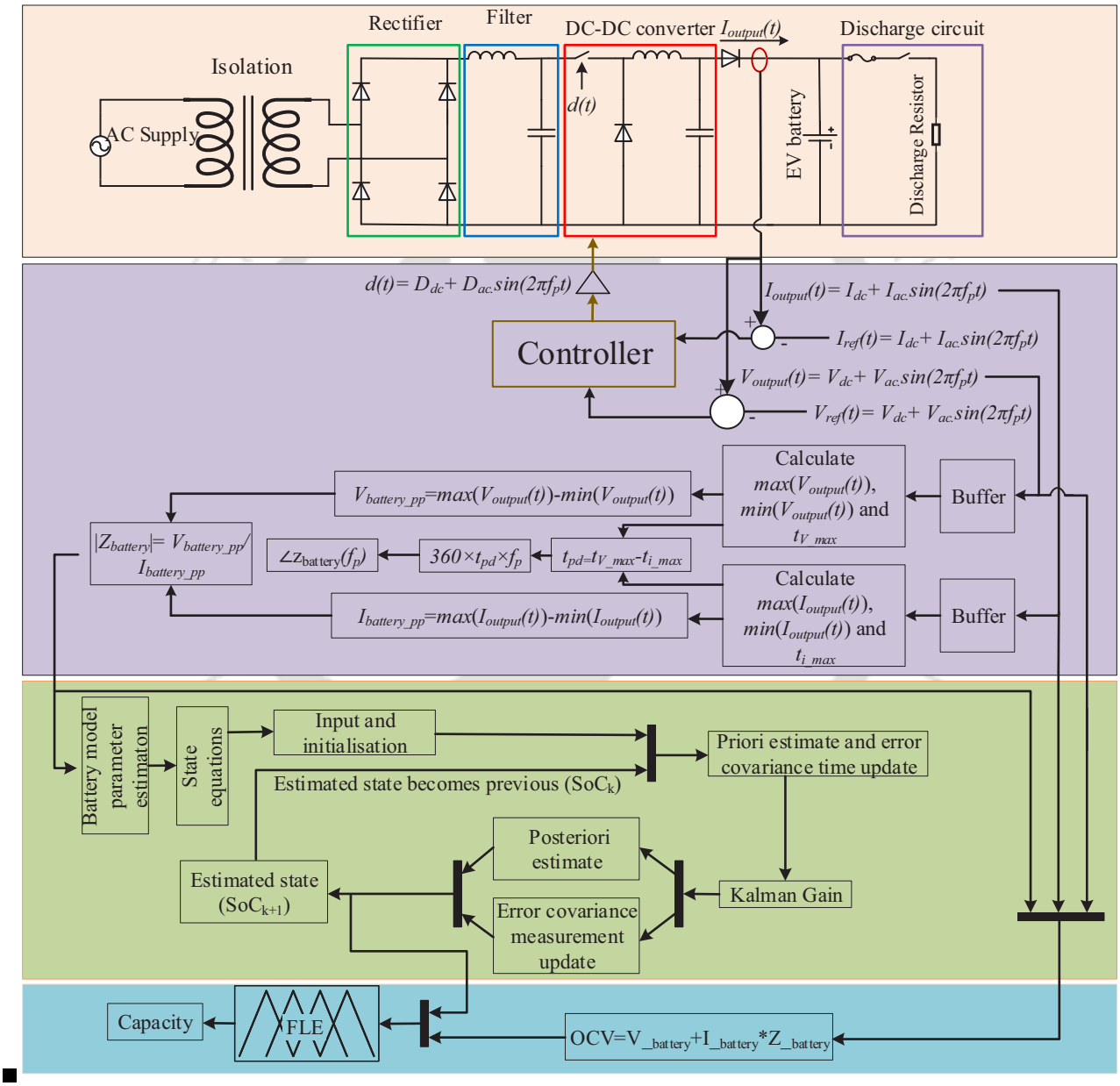

Fig. 5.6: A detailed schematic representation of all the estimations

The accurate estimation of the SoC requires determination of OCV. The OCV is estimated using (5.5). Further, OCV is a parameter which varies based on the changes in the equilibrium

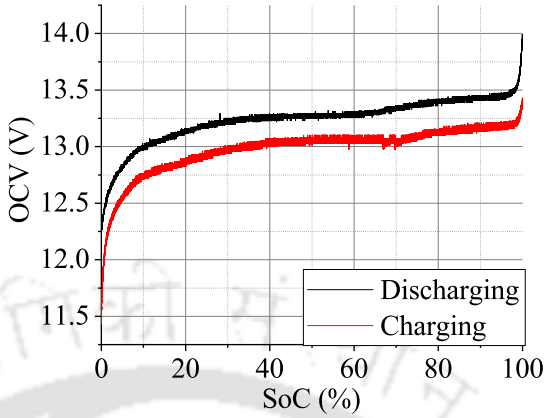

Fig. 5.7: OCV vs SoC plot of Old battery

potential of the battery. Hence, true OCV is determined either by allowing the battery to rest for an extended period such that the change in OCV is lower than 1mV/min or a very low (C/20) charging and discharging rate is used [190,203]. A very low charging and discharging rate allow the battery to remains close to electrochemical equilibrium. Using the relaxation time method is challenging, time consuming and have possible errors due to unknown relaxation times of battery. Hence C/20 charging and discharging method is used. The setup shown in Fig. 5.5 is used to perform the test.

SoC in this work is estimated using EKF based on the online ECM parameters estimated and the OCV-SoC curve. The working of the EKF is described in the previous section. The OCV-SoC curve is used to determine a relationship in the form of a higher-order polynomial equation. Although the work is focused on determining SoC during charging, both charging and discharging are done to record the effect of hysteresis in the battery due to ageing. The discharge test starts after inspecting the terminal voltage is 14.6 V, which infers to the full charge state of the battery. Since at a lower charge and discharge rate, the terminal voltage is equal to OCV, a constant discharge of C/20 is performed, monitoring the terminal voltage of the battery. On reaching 8 V, the cut-off voltage of the battery, the batteries are discharged at a constant voltage to reduce the discharge current to C/50. After complete discharge, the batteries are charged at C/20 rate up to 14.6 V. On reaching 14.6 V, the CV mode is activated until the charge current reduces to C/50.

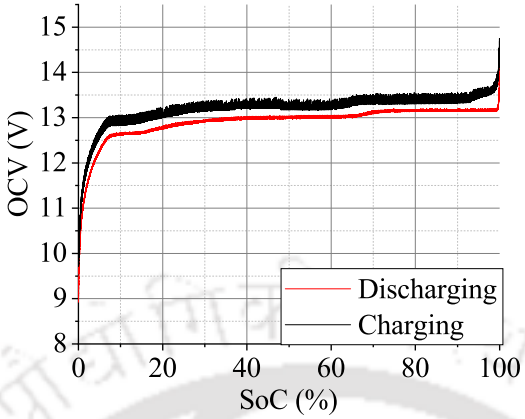

Fig. 5.8: OCV vs SoC plot of new battery

5.3.1.2 SoC and capacity estimation

The monitoring of the terminal voltage leads to the OCV values, and the current help to determine the SoC using the coulomb counting (CC) method 5.20.

$$SOC_k = SOC_0 - \int_{k_0}^{k} \eta_c I_L(\tau) d\tau / C_{nominal,k} \tag{5.20}$$

where, SOC_0 is the initial SoC of the battery, η_c is the charge or discharge efficiency, $I_L(\tau)$ is the charge or discharge current at time τ, and $C_{nominal,k}$ is the nominal capacity. While performing the charge-discharge test, since the terminal voltage is either maximum or minimum, the SOC_0 is taken as 100% or 0%, respectively. The SoC determined using CC is used as a reference while validating the estimated SoC using EKF. The OCV-SoC curve is shown in Figs. 5.3.1.1 and 5.3.1.1. The difference between charging voltage and the discharging voltage for the old battery is more signifying the increase in the hysteresis with the ageing of the battery. A ninth order polynomial fit is performed to use in the SoC estimation of battery using EKF. The coefficients are given in Table 5.4. The next subsection will present a robustness study in estimation based on the estimated parameters during different charging techniques.

The estimated SoC and OCV is used to estimate the capacity using FLE. Since SoC and OCV are translated into 10 and 20 MFs, respectively, 200 rules are formulated in the rule base supporting the inference system. The accuracy in the estimation of the FLE depends on the number of MFs. The capacity used for comparison is determined using the current and time

Table 5.4: Coefficients of the relation between OCV-SoC curve

Lithium Iron Phosphate					
Order	0	1	2	3	4
Coefficients	10.55	78.24	-1023.65	6957.22	-27107.4
Order	5	6	7	8	9
Coefficients	64068.09	-93549.8	82547.1	-40375.9	8409.49
Lithium polymer battery					
Order	0	1	2	3	4
Coefficients	12.08	21.65	-257.29	1741.58	-6968.4
Order	5	6	7	8	9
Coefficients	17171.5	-26373	24585.76	-12715.7	2795.31

data logged using the OCV-SoC test.

5.3.2 Validation of proposed algorithms for different charging techniques

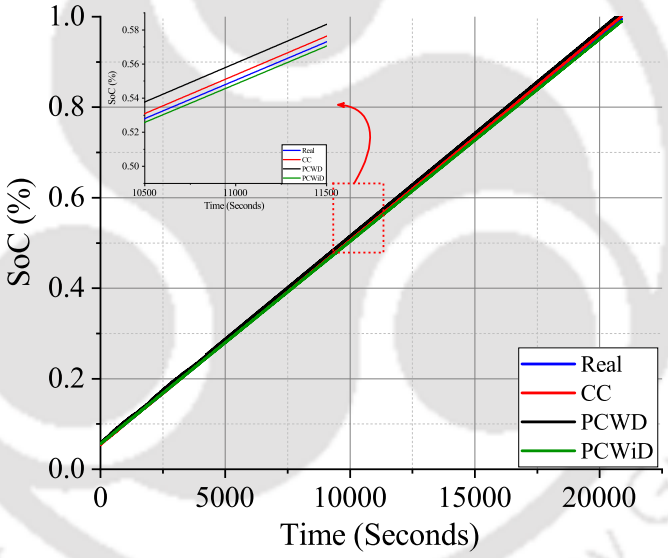

Fig. 5.9: Estimated SoC of new LFP battery

The estimation of impedance, SoC and capacity is validated for three different types of charging algorithms viz. constant current (CC), pulse charging without discharge (PCWD), and pulse charging with discharge (PCWiD). Constant current constant voltage (CCCV) is dominated by CC timing and have a very small change in SoC and capacity during CV. Further, the results of CCCV is identical to CC. Hence, the results are not shown in the plots given in this paper. All the experiments are performed at a fixed charging current of 2A. In case of PCWD and PCWiD, the average charging current is maintained at 2A. A period of 60 seconds are fixed for PCWD and PCWiD. The values of peak amplitude of current (I_{peak}), off time (t_{off}), on

time (t_{on}), rest period (t_{off} in PCWD and $2t_{off} + t_d$ in PCWiD) and discharge pulse period is determined based on (5.21) and (5.22).

$$I_{avg} = \frac{t_{on}}{t_{on} + t_{off}} \times I_{peak} \tag{5.21}$$

$$I_{avg} = \frac{t_{on}}{t_{on} + 2t_{off} + t_d} \times I_{peak} \tag{5.22}$$

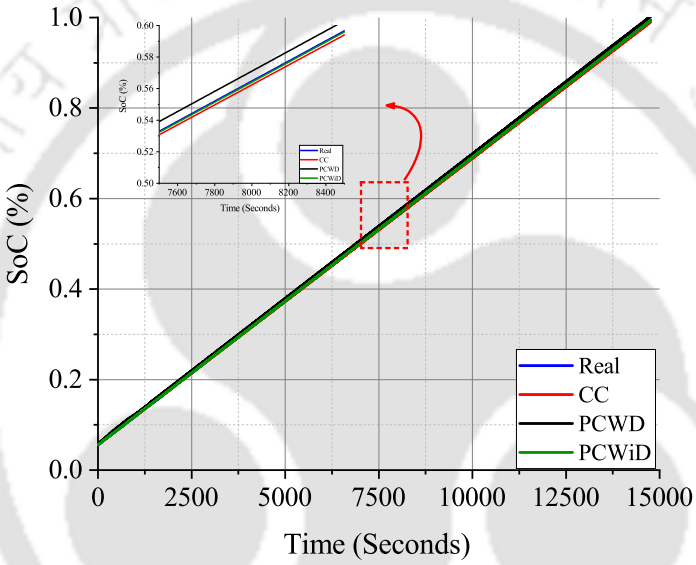

Fig. 5.10: Estimated SoC of the old LFP battery

With an increase in rest periods, the peak amplitude increases to maintain the same average current. Further, addition of a discharge pulse further add to an increase in the peak amplitude. In this work, the time period of a pulse for both PCWD and PCWiD is kept 60 seconds. Hence, for PCWD, to maintain an average current of 2 A, the I_{peak} is 2.5A for t_{on} = 48 seconds and t_{off}=12 seconds. Similarly, for PCWiD, for maintaining an average current of 2 A, the I_{peak} is 3.142 for t_{on}=48 seconds and t_{off}=6 seconds and t_d=6 seconds. The estimated SoC and capacity are shown in Fig. 5.3.2 – Fig. 5.3.2. In the plots, the real SoC and capacity are the values computed while determining OCV-SoC curves. The plots of SoC and capacity follows the real values for each charging technique. Further, robustness of the estimation algorithm is determined in next subsection.

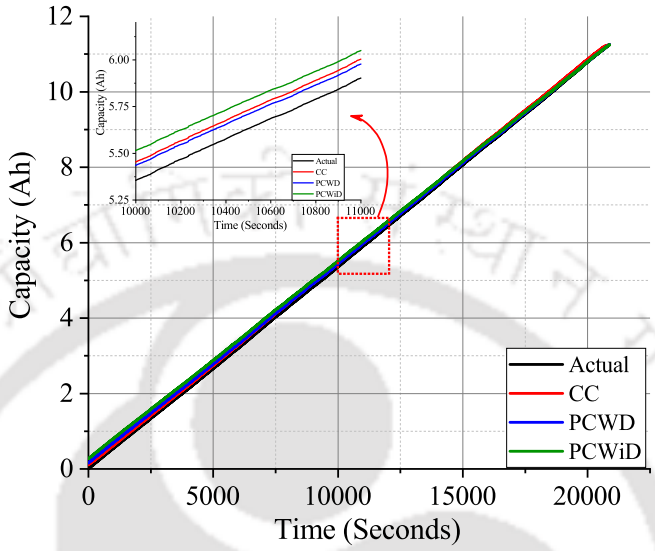

Fig. 5.11: Estimated capacity of the new LFP battery

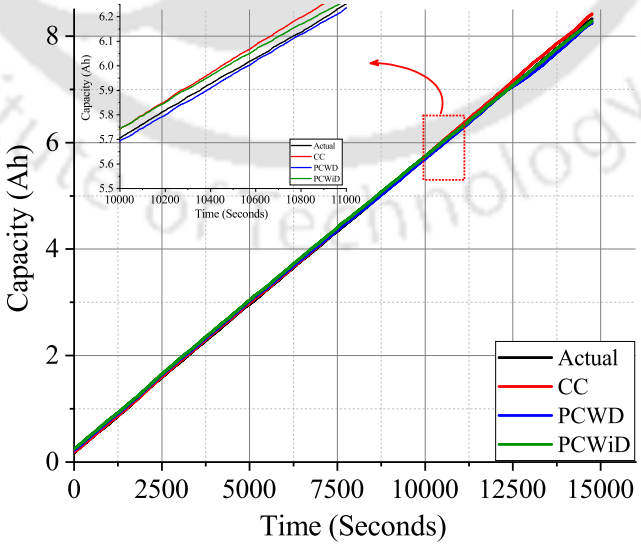

Fig. 5.12: Estimated capacity of the old LFP battery

5.3.3 Robustness study against variation of charging techniques

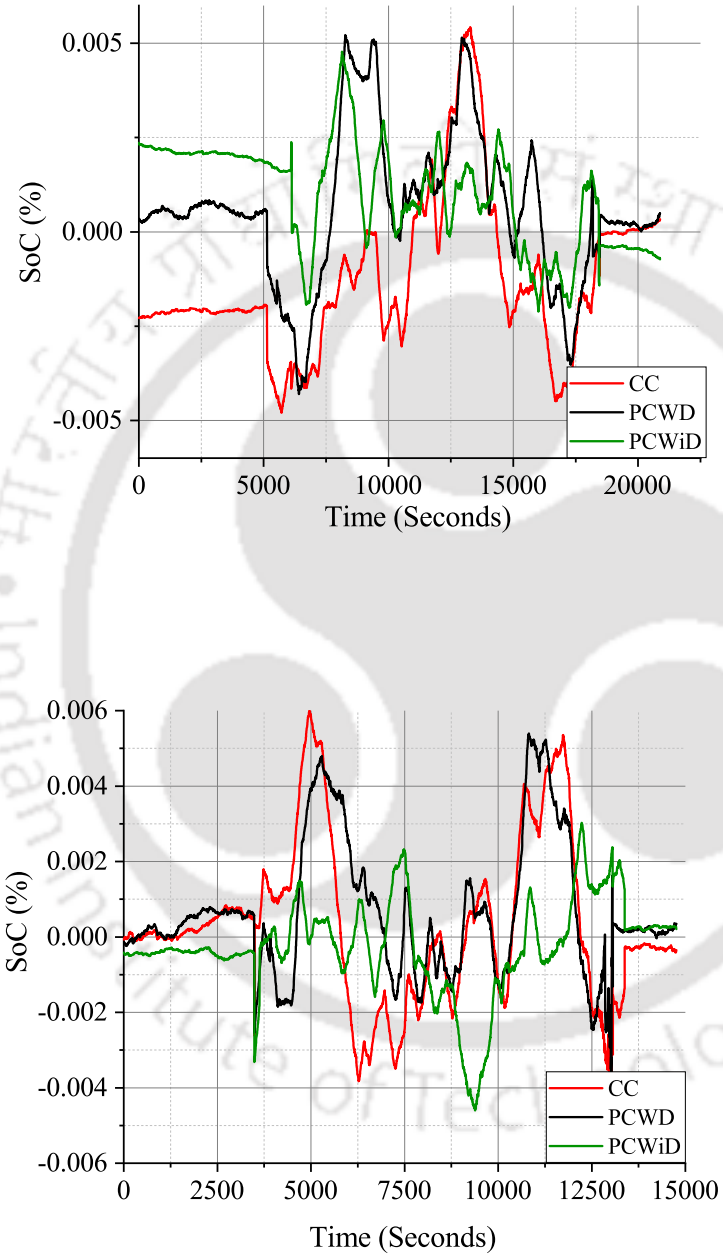

Fig. 5.13: Error in SoC estimation

The work in literature performs robustness study by varying the values of impedances and adding noise. In this work, the estimation is performed in a real time system with actual noise. Further, to verify the robustness with ageing an aged battery which has degraded by approximately 25% to its full capacity is considered. The mean average percentage error between

Table 5.5: MAPE of estimated quantities

		CC	PCWD	PCWiD
Old	SoC	0.00251	0.0023435	0.001699
New		0.002647	0.00252	0.00176
Old	Ah	0.05504	0.1404	0.137
New		0.09982	0.0988	0.0599

actual values and the estimated is calculated as a robustness parameter. The computed values are given in Table 5.5. The estimation error in SoC and capacity is least when CC technique is used while the estimation error is highest when PCWiD is used. The increase in the error is because of the changes in the voltage during periods of t_{on} and t_{off} in PCWD and additional t_d in PCWiD. The voltage fall to a small value during periods of t_{off} and t_d. The deviation from the OCV-SoC curve determined in Section X is a major reason for the error in both SoC and capacity estimation. However, less error in estimation of SoC and capacity even with deviation from OCV-SoC plot shows robustness in the proposed parameter estimation algorithm.

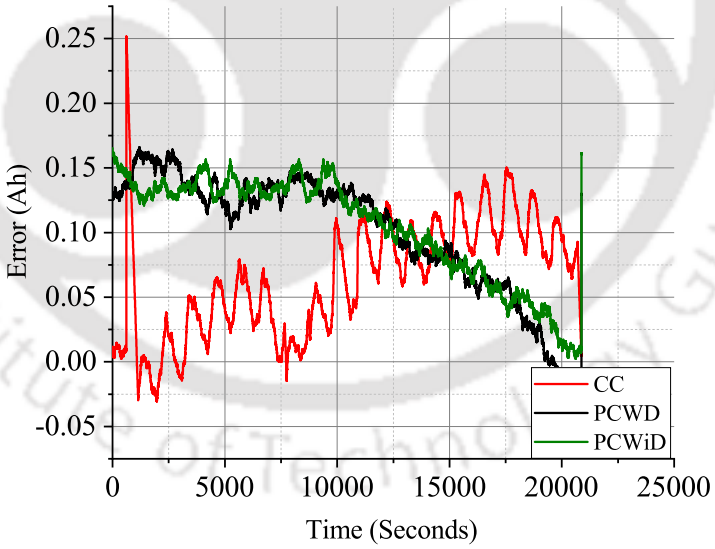

5.4 Conclusion

In this work, a proposal to estimate the parameters and states of the batteries is presented. Impedance and the ECM parameters are required when a model-based state estimation is performed. The impedance estimation is proposed to be performed without the requirement of any extra circuitry or formulation of a complex algorithm. The existing power electronics circuit,

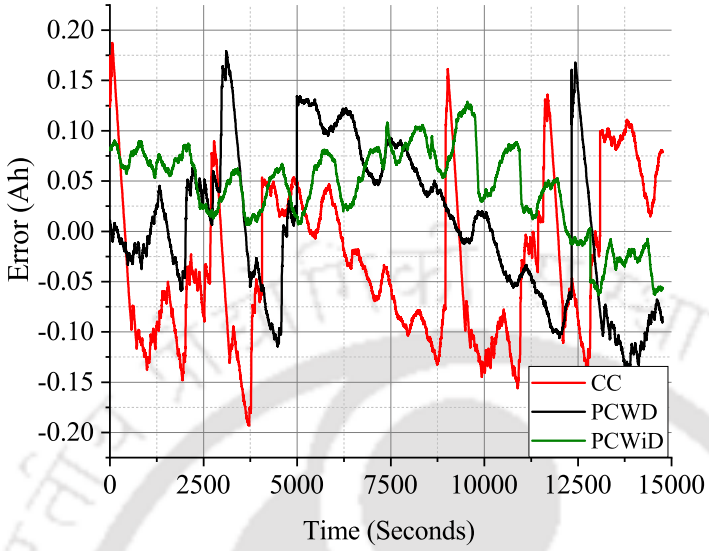

which is used to charge the battery, can generate required signals by modifying the reference signal. Hence, the work open directions for chargers with integrated parameter and state estimations. The impedance of a battery varies due to electrochemical changes leading to degradation of capacity or ageing. The real-time determination of parameters further adds accuracy in estimating related states such as SoC and capacity. The proposed algorithms for estimation of parameter and states of battery is implemented in an experimental setup. The accuracy of the algorithms are checked by using the algorithms while charging batteries by different charging types, viz CC, pulse charging without discharge, and pulse charging with discharge. Further, two types of LFP batteries- new and aged are used to validate the proposal to estimate accurately irrespective of a large change in impedance due to ageing. The accuracy of the proposed online estimation algorithm proves the competency and ability to reduce the impact of ageing.

6

Li-ion Battery Degradation: Developing Insight to Propose a new Charging Technique

Contents

"Man is made by his belief. As he believes, so he is!"

– Srimad Bhagwat Gita

6.1 Introduction

The study on the parameter variations of Li-ion batteries involves experimental procedures that require enormous time and precise measurement instruments. Mathematical models which capture various phenomena within the battery are replacements for the experiments. Hence, mathematical models are widely proposed and used in the literature to design new battery or manage battery systems. Butler-Volmer equations and Nernst's theory are the earliest approaches to describe the physics in batteries. The Butler-Volmer equation relates the current density and the overpotential in batteries [204]. In contrast, Nernst's equation describes the electric potential of the electrode and electrical charge in the battery [205]. These equations were simple, but it was not sufficient to describe the complex physics of advanced Li-ion chemistries. Newman et al. developed the porous electrode theory, which became a standard mathematical model for Li-ion batteries. The model is popularly reported as Doyle-Fuller-Newman (DFN) model in literature [206, 207]. The Butler-Volmer and Nernst equations use differential-algebraic equations, while the DFN model use partial differential equations. The equations of the DFN model are solved using a variety of numerical solving tools like control volumes, finite-difference methods, finite element methods, orthogonal collocation and others. The challenge in using DFN is the complexity to solve the equations even after using the listed variety of numerical solving tools.

Alternatively, equivalent circuit and simplified electrochemical models such as single-particle model and single-particle model with electrolyte are developed to meet the challenges of complexity, computational cost (speed and memory) and fast convergence to get results. Although alternative models solve the challenges, literature reports the requirement of correction factors to get appropriate results [208]. Hence, in this work, DFN is selected to analyse the battery's electrical, electrochemical, and mechanical parameters. The parameters of the battery used to simulate are given in Table 6.1 [2]. Apart from the parameters, various constant used in the

simulation are also given in the table.

Table 6.1: The table shows the parameters of cell used for simulating the different types of charging at different rates. The cell parameters are taken from [2] and the additional data required for the degradation models are those predefined in PyBaMM.

Parameter	Symbol	Units	Anode	Cathode
Length of the electrode	L_i	μm	88	80
Conductivity of electrode	σ	S/m	100	100
Volume fraction of solid phase	ϵ_1		0.49	0.59
Volume fraction of liquid phase	ϵ_2		0.485	0.385
Film thickness	δ	μm	2	2
Maximum Li ion in sold phase		mol/m^3	30555	51555
State of charge	θ_0		0.03	0.95
Diffusion coefficient of solid phase	D_1	m^2/s	3.9×10^{-14}	1×10^{-14}
Rate constant of electrochemical reactions	κ	$A/m^2/(mol/m^3)^{3/2}$	4.854×10^{-6}	2.252×10^{-6}
Anodic transfer coefficient of electrochemical reactions	α_a		0.5	0.5
Anodic transfer coefficient of electrochemical reactions	α_b		0.5	0.5
Initial Li ion in sold phase		mol/m^3	1000	1000
Diffusion coefficient of liquid phase	D2	m^2/s	7.5×10^{-14}	7.5×10^{-14}
Transference number of Li ion	t^+		0.363	0.363
Faraday constant	F	$C.mol^{-1}$		
Gas constant	R	$J.mol^{-1}K^{-1}$		

The governing equation of the DFN model is classified in three parts namely, charge conservation, molar conservation and electrochemical reactions. Each of them are discussed in detail in [208–210]. The experiments performed by simulating different charging techniques are focussed to meet the objective of proposing a battery friendly charging technique irrespective of change in ambient temperature and the requirements of any C_{rate}. The results obtained are analysed to find the impact of change in C_{rate}, charging technique, ambient temperature and increase or decrease in time period of pulses, t_{on}, t_{off}, amplitude of charge and discharge pulses in variants of pulse charging. The extensive simulation and analysis performed on the selected battery help to select charging techniques which is suitable for either energy extensive application or power extensive application.

Table 6.2: Summary of the variation of parameters with increase in the charging rate in different charging techniques. I_d is the amplitude of discharge current†, $^{\#}$, $\Downarrow$, $\Uparrow$, and * resembles decreasing, increasing, decreasing trend, increasing trend and negligible change, respectively.

Sl. No	Parameters	CC	CCCV	Pulse charging without discharge					Pulse charging with discharge			
									I_d			
		$C_{rate}{}^{\#}$	$C_{rate}{}^{\#}$	$t_{on}{}^{\dagger}$	$t_{on}{}^{\dagger}$	t_{on} & $t_{off}{}^{\dagger}$	$C_{rate}{}^{\#}$	t_{on}	0.5	1	2	$C_{rate}{}^{\#}$
1	X-averaged negative electrode inactive material volume fraction	$\Downarrow$	$\Downarrow$	$\Downarrow$	$\Downarrow$	$\Downarrow$	$\Downarrow$	$\Downarrow$	$\Downarrow$	$\Uparrow$	$\Downarrow$	$\Downarrow$
2	X-averaged total negative electrode SEI thickness [m]	$\Downarrow$	$\Downarrow$	$\Downarrow$	$\Downarrow$	$\Downarrow$	$\Downarrow$	$\Downarrow$	$\Downarrow$	$\Uparrow$	$\Downarrow$	$\Downarrow$
3	X-averaged negative electrode porosity	$\Downarrow$	$\Downarrow$	$\Downarrow$	$\Downarrow$	$\Downarrow$	$\Downarrow$	$\Downarrow$	$\Downarrow$	$\Uparrow$	$\Downarrow$	$\Downarrow$
4	X-averaged negative electrode tortuosity	$\Uparrow$	$\Uparrow$	$\Uparrow$	$\Uparrow$	$\Uparrow$	$\Uparrow$	$\Uparrow$	$\Uparrow$	$\Downarrow$	$\Uparrow$	$\Uparrow$
5	X-averaged negative electrode reaction overpotential [V]	$\Uparrow$	$\Uparrow$	$\Downarrow$	$\Downarrow$	$\Downarrow$	$\Uparrow$	$\Downarrow$	$\Uparrow$	$\Downarrow$	$\Uparrow$	$\Uparrow$
6	X-averaged negative electrode extent of lithiation	$\Downarrow$	$\Downarrow$	$\Downarrow$	$\Downarrow^{*}$	$\Downarrow$	$\Downarrow$	$\Downarrow$	$\Downarrow$	$\Uparrow$	$\Uparrow$	$\Downarrow$
7	X-averaged cell temperature [K]	$\Uparrow$	$\Uparrow$	$\Uparrow$	*	$\Downarrow$	$\Uparrow$	Low C_{rate} =$\Uparrow$ and High C_{rate} =$\Downarrow$	$\Downarrow$	Low C_{rate} =$\Uparrow$ and High C_{rate} =$\Downarrow$	$\Downarrow$	$\Uparrow$
8	Capacity fade	$\Uparrow$	$\Uparrow$	$\Downarrow$	$\Downarrow^{*}$	$\Downarrow$	$\Uparrow$	$\Uparrow$	$\Downarrow$	$\Uparrow$	$\Uparrow$	$\Uparrow$
9	X-averaged negative electrode particle crack length	$\Uparrow$	$\Uparrow$	$\Uparrow$	$\Uparrow$	$\Uparrow$	$\Uparrow$	$\Uparrow$	$\Downarrow$	$\Uparrow$	$\Uparrow$	$\Uparrow$

6.2 Variation of parameters in normal ambient temperature at different C_{rate} and charging techniques

6.2.1 SEI layer thickness

Side reactions in Li-ion batteries occur in three major regions viz. electrode-electrolyte interfaces, electrode-collector interface and electrolyte [211]. Change in the equilibrium potential of the reactions during charging and discharging leads to instability in the electrolyte. The instability is accompanied by the start of side reactions within battery [212]. The change in the equilibrium potential depends on the amplitude of the charging current and the types of charg-

ing. Hence, the concentration of the inactive materials and electrode-electrolyte interfaces or SEI layer thickness varies for different charging types and rates. Although the SEI layer is a by-product of side reactions, it is a required protective layer in graphite particles of negative electrodes in the battery. The lithium potential makes the electrolyte unstable and vulnerable to the reaction, which leads to the loss of lithium and a reduction in the overall capacity of batteries. Since it is a form of inactive material, the variation of the concentration of inactive material and the thickness of SEI layer are similar as shown in Fig. 6.5 and Fig. 6.2.1. The thickest SEI layer is formed in CC and CCCV, followed by CT9, which is pulse charging with discharge. The SEI layer thickness for all charging rates is also highest in CCCV. During CCCV, the time for the CV phase is higher and increases with an increase in the number of cycles. During CV, the stress due to electrochemical reactions and temperature is lower than the CC phase, leading to stable SEI formation [39]. Hence, with an increase in the number of cycles, the SEI layer keeps becoming thicker. Further, the formation of SEI is also higher at lower charging rates for the same reason as seen in Fig. 6.2.1.

The plot in Fig. 6.2.1 shows that pulse charging has the potential to reduce the SEI layer thickness. The SEI layer thickness in charge type 3 to 8, which is pulse charge without discharge, varies with the change in the t_{on}. The thickness is highest in charge type 3, which has the maximum t_{on}, while charge type 5 has the lowest because of the least t_{on}. The t_{off}, too, impacts the thickness of the SEI layer. With a decrease in the t_{off}, the SEI layer thickness is reduced. A reduced t_{on} as well as the t_{off} help to suppress the thickness of the SEI layer. A larger t_{on} at a lower C_{rate} act similar to CCCV. Even at a higher C_{rate}, the rest phase of the pulse will help to stabilise the SEI layer leading to thickening with an increase in the number of cycles. Hence, a decrease in t_{on} and t_{off} help reduce the SEI layer's thickening.

The variation in the change of SEI layer thickness for pulse charging with discharge is shown in charge type 9 to 15 in Fig. 6.2.1. Majority of the pulse charging with discharge charge type help in reducing the SEI layer thickness. The SEI layer thickness has a reducing trend for charge type 9 to 11, although the variation is not much for charge type 10 and 11. The amplitude of discharge current, too, had a role in the change in the SEI layer thickness. When

the amplitude of the discharge current is equal to the average current (charge type 9 to 11), with the reduction in t_{on}, the SEI layer thickness is also reduced.

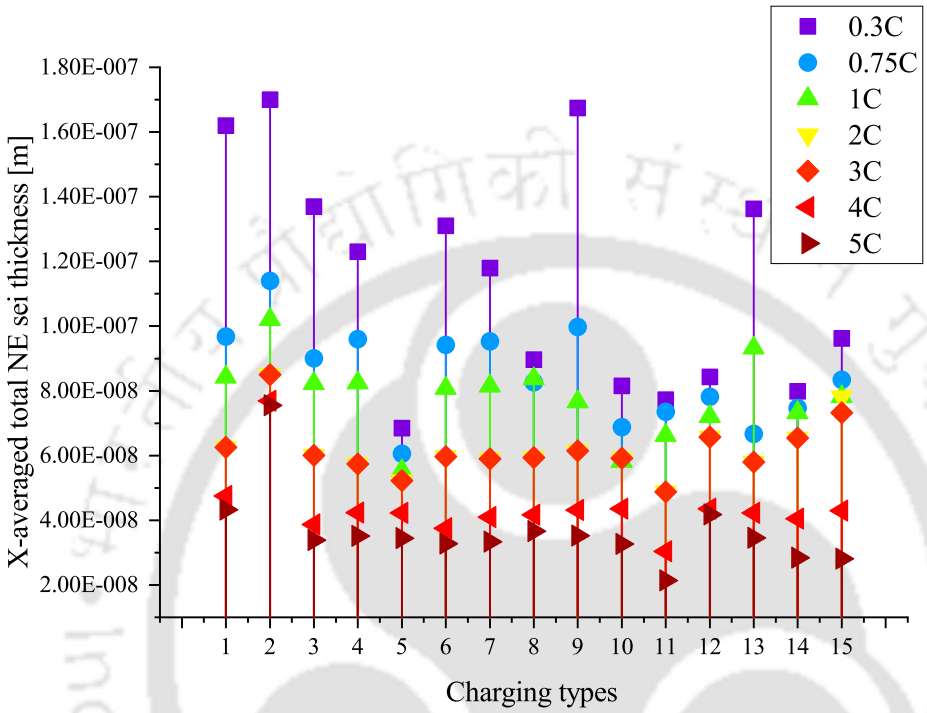

Fig. 6.1: Variation of parameters of the batteries at different charging techniques and charging rates : (a) The X-averaged total negative electrode SEI thickness [m] decreases with increase in C_{rate} as the chemical degradation is dominant at slower C_{rate}; (b) X-averaged negative electrode particle crack length increases with increase in C_{rate} because of the increased stress in electrode particles; (c) X-averaged cell temperature [K] is higher for higher C_{rate} due to the increase in chemical kinetics. The discharge pulses further instigates the phenomenon because of the change in the direction of motion of ions and masses;(d) Capacity is a function of chemical and mechanical parameters and internal change in temperature.

Further, when the amplitude of the discharge current is equal to half of the average current (charge type 12 and 13), a higher on-time resulted in less SEI layer thickness. On the contrary, when the amplitude of discharge current is equal to the twice average current, a higher on-time resulted in a thicker SEI layer. The change in the polarity of the charge pulses leads to a similar variation of equilibrium potential. When the amplitude of the current in the discharge pulse is more than the charge pulse, the equilibrium potential falls below the electrolyte's stability limits, accelerating the SEI formation. The rest phase further helps to stabilise the SEI formed, leading to a thick SEI layer in comparison when the amplitude of the current in the discharge pulse is less than or equal to the charge pulse. The charge type with amplitude of discharge

current equal to the average current and least t_{on} and rest time have thinnest SEI layer formed over the negative electrode.

6.2.2 Particle crack length

Particle cracking is a form of mechanical degradation in battery observed in the electrode particles. The stress in electrode particle are commonly modelled or experimentally reported due to intercalation/deintercalation reaction and changes in internal cell temperature variations or ambient temperature variations. The crack in the particles results in exposure to the surface of active materials leading to side reactions. These side reactions further lead to heat generations, amplifying the phenomenon of stress and side reactions due to an increase in cell kinetics [213]. Hence, an increase in mechanical degradation increases the chemical degradation and vice-versa.

Fig. 6.2.2 shows the variation of particle crack length on the application of different types of charging techniques at different charging rates. The slower charging rates resulted in the least particle cracking. There is an increase in the particle crack length on going from left to right. The CC and CCCV resulted in the least crack length, although CCCV has higher values when compared to CC. Since at higher potential of battery, the stress on the particles of electrodes is higher, CCCV resulted in higher crack length. In CC, the battery is allowed to settle with a reducing charge current. Since the battery is not allowed to settle and overpotential remains higher, the stress due to increased potential of battery and saturation of electrodes is not experienced. While in the case of CCCV, the battery keeps on charging after switching to CV. With increase in potential, the stress on particles of electrodes continue to increase. Hence, the particle crack length is more than CC.

The pulse charging techniques that resulted in a better candidate for fast charge when previous parameters were considered do not perform well. The reason behind the increase in the crack is related to the heat generation during the intercalation and deintercalation reaction. The heat generation adds to the internal battery temperature rise, increased chemical kinetics, and stress in the electrodes particle. The higher the rise in internal cell temperature (Fig. 6.2.3), the higher is the particle crack length. Hence, a change in the ambient temperature might result in

an increase or decrease in particle cracking. During pulse charging with discharge, the increase in the amplitude of the discharge pulse resulted in a further increase in the particle crack length.

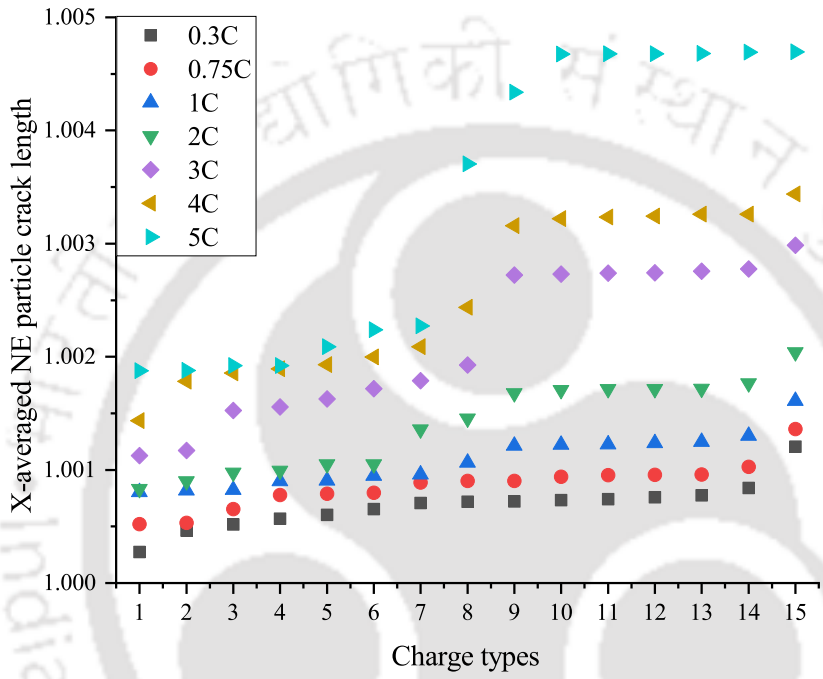

Fig. 6.2: Variation of parameters of the batteries at different charging techniques and charging rates : (a) The X-averaged total negative electrode SEI thickness [m] decreases with increase in C_{rate} as the chemical degradation is dominant at slower C_{rate}; (b) X-averaged negative electrode particle crack length increases with increase in C_{rate} because of the increased stress in electrode particles; (c) X-averaged cell temperature [K] is higher for higher C_{rate} due to the increase in chemical kinetics. The discharge pulses further instigates the phenomenon because of the change in the direction of motion of ions and masses;(d) Capacity is a function of chemical and mechanical parameters and internal change in temperature.

6.2.3 Cell temperature

The internal cell temperature is a major factor impacting the capacity fade of batteries. The temperature brings changes in equilibrium potential of reactions within the battery, the chemical kinetics which affects the rate of side reactions, SEI layer formation and erosion, the diffusivity of charge and mass in electrodes, stress in battery, structure disordering or electrodes and overall geometry, and safety in the operation of battery [64, 146].

A higher C_{rate} resulted in an increase in the heat generation due to rapid diffusivity of charges

and increased stress in the electrode particles. The conventional CC and CCCV had control on the rise in the internal cell temperature. However, during pulse charging with discharge, the temperature rose to a very high value. The temperature rise is related to the ease in the diffusivity of charge in the battery both during intercalation and intercalation. With an increase in the SEI layer thickness, decrease in porosity and increase in the tortuosity of electrodes, the charge and mass transfer are offered resistance. The increase in the resistance adds to the heat generation and impacts the stability of electrolyte.

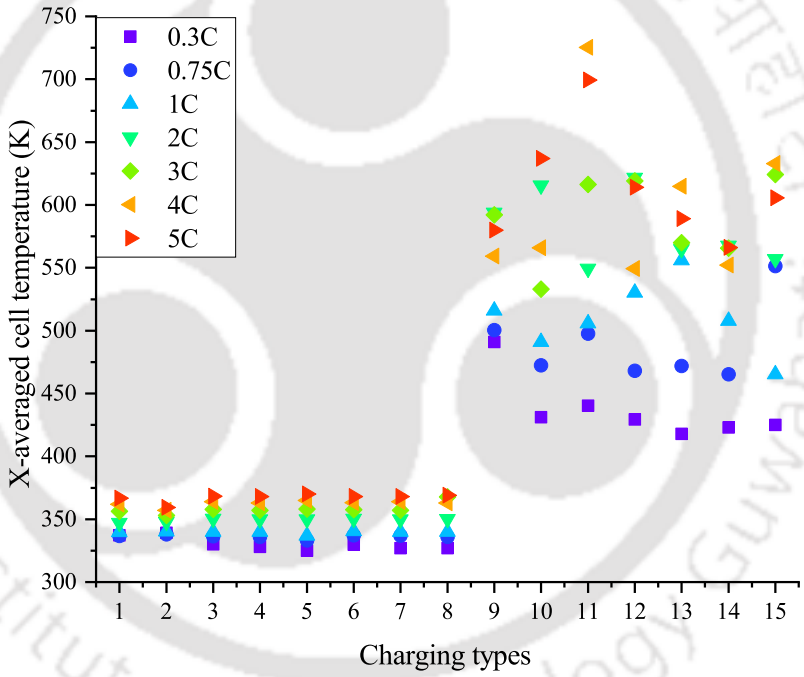

Fig. 6.3: Variation of parameters of the batteries at different charging techniques and charging rates : (a) The X-averaged total negative electrode SEI thickness [m] decreases with increase in C_{rate} as the chemical degradation is dominant at slower C_{rate}; (b) X-averaged negative electrode particle crack length increases with increase in C_{rate} because of the increased stress in electrode particles; (c) X-averaged cell temperature [K] is higher for higher C_{rate} due to the increase in chemical kinetics. The discharge pulses further instigates the phenomenon because of the change in the direction of motion of ions and masses;(d) Capacity is a function of chemical and mechanical parameters and internal change in temperature.

The impact of the increase in internal cell temperature is deteriorating in nature. The increase in the temperature induces stress in the electrode particles and erodes the SEI layer. On erosion, the surface of active material or electrode particles are unlatched to further side re-

actions. Apart from forming the SEI layer, the side reactions leave behind residual inactive materials and gases, which are generated due to phase transition from solid to gas or liquid to gas. An uncontrolled rise in the temperature is imperative to lead to thermal runaway and harm the safety of the battery being charged pr discharged. Fig. 6.2.3 infers that conventional CC and CCCV and pulse charging without discharge are effective methods to perform fast charge with a limited rise in internal battery temperature.

6.2.4 Discharge capacity

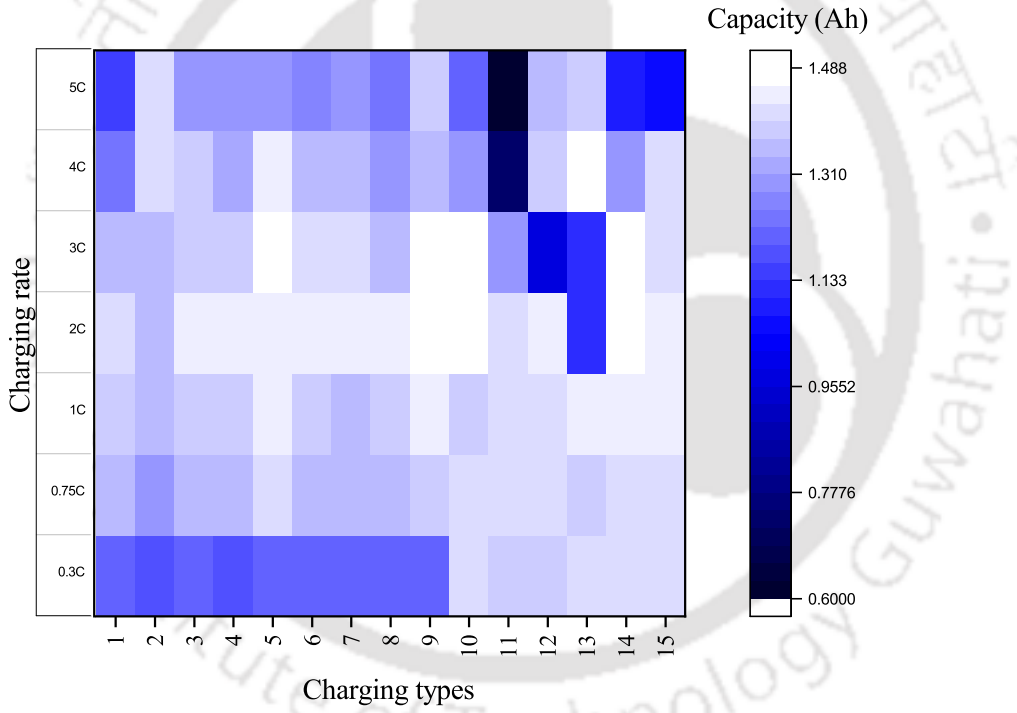

Fig. 6.4: Variation of parameters of the batteries at different charging techniques and charging rates : (a) The X-averaged total negative electrode SEI thickness [m] decreases with increase in C_{rate} as the chemical degradation is dominant at slower C_{rate}; (b) X-averaged negative electrode particle crack length increases with increase in C_{rate} because of the increased stress in electrode particles; (c) X-averaged cell temperature [K] is higher for higher C_{rate} due to the increase in chemical kinetics. The discharge pulses further instigates the phenomenon because of the change in the direction of motion of ions and masses;(d) Capacity is a function of chemical and mechanical parameters and internal change in temperature.

Discharge capacity is the final parameter of the battery, which determines the performance of the battery. Discharge capacity depends on various parameters discussed in previous subsections. The reduction in capacity fade depends on the C_{rate} and the types of charging techniques

as shown in Fig. 6.2.4. The C_{rate} impacts the rate of chemical kinetics, equilibrium potential and stress due to intercalation reactions. An increase in the mentioned parameters increases the overpotential while vice-versa reduce the overpotential. At higher C_{rates}, the overpotential rises and leads to an increase in the terminal voltage. Since the battery terminal voltage reaches the cut-off potential much earlier, the electrode is not lithiated fully.

The battery does not charge to the full range of SoC. When CCCV is used to charge, the CV part of charging allows the battery to be charged in a wider SoC range as the rise in overpotential is countered by a fall in current. Further, the time to charge also impacts the reduction in discharge capacity. A larger time period will lead to increased stress on electrode particles due to increased concentration gradients [1]. Increased stress adds to SEI erosion and further side reactions leading to loss of active particles and Li-ions [214].

In Fig. 6.2.4, it can be seen that CCCV leads to larger capacity loss at slower C_{rate} when compared to CC, but at a higher C_{rate}, the CC leads to larger capacity loss. A similar pattern is seen in the case of pulse charging without discharge also. The t_{on} and t_{off} time also impacts the reduction in discharge capacity. A decrease in t_{on} and t_{off} are instrumental in countering the reduction in discharge capacity. Contemplating, it is observed that higher charging rates are a possible solution with pulse charging without discharge. However, 2C is found to be an optimal C_{rate}.

Looking into the pulse charging with discharge, an increased t_{on} leads to a similar pattern of reduction in discharge capacity. The reduction in t_{on} helps to reduce the rate of reduction of discharge capacity. The amplitude of discharge pulse during charging too impacted the change in discharge capacity. When the amplitude of discharge pulse is more than or equal to the average charging current, the discharge capacity reduces drastically. The drastic reduction can be related to the change in the equilibrium potential of reactions and the overpotential during charge, rest and discharge durations. The rise in internal cell temperature due to an increase in cell kinetics cannot be neglected while selecting an optimal charging technique to fast charge. The pulse charging with discharge increases the internal cell temperature to a higher value, leading to thermal runaway. Considering the reduction in discharge capacity, CT5 is the best

technique to charge the battery at higher C_{rate}.

6.2.5 Inactive material concentration

Li-ion batteries have active and inactive materials. Those materials that contribute to the energy storage process, such as storing lithium, are the active materials. The inactive materials include separator, binders, current collectors, electrolyte, additives and packaging components [215, 216]. These inactive materials constitute almost 60% of the battery weight and hence, are a crucial parameter affecting the battery energy and power density [217]. The concentration of inactive materials keeps increasing with the age of the battery. The side reactions in the battery are a major cause supporting the conversion of active materials to inactive [61, 215, 218].

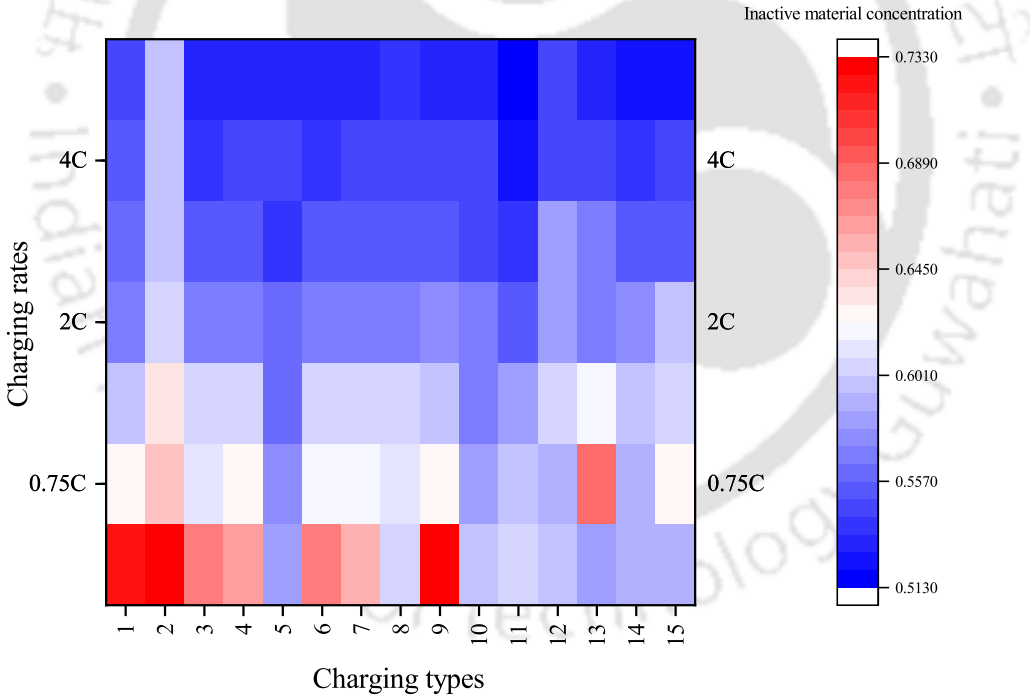

Fig. 6.5: The variation of X-averaged negative electrode inactive material volume fraction when the elected battery us charged using different types of charging techniques at different C_{rate} is shown. The lower charging rates results in maximum formation of inactive materials because chemical degradation dominates at lower C_{rate}.

Fig. 6.5 shows the formation of inactive material in the battery when different types of charging are used at different charging rates. The inactive material formation is the highest at lower charging rates. The charging technique 1 (CC), 2 (CCCV) and 9 (pulse charge with

discharge) shows the highest concentration of inactive material at the end of 350 cycles of charge and discharge at low discharging rates. With an increase in the charging rates, the amount of inactive material concentration reduced. The reduction in the formation of inactive material is related to two primary reasons: i) the battery reaches the cutoff potential faster because of the increased overpotential, and ii) the time to charge is reduced. The first reason is, a higher C_{rate} leads to an increase in chemical kinetics, charge transfer via diffusion and change in equilibrium potential. Since the overpotential is high, the cutoff voltage is reached faster, and the battery is considered to be charged. A larger time frame to charge at a slower C_{rate} leads to a larger time for side reactions.. Hence, the concentration of inactive materials is higher at slow C_{rate}.

CCCV and variants of pulse charging have shown reasonable changes in the concentration of inactive material formation. During CCCV, although the battery is charged at high currents during initial states, the charging end with a reduction in the C_{rate} or fall of charging current to 50 mA during CV mode. Hence, CCCV is the only technique in which there is the least variation of the concentration of inactive material followed by the pulse charging with discharge (charging type 12 and 13). Fig. 6.5 shows the impact of the duty cycle, rest time and the amplitude of discharge pulse in different variants of pulse charging. The rest period during the pulse charge provides a settling time to the batteries. During the settling time, the increase in the chemical kinetics, charge transfer rate, and change in equilibrium potential is reduced or halted. Hence, the formation of inactive material is also less when compared to CC and CCCV. However, there are variations due to the parameters of the pulses. The interpretation of the concentration of inactive material for pulse charging without discharge is shown in charging type 3 to 8. The decrease in the concentration of inactive material is seen with a reduction of the t_{on}. For a higher t_{on}, the charging technique tends to behave like CC or CCCV; hence, a similar concentration is seen, although it is less than CC and CCCV. The t_{off} also impacts the formation of inactive materials. A reduction in the t_{off} leads to a reduction in the formation of inactive material. In general, a reduced t_{on} and t_{off} reduces the increase in the concentration of inactive material volume concentration.

The pulse charging with discharge leads to the least increase in the concentration of inactive

material compared to CC, CCCV and pulse charge without discharge. Charge type 9 to 15 in Fig. 6.5 shows the variation of the concentration of inactive material. The charge type 9, 10 and 11 are having a reduction t_{on} for a constant t_{off} and discharge time, resulting in reduced inactive material concentration. The results obtained follows a similar trend as observed in pulse charging without discharge. Further investigation on the impact of discharge pulse is studied by changing the amplitude. For simulations in which the amplitude of discharge current is equal to average current, but the on-time varies from highest to lowest (charge type 9, 10 and 11), the inactive material concentration is least for the smallest t_{on}. When the amplitude of discharge current is reduced to half of the average current, higher on-time resulted in the formation of less inactive material. In contrast, when the amplitude of discharge pulse is double the average current, inactive material volume concentration is more for a higher on-time. Hence, for pulse charging with discharge, with charge type in which the amplitude of discharge current equals the average current, and have least on-time results in the formation of least inactive material. The battery discharge process also renders a similar change in the equilibrium potential of the reactions in the batteries. Hence, an increase in the discharge pulse leads to a rise in the formation of inactive materials.

6.2.6 Reaction overpotential

The deviation of the battery potential from the electrode equilibrium potential to meet the requirements of current during charge or discharge is commonly called overpotential. A simplistic example of overpotential can be visualised by observing the increase in the terminal voltage of a battery when a charger is connected to it after allowing it to rest for an hour or more. Hence, a higher charge or discharge current will lead to an increase in the overpotential of the battery. Different types of overpotential are described in the literature. Those include thermodynamic, charge-transfer, ohmic and concentration overpotential. Splitting the overall overpotential is not done in this work. The literature describes that an increase in the SEI layer thickness (ohmic overpotential) add to the increase in the overpotential [1].

Fig.6.6 shows the changes in the overpotential with an increase in the charging rates and change in the charging types. During CC and CCCV, the highest overpotential is seen during

low C_{rate}. Since at low C_{rate}, the SEI formed is stable and thick, the ohmic overpotential due to SEI layer formation is dominant. Further, CCCV have higher overpotential when compared to CC, which is similar to the SEI layer thickness. Moving right in Fig.6.6, the variation of overpotential when variants of pulse charging are done is described. The rise in the overpotential is the least in CT5, which is attributed to SEI layer formation. With the decrease in t_{on} and t_{off}, the rise in overpotential decreases. The rest period in the pulse charge provided time to settle. Hence, the overpotential due to thermodynamics, charge transfer, and concentration reduces. Further, the growth of the SEI layer is also constrained due to the least deviation from equilibrium potential.

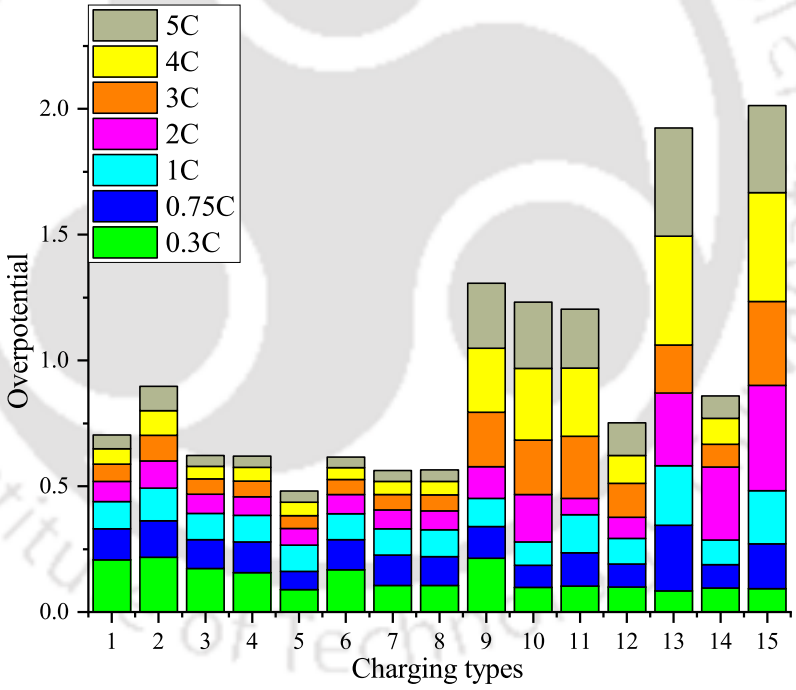

Fig. 6.6: The variation of X-averaged negative electrode reaction overpotential [V] when the battery is charged using different charging techniques at different C_{rate} is shown. The overpotential is higher at lower C_{rate} as the inactive material formation and SEI thickness is more.

The pulse charging without discharge is found to reduce the rise in the overpotential. However, when the pulse charging with discharge is observed, a sudden increase in the overpotential is visible. Although the rise in the overpotential follows the trend of decreasing t_{on}, the SEI layer thickness is not the highest compared to Fig. 6.2.1. Hence, in pulse charge with discharge, it

is not the ohmic overpotential that dominates; it is the thermodynamics and the charge transfer overpotential that dominates. The claim is corroborated by the rise in cell temperature as seen in Fig. 6.2.3. The charge transfer overpotential increases with an increase in the C_{rate}. Hence, with an increase in the amplitude of the discharge pulse, from half of the average charging current to double the charge current, the overpotential rises. Both thermodynamic and charge transfer overpotential dominates the rise in overpotential when pulse charging with discharge is performed with a higher amplitude discharge pulse. CT5 and CT8 resulted in the best charging types when the increase in overpotential is accounted for.

6.2.7 Extent of lithiation

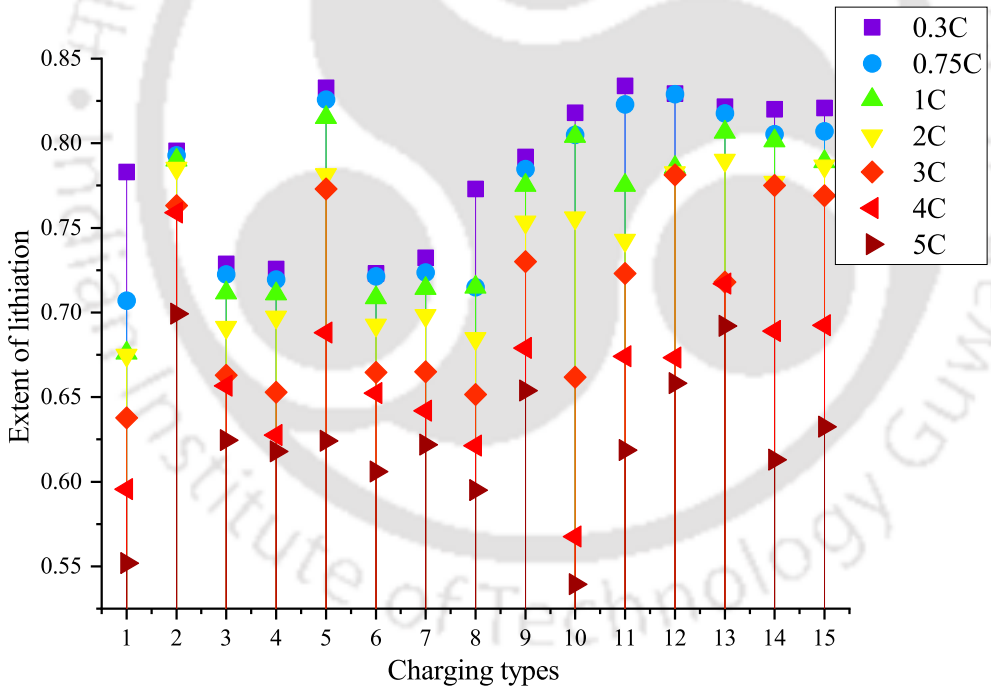

Fig. 6.7: The X-averaged negative electrode extent of lithiation for different types of charging and at different C_{rate} is shown. Lower C_{rate} results in better lithiation while higher C_{rate} reduces it. A better lithiation is related to overpotential and the chemical kinetics which impact the settlement of ions in electrodes.

Lithiation is the intercalation of Li-ions in the negative electrode during charging. The extent of lithiation happening prominently impacts the capacity of the battery during charging. The formation cycle, which is done after the manufacturing of the battery, involves the process of

prelithiate anode, which is also accompanied by SEI layer formation and a rise in overpotential during formation. Hence, the extent of lithiation is also related to SEI layer thickness, and overpotential [219]. Fig. 6.7 shows the variation of lithiation at different charging techniques and rate.

The change in the extent of lithiation in CCCV is the least for different charging rates. A larger impact of C_{rate} is seen in CC. The process of lithiation is dependant on the ease to intercalate in the electrodes. The ease to intercalate further depends on the diameter of the pores. With the growth of the SEI layer, the diameter decreases and add resistance to the diffusion of ions. Hence, lithiation reduces with the ageing of the battery. At the lower C_{rate}, the SEI layer formed is thick and stable; hence, lithiation reduces.

On the contrary, although the SEI layer is less thick than the lower C_{rate}, the lithiation is less in the higher C_{rate}. Hence, there are other factors also that impacts the extent of lithiation. The higher C_{rate} leads to an increase in the chemical kinetics in the battery. The equilibrium potential and overpotential also increases with an increase in the cell temperature. The overall change in the battery makes does not allow the Li-ion to settle in and stimulate various side reactions.

A few patterns of pulse charging shows better results when compared to conventional CC and CCCV. The variation of t_{on} and t_{off} shows similar changes in the variation of extent of lithiation. A decrease in the t_{on} and t_{off} leads to better lithiation. A larger t_{on} allows accumulative growth of SEI layer and cell temperature, and the t_{off} helps to settle the processes in the battery. A reduction in t_{on} time ensures a reduction in the accumulative growth of the SEI layer and temperature. The pulse charging with discharge good results in low charging rates, but the extent of lithiation reduced drastically at higher charging rates. The decrease in t_{on} is visible here as well, with improvement in the extent of lithiation. The amplitude of discharge pulse also impacts the lithiation, but visible changes are seen only at higher C_{rate}. At higher C_{rate}, the impact of SEI layer thickness and the processes leading to an increase in temperature dominates convolutes. However, the impact of the SEI layer is dominant only at low C_{rate}.

6.2.8 Porosity

The porosity of the electrodes is an important parameter that impacts the capacity of the Li-ion battery. The porosity of pores in the electrode is varied with the deposition of inactive materials, which is the SEI layer. With an increase in the thickness of the SEI layer, the pores get clogged, leading to a reduction in the intercalation reactions, as discussed in previous sub-sections [158]. Hence, the porosity also varies similarly as the inactive material, and SEI layer thickness varies. Fig. 6.2.9 shows the variation of porosity of the negative electrode after 350 charge-discharge cycles. The porosity is the least in the case of CCCV and CC, followed by CT9. The variation in porosity in Fig. 6.2.9 demonstrates that change in charging types have an impact on the performance of the battery, especially when looked into the variants of pulse charging.

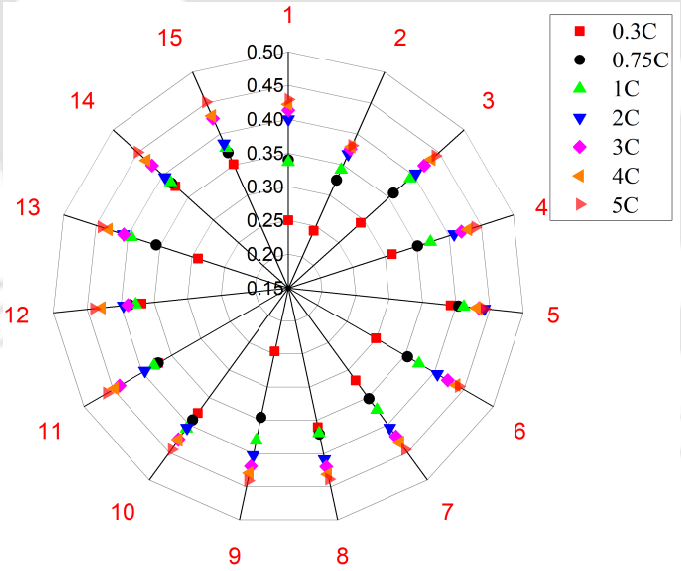

Fig. 6.8: The X-averaged negative electrode porosity for different types of charging and at different C_{rate} is shown. The porosity depends on the SEI layer thickness over particles in electrodes. Hence, at lower C_{rate}, when SEI layer thickness increases, the porosity of the electrodes is also reduces.

The porosity impacts from the t_{on} and t_{off} for pulse charge without discharge. It is observed that for a lower value of on-time, the impact on the porosity is least and retain a higher value. A lower off-time too have a similar impact on the porosity. The charge type 5 shows the least variation in the porosity for different charge rates. With an increase in the C_{rate}, the change in

the value of porosity is reduced. In contrast, a lower charging rate leads to a higher reduction of porosity with an increase in the number of cycles. As described in previous subsections, the SEI layer formed is thicker and stable at lower charging rates. Hence, porosity is reduced drastically, and the impact of pulse charging is also negligible. The pulse charging without discharge is capable of controlling the reduction in the porosity of the negative electrode. However, pulse charge with the discharge has shown similar benefits when the variation of t_{on} and t_{off} is investigated.

The variation of pulse charging with discharge is shown in charge type 9 to 15. The change in the porosity is reduced with the use of pulse charge with discharge because of the reduction in the SEI layer thickness as shown in Fig. 6.2.1. The decrease in the t_{on} in this technique also impacts the porosity. For a higher value of on-time, the change in the porosity is greater at lower charging rates. For higher charging rates, the change in porosity is the least. The charge types-9, 10, and 11 shows a reduction in the change in the porosity because of the reduction in t_{on}. The reduction in t_{on} stops a consistent rise in the rate of side reactions, and the t_{off} allows to settle processes. The amplitude of the discharge pulse also impacts the change in the porosity of the electrodes. For cases where the amplitude of discharge pulse is equal to the average current, the difference in porosity is with the reduction in t_{on}, the change in the porosity reduces. On the contrary, a more significant change in porosity is found when the amplitude of discharge current is equal to half of the average current.

A larger difference in porosity is observed for case the amplitude of discharge current is double the average current. The change in the porosity is related to the equilibrium potential, which on the increase in the magnitude, fall below the stability limits of the electrolyte leading to SEI formation. The rest period after the discharge pulse helps to stabilise the SEI layer. Hence, in the case of low C_{rate}, which also generates a stable SEI layer, the larger reduction in porosity is visible even when pulse charging with discharge is used.

6.2.9 Tortuosity

Tortuosity is an important factor relating to the mass and charge transport in an electrochemical device [220]. Although this factor plays a major role in the fast charging of batteries,

it has not been widely discussed in works dealing with the capacity fade of batteries. Tortuosity is a microstructural characteristic that defines the ease of flow of ions during charging and discharging [221–223]. However, tortuosity should not be misunderstood with the geometric property of microstructure rather interpreted as the effective diffusibility of mass in a porous object [220]. A higher value of tortuosity infers that the travel path through the porous structure is not smooth or short for the charge. Hence, the lower the value of tortuosity, the better the charge and mass transport in the battery's electrodes [223].

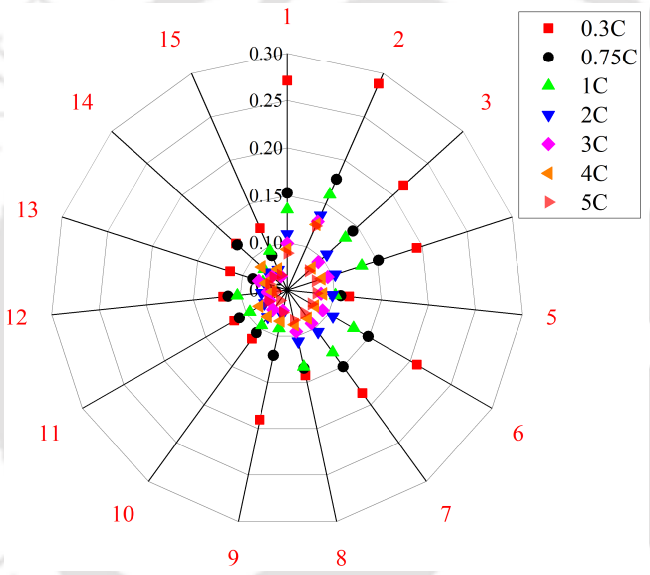

Fig. 6.9: The X-averaged negative electrode tortuosity for different types of charging and C_{rate} is shown. Tortuosity is inversely related to porosity. Hence, the variation follows a trend but opposite to the porosity.

Fig. 6.9 shows the variation of values of tortuosity for different types of charging at various C_{rates}. The lower charging rates in all the techniques showed resulted in the highest value of tortuosity. The conventional CC and CCCV have the maximum variation in the tortuosity, especially at low C_{rate}. At lower C_{rate} other parameters such as concentration of inactive materials and the SEI layer thickness is higher. The SEI layer is a type of inactive material that is formed on the surface of electrode particles. These particles are kept together using binders and have spaces in between them, which are called pores. These pores allow the Li-ion to settle during intercalation reaction or charging. When the SEI layer thickness increases, the pores start get-

ting clogged and restrain the movement of charges [158, 220]. Hence, during charge transfer or diffusion, a larger path is required, which leads to an increase in tortuosity. Since the porosity of electrodes is related to tortuosity, the calculation also involves the value of porosity.

On the introduction of pulse charge techniques, the change in the values of tortuosity reduces as compared to CC and CCCV. The t_{on} and t_{off} have impact on the change in the tortuosity similar porosity changes shown in Fig. 6.2.9. The decrease in the t_{on} and t_{off} reduces the tortuosity changes due to similar reasons as described in the previous subsection explaining the less change in the porosity and SEI layer thickness. Looking at the pulse charging with discharge, the change in tortuosity over different charging rates are the least except for a low C_{rate} in CT9. CT9 has a high t_{on}, therefore at low C_{rate}, the formation of SEI to constrain the diffusivity of charge is least. On an increase of C_{rate}, the internal cell temperature increases, boosting the diffusivity of charge. Further, the increase in the amplitude of discharge pulse in pulse charging with discharge also increases the internal cell temperature. Hence, for CT13 and CT15, in which the amplitude of discharge pulse is twice the average charge current, the tortuosity changes are minimal. The pulse charge with discharge turns out to be a good alternative to fast charge batteries if the only tortuosity is considered under study.

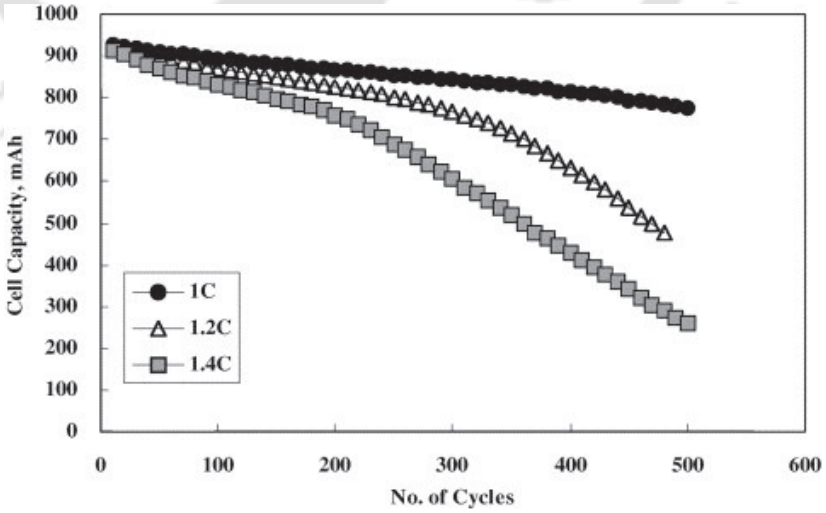

Fig. 6.10: The acceleration of capacity fade with increase in charging rate as described in [1]

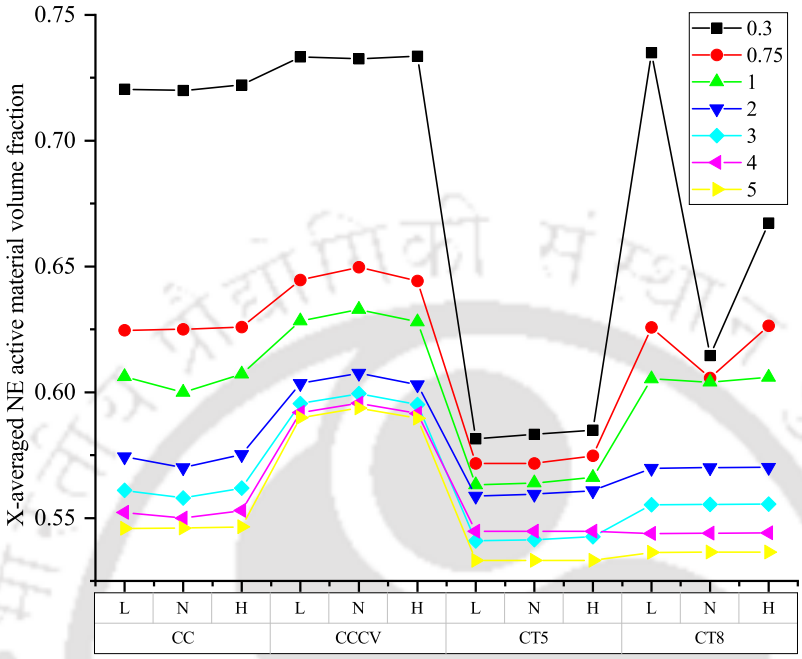

Fig. 6.11: Variation of X-averaged NE active material volume fraction

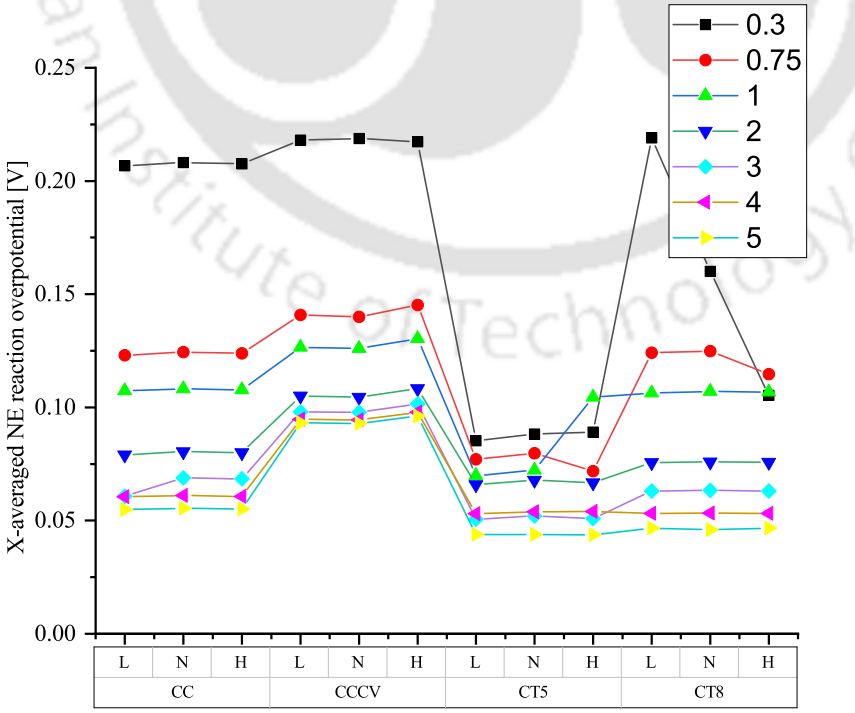

Fig. 6.12: Variation of X-averaged NE reaction overpotential [V]

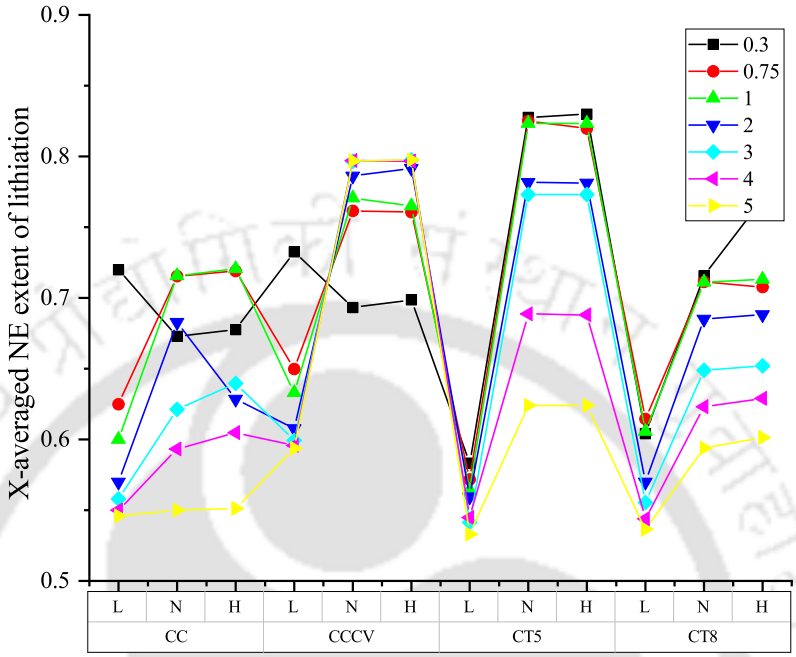

Fig. 6.13: Variation of X-averaged NE extent of lithiation

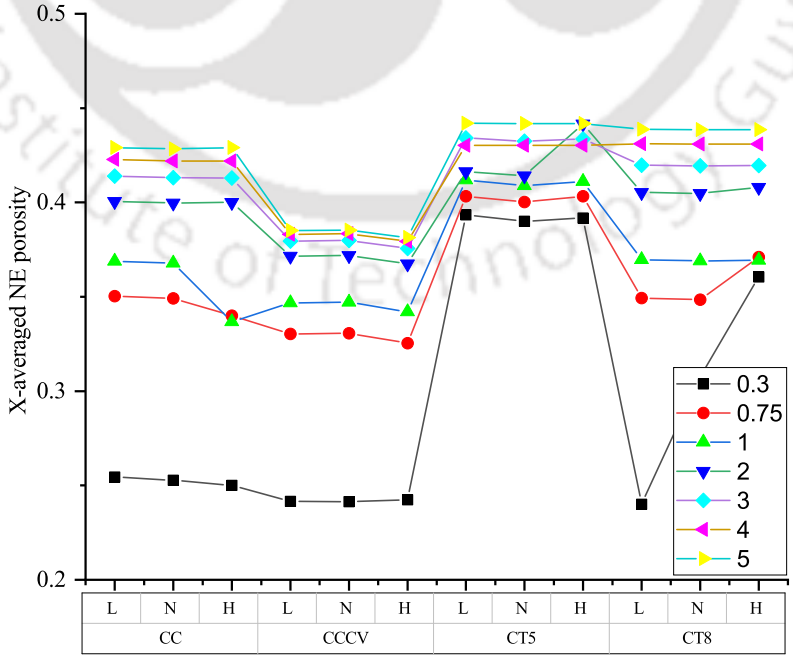

Fig. 6.14: Variation of X-averaged NE porosity

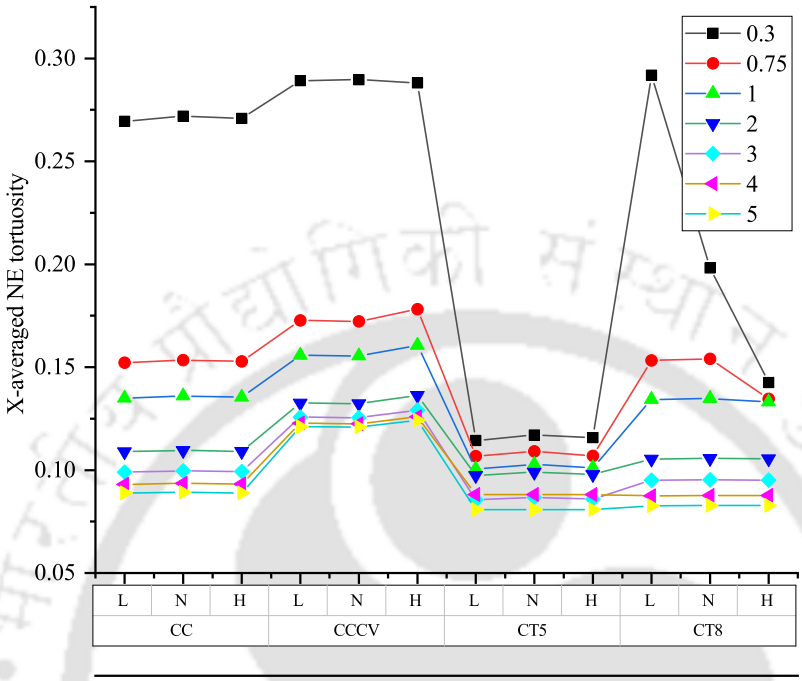

Fig. 6.15: Variation of X-averaged NE tortuosity

6.3 Comparison of the results with the change in ambient temperature

Various works in literature have reported the impact of ambient temperature in operation and ageing mechanisms of the battery at different C_{rate}. However, the effect of the charging types is a not widely discussed topic in the literature, although a few works suggest charging techniques for extreme temperature conditions [168]. Hence, this work is further extended to analyse the impact of the charging technique at two extreme temperatures - 318.15 K (45 ^{o}C) and 273.5 K (0 ^{o}C). The temperature changes the rate of formation of inactive materials, including SEI, erosion or decomposition of SEI and instability in electrolyte resulting in reduction reactions with active material. Rise of internal temperature above a certain level (125^{o}C to 180^{o}C) can lead to thermal runaway, venting, and complete damage of battery [224].

The previous results, which were at 298.15 K (25 ^{o}C), are compared with the results obtained at two extreme temperature for selected four types of charging techniques. CT5 and CT8 variants of pulse charge with discharge resulted in the best performing charging types based on the previous simulations at normal ambient temperature. Hence, to reduce the simulation

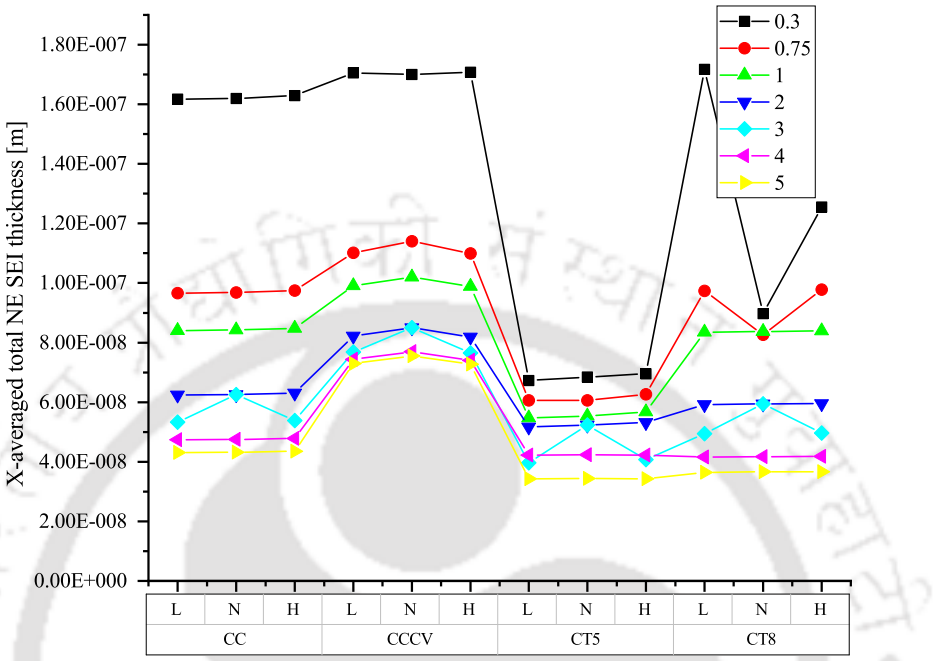

Fig. 6.16: Variation of X-averaged total NE SEI thickness [m]

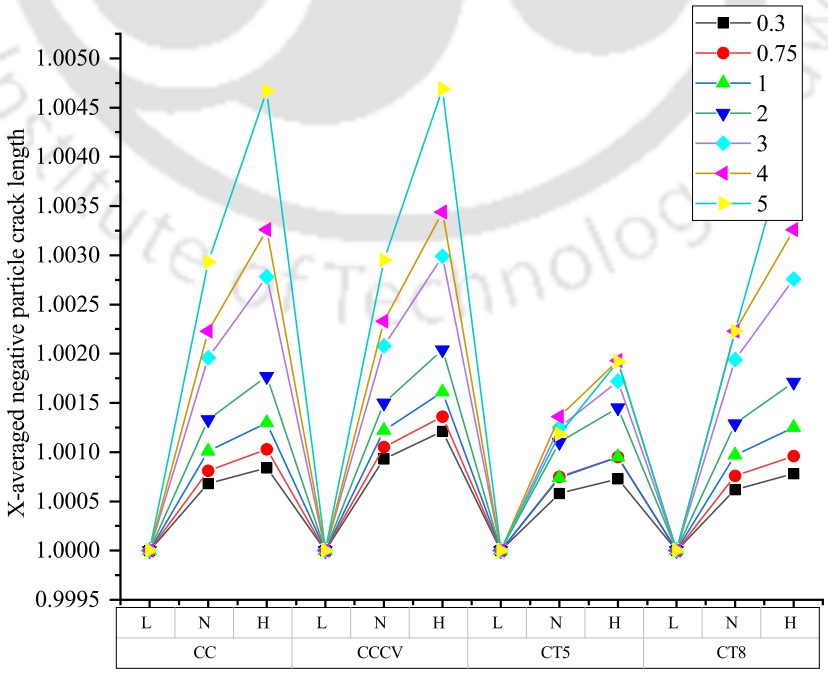

Fig. 6.17: Variation of X-averaged negative particle crack length

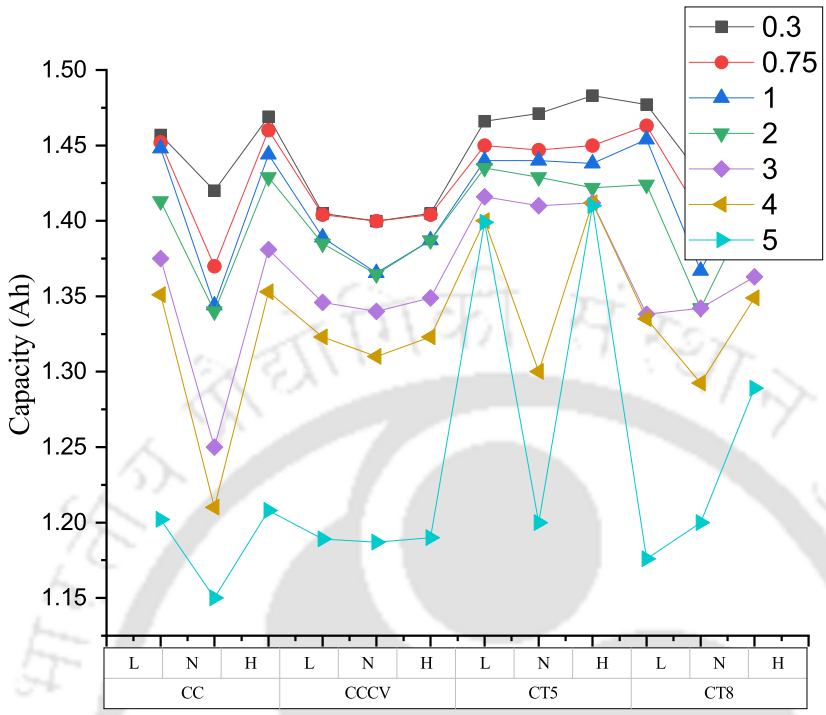

Fig. 6.18: Variation of capacity (Ah)

time, further simulations are performed on only four types of charging techniques, viz. CC and CCCV being conventional, and CT5 and CT8 are only simulated at two extreme temperatures.

Fig. 6.2.9 – Fig. 6.3 shows all the parameters studied to determine the performance of the battery at different charging rates and temperatures. Three different temperatures are represented by "L" (273.5 K (0 ^{o}C)), "N" (298.15 K (25 ^{o}C)) and "H" (318.15 K (45 ^{o}C)). The parameters analysed are those presented in Fig. 6.4. The difference in the formation of inactive material for different C_{rate} is the least in the case of CT5. For CC, at lower C_{rate}, the variation in the formation of inactive material is negligible with a change in the temperature. The change in overpotential of the battery is also less; thereby, the changes in SEI layer thickness, porosity, and tortuosity also follows a similar pattern. The parameter which shows differences are the lithiation, particle crack length and capacity. The changes in the lithiation is related to the rate of diffusivity, which changes with the change in the temperature. At lower temperature, higher resistance to diffusivity is found in the batteries, resulting in decreased lithiation. With an increase in the temperature, the Li-ions and mass transfer rate increases with an increase in chemical kinetics. As the lithiation increases, there is an increase in the stress in the particles of

the electrode. Hence, as expected, the particle cracking increases with the temperature.

The changes in temperature does not results in a major change in the parameter when CCCV is used, although there is a rise in the formation of inactive materials, SEI layer thickness, overpotential, lithiation and tortuosity. Porosity decreases while particle crack length does not show any major difference with CC. CT5, which is found to be the best charging technique, shows the least variation in values of parameters at different charging rates. The decrease in the t_{on} and t_{off} resulting in the changes as described in previous subsections. The results with reduced t_{on} and t_{off} aligns with the finding in [225] where it is shown that a low-frequency diffusion leads to higher impedance of the battery. The impedance of the battery is due to an increase in the growth of the SEI layer and the formation of inactive materials. CT8, which follows the CT5 in performance, has a similar results pattern as found in CC, CCCV and CT5.

6.4 Suitability of type of charging for high power or high energy applications

The degradation of Li-ion batteries in EVs also depends on the application. The EVs in transport sector ranges from small two-wheeler to large bus application. The fast EV racing cars are not far behind in tracks. The variation in the requirements of torque and speed of EV motor changes the discharge pattern of batteries. Hence, the rate of degradation also varies for the same battery used in a different application. In this work, an analysis to determine the performance of battery for the higher energy or higher power applications is also done. Fig. 6.4 – Fig. 6.4 shows the plots of terminal power vs energy plots for different charging techniques and C_{rate}.

Fig. 6.4 shows the plot for lower ambient temperature. CT5 performs the best up to $2C_{rate}$ for all the temperature conditions under study. The CCCV becomes a competitor at normal temperature conditions, but CT5 still outpaces. Further, CCCV is performs worst at low and high ambient temperature regions. The results clearly depict the requirements of different charging pattern for different types of vehicles. Fig. 6.4 is the plot for normal ambient temperature range. CT5 and CCCV are close competitors while CT8 and CC are far behind and not suitable for

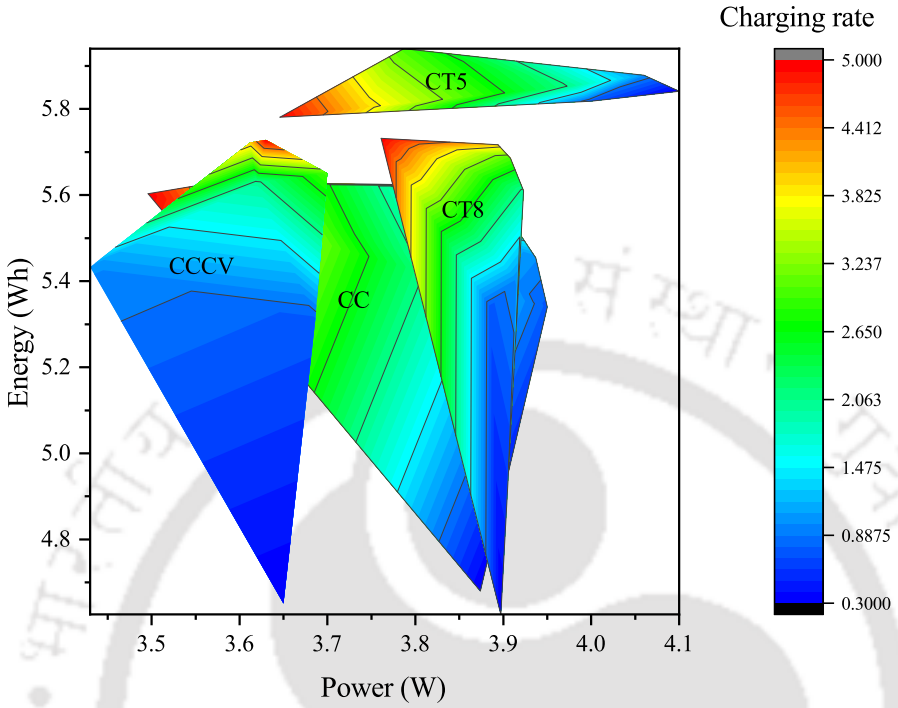

Fig. 6.19: Energy vs power plot at low temperature

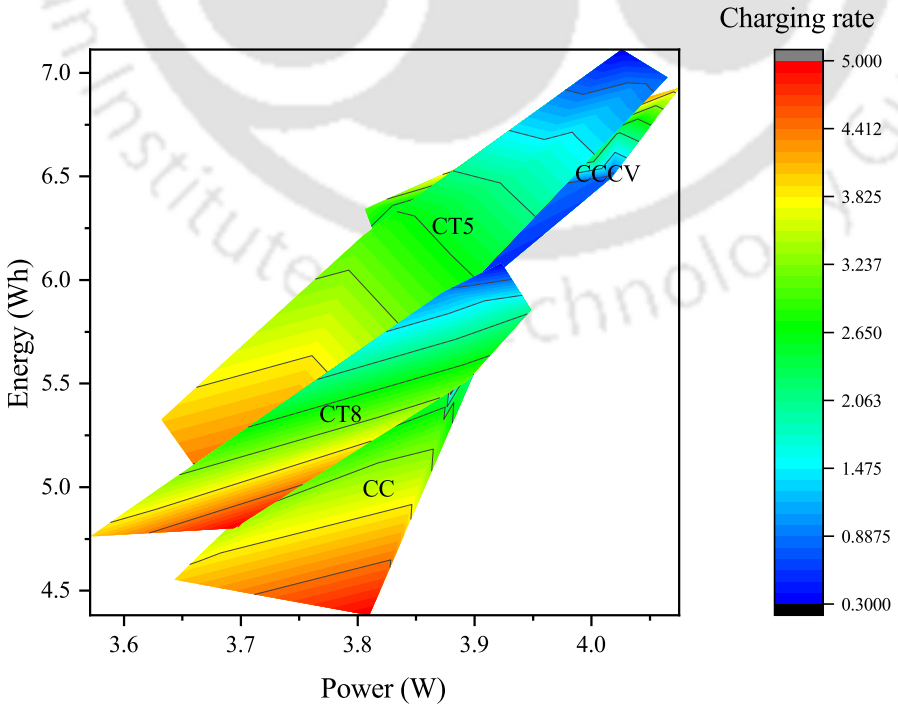

Fig. 6.20: Energy vs power plot at medium temperature

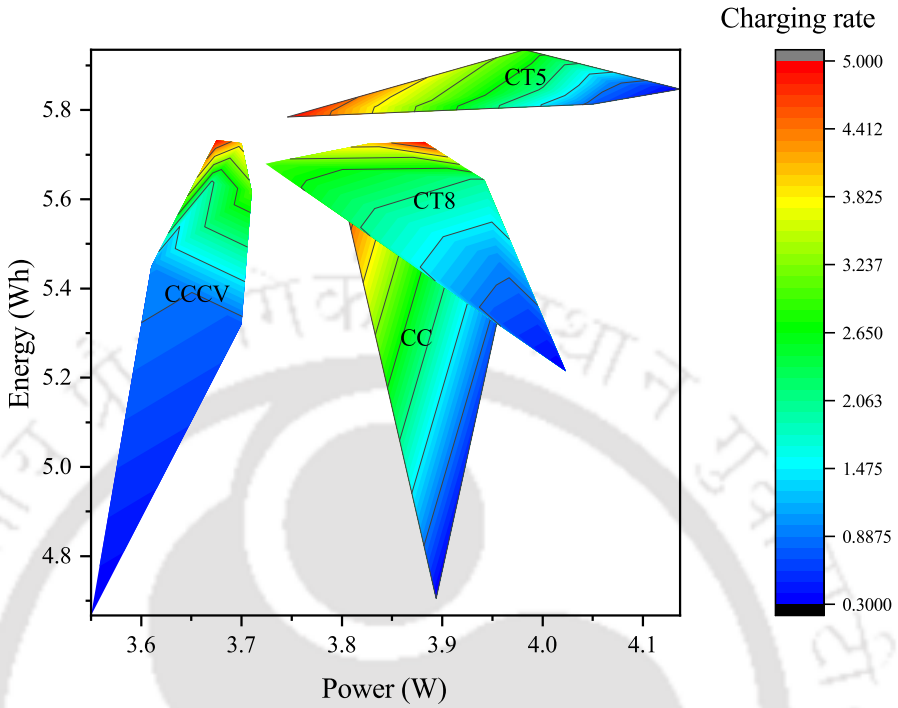

Fig. 6.21: Energy vs power plot at high temperature

use. From Fig. 6.4, which is the plot for higher ambient temperature range, CT5 resulted in the best charging technique. The higher charging rate still remains a challenge for all the ambient temperature conditions. The solution to the problem is discussed in the next section.

6.5 Discussions on the variations of parameters in direction to propose a novel charging techniques

6.6 Discussion

The benefits of Li-ion batteries and their wide application in EVs have developed research interest to meet the challenges. All the challenges in EVs converge to one- battery degradation [21, 39]. The rate of battery degradation changes with the change in utilisation of EV battery. The utilisation depends on the EV driver behaviour, temperature of the environments and type of utilisation of EVs (high energy or high power applications). Higher energy and power density requirements result in a series-parallel connection of cells, which adds to the challenges of making the pack safe, durable, and lower cost. The battery degradation is triggered by the change in the equilibrium potential of the reactions in the battery. The thermodynamic force

to drive the reactions in the battery is associated with equilibrium potential. Hence, changes in the internal battery or external ambient temperature lead to a variety of chemical and structural alternations [226].

An increase in the temperature leads to heighten kinetics of both intercalation-deintercalation and side reactions. The inactive material formed during elevated temperature has a different morphology in comparison with normal temperature. Most importantly, the SEI layer composition changes. Studies are performed using differential scanning calorimetry and accelerated rate calorimetry to determine the cell or electrode behaviour [227, 228]. These studies disclosed the phenomenon of self-heating due to exothermic side reactions. The selection of electrolyte salt has a significant role in the temperature rise. The elevated temperature further erodes the existing SEI layer over the active material. The eroded SEI either dissolve or re-precipitate, leading to the restructuring of damaged SEI and more side reactions. More stable SEI and inorganic products are formed, such as lithium fluoride and lithium carbonate [229]. Further, these stable products are less penetrable for Li-ions, thereby decreasing SEI's overall diffusivity and ionic conductivity.

At low temperatures, the degradation of the battery is not dominated due to changes in the SEI formation instead by the phenomenon of lithium plating and dendrite formation [61, 230]. This study does not consider these two phenomena. Hence the related results are not presented. However, the literature states that, at low temperature, the equilibrium potential of intercalation reactions drops close to the lithium metal potential [231]. Further, the viscosity changes in the electrolytes are observed, leading to a decrease in the diffusivity of li-ion into electrolytes and electrodes. Li-metal reactions in the electrolyte lead to side reactions, which accelerated the ageing process and increased capacity loss. The saturation of electrodes due to slow diffusion and Li's settlement around electrodes adds to the increase in local potential. Hence, the possibility of Li metal plating or dendrite formation increases.

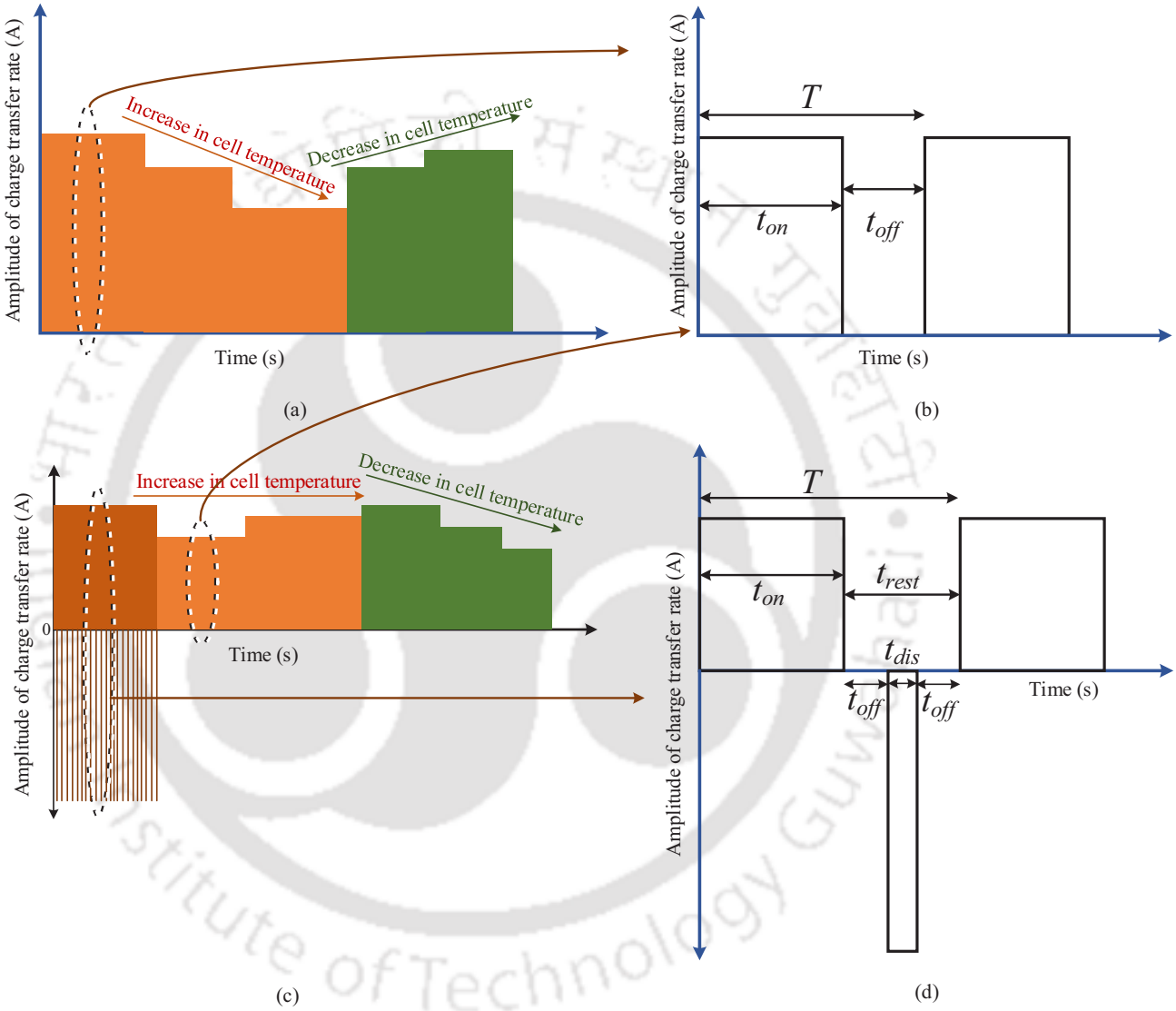

Fig. 6.22: Proposed charging technique: (a) The charging pattern that is suitable for charging at normal or high ambient temperature. The increase and decrease in cell temperature is countered by reducing and increasing the amplitude of positive pulse current. (b) The pattern of pulse in which T, t_{on} and t_{off} are required to be computed to constrain battery degradation. (c) The charging pattern that is suitable for charging at extreme low temperatures. The discharge pulse of more than average charging current help to increase internal cell temperature. The increase and decrease in this case is controlled by shifting from pulse charging with discharge to without discharge and increasing or decreasing the amplitude of charge current.

6.7 Proposal of a new battery friendly charging technique

The discussions in this subsection help gain insights into different types of charging techniques discussed in this work. The conventional techniques viz CC and CCCV have shown increased chemical degradation during lower C_{rate} and increased mechanical degradation during higher C_{rate}. The inactive materials and SEI layer formed at all the C_{rate} is higher when compared to pulse charging without discharge, as seen in Fig. 6.2.9 and Fig. 6.3. Similarly, the particle cracking length is also higher. The CT5 has shown the best results in terms of all the parameters analysed in Fig. 6.2.9 – Fig. 6.3. Even when the ambient temperature is taken into consideration, the performance does not deteriorate. Hence, pulse charging technique without discharge pulse with a reduced t_{on} and t_{on} can be a suitable option to go for fast charging and constrain the battery degradation. The value of t_{on} and t_{off} is an optimization problem given in [232].

Although the CT5 results are optimal for all temperature conditions analysed in this work, the design of new charging techniques will be indispensable at extreme temperatures such as -20 ^oC and 80 ^oC. Further, each charging technique has advantages and disadvantages that can be utilised to charge in extreme environmental conditions. The amalgamation of the charging techniques directs us towards the developing a new rule-based charging strategy for Li-ion batteries. Further, for high energy and high power applications as well, the rules can be framed by selecting the suitability of charging type from Fig. 6.4 – Fig. 6.4, monitoring the rise in internal battery temperature, and appropriately varying the C_{rate}.

The rule-based charging strategy should incorporate the battery electrochemistry, present battery health parameters, environmental conditions, user requirements and grid conditions. Hence, a new rule-based charging strategy is proposed to fast charge with reduced battery degradation in this work. Different types of electrochemistry of Li-ion battery are commercially available such as Lithium Cobalt Oxide (LCO), Lithium Manganese Oxide (LMO), Lithium Iron Phosphate (LFP), and Lithium Titanate (LTO). The battery electrochemistry is to be considered because of the variation in ability to fast charge, performance, lifespan, specific power,

and energy. The present battery health conditions will help to determine the ageing of the battery. Capacity estimated by the BMS or any types of the model or the previous battery charge and discharge profile data will help determine the battery's ageing. The environmental condition includes the temperature of the region. User requirements can be a fast, medium and slow charge. The grid conditions should also be incorporated to avoid the impact of uncoordinated charging, which leads to voltage imbalance and instability [19, 20, 233]. The electric grid can be at peak load, off-peak load or normal condition.

Assume an EV arrives at a charging station with LTO battery electrochemistry. The battery is new and can charge to full capacity as communicated by the BMS. The temperature of the region of the charging station is below normal (-10 ^{o}C). The user opts to fast charge, and the grid is at peak load condition. For the given scenario, if a fast charge is performed, the grid will be overburdened. Hence, the user will be given an option to go with a slow or medium charge rate. If the user wants to continue the fast charge, the service will not be denied, and fast charging will be selected. The only condition to be evaluated is the ambient temperature. Since the temperature is very low, the battery is under stress, and the internal resistance is high. The rise of the internal resistance is due to the low ionic and mass diffusivity. Suppose the battery's internal temperature is increased, the viscosity of the electrolyte and the overall rate of diffusion can be brought to normal. The analysis in the previous subsection has shown that pulse charging with discharge can help in increasing battery's internal temperature. Hence, the battery undergoes a pulse charging with discharge for a period of time until the battery's internal temperature becomes normal. Later, with controlled battery temperature monitoring, fast charging can be performed using a charging pattern, leading to the least battery degradation. For instance, in this work, CT5 is found to be the best performer. Similarly, for LTO battery, an optimal charging pattern can be proposed.

The advantages of the rule-based charging system lie in the ease of implementation. The charging station developer can predefine a set of rules based on the changes in the climatic condition, nature of the user and their requirements of fast charge, condition of the electric grid over a period of time. The charger should be designed to meet the requirements of different

charging strategies. A set of rules can be framed and fed to the controller of the charger. Every time a user connects for the charge, as per requirements, the rule will ensure the best services for both EV user and the electric grid. The assurance of the least battery degradation will advantage the EV user, and the electric grid will have the least impact of uncoordinated fast charge.

The disadvantages of such rule-based charging are data requirements related to battery parameters that need to be considered to fast charge with reduced battery degradation. Further, robust communication needs to be established with the grid for real-time monitoring of loading. The charger should also be capable of communicating with EV battery BMS. A computational signal processing board or connected infrastructure is also required to monitor and control the charging of EV batteries. These requirements make the charging systems costly, but an increase in cost will be compensated by avoiding ageing of battery and losses of power system operators due to uncoordinated charging. The benefits of Li-ion batteries and their wide application in EVs have developed research interest to meet the challenges. All the challenges in EVs converge to one- battery degradation Table 6.3 shows a rule base developed considering all the five parameters.

Table 6.3: Example rule set for charging: The set of rules are designed based on the results obtained for the selected battery in this work. The user selection is not demonstrated in the process when the grid is in peak load hours. Further, frequency, duty cycle of the pulses and amplitude of charge and discharge pulse should be either computed online by preset optimisation algorithms or set as a predefined value determined based on experiments/simulations for any charge technique (CT5, CT9 or any pulse charging with discharge) defined in the table.

Sl.No	Present battery health	Environmental condition	User requirement	Charge technique
1	New	Low	Fast	Start charging by a high charge current pulse or pulse charging with discharge (similar to CT9*). With an increase in the internal cell temperature, charge technique similar to CT5* can be used to fully charge.
2	New	Normal	Fast	Start charging with charging technique similar to CT5*.

3	New	High	Fast	Start charging by a technique similar to CT5* and monitor the internal temperature. With the rise in the internal cell temperature, the C_{rate} should be reduced to constrain the rise. On stabilising the rise in internal cell temperature, C_{rate} can be increased again.
4	Half-life	Low	Fast	Start charging by using a technique similar to CT9*, with amplitude of discharge pulse lower than the average charge current. Monitor the rise in internal cell temperature. With the rise in internal cell temperature, shift charging to CT5. The internal cell temperature should be monitored to reduce C_{rate} on a rapid rise.
5	Half-life	Normal	Fast	Start charging using a technique similar to CT5 while monitoring the internal cell temperature. An increase in internal cell temperature near stability limits should be constrained by reducing C_{rate}.
6	Half-life	High	Fast	Start charging using a technique similar to CT5 and monitor the rise in internal temperature. Constrain the rise in internal cell temperature by reducing the C_{rate}. On decreased and stabilising the internal cell temperature, C_{rate} can be increased.
7	Degraded	Low	Fast	Start charging by deploying pulse charging with the discharge with amplitude of discharge pulse higher than the average charge current. The rise in internal cell temperature should be monitored. The charging should shift to a technique similar to CT5 on rise in temperature. The internal cell temperature should be monitored and a reduction in C_{rate} should be used to constrain the rise.
8	Degraded	Normal	Fast	The charging should be performed using a technique similar to CT5 and internal cell temperature should be monitored. C_{rate} should be decreased to constrain the rise in internal cell temperature after a certain safe value.
9	Degraded	High	Fast	The charging should start by a technique similar to CT5 and internal cell temperature should be monitored. With an increase in the internal cell temperature above a certain safe value, the C_{rate} should be reduced. The C_{rate} can be increased again once the cell reaches the level of normal internal cell temperature.

10	New	Low	Slow	Start charging using a technique similar to pulse charging with the discharge with amplitude of pulse discharge greater than the average charge current. The rise in temperature should be monitored and with an increase, shift to a technique similar to CT5. The C_{rate} should be decreased if the rise in internal cell temperature is observed around stability limits.
11	New	Normal	Slow	A technique similar to CT5 should be used to charge and regular monitoring of rise in internal cell temperature should be done. The rise in internal cell temperature near stability limits should be constrained by decreasing C_{rate}.
12	New	High	Slow	Start charging using a technique similar to CT5 and monitor the rise in internal cell temperature. Reduce C_{rate} to control the rise in internal cell temperature.
13	Half-life	Low	Slow	The charging should start using a pulse charging with the discharge with amplitude of pulse discharge greater than the average charge current. The rise in internal cell temperature should lead to shifting to CT5 or CT8. Reduce C_{rate} to control the rise in internal cell temperature.
14	Half-life	Normal	Slow	The charging should be done using a technique similar to CT5. The internal cell temperature should be monitored and C_{rate} should be changed to constrain the rise in internal cell temperature.
15	Half-life	High	Slow	Start charging using a technique similar to CT5 and monitor internal cell temperature. Modify the C_{rate} to control the rise in internal cell temperature.
16	Degraded	Low	Slow	Start charging using pulse charging with the discharge with amplitude of discharge pulse higher than the average charge current. Monitor the rise in internal cell temperature, and shift charging to CT5 once temperature rises. The internal cell temperature should be monitored to modify the C_{rate} on rise around safety limits.
17	Degraded	Normal	Slow	A charging technique similar to CT5 should be performed with monitoring of internal cell temperature. The C_{rate} should be modified to constrain the rise in internal cell temperature above safety limits.
18	Degraded	High	Slow	Start charging similar to CT5 and monitor the rise in internal cell temperature. With an increase in the internal cell temperature around safety limits, the C_{rate} should be reduced and on reaching normal internal cell temperature, C_{rate} can be ageing increased.

6.8 Conclusion

This work shows that by developing a methodology of charging, the rate of degradation in the battery is constrained irrespective of extreme changes in the ambient temperature and requirements of fast charge by the EV users. Insightful analysis is performed by developing a set of experiments that help to find the impact on the causes and the rate of battery degradation due to change in charging techniques, C_{rate}, ambient temperature and various parameters of a charge pulse invariants of pulse charging. Although the use of the proposed charging methodology requires pre-analysis on the battery to be charged in a charging station, if used by the charging service providers, the proposed charging technique can reduce the overall cost spent on purchasing the batteries per year for EVs. Further, the proposed charging technique also considers the condition of the electric grid (peak load, off-peak load hours) while deciding the C_{rate} to charge batteries. Hence, the impact of charging in the electric grid is also reduced. The analysis further guides in selecting the charging technique for utilisation in energy-extensive or power-extensive applications at different ambient temperatures. The insight developed based on the extensive analysis is not limited to propose a battery-friendly charging technique but also to develop a rational and new way to approach the development of charging techniques in future.

7

Discussion and Suggestions for Future Work

Contents

"No one who does good work will ever come to a bad end, either here or in the world to come."

– Srimad Bhagwat Gita

7.1 Summary of Contributions

The summary of the findings and the inferences are drawn while working on the works described in the thesis are presented below:

✔ **Proposals of modification in a controller for a V2G system**

The controller is the core of a coordinated charging system. The coordinated charging system explores the idea of the bidirectional flow of power between EVs and the electric grid, also called a V2G system. The amount of power flow between the electric grid and the EVs is decided by a central or distributed controller in a V2G system. The work infers that a preprocessing of data is required in a V2G system where data between entities are communicated using a variety of channels and at different sampling rates. Preprocessing involves a process of synchronisation in the discrete domain. The work also found that a faster sampling rate is required for an optimal operation of the controller. Further, the work concluded that irrespective of the requirements of a faster sampling rate, improvisations in the controller could ensure the best operations even with slower sampling rates. The slower sampling rates of data will help in a reduction in capital investment while upgrading the conventional electric grid.

✔ **Proposals of an intelligent controller for a V2G system**

The sampling rate and synchronisation are challenges in developing a reliable EV charging infrastructure. However, another aspect of challenges in the communication is related to the data loss and delay due to the use of different communication channels. In this work, a proposal for developing an intelligent controller is described to mitigate the challenge. An initial study on the impact of data loss and delay in the data exchange between entities was analysed in a V2G system. Since the issue was real, a support system to perform data integrity checks and corrections before the controller is developed. The data integrity check is performed using a trained ANN and a tolerance value. The correction

involved the use of forecasted values from trained ANN. The results inferred that the issue could be mitigated by appropriately using a sufficient amount of data to develop a trained ANN and selecting ample samples while calculating tolerance.

✔ **Proposals of a charger integrated estimation of parameters and states of the battery**

The electric grid side is one end of the EV charging infrastructure. The other end is the EV users who have to deal with the challenge of battery degradation. Hence, in this work, a proposal of charger integrated estimation of parameters and states of the battery. The benefit of the proposed estimation lies in the fact that degradation in the battery leads to an increase in the overall impedance of the battery. The change in impedance further impacts the estimation of other states of the battery. Hence, the work described the estimation process of impedance using chargers as an initial step to start the estimation process. Based on the impedance, other states can be estimated, which improves the accuracy of values. The accuracy in estimated states such as SoC and capacity guides EV users to perform appropriate charging or select appropriate charging rates to constrain degradation.

✔ **Proposals of a novel charging technique to mitigate the challenges of the electric grid and EV users**

The literature studies batteries as an electrical circuit model and as an electrochemical model. The definition of parameters while using electrical circuit models are based on the electrochemical phenomenon. Further, the battery is an electrochemical system. Hence, it is essential to look into the electrochemical parameters to get a deeper insight into the causes of battery degradation and define proposals to constrain them. In this work, a proposal of a new charging technique is presented, which considers the requirements of fast charge from the users, maintaining the charging rate based on the changes in the internal temperature, changing the types of charging appropriately, and considering the electric grid conditions. The proposal ensured that a reliable EV charging infrastructure is developed that caters to both the electric grid and the EV users.

7.2 Suggestions for the Future Work

The works described in this thesis is have opened directions to study various other aspects of the EV charging infrastructure as a complete system. The challenges in the electric grid side, controllers, aggregators, charging stations, EV users, and subsystems of EVs such as batteries and its management system. A few possible works to be explored are given below:

- The work done in this thesis considers the deployment of controllers and aggregators in substations. However, the deployment will require special arrangements to be made at the substations. Another alternative is to explore the possibility of using cloud services to deploy the aggregators and controllers.
- The development of the intelligent controller uses conventional ANN-based techniques to perform data integrity checks and corrections. Various new and efficient machine learning techniques are being regularly proposed in the literature. The selection and utilisation of these techniques for data integrity check and corrections can be another work. Further, these techniques require a large amount of data and high-performance computational devices. Hence, the support system to perform data integrity checks and corrections can be shifted to the online cloud servers. The challenges to shift in the cloud and integrate into the existing infrastructure can be explored.
- The algorithms of determining the parameters and states of the battery are developed for charging processes. However, the battery also degrades during the process of discharging. Hence, incorporating the battery's impedance estimation while estimating the battery's states during the discharging process can be one of the future work.
- With the addition of different algorithms to meet the requirements of different stakeholders, the EV charging infrastructure has increased complexity in the overall system. A monitoring and correction system for the complete infrastructure is a must to ensure the least impact on any connected entities due to failure of any entity or system, or algorithms. The digital twin is a concept widely used popularised worldwide to perform monitoring, control and correction. Hence, the work can be further extended to incorporate the digital twin concept in the EV charging infrastructure.

Bibliography

[1] C. M. Snyder, "The rate depedency of li-ion battery degradation mechanisms." Sandia National Lab.(SNL-NM), Albuquerque, NM (United States), Tech. Rep., 2016.

[2] P. Ramadass, B. Haran, P. M. Gomadam, R. White, and B. N. Popov, "Development of first principles capacity fade model for li-ion cells," *Journal of the Electrochemical Society*, vol. 151, no. 2, p. A196, 2004.

[3] Z. Zhongming, L. Linong, Z. Wangqiang, L. Wei *et al.*, "Ar6 climate change 2021: The physical science basis," 2021.

[4] "We promote sustainable, low-emission transport and work to reduce the sector's contribution to air pollution and climate change." https://www.unep.org/explore-topics/energy/what-we-do/transport, accessed: 2021-09-08.

[5] U. N. E. P. 2016, "GEO-6: Global Environment Outlook," 2016.

[6] R. P. Cornell, "The environmental benefits of electric vehicles as a function of renewable energy," Ph.D. dissertation, 2017.

[7] C. Sabel, "Urban reduction of GHG emissions in china and europe," University of Bristol, Tech. Rep., 2015.

[8] A. Bailie, "Clean air benefits from electric vehicles," The Pembina Institute, Tech. Rep., 2013.

[9] D. Zhili, L. Boqiang, and G. Chunxu, "Development path of electric vehicles in china under environmental and energy security constraints," *Resources, Conservation and Recycling*, vol. 143, pp. 17 – 26, 2019.

[10] P. N. Leiby, *Estimating the energy security benefits of reduced US oil imports*. Oak Ridge National Laboratory, Oak Ridge, Tennessee, 2007.

[11] J. J. Michalek, M. Chester, P. Jaramillo, C. Samaras, C.-S. N. Shiau, and L. B. Lave, "Valuation of plug-in vehicle life-cycle air emissions and oil displacement benefits," *Proceedings of the National Academy of Sciences*, vol. 108, no. 40, pp. 16 554–16 558, 2011.

[12] B. Tarroja, B. Shaffer, and S. Samuelsen, "The importance of grid integration for achievable greenhouse gas emissions reductions from alternative vehicle technologies," *Energy*, vol. 87, pp. 504 – 519, 2015.

[13] P. Capros, L. Mantzos, L. Parousos, N. Tasios, G. Klaassen, and T. V. Ierland, "Analysis of the EU policy package on climate change and renewables," *Energy Policy*, vol. 39, no. 3, pp. 1476 – 1485, 2011.

[14] S. Sarabi, A. Davigny, V. Courtecuisse, Y. Riffonneau, and B. Robyns, "Potential of vehicle-to-grid ancillary services considering the uncertainties in plug-in electric vehicle availability and service/localization limitations in distribution grids," *Applied Energy*, vol. 171, pp. 523 – 540, 2016.

[15] K. M. Tan, V. K. Ramachandaramurthy, and J. Y. Yong, "Integration of electric vehicles in smart grid: A review on vehicle to grid technologies and optimization techniques," *Renewable and Sustainable Energy Reviews*, vol. 53, pp. 720 – 732, 2016.

[16] L. Noel, G. Z. de Rubens, J. Kester, and B. K. Sovacool, "The technical challenges to V2G," *Vehicle-to-Grid*, pp. 65–89, 2019.

[17] W. Kempton and J. Tomić, "Vehicle-to-grid power implementation: From stabilizing the grid to supporting large-scale renewable energy," *Journal of power sources*, vol. 144, no. 1, pp. 280–294, 2005.

[18] M. Singh, P. Kumar, and I. Kar, "Implementation of vehicle to grid infrastructure using fuzzy logic controller," *IEEE Transactions on Smart Grid*, vol. 3, no. 1, pp. 565–577, 2012.

[19] B. Sah, P. Kumar, R. Rayudu, S. K. Bose, and K. P. Inala, "Impact of sampling in the operation of vehicle to grid and its mitigation," *IEEE Transactions on Industrial Informatics*, vol. 15, no. 7, pp. 3923–3933, 2018.

[20] B. Sah, P. Kumar, and S. K. Bose, "A fuzzy logic and artificial neural network-based intelligent controller for a vehicle-to-grid system," *IEEE Systems Journal*, vol. 15, no. 3, pp. 3301 – 3311, 2021.

[21] A. Masias, J. Marcicki, and W. A. Paxton, "Opportunities and challenges of lithium ion batteries in automotive applications," *ACS Energy Letters*, vol. 6, no. 2, pp. 621–630, 2021.

[22] L. Noel, G. Z. de Rubens, J. Kester, and B. K. Sovacool, "The economic and business challenges to V2G," in *Vehicle-to-Grid*. Springer, 2019, pp. 91–116.

[23] L. Ellingsen and C. Hung, "Research for TRAN committee-battery-powered electric vehicles: market development and lifecycle emissions," *STUDY, European Parliament, Directorate General for Internal Policies, Policy Department for Structural and Cohesion Policies, Transport and Tourism*, vol. 10, p. 944056, 2018.

[24] F. Li, W. Qiao, H. Sun, H. Wan, J. Wang, Y. Xia, Z. Xu, and P. Zhang, "Smart transmission grid: Vision and framework," *IEEE transactions on Smart Grid*, vol. 1, no. 2, pp. 168–177, 2010.

[25] M. Singh, P. Kumar, and I. Kar, "A multi charging station for electric vehicles and its utilization for load management and the grid support," *IEEE Transactions on Smart Grid*, vol. 4, no. 2, pp. 1026–1037, June 2013.

[26] R. Das, K. Thirugnanam, P. Kumar, R. Lavudiya, and M. Singh, "Mathematical modeling for economic evaluation of electric vehicle to smart grid interaction," *IEEE Transactions on Smart Grid*, vol. 5, no. 2, pp. 712–721, 2013.

[27] X. Bai and W. Qiao, "Robust optimization for bidirectional dispatch coordination of large-scale V2G," *IEEE Transactions on Smart Grid*, vol. 6, no. 4, pp. 1944–1954, 2015.

[28] R. Shi, S. Li, P. Zhang, and K. Y. Lee, "Integration of renewable energy sources and electric vehicles in v2g network with adjustable robust optimization," *Renewable Energy*, vol. 153, pp. 1067–1080, 2020.

[29] H. Liang, B. J. Choi, W. Zhuang, and X. Shen, "Optimizing the energy delivery via V2G systems based on stochastic inventory theory," *IEEE Transactions on Smart Grid*, vol. 4, no. 4, pp. 2230–2243, 2013.

[30] A. Y. Saber and G. K. Venayagamoorthy, "Intelligent unit commitment with vehicle-to-grid—a cost-emission optimization," *Journal of Power Sources*, vol. 195, no. 3, pp. 898–911, 2010.

[31] H. U. R. Habib, U. Subramaniam, A. Waqar, B. S. Farhan, K. M. Kotb, and S. Wang, "Energy cost optimization of hybrid renewables based V2G microgrid considering multi objective function by using artificial bee colony optimization," *IEEE Access*, vol. 8, pp. 62 076–62 093, 2020.

[32] M. Ebrahimi, M. Rastegar, M. Mohammadi, A. Palomino, and M. Parvania, "Stochastic charging optimization of V2G-capable PEVs: A comprehensive model for battery aging and customer service quality," *IEEE Transactions on Transportation Electrification*, vol. 6, no. 3, pp. 1026–1034, 2020.

[33] J. Kester, L. Noel, G. Z. de Rubens, and B. K. Sovacool, "Promoting vehicle to grid (V2G) in the nordic region: Expert advice on policy mechanisms for accelerated diffusion," *Energy Policy*, vol. 116, pp. 422–432, 2018.

[34] B. K. Sovacool, J. Kester, L. Noel, and G. Z. de Rubens, "Energy injustice and nordic electric mobility: Inequality, elitism, and externalities in the electrification of vehicle-to-grid (v2g) transport," *Ecological economics*, vol. 157, pp. 205–217, 2019.

[35] Z. U. Zahid, Z. M. Dalala, R. Chen, B. Chen, and J.-S. Lai, "Design of bidirectional DC–DC resonant converter for vehicle-to-grid (V2G) applications," *IEEE Transactions on Transportation Electrification*, vol. 1, no. 3, pp. 232–244, 2015.

[36] S. H. Hosseini, R. Ghazi, and H. Heydari-Doostabad, "An extendable quadratic bidirectional DC–DC converter for V2G and G2V applications," *IEEE Transactions on Industrial Electronics*, vol. 68, no. 6, pp. 4859–4869, 2020.

[37] D. Das, N. Weise, K. Basu, R. Baranwal, and N. Mohan, "A bidirectional soft-switched DAB-based single-stage three-phase AC–DC converter for V2G application," *IEEE Transactions on Transportation Electrification*, vol. 5, no. 1, pp. 186–199, 2018.

[38] M. Su, H. Wang, Y. Sun, J. Yang, W. Xiong, and Y. Liu, "AC/DC matrix converter with an optimized modulation strategy for V2G applications," *IEEE transactions on power electronics*, vol. 28, no. 12, pp. 5736–5745, 2013.

[39] J. Vetter, P. Novák, M. R. Wagner, C. Veit, K.-C. Möller, J. Besenhard, M. Winter, M. Wohlfahrt-Mehrens, C. Vogler, and A. Hammouche, "Ageing mechanisms in lithium-ion batteries," *Journal of power sources*, vol. 147, no. 1-2, pp. 269–281, 2005.

[40] M. R. Palacín, "Understanding ageing in li-ion batteries: a chemical issue," *Chemical Society Reviews*, vol. 47, no. 13, pp. 4924–4933, 2018.

[41] X. Han, L. Lu, Y. Zheng, X. Feng, Z. Li, J. Li, and M. Ouyang, "A review on the key issues of the lithium ion battery degradation among the whole life cycle," *eTransportation*, vol. 1, p. 100005, 2019. [Online]. Available: https://www.sciencedirect.com/science/article/pii/S2590116819300050

[42] B. Sah, P. Kumar, and D. Kothari, "Application of fuzzy logic in the operation of a V2G system in the smart grid," in *Applications of Fuzzy Logic in Planning and Operation of Smart Grids*. Springer, 2021, pp. 153–185.

[43] N. I. Nimalsiri, E. L. Ratnam, C. P. Mediwaththe, D. B. Smith, and S. K. Halgamuge, "Coordinated charging and discharging control of electric vehicles to manage supply voltages in distribution networks: Assessing the customer benefit," *Applied Energy*, vol. 291, p. 116857, 2021.

[44] V. S. Kasani, D. Tiwari, M. R. Khalghani, S. K. Solanki, and J. Solanki, "Optimal coordinated charging and routing scheme of electric vehicles in distribution grids: Real grid cases," *Sustainable Cities and Society*, p. 103081, 2021.

[45] B. Sah and P. Kumar, "Smart charging: an outlook towards its role and impacts, enablers, markets, and the global energy system," in *Smart Charging Solutions on Hybrid and Electric Vehicles*.

[46] K. P. Inala, B. Sah, P. Kumar, and S. K. Bose, "Impact of V2G communication on grid node voltage at charging station in a smart grid scenario," *IEEE Systems Journal*, 2020.

[47] M. Yilmaz and P. T. Krein, "Review of the impact of vehicle-to-grid technologies on distribution systems and utility interfaces," *IEEE Transactions on power electronics*, vol. 28, no. 12, pp. 5673–5689, 2012.

[48] L. Noel, G. Z. de Rubens, J. Kester, and B. K. Sovacool, "Beyond emissions and economics: Rethinking the co-benefits of electric vehicles (EVs) and vehicle-to-grid (V2G)," *Transport Policy*, vol. 71, pp. 130–137, 2018.

[49] B. Sah and P. Kumar, "An insight into the battery degradation for a proposal of a battery friendly charging technique," *PREPRINT*, 2021.

[50] M. A. Ahmed and Y.-C. Kim, "Performance analysis of communication networks for EV charging stations in residential grid," in *Proc. of the 6th ACM Symp. on Develop. and Anal. of Intell. Veh. Netw. and Appl.*, ser. DIVANet '17. New York, NY, USA: ACM, 2017, pp. 63–70.

[51] X. Ye, F. Wen, S. P. Ang, and M. A. Salam, "OPNET-based performance analysis of the communication network in a charging station of electric vehicles," in *Proc. of 2014 IEEE PES Asia-Pacific Power and Energy Eng. Conf. (APPEEC)*, Dec 2014, pp. 1–6.

[52] Y. Sun, X. Hu, X. Liu, X. He, and K. Wang, "A software-defined green framework for hybrid EV-charging networks," *IEEE Commun. Mag.*, vol. 55, no. 11, pp. 62–69, NOVEMBER 2017.

[53] K. M. Liyanage, A. Yokoyama, Y. Ota, T. Nakajima, and H. Taniguchi, "Impacts of communication delay on the performance of a control scheme to minimize power fluctuations introduced by renewable generation under varying V2G vehicle pool size," in *Proc. of 2010 First IEEE Int. Conf. on Smart Grid Commun.*, Oct 2010, pp. 85–90.

[54] Y. Zhang, S. Gjessing, H. Liu, H. Ning, L. T. Yang, and M. Guizani, "Securing vehicle-to-grid communications in the smart grid," *IEEE Wireless Commun.*, vol. 20, no. 6, pp. 66–73, December 2013.

[55] H. Guo, Y. Wu, F. Bao, H. Chen, and M. Ma, "UBAPV2G: A unique batch authentication protocol for vehicle-to-grid communications," *IEEE Trans. on Smart Grid*, vol. 2, no. 4, pp. 707–714, Dec 2011.

[56] L. Zhang, H. Ma, D. Shi, P. Wang, G. Cai, and X. Liu, "Reliability oriented modeling and analysis of vehicular power line communication for vehicle to grid (V2G) information exchange system," *IEEE Access*, vol. 5, pp. 12 449–12 457, 2017.

[57] M. Sayed, A. E. Shafie, M. Elgenedy, R. C. Chabaan, and N. Al-Dhahir, "Enhancing the reliability of two-way vehicle-to-grid communications," in *in Proc. of 2017 IEEE Intell. Vehicles Symp. (IV)*, June 2017, pp. 1922–1927.

[58] Santoshkumar and R. Y. Udaykumar, "Performance investigation of mobile WiMAX protocol for aggregator and electrical vehicle communication in vehicle-to-grid(v2g)," in *Proc. of 2014 IEEE 27th Canadian Conf. on Elect. and Comput. Eng. (CCECE)*, May 2014, pp. 1–6.

[59] V. T. Kilari, S. Misra, and G. Xue, "Revocable anonymity based authentication for vehicle to grid (V2G) communications," in *Proc. of 2016 IEEE Int. Conf. on Smart Grid Commun. (SmartGridComm)*, Nov 2016, pp. 351–356.

[60] J. R. Harish Ramakrishnan, *Power Topology Considerations for Electric Vehicle Charging Stations*.

[61] P. Arora, R. E. White, and M. Doyle, "Capacity fade mechanisms and side reactions in lithium-ion batteries," *Journal of the Electrochemical Society*, vol. 145, no. 10, p. 3647, 1998.

[62] K. P. Inala, P. Kumar, and S. K. Bose, "Impact of communication systems on grid node voltage and operation of a vehicle-to-grid controller in a smart-grid scenario," *IET Power Electronics*, vol. 12, no. 13, pp. 3499–3509, 2019.

[63] D. Lisbona and T. Snee, "A review of hazards associated with primary lithium and lithium-ion batteries," *Process Safety and Environmental Protection*, vol. 89, no. 6, pp. 434–442, 2011.

[64] S. Pelletier, O. Jabali, G. Laporte, and M. Veneroni, "Battery degradation and behaviour for electric vehicles: Review and numerical analyses of several models," *Transportation Research Part B: Methodological*, vol. 103, pp. 158–187, 2017.

[65] H. V. P. Ekram Hossain, Zhu Han, *Smart Grid Communications and Networking*. Cambridge University Press, June 2012.

[66] W. Xu and Y. Mansour, "Voltage stability analysis using generic dynamic load models," *IEEE Transactions on Power Systems*, vol. 9, no. 1, pp. 479–493, 1994.

[67] Y. Tang, *Voltage stability analysis of power system*. Springer, 2021.

[68] W. Kempton and S. E. Letendre, "Electric vehicles as a new power source for electric utilities," *Transportation Research Part D: Transport and Environment*, vol. 2, no. 3, pp. 157 – 175, 1997.

[69] J. G. Pinto, V. Monteiro, H. Gonçalves, B. Exposto, D. Pedrosa, C. Couto, and J. L. Afonso, "Bidirectional battery charger with grid-to-vehicle, vehicle-to-grid and vehicle-to-home technologies," in *IECON 2013 - 39th Annual Conference of the IEEE Industrial Electronics Society*, Nov 2013, pp. 5934–5939.

[70] W. Choi, Y. Wu, D. Han, J. Gorman, P. C. Palavicino, W. Lee, and B. Sarlioglu, "Reviews on grid-connected inverter, utility-scaled battery energy storage system, and vehicle-to-grid application - challenges and opportunities," in *2017 IEEE Transportation Electrification Conference and Expo (ITEC)*, June 2017, pp. 203–210.

[71] S. Habib, M. Kamran, and U. Rashid, "Impact analysis of vehicle-to-grid technology and charging strategies of electric vehicles on distribution networks – a review," *Journal of Power Sources*, vol. 277, pp. 205 – 214, 2015.

[72] K. Clement-Nyns, E. Haesen, and J. Driesen, "The impact of charging plug-in hybrid electric vehicles on a residential distribution grid," *IEEE Transactions on Power Systems*, vol. 25, no. 1, pp. 371–380, Feb 2010.

[73] T. S. Ustun, A. Zayegh, and C. Ozansoy, "Electric vehicle potential in australia: Its impact on smartgrids," *IEEE Industrial Electronics Magazine*, vol. 7, no. 4, pp. 15–25, Dec 2013.

[74] C. Liu, K. T. Chau, D. Wu, and S. Gao, "Opportunities and challenges of vehicle-to-home, vehicle-to-vehicle, and vehicle-to-grid technologies," *Proceedings of the IEEE*, vol. 101, no. 11, pp. 2409–2427, Nov 2013.

[75] M. D. Galus, R. A. Waraich, F. Noembrini, K. Steurs, G. Georges, K. Boulouchos, K. W. Axhausen, and G. Andersson, "Integrating power systems, transport systems and vehicle technology for electric mobility impact assessment and efficient control," *IEEE Transactions on Smart Grid*, vol. 3, no. 2, pp. 934–949, June 2012.

[76] X. Jiang, J. Wang, Y. Han, and Q. Zhao, "Coordination dispatch of electric vehicles charging/discharging and renewable energy resources power in microgrid," *Procedia Computer Science*, vol. 107, pp. 157 – 163, 2017, advances in Information and Communication Technology: Proceedings of 7th International Congress of Information and Communication Technology (ICICT2017).

[77] V. O. K. Li, F. F. Wu, and J. Zhong, "Communication requirements for risk-limiting dispatch in smart grid," in *2010 IEEE International Conference on Communications Workshops*, May 2010, pp. 1–5.

[78] J. Lin, K. C. Leung, and V. O. K. Li, "Optimal scheduling with vehicle-to-grid regulation service," *IEEE Internet of Things Journal*, vol. 1, no. 6, pp. 556–569, Dec 2014.

[79] C. Wu, H. Mohsenian-Rad, and J. Huang, "Vehicle-to-aggregator interaction game," *IEEE Transactions on Smart Grid*, vol. 3, no. 1, pp. 434–442, March 2012.

[80] S. Shao, M. Pipattanasomporn, and S. Rahman, "Grid integration of electric vehicles and demand response with customer choice," *IEEE Transactions on Smart Grid*, vol. 3, no. 1, pp. 543–550, March 2012.

[81] H. Zhang, Z. Hu, Z. Xu, and Y. Song, "Evaluation of achievable vehicle-to-grid capacity using aggregate PEV model," *IEEE Transactions on Power Systems*, vol. 32, no. 1, pp. 784–794, Jan 2017.

[82] Y. Tang, J. Zhong, and M. Bollen, "Aggregated optimal charging and vehicle-to-grid control for electric vehicles under large electric vehicle population," *IET Generation, Transmission Distribution*, vol. 10, no. 8, pp. 2012–2018, 2016.

[83] G. Kiokes, E. Zountouridou, C. Papadimitriou, A. Dimeas, and N. Hatziargyriou, "Development of an integrated wireless communication system for connecting electric vehicles to the power grid," in *Proc. of 2015 Int. Symp. on Smart Elect. Distribution Syst. and Technologies (EDST)*, Sept 2015, pp. 296–301.

[84] R. Yu, W. Zhong, S. Xie, C. Yuen, S. Gjessing, and Y. Zhang, "Balancing power demand through EV mobility in vehicle-to-grid mobile energy networks," *IEEE Transactions on Industrial Informatics*, vol. 12, no. 1, pp. 79–90, Feb 2016.

[85] A. Kavousi-Fard, M. A. Rostami, and T. Niknam, "Reliability-oriented reconfiguration of vehicle-to-grid networks," *IEEE Transactions on Industrial Informatics*, vol. 11, no. 3, pp. 682–691, June 2015.

[86] L. Rubino, C. Capasso, and O. Veneri, "Review on plug-in electric vehicle charging architectures integrated with distributed energy sources for sustainable mobility," *Applied Energy*, 2017.

[87] F. Mwasilu, J. J. Justo, E.-K. Kim, T. D. Do, and J.-W. Jung, "Electric vehicles and smart grid interaction: A review on vehicle to grid and renewable energy sources integration," *Renewable and Sustainable Energy Reviews*, vol. 34, pp. 501 – 516, 2014.

[88] A. Ahmadi, A. Tavakoli, P. Jamborsalamati, N. Rezaei, M. R. Miveh, F. H. Gandoman, A. Heidari, and A. E. Nezhad, "Power quality improvement in smart grids using electric vehicles: a review," *IET Electrical Systems in Transportation*, vol. 9, no. 2, pp. 53–64, 2019.

[89] M. J. M. Al Essa, "Power quality of electrical distribution systems considering PVs, EVs and DSM," *Journal of Control, Automation and Electrical Systems*, vol. 31, no. 6, pp. 1520–1532, 2020.

[90] W. Han and Y. Xiao, "Privacy preservation for V2G networks in smart grid: A survey," *Computer Communications*, vol. 91, pp. 17–28, 2016.

[91] F. Berthold, A. Ravey, B. Blunier, D. Bouquain, S. Williamson, and A. Miraoui, "Design and development of a smart control strategy for plug-in hybrid vehicles including vehicle-to-home functionality," *IEEE Transactions on Transportation Electrification*, vol. 1, no. 2, pp. 168–177, Aug 2015.

[92] M. B. Naik, P. Kumar, and S. Majhi, "Optimal number of e-buses in the solar-assisted smart public transit system and its failure analysis," *IET Electrical Systems in Transportation*, vol. 8, no. 1, pp. 61–70, 2018.

[93] A. Agrawal, M. Kumar, D. K. Prajapati, M. Singh, and P. Kumar, "Smart public transit system using an energy storage system and its coordination with a distribution grid," *IEEE Transactions on Intelligent Transportation Systems*, vol. 15, no. 4, pp. 1622–1632, Aug 2014.

[94] M. B. Naik, P. Kumar, and S. Majhi, "Small-scale solar plants coupled with smart public transport system and its coordination with the grid," *IET Electrical Systems in Transportation*, vol. 7, no. 2, pp. 135–144, 2017.

[95] M. Singh, K. Thirugnanam, P. Kumar, and I. Kar, "Real-time coordination of electric vehicles to support the grid at the distribution substation level," *IEEE Systems Journal*, vol. 9, no. 3, pp. 1000–1010, Sept 2015.

[96] K. Kaur, R. Rana, N. Kumar, M. Singh, and S. Mishra, "A colored petri net based frequency support scheme using fleet of electric vehicles in smart grid environment," *IEEE Transactions on Power Systems*, vol. 31, no. 6, pp. 4638–4649, Nov 2016.

[97] K. Kaur, A. Dua, A. Jindal, N. Kumar, M. Singh, and A. Vinel, "A novel resource reservation scheme for mobile phevs in V2G environment using game theoretical approach," *IEEE Transactions on Vehicular Technology*, vol. 64, no. 12, pp. 5653–5666, Dec 2015.

[98] S. Singh, M. Singh, and S. C. Kaushik, "Optimal power scheduling of renewable energy systems in microgrids using distributed energy storage system," *IET Renewable Power Generation*, vol. 10, no. 9, pp. 1328–1339, 2016.

[99] C. Li, Y. Cao, Y. Kuang, and B. Zhou, "The response of EV charging load to the grid voltage," in *Influences of Electric Vehicles on Power System and Key Technologies of Vehicle-to-Grid*. Springer, 2016, pp. 37–48.

[100] O. Tremblay and L.-A. Dessaint, "Experimental validation of a battery dynamic model for ev applications," *World Electric Vehicle Journal*, vol. 3, no. 2, pp. 289–298, 2009.

[101] MathWorks, "Battery, implement generic battery model." [Online]. Available: https://in.mathworks.com/help/physmod/sps/powersys/ref/battery.html

[102] J. J. Escudero-Garzas, A. Garcia-Armada, and G. Seco-Granados, "Fair design of plug-in electric vehicles aggregator for V2G regulation," *IEEE Transactions on Vehicular Technology*, vol. 61, no. 8, pp. 3406–3419, Oct 2012.

[103] A. Wu, M. Ju, and Y. Tsuei, "Comparison of fuzzy logic and self-tuning adaptive control of single-link flexible arm," *Mechatronics*, vol. 3, no. 4, pp. 451 – 464, 1993.

[104] S. G. Li, S. M. Sharkh, F. C. Walsh, and C. N. Zhang, "Energy and battery management of a plug-in series hybrid electric vehicle using fuzzy logic," *IEEE Transactions on Vehicular Technology*, vol. 60, no. 8, pp. 3571–3585, Oct 2011.

[105] S. M. T. Bathaee, A. H. Gastaj, S. R. Emami, and M. Mohammadian, "A fuzzy-based supervisory robust control for parallel hybrid electric vehicles," in *2005 IEEE Vehicle Power and Propulsion Conference*, Sept 2005, pp. 7 pp.–.

[106] W. Pedrycz, "Why triangular membership functions?" *Fuzzy Sets and Syst.*, vol. 64, no. 1, pp. 21 – 30, 1994.

[107] T. Ross, *Fuzzy logic with engineering applications*. McGraw-Hill, 1995.

[108] R. Lowen, *Fuzzy Set Theory: Basic Concepts, Techniques and Bibliography*. Springer Netherlands, 1996.

[109] M. P. Jay Giri and D. Wilson, "Synchrophasor PMU data analysis for enhanced control centre operations," in *IEEE General Meeting, 2011*.

[110] P. Kundur, N. J. Balu, and M. G. Lauby, "Power system stability and control," 1994.

[111] S. Mikkili and A. K. Panda, "Simulation and real-time implementation of shunt active filter id-iq control strategy for mitigation of harmonics with different fuzzy membership functions," *IET Power Electronics*, vol. 5, no. 9, pp. 1856–1872, November 2012.

[112] P. García-Triviño, J. P. Torreglosa, L. M. Fernández-Ramírez, and F. Jurado, "Decentralized fuzzy logic control of microgrid for electric vehicle charging station," *IEEE Journal of Emerging and Selected Topics in Power Electronics*, vol. 6, no. 2, pp. 726–737, June 2018.

[113] X. Lin and Y. Lei, "Coordinated control strategies for SMES-battery hybrid energy storage systems," *IEEE Access*, vol. 5, pp. 23 452–23 465, 2017.

[114] S. Falahati, S. A. Taher, and M. Shahidehpour, "Grid secondary frequency control by optimized fuzzy control of electric vehicles," *IEEE Transactions on Smart Grid*, pp. 1–1, 2017.

[115] M. Datta and T. Senjyu, "Fuzzy control of distributed PV inverters/energy storage systems/electric vehicles for frequency regulation in a large power system," *IEEE Transactions on Smart Grid*, vol. 4, no. 1, pp. 479–488, March 2013.

[116] T. Ma and O. A. Mohammed, "Optimal charging of plug-in electric vehicles for a car-park infrastructure," *IEEE Transactions on Industry Applications*, vol. 50, no. 4, pp. 2323–2330, July 2014.

[117] Asia-Pacific Economic Coorperation, *The Impact of Government Policy on PromoPromoting New Energy Vehicles (NEVs)– The Evidence in APEC Economies*, 2017.

[118] R. C. Green, L. Wang, and M. Alam, "The impact of plug-in hybrid electric vehicles on distribution networks: A review and outlook," *Renewable and Sustain. Energy Rev.*, vol. 15, no. 1, pp. 544 – 553, 2011.

[119] D. B. Richardson, "Electric vehicles and the electric grid: A review of modeling approaches, impacts, and renewable energy integration," *Renewable and Sustain. Energy Rev.*, vol. 19, pp. 247 – 254, 2013.

[120] T. Markel, A. Meintz, K. Hardy, B. Chen, and T. Bohn, "Multi-lab EV smart grid integration requirements study [internet]. golden, colorado: Nrel; 2015 may [cited 2016 may 22]," *Report No.: NREL/TP-5400-63963*, p. 91, 2015.

[121] C. Nelder, J. Newcomb, and G. Fitzgerald, "Electric vehicles as distributed energy resources," *Rocky Mountain Institute*, 2016.

[122] S. Vachirasricirikul and I. Ngamroo, "Robust LFC in a smart grid with wind power penetration by coordinated V2G control and frequency controller," *IEEE Trans. Smart Grid*, vol. 5, no. 1, pp. 371–380, Jan 2014.

[123] V. Lakshminarayanan, V. G. S. Chemudupati, S. K. Pramanick, and K. Rajashekara, "Real-time optimal energy management controller for electric vehicle integration in workplace microgrid," *IEEE Trans. Transport. Electrific.*, vol. 5, no. 1, pp. 174–185, Mar 2019.

[124] S. Debbarma and A. Dutta, "Utilizing electric vehicles for LFC in restructured power systems using fractional order controller," *IEEE tran. Smart Grid*, vol. 8, no. 6, pp. 2554–2564, 2016.

[125] Y. Tang, J. Yang, J. Yan, and H. He, "Intelligent load frequency controller using GrADP for island smart grid with electric vehicles and renewable resources," *Neurocomputing*, vol. 170, pp. 406–416, 2015.

[126] H. Khayyam, H. Ranjbarzadeh, and V. Marano, "Intelligent control of vehicle to grid power," *J. Power Sources*, vol. 201, pp. 1 – 9, 2012.

[127] E. Sortomme, M. M. Hindi, S. D. J. MacPherson, and S. S. Venkata, "Coordinated charging of plug-in hybrid electric vehicles to minimize distribution system losses," *IEEE Trans. Smart Grid*, vol. 2, no. 1, pp. 198–205, Mar 2011.

[128] Z. Xu, Z. Hu, Y. Song, H. Zhang, and X. Chen, "Coordinated charging strategy for PEV charging stations based on dynamic time-of-use tariffs," *Proc. CSEE*, vol. 34, no. 22, pp. 3638–3646, 2014.

[129] J. Zhang, M. Cui, B. Li, H. Fang, and Y. He, "Fast solving method based on linearized equations of branch power flow for coordinated charging of evs (evcc)," *IEEE Trans. Veh. Technol.*, vol. 68, no. 5, pp. 4404–4418, May 2019.

[130] H. V. Padullaparti, P. Chirapongsananurak, S. Santoso, and J. A. Taylor, "Edge-of-grid voltage control: Device modeling, strategic placement, and application considerations," *IEEE Power and Energy Technol. Syst. J.*, vol. 4, no. 4, pp. 106–114, 2017.

[131] A. Ramachandran, A. Balakrishna, P. Kundzicz, and A. Neti, "Predicting electric vehicle charging station usage: Using machine learning to estimate individual station statistics from physical configurations of charging station networks," *arXiv preprint arXiv:1804.00714*, 2018.

[132] C. Huang, F. Li, D. Zhou, J. Guo, Z. Pan, Y. Liu, and Y. Liu, "Data quality issues for synchrophasor applications Part I: A review," *J. of Modern Power Syst. and Clean Energy*, vol. 4, no. 3, pp. 342–352, Jul 2016.

[133] D. E. Bakken, A. Bose, C. H. Hauser, D. E. Whitehead, and G. C. Zweigle, "Smart generation and transmission with coherent, real-time data," *Proc. of the IEEE*, vol. 99, no. 6, pp. 928–951, June 2011.

[134] A. B. Forouzan, *Data communications & networking (sie)*. Tata McGraw-Hill Education, 2007.

[135] P. E. Sørensen, P. H. Madsen, A. Vikkelsø, K. K. Jensen, K. Fathima, A. Unnikrishnan, and Z. Lakaparampil, *Power quality and integration of wind farms in weak grids in India*, 2000.

[136] C. Richts, P. Strauss, and D. Heinemann, "Report on forecasting, concept of renewable energy management centres and grid balancing," *Indo-German Energy Programme—Green Energy Corridors, GIZ GmbH*, 2015.

[137] A. Bakshi, A. Velayutham, S. Srivastava, K. Agrawal, R. Nayak, S. Soonee, and B. Singh, "Report of the enquiry committee on grid disturbance in northern region on 30th july 2012 and in northern, eastern & north-eastern region on 31st july 2012," *New Delhi, India*, 2012.

[138] B. Sah, P. Kumar, R. Rayudu, S. K. Bose, and K. P. Inala, "Impact of sampling in the operation of vehicle to grid and its mitigation," *IEEE Trans. on Ind. Informat.*, pp. 1–1, 2018.

[139] L. Noel, G. Zarazua de Rubens, B. K. Sovacool, and J. Kester, "Fear and loathing of electric vehicles: The reactionary rhetoric of range anxiety," *Energy Research & Social Science*, vol. 48, pp. 96–107, 2019. [Online]. Available: https://www.sciencedirect.com/science/article/pii/S2214629618304456

[140] H. A. Kiehne, *Battery technology handbook*. CRC Press, 2003, vol. 118.

[141] Y. Ma, H. Zhang, B. Wu, M. Wang, X. Li, and H. Zhang, "Lithium sulfur primary battery with super high energy density: based on the cauliflower-like structured c/s cathode," *Scientific reports*, vol. 5, no. 1, pp. 1–10, 2015.

[142] J. Lopez, D. G. Mackanic, Y. Cui, and Z. Bao, "Designing polymers for advanced battery chemistries," *Nature Reviews Materials*, vol. 4, no. 5, pp. 312–330, 2019.

[143] N. Chawla, "Recent advances in air-battery chemistries," *Materials Today Chemistry*, vol. 12, pp. 324–331, 2019.

[144] J. T. Warner, *Lithium-Ion Battery Chemistries: A Primer*. Elsevier, 2019.

[145] M. Kabir and D. E. Demirocak, "Degradation mechanisms in li-ion batteries: a state-of-the-art review," *International Journal of Energy Research*, vol. 41, no. 14, pp. 1963–1986, 2017.

[146] L. Lu, X. Han, J. Li, J. Hua, and M. Ouyang, "A review on the key issues for lithium-ion battery management in electric vehicles," *Journal of power sources*, vol. 226, pp. 272–288, 2013.

[147] F. Conte, "Battery and battery management for hybrid electric vehicles: a review," *e & i Elektrotechnik und Informationstechnik*, vol. 123, no. 10, pp. 424–431, 2006.

[148] P. Keil, S. F. Schuster, J. Wilhelm, J. Travi, A. Hauser, R. C. Karl, and A. Jossen, "Calendar aging of lithium-ion batteries," *Journal of The Electrochemical Society*, vol. 163, no. 9, p. A1872, 2016.

[149] A. Raj, M.-T. F. Rodrigues, and D. P. Abraham, "Rate-dependent aging resulting from fast charging of li-ion cells," *Journal of The Electrochemical Society*, vol. 167, no. 12, p. 120517, 2020.

[150] K. Maher and R. Yazami, "A study of lithium ion batteries cycle aging by thermodynamics techniques," *Journal of Power Sources*, vol. 247, pp. 527–533, 2014.

[151] A. Tomaszewska, Z. Chu, X. Feng, S. O'Kane, X. Liu, J. Chen, C. Ji, E. Endler, R. Li, L. Liu, Y. Li, S. Zheng, S. Vetterlein, M. Gao, J. Du, M. Parkes, M. Ouyang, M. Marinescu, G. Offer, and B. Wu, "Lithium-ion battery fast charging: A review," *eTransportation*, vol. 1, p. 100011, 2019. [Online]. Available: https://www.sciencedirect.com/science/article/pii/S2590116819300116

[152] D. Zhang, B. Haran, A. Durairajan, R. E. White, Y. Podrazhansky, and B. N. Popov, "Studies on capacity fade of lithium-ion batteries," *Journal of Power Sources*, vol. 91, no. 2, pp. 122–129, 2000.

[153] P. Ramadass, B. Haran, R. White, and B. N. Popov, "Capacity fade of sony 18650 cells cycled at elevated temperatures: Part i. cycling performance," *Journal of power sources*, vol. 112, no. 2, pp. 606–613, 2002.

[154] P. Keil and A. Jossen, "Charging protocols for lithium-ion batteries and their impact on cycle life—an experimental study with different 18650 high-power cells," *Journal of Energy Storage*, vol. 6, pp. 125–141, 2016.

[155] J. Liu, Q. Duan, M. Ma, C. Zhao, J. Sun, and Q. Wang, "Aging mechanisms and thermal stability of aged commercial 18650 lithium ion battery induced by slight overcharging cycling," *Journal of Power Sources*, vol. 445, p. 227263, 2020.

[156] G. Sikha, P. Ramadass, B. Haran, R. E. White, and B. N. Popov, "Comparison of the capacity fade of sony us 18650 cells charged with different protocols," *Journal of power sources*, vol. 122, no. 1, pp. 67–76, 2003.

[157] L. Patnaik, A. Praneeth, and S. S. Williamson, "A closed-loop constant-temperature constant-voltage charging technique to reduce charge time of lithium-ion batteries," *IEEE Transactions on Industrial Electronics*, vol. 66, no. 2, pp. 1059–1067, 2018.

[158] G. Sikha, B. N. Popov, and R. E. White, "Effect of porosity on the capacity fade of a lithium-ion battery: Theory," *Journal of the Electrochemical Society*, vol. 151, no. 7, p. A1104, 2004.

[159] M. B. Pinson and M. Z. Bazant, "Theory of SEI formation in rechargeable batteries: capacity fade, accelerated aging and lifetime prediction," *Journal of the Electrochemical Society*, vol. 160, no. 2, p. A243, 2012.

[160] S. Schindler, M. Bauer, H. Cheetamun, and M. A. Danzer, "Fast charging of lithium-ion cells: identification of aging-minimal current profiles using a design of experiment approach and a mechanistic degradation analysis," *Journal of Energy Storage*, vol. 19, pp. 364–378, 2018.

[161] S. S. Zhang, "The effect of the charging protocol on the cycle life of a li-ion battery," *Journal of power sources*, vol. 161, no. 2, pp. 1385–1391, 2006.

[162] S. Li, Q. Wu, D. Zhang, Z. Liu, Y. He, Z. L. Wang, and C. Sun, "Effects of pulse charging on the performances of lithium-ion batteries," *Nano Energy*, vol. 56, pp. 555–562, 2019.

[163] J. Li, E. Murphy, J. Winnick, and P. A. Kohl, "The effects of pulse charging on cycling characteristics of commercial lithium-ion batteries," *Journal of Power Sources*, vol. 102, no. 1-2, pp. 302–309, 2001.

[164] F. Savoye, P. Venet, M. Millet, and J. Groot, "Impact of periodic current pulses on li-ion battery performance," *IEEE Transactions on Industrial Electronics*, vol. 59, no. 9, pp. 3481–3488, 2011.

[165] H. Lv, X. Huang, and Y. Liu, "Analysis on pulse charging–discharging strategies for improving capacity retention rates of lithium-ion batteries," *Ionics*, pp. 1–22, 2020.

[166] S. Li, Q. Wu, D. Zhang, Z. Liu, Y. He, Z. L. Wang, and C. Sun, "Effects of pulse charging on the performances of lithium-ion batteries," *Nano Energy*, vol. 56, pp. 555–562, 2019. [Online]. Available: https://www.sciencedirect.com/science/article/pii/S2211285518308826

[167] P. H. Notten, J. O. het Veld, and J. Van Beek, "Boostcharging li-ion batteries: A challenging new charging concept," *Journal of Power Sources*, vol. 145, no. 1, pp. 89–94, 2005.

[168] M. F. Hasan, C.-F. Chen, C. E. Shaffer, and P. P. Mukherjee, "Analysis of the implications of rapid charging on lithium-ion battery performance," *Journal of the Electrochemical Society*, vol. 162, no. 7, p. A1382, 2015.

[169] L.-R. Chen, S.-L. Wu, D.-T. Shieh, and T.-R. Chen, "Sinusoidal-ripple-current charging strategy and optimal charging frequency study for li-ion batteries," *IEEE Transactions on Industrial Electronics*, vol. 60, no. 1, pp. 88–97, 2012.

[170] Y. Lee and S. Park, "Electrochemical state-based sinusoidal ripple current charging control," *IEEE Transactions on Power Electronics*, vol. 30, no. 8, pp. 4232–4243, 2015.

[171] J. Chen, Y. Lee, and S. Park, "Adaptive PI gain control to realize sinusoidal ripple current charging," in *2015 9th International Conference on Power Electronics and ECCE Asia (ICPE-ECCE Asia)*, 2015, pp. 2582–2589.

[172] M. Bayati, M. Abedi, G. B. Gharehpetian, and M. Farahmandrad, "Sinusoidal-ripple current control in battery charger of electric vehicles," *IEEE Transactions on Vehicular Technology*, vol. 69, no. 7, pp. 7201–7210, 2020.

[173] H. Vazini, "Sinusoidal charging of li-ion battery based on frequency detection algorithm by pole placement control method," *IET Power Electronics*, vol. 12, pp. 421–429(8), March 2019.

[174] Z. Zhang, Z. L. Wang, and X. Lu, "Suppressing lithium dendrite growth via sinusoidal ripple current produced by triboelectric nanogenerators," *Advanced Energy Materials*, vol. 9, no. 20, p. 1900487, 2019. [Online]. Available: https://onlinelibrary.wiley.com/doi/abs/10.1002/aenm.201900487

[175] A. Bessman, R. Soares, S. Vadivelu, O. Wallmark, P. Svens, H. Ekström, and G. Lindbergh, "Challenging sinusoidal ripple-current charging of lithium-ion batteries," *IEEE Transactions on Industrial Electronics*, vol. 65, no. 6, pp. 4750–4757, 2018.

[176] X. Lin, X. Hao, Z. Liu, and W. Jia, "Health conscious fast charging of li-ion batteries via a single particle model with aging mechanisms," *Journal of Power Sources*, vol. 400, pp. 305–316, 2018.

[177] H. Perez, S. Dey, X. Hu, and S. Moura, "Optimal charging of li-ion batteries via a single particle model with electrolyte and thermal dynamics," *Journal of The Electrochemical Society*, vol. 164, no. 7, p. A1679, 2017.

[178] S. Pramanik and S. Anwar, "Electrochemical model based charge optimization for lithium-ion batteries," *Journal of Power Sources*, vol. 313, pp. 164–177, 2016.

[179] T. Waldmann, M. Kasper, and M. Wohlfahrt-Mehrens, "Optimization of charging strategy by prevention of lithium deposition on anodes in high-energy lithium-ion batteries–electrochemical experiments," *Electrochimica Acta*, vol. 178, pp. 525–532, 2015.

[180] F. B. Spingler, W. Wittmann, J. Sturm, B. Rieger, and A. Jossen, "Optimum fast charging of lithium-ion pouch cells based on local volume expansion criteria," *Journal of Power Sources*, vol. 393, pp. 152–160, 2018.

[181] C. Zou, X. Hu, Z. Wei, T. Wik, and B. Egardt, "Electrochemical estimation and control for lithium-ion battery health-aware fast charging," *IEEE Transactions on Industrial Electronics*, vol. 65, no. 8, pp. 6635–6645, 2017.

[182] M. Song and S.-Y. Choe, "Fast and safe charging method suppressing side reaction and lithium deposition reaction in lithium ion battery," *Journal of Power Sources*, vol. 436, p. 226835, 2019.

[183] T. Osaka, S. Nakade, M. Rajamäki, and T. Momma, "Influence of capacity fading on commercial lithium-ion battery impedance," *Journal of power sources*, vol. 119, pp. 929–933, 2003.

[184] A. Waligo and P. Barendse, "A comparison of the different broadband impedance measurement techniques for lithium-ion batteries," in *2016 IEEE Energy Conversion Congress and Exposition (ECCE)*, 2016, pp. 1–7.

[185] D. Depernet, O. Ba, and A. Berthon, "Online impedance spectroscopy of lead acid batteries for storage management of a standalone power plant," *Journal of Power Sources*, vol. 219, pp. 65–74, 2012. [Online]. Available: https://www.sciencedirect.com/science/article/pii/S0378775312011780

[186] W. Huang and J. A. Abu Qahouq, "An online battery impedance measurement method using DC–DC power converter control," *IEEE Transactions on Industrial Electronics*, vol. 61, no. 11, pp. 5987–5995, 2014.

[187] D. A. Howey, P. D. Mitcheson, V. Yufit, G. J. Offer, and N. P. Brandon, "Online measurement of battery impedance using motor controller excitation," *IEEE Transactions on Vehicular Technology*, vol. 63, no. 6, pp. 2557–2566, 2014.

[188] R. Koch, R. Kuhn, I. Zilberman, and A. Jossen, "Electrochemical impedance spectroscopy for online battery monitoring - power electronics control," in *2014 16th European Conference on Power Electronics and Applications*, 2014, pp. 1–10.

[189] Y.-D. Lee, S.-Y. Park, and S.-B. Han, "Online embedded impedance measurement using high-power battery charger," *IEEE Transactions on Industry Applications*, vol. 51, no. 1, pp. 498–508, 2015.

[190] T. N. Gücin and L. Ovacik, "Online impedance measurement of batteries using the cross-correlation technique," *IEEE Transactions on Power Electronics*, vol. 35, no. 4, pp. 4365–4375, 2019.

[191] G. S. Misyris, D. I. Doukas, T. A. Papadopoulos, D. P. Labridis, and V. G. Agelidis, "State-of-charge estimation for li-ion batteries: A more accurate hybrid approach," *IEEE Transactions on Energy Conversion*, vol. 34, no. 1, pp. 109–119, 2018.

[192] T. Ouyang, P. Xu, J. Lu, X. Hu, B. Liu, and N. Chen, "Co-estimation of state-of-charge and state-of-health for power batteries based on multi-thread dynamic optimization method," *IEEE Transactions on Industrial Electronics*, 2021.

[193] E. Chemali, P. J. Kollmeyer, M. Preindl, and A. Emadi, "State-of-charge estimation of li-ion batteries using deep neural networks: A machine learning approach," *Journal of Power Sources*, vol. 400, pp. 242–255, 2018. [Online]. Available: https://www.sciencedirect.com/science/article/pii/S0378775318307080

[194] G. Sethia, S. K. Nayak, and S. Majhi, "An approach to estimate lithium-ion battery state of charge based on adaptive lyapunov super twisting observer," *IEEE Transactions on Circuits and Systems I: Regular Papers*, vol. 68, no. 3, pp. 1319–1329, 2020.

[195] T. Ouyang, P. Xu, J. Lu, X. Hu, B. Liu, and N. Chen, "Co-estimation of state-of-charge and state-of-health for power batteries based on multi-thread dynamic optimization method," *IEEE Transactions on Industrial Electronics*, 2021.

[196] M. Verbrugge, "Adaptive, multi-parameter battery state estimator with optimized time-weighting factors," *Journal of applied electrochemistry*, vol. 37, no. 5, pp. 605–616, 2007.

[197] H. Rahimi-Eichi, F. Baronti, and M.-Y. Chow, "Online adaptive parameter identification and state-of-charge coestimation for lithium-polymer battery cells," *IEEE Transactions on Industrial Electronics*, vol. 61, no. 4, pp. 2053–2061, 2013.

[198] J. Li and M. Liu, "State-of-charge estimation of lithium-ion batteries using composite multi-dimensional features and a neural network," *IET Power Electronics*, vol. 12, no. 6, pp. 1470–1478, 2019.

[199] K. Zhu, Y. Wan, C. Li, and X. Luo, "Battery parameter identification using recursive least squares with variable directional forgetting," in *2020 IEEE 16th International Conference on Control & Automation (ICCA)*. IEEE, 2020, pp. 755–760.

[200] H.-S. Shin and H.-I. Lee, "A new exponential forgetting algorithm for recursive least-squares parameter estimation," *arXiv preprint arXiv:2004.03910*, 2020.

[201] S. Yang, S. Zhou, Y. Hua, X. Zhou, X. Liu, Y. Pan, H. Ling, and B. Wu, "A parameter adaptive method for state of charge estimation of lithium-ion batteries with an improved extended kalman filter," *Scientific reports*, vol. 11, no. 1, pp. 1–15, 2021.

[202] P. Xu, B. Liu, X. Hu, T. Ouyang, and N. Chen, "State-of-charge estimation for lithium-ion batteries based on fuzzy information granulation and asymmetric gaussian membership function," *IEEE Transactions on Industrial Electronics*, 2021.

[203] T. N. Gücin and L. Ovacik, "Online impedance measurement of batteries using the cross-correlation technique," *IEEE Transactions on Power Electronics*, vol. 35, no. 4, pp. 4365–4375, 2019.

[204] E. J. Dickinson and A. J. Wain, "The butler-volmer equation in electrochemical theory: Origins, value, and practical application," *Journal of Electroanalytical Chemistry*, vol. 872, p. 114145, 2020, dr. Richard Compton 65th birthday Special issue. [Online]. Available: https://www.sciencedirect.com/science/article/pii/S1572665720303283

[205] A. Seaman, T.-S. Dao, and J. McPhee, "A survey of mathematics-based equivalent-circuit and electrochemical battery models for hybrid and electric vehicle simulation," *Journal of Power Sources*, vol. 256, pp. 410–423, 2014. [Online]. Available: https://www.sciencedirect.com/science/article/pii/S0378775314000810

[206] M. Doyle, T. F. Fuller, and J. Newman, "Modeling of galvanostatic charge and discharge of the lithium/polymer/insertion cell," *Journal of the Electrochemical society*, vol. 140, no. 6, p. 1526, 1993.

[207] C. M. Doyle, "Design and simulation of lithium rechargeable batteries," 1995.

[208] S. G. Marquis, V. Sulzer, R. Timms, C. P. Please, and S. J. Chapman, "An asymptotic derivation of a single particle model with electrolyte," *Journal of The Electrochemical Society*, vol. 166, no. 15, p. A3693, 2019.

[209] R. Timms, S. G. Marquis, V. Sulzer, C. P. Please, and S. J. Chapman, "Asymptotic reduction of a lithium-ion pouch cell model," *SIAM Journal on Applied Mathematics*, vol. 81, no. 3, pp. 765–788, 2021.

[210] V. Sulzer, S. G. Marquis, R. Timms, M. Robinson, and S. J. Chapman, "Python Battery Mathematical Modelling (PyBaMM)," *Journal of Open Research Software*, vol. 9, no. 1, p. 14, 2021.

[211] B. Balagopal and M.-Y. Chow, "The physical manifestation of side reactions in the electrolyte of lithium-ion batteries and its impact on the terminal voltage response," *Batteries*, vol. 6, no. 4, p. 53, 2020.

[212] M. H.-M. Tang, "Side reactions in lithium-ion batteries," Ph.D. dissertation, UC Berkeley, 2012.

[213] X. Zhang, A. M. Sastry, and W. Shyy, "Intercalation-induced stress and heat generation within single lithium-ion battery cathode particles," *Journal of The Electrochemical Society*, vol. 155, no. 7, p. A542, 2008.

[214] R. Xiong, Y. Pan, W. Shen, H. Li, and F. Sun, "Lithium-ion battery aging mechanisms and diagnosis method for automotive applications: Recent advances and perspectives," *Renewable and Sustainable Energy Reviews*, vol. 131, p. 110048, 2020.

[215] Z. Yan and M. Obrovac, "Selecting inactive materials with low electrolyte reactivity for lithium-ion cells," *Journal of Power Sources*, vol. 397, pp. 374–381, 2018. [Online]. Available: https://www.sciencedirect.com/science/article/pii/S037877531830750X

[216] C. J. Orendorff, G. Nagasubramanian, T. N. Lambert, K. R. Fenton, C. A. Apblett, C. R. Shaddix, M. Geier, and E. P. Roth, "Advanced inactive materials for improved lithium-ion battery safety," *Sandia Report SAND*, vol. 9186, p. 2012, 2012.

[217] E. Foreman, W. Zakri, M. Hossein Sanatimoghaddam, A. Modjtahedi, S. Pathak, A. G. Kashkooli, N. G. Garafolo, and S. Farhad, "A review of inactive materials and components of flexible lithium-ion batteries," *Advanced Sustainable Systems*, vol. 1, no. 11, p. 1700061, 2017.

[218] X.-G. Yang, Y. Leng, G. Zhang, S. Ge, and C.-Y. Wang, "Modeling of lithium plating induced aging of lithium-ion batteries: Transition from linear to nonlinear aging," *Journal of Power Sources*, vol. 360, pp. 28–40, 2017.

[219] Y. Jeon, H. K. Noh, and H.-K. Song, "A lithium-ion battery using partially lithiated graphite anode and amphi-redox $limn_2o_4$ cathode," *Scientific reports*, vol. 7, no. 1, pp. 1–9, 2017.

[220] T. R. Ferguson, "Lithium-ion battery modeling using non-equilibrium thermodynamics," Ph.D. dissertation, Massachusetts Institute of Technology, 2014.

[221] T.-T. Nguyen, A. Demortière, B. Fleutot, B. Delobel, C. Delacourt, and S. J. Cooper, "The electrode tortuosity factor: why the conventional tortuosity factor is not well suited for quantifying transport in porous li-ion battery electrodes and what to use instead," *npj Computational Materials*, vol. 6, no. 1, pp. 1–12, 2020.

[222] J. Landesfeind, J. Hattendorff, A. Ehrl, W. A. Wall, and H. A. Gasteiger, "Tortuosity determination of battery electrodes and separators by impedance spectroscopy," *Journal of The Electrochemical Society*, vol. 163, no. 7, p. A1373, 2016.

[223] B. Tjaden, D. J. Brett, and P. R. Shearing, "Tortuosity in electrochemical devices: a review of calculation approaches," *International Materials Reviews*, vol. 63, no. 2, pp. 47–67, 2018.

[224] D. H. Doughty and C. C. Crafts, "Freedomcar: electrical energy storage system abuse test manual for electric and hybrid electric vehicle applications." Sandia National Laboratories, Tech. Rep., 2006.

[225] X. Zhou, J. Huang, Z. Pan, and M. Ouyang, "Impedance characterization of lithium-ion batteries aging under high-temperature cycling: Importance of electrolyte-phase diffusion," *Journal of Power Sources*, vol. 426, pp. 216–222, 2019.

[226] A. Andersson and K. Edström, "Chemical composition and morphology of the elevated temperature sei on graphite," *Journal of the Electrochemical Society*, vol. 148, no. 10, p. A1100, 2001.

[227] M. Richard and J. Dahn, "Accelerating rate calorimetry study on the thermal stability of lithium intercalated graphite in electrolyte. i. experimental," *Journal of The Electrochemical Society*, vol. 146, no. 6, p. 2068, 1999.

[228] H. Maleki, G. Deng, A. Anani, and J. Howard, "Thermal stability studies of li-ion cells and components," *Journal of The electrochemical society*, vol. 146, no. 9, p. 3224, 1999.

[229] D. MacNeil, D. Larcher, and J. Dahn, "Comparison of the reactivity of various carbon electrode materials with electrolyte at elevated temperature," *Journal of the electrochemical society*, vol. 146, no. 10, p. 3596, 1999.

[230] P. Arora, M. Doyle, and R. E. White, "Mathematical modeling of the lithium deposition overcharge reaction in lithium-ion batteries using carbon-based negative electrodes," *Journal of The Electrochemical Society*, vol. 146, no. 10, p. 3543, 1999.

[231] C.-K. Huang, J. Sakamoto, J. Wolfenstine, and S. Surampudi, "The limits of low-temperature performance of li-ion cells," *Journal of the Electrochemical Society*, vol. 147, no. 8, p. 2893, 2000.

[232] L.-R. Chen, "A design of an optimal battery pulse charge system by frequency-varied technique," *IEEE Transactions on Industrial Electronics*, vol. 54, no. 1, pp. 398–405, 2007.

[233] M. Muratori, "Impact of uncoordinated plug-in electric vehicle charging on residential power demand," *Nature Energy*, vol. 3, no. 3, pp. 193–201, 2018.